The pre-depositional history of the Applecross Formation, Northwest Highlands, Scotland.

Samuel John Holmes

BSc (Hons)

Submitted in fulfilment of the requirements for the

Degree of Master of Science

School of Geographical and Earth Sciences

College of Science and Engineering

University of Glasgow

November 2018

Abstract

The provenance of Applecross Formation sedimentary rocks (Torridon Group, Northwest Scotland) is a topic of significant debate owing to difficulties in clearly correlating various datasets for the region (detrital mineral studies, sedimentology, and palinspastic restorations) to create an accepted palaeogeographic reconstruction. This study aims to elucidate the source area of Applecross sedimentary rocks and modes of deposition and transportation.

LA-ICP-MS $^{206}Pb/^{238}U$ dating of detrital zircon samples from various stratigraphic levels within the Applecross Formation type area is utilised to assess variations in the source over time. Sampling is spread through ~2000m of stratigraphy, along a ~15km outcrop parallel transect between Applecross and Loch Kishorn. Data reduction is undertaken using Iolite data reduction software.

U-Pb detrital zircon peaks of Mesoproterozoic (1280-1520Ma) and late Palaeoproterozoic (1680-1980Ma) age are dominant throughout the Applecross Formation. Minor early Palaeoproterozoic (2191-2265Ma) and Archean components up to 3346±43Ma are present. These data are in broad agreement with detrital zircon data from elsewhere in the Applecross Formation presented by Rainbird, Hamilton and Young (2001) and Krabbendam *et al.* (2017), suggesting a uniform input of well mixed sediment from a single source. Terranes in the foreland basin of the Grenville Orogen are favoured as source areas, with transport in an orogen axial foreland trunk system. Detrital Zircon U-Pb geochronology is combined with sedimentological context to determine depositional style. Deposition is interpreted to occur in a large scale distributive system similar to the Okavango Delta, Botswana, with unconfinement occurring during an extensional phase of the Grenville Orogen associated with rotation of Baltica relative to Laurentia at the time of deposition (see Rivers, 1997; Cawood *et al.*, 2007). This proposal correlates known detrital mineral and sedimentological datasets. Further work is required to support the model; additional detrital zircon datasets are required to confirm the validity of a single sediment input. Further evidence for localised extension in the Applecross region is required to substantiate unconfinement of an established foreland trunk river system.

Table of Contents

List of Tables and Figures

Acknowledgements

I would like to thank my supervisor Dr. Cristina Persano and co-supervisor Dr. Amanda Owen for their support, advice, and numerous discussions over the course of the year, without which I would most likely still be lost on a hill in Applecross. To that end I would also like to thank Ben Martin who travelled a very long way at short notice to carry several tonnes of rock down the mountain in the sleet and snow.

I enjoyed the advice and jokes of skilled technicians Robert MacDonald and John Gilleece while preparing samples. I would also like to thank Peter Chung of ISAAC for the use of and training on the ISAAC SEM without which accurate analysis would have been impossible.

Within the Solid Earth and LA-ICP-MS research groups I benefited greatly from the experience of Charlotte Slaymark, Eamon McKenna, and Awara Amin in understanding techniques, avoiding mistakes, and learning how to prepare and run various analysis. I would particularly like to thank Dr. Amy Riches for her assistance in completing later analyses for which there would not otherwise have been time.

I would like to thank GES staff Professor Rod Brown and Dr. Tim Dempster for their expertise during various areas of the project. I would like to thank the GES postgraduate cohort; few groups could be as universally welcoming and supportive to each other.

Finally, I can't thank enough the continued support and patience of my parents. I'll go and do something that pays now, I swear.

Author's Declaration

I declare that except where explicit reference is made to the contribution of others, that this thesis is the result of my own work and has not been submitted for any other degree at the University of Glasgow or any other institution.

Samuel John Holmes

Chapter 1 Introduction

The Torridon Group of Northwest Scotland forms the dramatic mountains and landscapes of the Scottish seaboard. The group is a sedimentary succession divided into four formations: the lowermost Diabaig Formation at the base of the sequence, overlain by the coarser Applecross and Aultbea Formations (classified as a single formation by Stewart, 2002). The Torridon Group is overlain by the Cailleach Head Formation. The Torridon Group was deposited by a number of fluvial processes in a pre-vegetation landscape; understanding the context of these processes is key to interpreting the landscape of the Mesoproterozoic. This study will focus on elucidating the source area of the Applecross Formation, which is the most extensive formation within the Torridon Group.

The source area of the Applecross Formation sandstones is a matter of debate. Numerous proposals have been made in an effort to elucidate the proximity and age of potential basement and supracrustal sources; in spite of this, it is difficult to bring the available evidence together in a unifying theory as several datasets appear to contradict each other. The style of transport and deposition are also a key topic of discussion. Ongoing collection of palaeocurrent data frequently leads to new proposals concerning the regional structure of the Applecross Formation. For example, it is unclear whether structures such as the Cape Wrath Megafan (see Williams, 2001) represent isolated features within braidplain settings or exposed remnants of a broader belt of alluvial fans as subsequent datasets lend support to different settings.

Understanding the precise nature of the Applecross Formation will provide insight into the relationship between ongoing fluvial styles and processes in modern landscapes and those in ancient, pre-vegetation fluvial systems. Such understanding has implications for our understanding of processes in remote locations and potential applications in the search for liquid water on other planets.

1.1 Objectives

This study aims to clarify the provenance of the Applecross sandstones and the style of their deposition. This is to be achieved through production of a new and extensive U-Pb detrital zircon dataset, covering both a range of stratigraphic levels within the Applecross Formation and a geographic transect within the formation type area at Applecross; these will be compared with previous low-quanta datasets for the formation from Rainbird, Hamilton and Young (2001) and Krabbendam *et al*. (2017).

Detrital zircon U-Pb data will be used to establish possible basement sources for the Applecross Formation. To further elucidate the source, this study will assess previous proposals of both source area and fluvial regime. Potential sources will be further constrained by extant sedimentological evidence from previous authors. This study will attempt to unify geochronological and sedimentological evidence to determine the most likely source of sediments for the Applecross Formation and the processes of deposition.

1.2 Setting

The outcrop of the Applecross Formation extends for ~200km through the Northwest Highlands of Scotland (Figure 1) forming a high relief landscape with abundant exposure (Figure 2). The Applecross Formation alone is ~3500m thick, however Stewart (2002) supports reclassification of the Aultbea Formation as part of the Applecross Formation providing a total thickness of ~4500m (See Figure 3). The vertical extent of exposure provides opportunity to assess the stratigraphy of the formation directly in the field. The Applecross Formation is largely homogenous, consisting of coarse arkosic sandstones with a varied pebble suite (see Moorbath, 1969; Williams and Foden, 2011,Table 2, section 3.2.2); occasional mud clasts also occur.

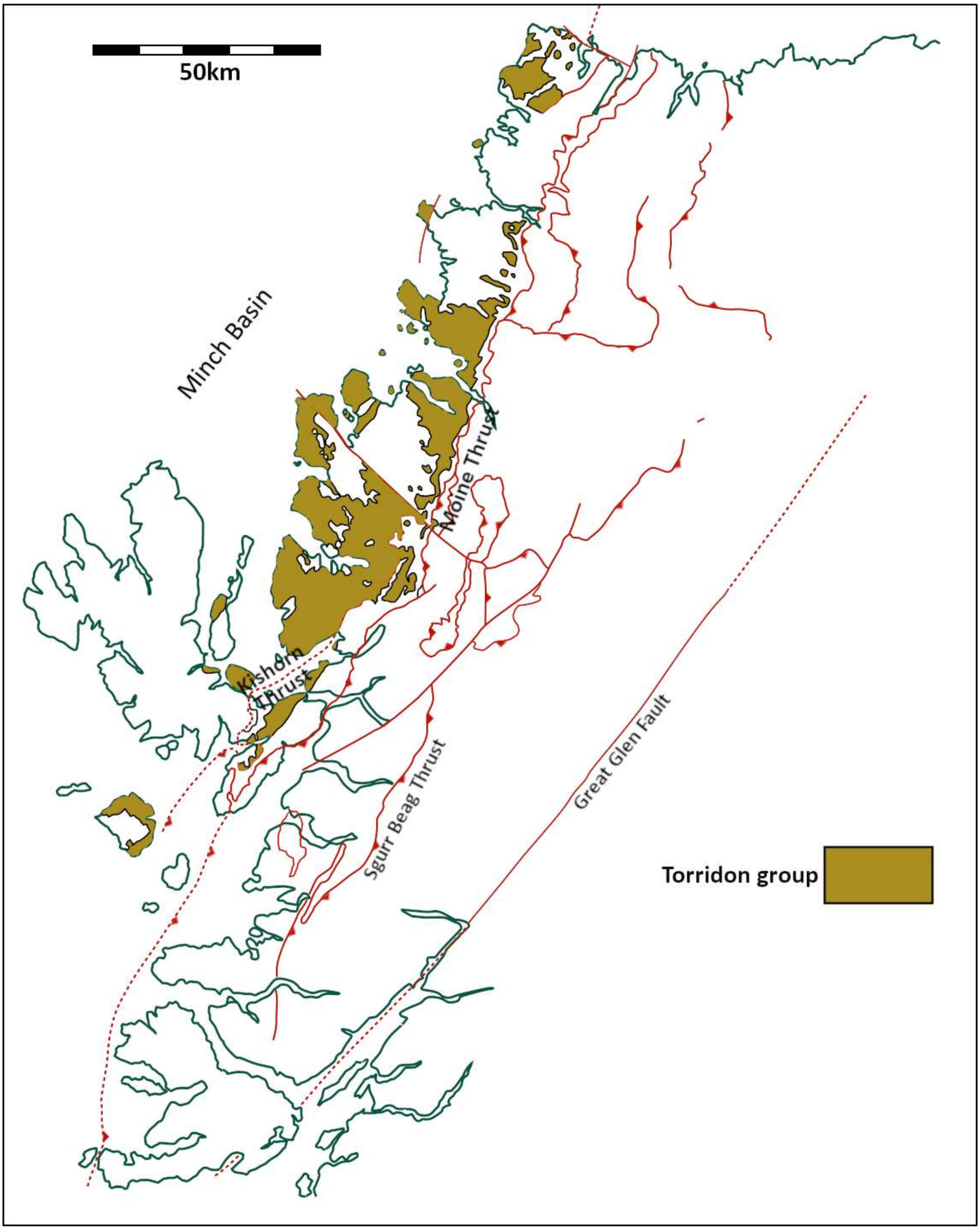

Figure 1: Extent of Torridonian outcrop in Northwest Scotland. After (Rainbird, Hamilton and Young, 2001; Krabbendam *et al.*, 2017). The Torridon Group is confined to the Northwest Highlands west of the Moine Thrust zone, lithologies extend into the Minch basin to the west.

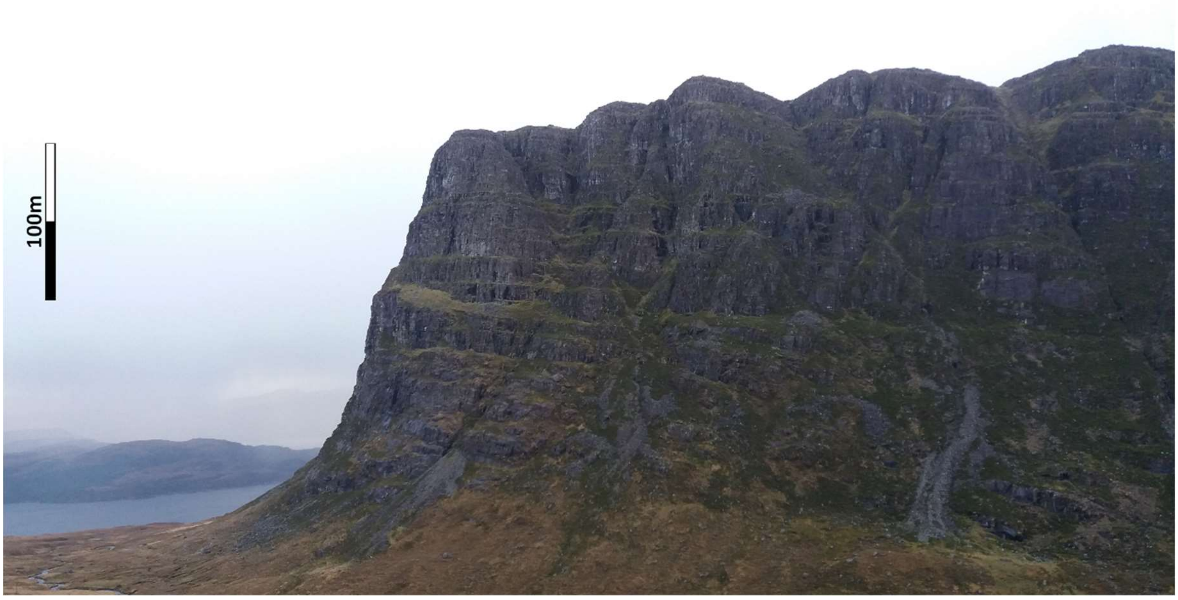

Figure 2: Photograph of Creag a Chumhaing taken from grid reference OS428, 7944 4120. Viewing direction 154°. Creag a Chumhaing lies in the Applecross type area near Loch Kishorn. Exposure of this type is typical of the Applecross type area and localities further north in mainland Scotland.

The Applecross Formation underwent early diagenesis between 994±48Ma and 977±39Ma (Turnbull, Whitehouse and Moorbath, 1996), placing a minimum age of deposition at ~980Ma. During this period Northwest Scotland formed a promontory on the edge of the Laurentian craton, which formed the core of the supercontinent Rodinia (Pisarevsky *et al.*, 2003; Cawood *et al.*, 2007, 2010; Bingen *et al.*, 2008; Li *et al.*, 2008; Rainbird *et al.*, 2017). At the time of deposition Laurentia and Baltica (Scandinavian craton) were undergoing a complex accretion and collision process involving rotation of Baltica around Laurentia and several periods of extension (Rivers, 1997; Cawood *et al.*, 2007), see Figure 4. Accretion of Rodinia lead to the formation of the extensive Grenville-Sveconorwegian Orogen along the southern boundary of Laurentia and Baltica; it is likely that the Applecross Formation, although not influenced by Grenvillian metamorphism, lay within the foreland of the Mesoproterozoic Grenville Orogen.

The Applecross Formation was deposited on a Lewisian palaeolandscape. Since the 1800's, the palaeoclimate at the time of deposition has been interpreted as warm and semi-arid, on the basis of abundant red sandstones; however mid-palaeolatitudes (30°-40°S) and a position closer to the Laurentian interior may have provided a cooler, more temperate setting (van de Kamp and Leake, 1997; Owen and Santos, 2014).

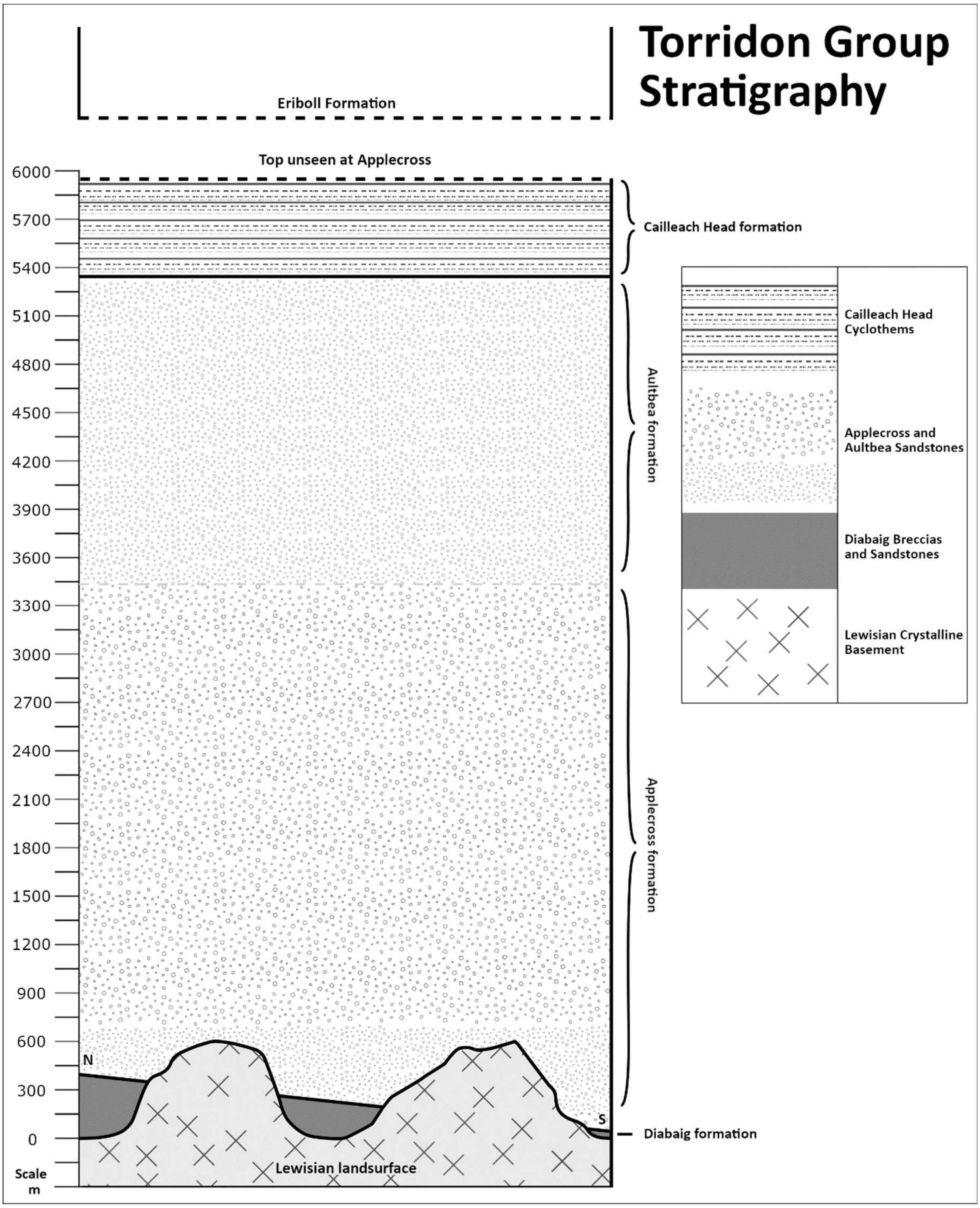

Figure 3: Simplified schematic stratigraphy of the Torridon Group. After (Selley, 1965; Stewart and Donnellan, 1992; Rainbird, Hamilton and Young, 2001; Williams, 2001; Stewart, 2002; Krabbendam, Prave and Cheer, 2008; Williams and Foden, 2011; Krabbendam *et al.*, 2017). The Torridon Group is deposited directly onto a Lewisian landscape, with formations such as the Diabaig varying significantly in thickness. (Stewart, 2002). The Applecross Formation overlies the Diabaig. Some workers (Stewart, 2002) have proposed that division of the Applecross and Aultbea is a misclassification, preferring to interpret them as a single formation. Both the Applecross and Aultbea Formations vary greatly in thickness, with estimates of thickness for the Aultbea ranging from ~500m to ~2000m; subsequently the thicknesses displayed are intended to be representative of the maximum thickness and may not resemble specific localities. The Cailleach Head Formation tops overlies the Aultbea Formation, in the study area (Applecross Peninsula) the formation is unseen. Further north the Cailleach Head Formation is overlain unconformably by the Eriboll Formation (Stewart, 2002; Krabbendam *et al.*, 2017).

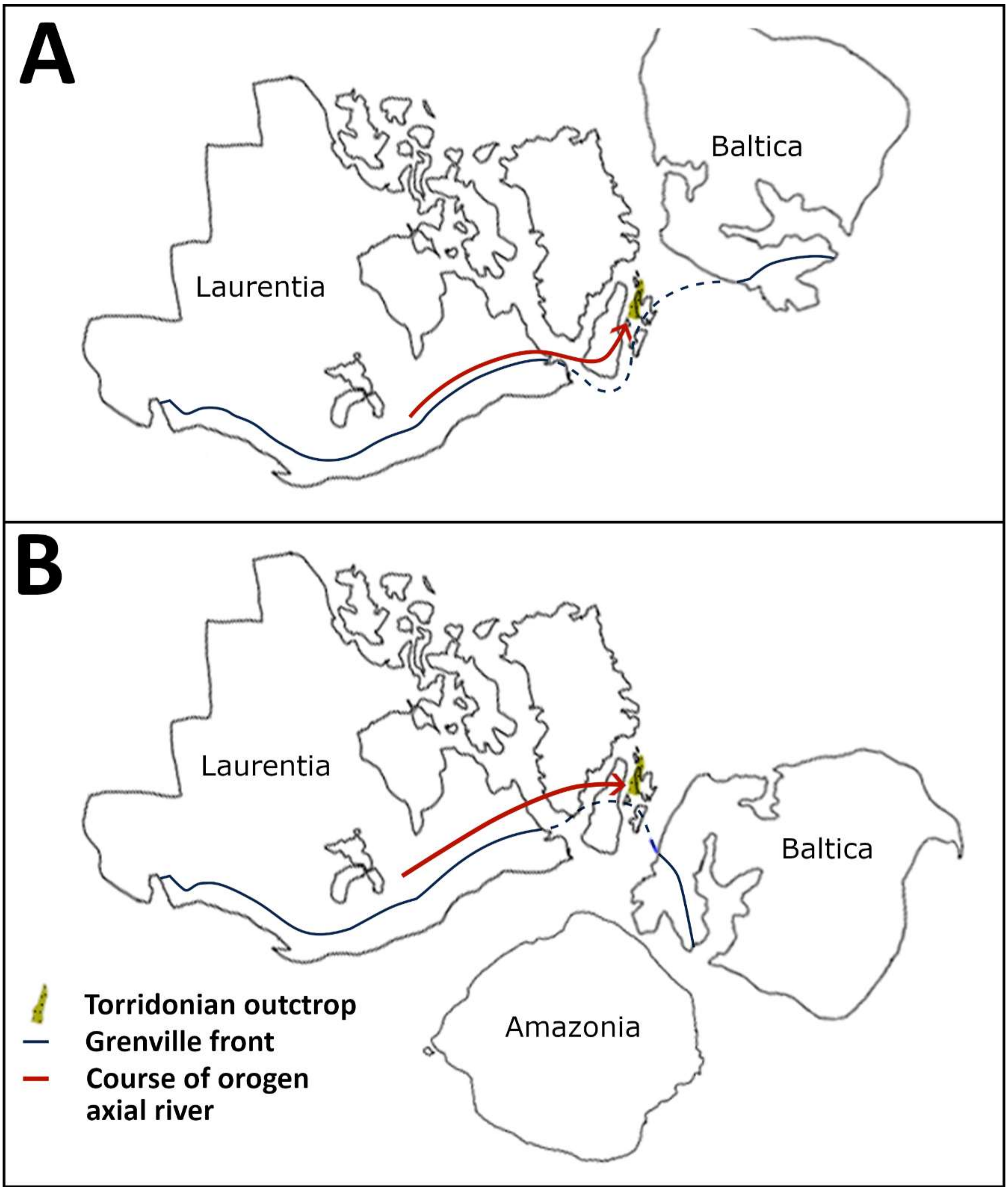

Figure 4: Relative positions of Laurentia and Baltica at (A) ~1200Ma and (B) during deposition of the Torridon. After (Li *et al.*, 2008; Cawood *et al.*, 2010; Williams and Foden, 2011; Krabbendam *et al.*, 2017; Rainbird *et al.*, 2017). Between 1200Ma (A)-980Ma (B) Baltica rotated around and in relation to Laurentia. This complex rotation may have facilitated periods of localised extension coeval with deposition of the Torridon Group.

1.3 Detrital zircon geochronology

The robust nature and high crystallization temperature of zircon render the mineral resilient to weathering processes and erosion. Zircon is able to survive multiple cycles of deposition and reworking, after initial removal from magmatic or metamorphic basement sources. Uranium commonly replaces zirconium in the crystal lattice of zircon. The combination of these features render zircon an excellent chronometer for provenance studies. By generating detrital zircon U-

Pb datasets over different levels in the Applecross Formation, variations in the source over time can be measured and comparisons may be drawn between zircon age clusters and terranes of relevant age. Comparison of conclusions from geochronological provenance studies with known sedimentological context and palaeogeographic reconstructions allows for robust determination of possible source areas.

1.4 Previous work

Current understanding of the Applecross Formation and related units has been developed by numerous authors, particularly since the 1960's with the advancement of detrital mineral studies.

Williams (1966) identified broadly northwest to west-northwest radial palaeocurrents in the Applecross Formation, interpreting these as the product of two large coalescing alluvial fans deposited at the foot of a retreating mountain front to the immediate northwest. Sediments were interpreted to be sourced from weathered Lewisian basement within the retreating belt (Williams, 1966).

Later analysis of palaeocurrents and sedimentology in the Applecross Formation revealed the presence of large scale bar structures (Nicholson, 1993) interpreted as the product of large scale rivers present alongside the fan deposits. A greater degree of variability in palaeoflow than previously recognised suggests that regional flow vectors may not support fan formation throughout the Applecross Formation (Nicholson, 1993). Nicholson (1993) instead supports deposition in a broader extensional basin setting, without active basin bounding faults, with sediment supplied by rivers over 500km in length.

Further evidence and constraints for a distal Applecross source area are provided by detrital zircon analysis (Rainbird, Hamilton and Young, 2001). Detrital zircon data support a source area in the foreland of the Grenville Orogen. Deposition by a northeast flowing foreland trunk river system axial to the Grenville Orogen is proposed (Rainbird, Hamilton and Young, 2001), supporting the distal fluvial setting of Nicholson (1993). Any northeast flowing trunk river system would be required to turn approximately east or southeast to generate the observed palaeocurrents in the Applecross Formation (Figure 5).

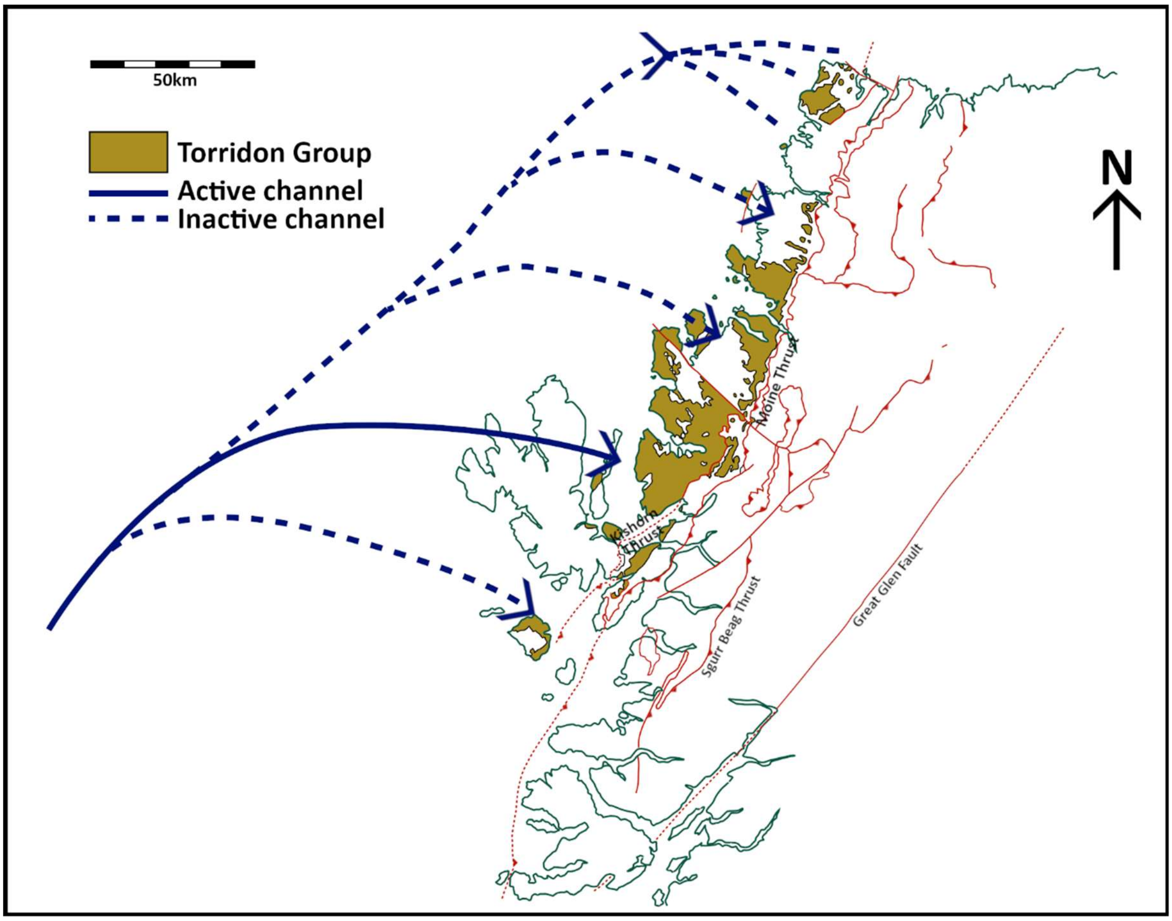

Figure 5: Alteration of flow direction in distal channels. Trunk river systems flowing to the northeast would require a significant change in direction to provide the palaeocurrents seen in the Applecross Formation outcrop.

The presence of a large scale alluvial fan with an overall east-directed flow is confirmed by extensive palaeocurrent analysis at Cape Wrath (Williams, 2001). In light of evidence for large scale rivers (Nicholson, 1993) Williams (2001) proposes deposition of the Applecross Formation in two main stages;

1. Deposition of the ~50km diameter Cape Wrath Megafan, following uplift of an adjacent source area to the northwest;

2. Deposition of the southern Applecross Formation in a braidplain setting at the distal end of alluvial fans, following uplift of the source area further to the southwest.

The proposed proximal source area may have reached up to 250km west from the Outer Hebrides, with uplift occurring along the line of the Minch Fault or

Outer Hebrides Fault Zone (OHFZ) (Williams, 2001) supporting a syn-depositional extensional setting.

Previous interpretations of the Applecross Formation as the result of deposition in an extensional basin are refuted by Kinnaird *et al.* (2007). Kinnaird *et al.* (2007) interpret the Applecross Formation as a non-marine molasse deposited by distal river systems and genetically unrelated to the adjacent Sleat and Stoer Groups.

Williams and Foden (2011) attempt to create a compromise model between detrital mineral datasets and local stratigraphic and palaeocurrent evidence, as some distal source proposals are not compatible with palaeocurrents observed in the Applecross Formation. A supracrustal series overlying the Lewisian to the west-northwest is proposed as the source area, with minimal contributions from the local Lewisian basement (Williams and Foden, 2011). The setting is proposed to be extensional with sediment filling the basin laterally from the relatively uplifted proximal source area (Williams and Foden, 2011). In response, Krabbendam and Rainbird (2012) refute the proposal of a proximal supracrustal source area citing a lack of evidence for such an outcrop, or for movement of appropriate age along the Minch Fault.

Owen and Santos (2014) support both a distal source and a distributive setting in a study of soft sediment deformation within the Applecross Formation. Ielpi and Ghinassi (2015) detail the drainage patterns of the Applecross Formation at the Stoer Peninsula, identifying low sinuosity braided rivers with well-defined but rarely preserved levees and abundantly preserved bar sheets. Evidence for discharge cycles is presented and the potential for distal transport in the Applecross Formation fluvial system supported.

Further detrital zircon studies constrain potential extant source areas to the proximal Canadian sector of the Grenville Orogen (Krabbendam *et al.*, 2017), which represents a distal source to the southwest. Distal transport in a trunk river system is supported (Krabbendam *et al.*, 2017), however transport to the northeast remains unjustified to the observed east-southeast palaeocurrents in the Applecross Formation.

The proposals outlined are difficult to rectify with each other as strong evidence for a Grenvillian source area is presented, however few proposals attempt to explain the difference between observed flow vectors (southeast) and the proposed direction of travel from the source area (northeast). A robust determination of the setting and regional fluvial style within the extant Applecross outcrop is required to understand the palaeogeographic relationship between the sediments and their source, and subsequently to provide better context to the Applecross Formation.

In this thesis, new detrital zircon samples from the Applecross Formation are collected and prepared. Zircon grains are separated from sandstones through conventional crushing, washing, and density separation techniques prior to hand picking and mounting of grains in resin. Cathodoluminescence (CL) images of polished grains are produced using the ISAAC (Imaging Spectroscopy and Analysis Centre) SEM at the University of Glasgow. New LA-ICP-MS (Laser Ablation-Inductively Coupled Plasma-Mass Spectrometry) U/Pb ages for the Applecross Formation are presented (see Chapter 3, Results) and discussed (see Chapter 4, Discussion) in order to clarify the source of Applecross sedimentary rocks and their mode of deposition (see Chapter 5, Conclusions).

1.5 Rodinia configuration

Deposition of the Torridon Group occurred between 994±48Ma and 977±39Ma (Rb-Sr whole rock study of lower and middle Torridonian respectively, Turnbull, Whitehouse And Moorbath, 1996; Rainbird, Hamilton And Young, 2001). The unconformably underlying Stoer Group is interpreted to be significantly older (1199±70Ma; e.g. Turnbull, Whitehouse and Moorbath, 1996, ~1180Ma from Stewart, 2002). The unconformity represents a time interval of 200-300Ma between 1177-994Ma (Williams, 2001).

In order to understand the depositional setting and provenance of the Applecross Formation (Torridon Group), it is important to consider the configuration and tectonics of the supercontinent Rodinia, widely believed to have incorporated the majority of continental plates at the time of deposition of the Torridon Group (Rivers, 1997; Rainbird *et al.*, 1997, 2017; Dalziel, Mosher and Gahagan, 2000; Rainbird, Hamilton and Young, 2001; Pisarevsky *et al.*, 2003; Cawood *et al.*, 2007, 2010; Bingen *et al.*, 2008; Li *et al.*, 2008; Williams and Foden, 2011; Krabbendam *et al.*, 2017). Precise continental configuration varies between authors, however the Laurentian craton is commonly placed near the core of Rodinia, on the basis of evidence for late Neoproterozoic passive margins around the craton (see Bond, Nickeson and Kominz, 1984; Pisarevsky *et al.*, 2003; Davidson, 2008), (See Figure 6, Figure 7).

In previous provenance studies of the Torridonian two primary models for the relative position of the Laurentian and Baltican cratons have been utilised (Figure 7). Williams and Foden (2011) utilise models after Li *et al.* (2008) and Cawood *et al.* (2010) positioning Baltica adjacent to Greenland and Amazonia at the time of deposition (Figure 7A). This configuration supports an oroclinal configuration for the Grenville Orogen when correlated with the Sveconorwegian Orogen in Baltica, passing near or through the southern parts of Scotland and Ireland (present position), see (Pisarevsky *et al.*, 2003; Piper and Darabi, 2005; Cawood *et al.*, 2007; Bingen *et al.*, 2008; Li *et al.*, 2008; Williams and Foden, 2011; Krabbendam *et al.*, 2017).

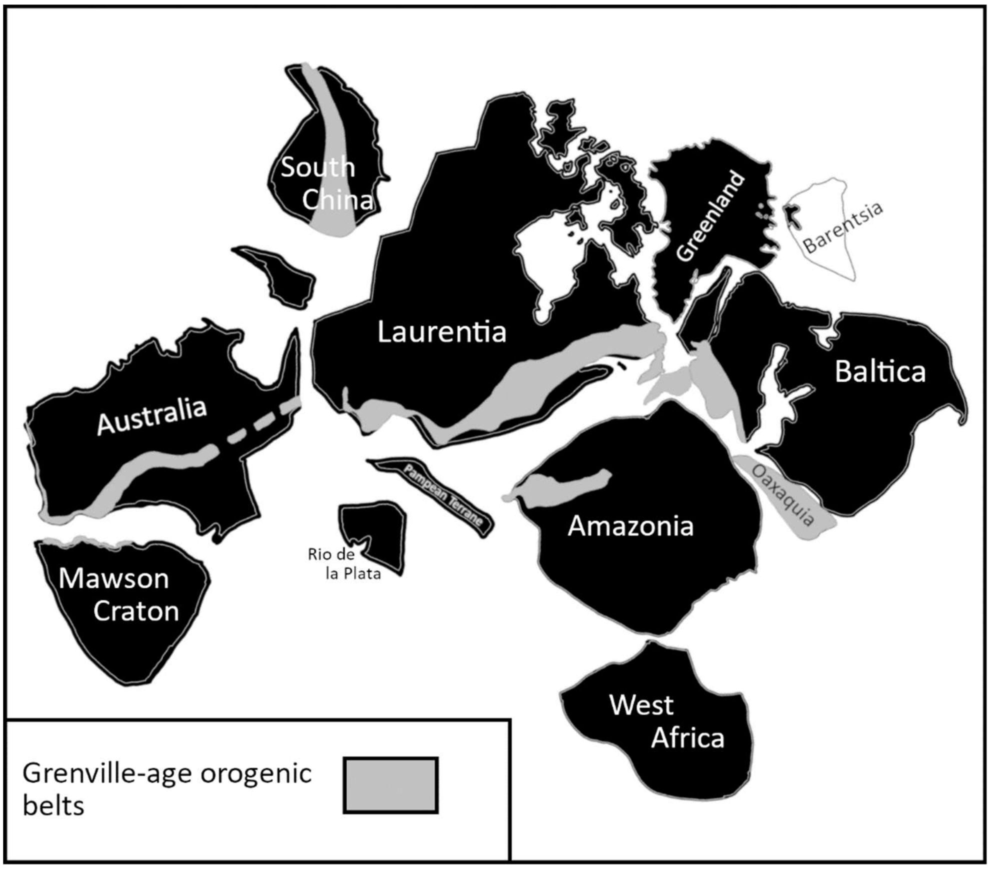

Figure 6: Cratonic layout of supercontinent Rodinia. After (Pisarevsky *et al.*, 2003). Possible reconstruction of the supercontinent Rodinia at 990Ma, coeval with deposition of the Applecross Formation. Grey bands display orogens of Grenvillian age.

This study is primarily concerned with the nature and provenance of Applecross Formation sediments in the Torridon Group; subsequently only the immediately relevant cratons are discussed further, namely Laurentia, Baltica, and Amazonia (see Figure 6, Figure 7).

Reconstructions of Rodinia at the time of deposition of the Stoer Group (~180Ma prior to deposition of the Applecross and associated formations, Williams and Foden, 2011) position Baltica widdershins of its late Mesoproterozoic position relative to Laurentia (see Figure 7A) (Li *et al.*, 2008; Cawood *et al.*, 2010). Krabbendam *et al.*, (2017) utilise a less drastically oroclinal model of the Grenville Orogen (Figure 7B) to establish a provenance for the Sleat Group. Although this layout for the orogen and resultant foreland provide a good fit with the Sleat and Morar (correlated with the lower Torridon in Krabbendam *et al.*, 2017) palaeocurrents, no explanation is given for the discordance of Applecross Formation palaeocurrents with the north easterly flowing orogen axial trunk river system proposed by Krabbendam *et al.* (2017). Applecross Formation palaeocurrents support a flow direction to the southeast (Gracie and Stewart, 1967; Nicholson, 1993; Williams, 2001; Owen and Santos, 2014; Ielpi and Ghinassi, 2015). In an oroclinal setting taking into account the clockwise rotation and movement of Baltica relative to Rodinia between 1265-1000Ma (Cawood *et al.*, 2010), an orogen axial foreland basin may facilitate southeastward flow during the deposition of the Applecross Formation whilst preserving northeastward flow into the earlier Sleat Formation.

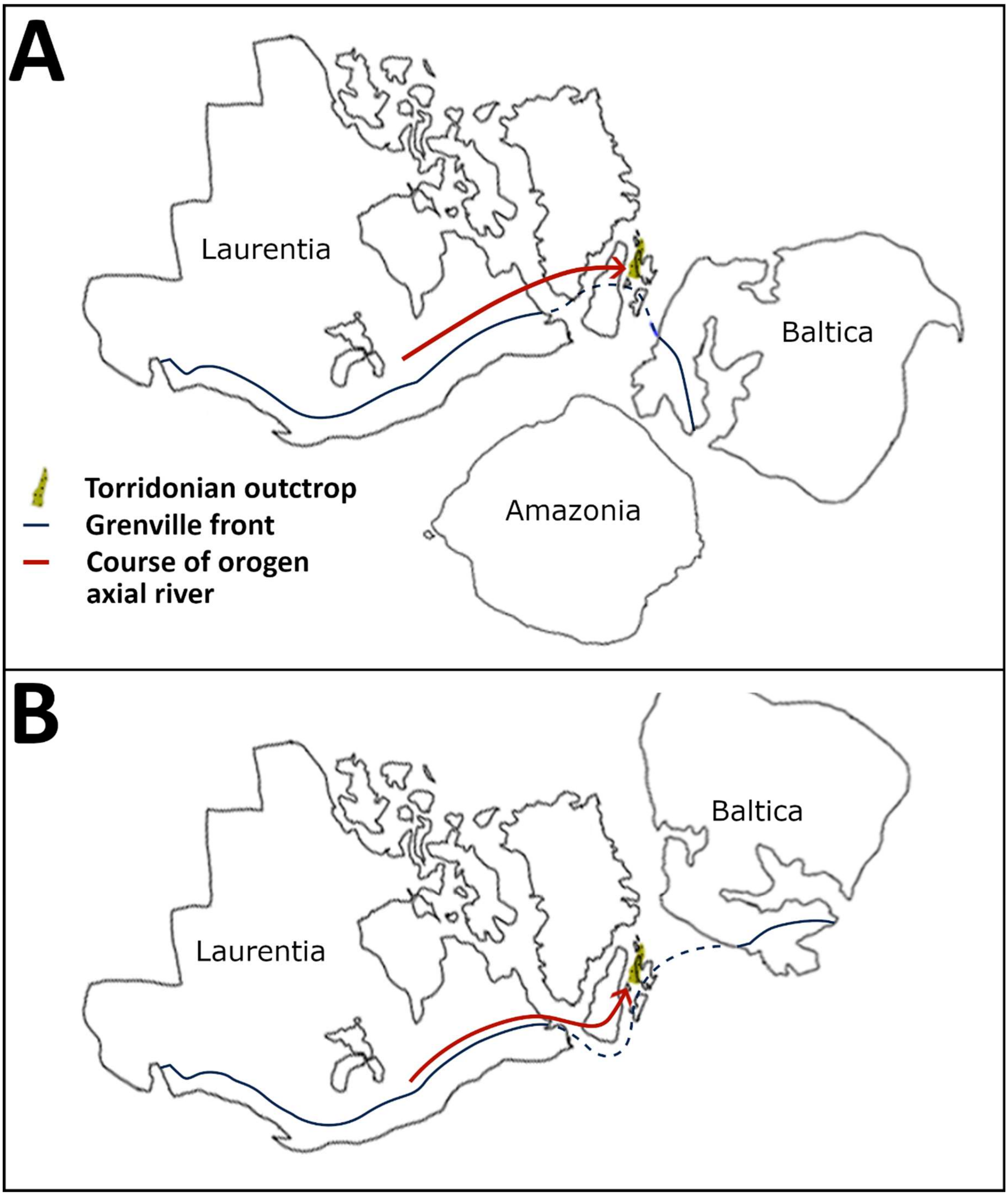

Figure 7: Schematic continental configuration of Laurentia, Baltica, and Amazonia. After (Li *et al.*, 2008; Cawood *et al.*, 2010; Williams and Foden, 2011; Krabbendam *et al.*, 2017; Rainbird *et al.*, 2017) Comparison of the continental layouts adopted by different authors. **A)** Configuration adopted by this study displaying Laurentia, Baltica and Amazonia in their positions ~950-1000Ma, coeval with Torridonian deposition. **B)** After (Krabbendam *et al.*, 2017; Rainbird *et al.*, 2017). Configuration displaying Laurentia and Baltica in their earlier Palaeoproterozoic positions. Blue lines indicate the approximate position of Grenville-Sveconorwegian fronts, red arrows indicate broad flow directions of possible orogen axial rivers entering the Torridonian (highlighted).

Within Laurentia, a variety of fluvial systems and source areas for the Torridon Group have been proposed. An extensional half graben setting invoking a supracrustal source overlying a previously uplifted Lewisian terrane along the western margin of the Minch is supported by Stewart and Donnellan (1992) and Williams and Foden (2011). This proximal source is based on palaeocurrents within the Torridon Group, indicating the presence of a megafan ~50km wide with an apex ~30km west of the Scottish mainland in the Cape Wrath member at the norther end of the exposure (Williams, 2001; Williams and Foden, 2011). The southern end of the basin is in this model filled laterally by braidplain deposits suggested to represent the distal deposits of a series of alluvial fans further west (Williams, 1969; Williams, 2001; Williams and Foden, 2011), although Nicholson (1993) refutes the presence of alluvial fans in the southern exposures of the Torridonian.

Alternative viewpoints include those of Rainbird, Hamilton and Young (2001) and Krabbendam *et al.* (2017) who support distal sediment transport in an orogen axial trunk river system from a distal source. This model is supported by evidence for pan-continental river systems across Laurentia (Rainbird *et al.*, 1997) distributing detritus from the Grenville Orogen to basins throughout Laurentia (see Krabbendam *et al.*, 2017). This fluvial system provides transport broadly to the northeast relative to the present position of the Torridonian, however transport direction may have varied with local structure and tectonics.

1.6 Grenville configuration and basements

Palaeocurrents within the Applecross Formation indicate transport from Laurentia in the west (south east palaeocurrents, see Gracie and Stewart, 1967; Nicholson, 1993; Williams, 2001; Owen and Santos, 2014). The proximity of the source varies between authors, with grain abrasion supporting a more distal source for the Applecross than that of the Sleat and Stoer Groups (Rainbird, Hamilton and Young, 2001). In light of these suggestions, Laurentian basement and sediments are of key interest as potential source areas, particularly those of composition suitable to form the arkoses of the Applecross Formation (primarily quartzofeldspathic crystalline rocks and pre-existing sedimentary sequences).

At the time of deposition of the Torridon Group, basement rocks and orogens from a broad range of time periods are present across Laurentia (see Figure 8). Archean cratons (<2500Ma are located across central Laurentia, Greenland, and the Rockall Plateau, as well as areas of Baltica to the east (Rivers, 1997; Li *et al.*, 2008; Krabbendam *et al.*, 2017; Rainbird *et al.*, 2017). There is evidence for Early-mid Palaeoproterozoic orogens (2500-1900Ma) in southern Canada and the United States (present position), Rockall Plateau, and Baltica (Rivers, 1997; Li *et al.*, 2008), with late Palaeoproterozoic belts occurring in adjacent areas (Rivers, 1997; Cawood *et al.*, 2007; Li *et al.*, 2008; Krabbendam *et al.*, 2017; Rainbird *et al.*, 2017). Rivers (1997) highlights major Palaeoproterozoic-Mesoproterozoic orogenic fronts in Laurentia (Figure 8b), which may have formed areas of relief during this period. Orogens within the 1820-1600Ma period are focused in southern Laurentia, with some occurences in Baltica (Figure 8A) (Krabbendam *et al.*, 2017; Rainbird *et al.*, 2017). The Makkovik-Ketilidian-Rhinian events (collectively referred to as the MKR) are found in southern Greenland and possibly on the Rockall Plateau (Rivers, 1997; Krabbendam *et al.*, 2017; Rainbird *et al.*, 2017). Emplacement of a granite-rhyolite belt into and onto pre-existing crust occurred between 1500-1300Ma in central Laurentia, concluding shortly before earliest for events preceding the Grenville Orogen (Rivers, 1997; Cawood *et al.*, 2007; Li *et al.*, 2008; Krabbendam *et al.*, 2017; Rainbird *et al.*, 2017). Crystalline rocks between 1300-950Ma occur in east Greenland and northern Laurentia (Figure 8) (Li *et al.*, 2008). Mesoproterozoic AMCG (anorthosite-mangerite-charnockite granites) plutonic suites are found in eastern Canada (Rainbird *et al.*, 2017). Arc related rocks between 1300-1100Ma are found on the rear side of the Grenville Orogen (Li *et al.*, 2008) and subsequently are not of interest to this study. During the late Mesoproterozoic (1200-1100Ma) a mid-continent rift system developed in central Laurentia (Vervoort *et al.*, 2007).

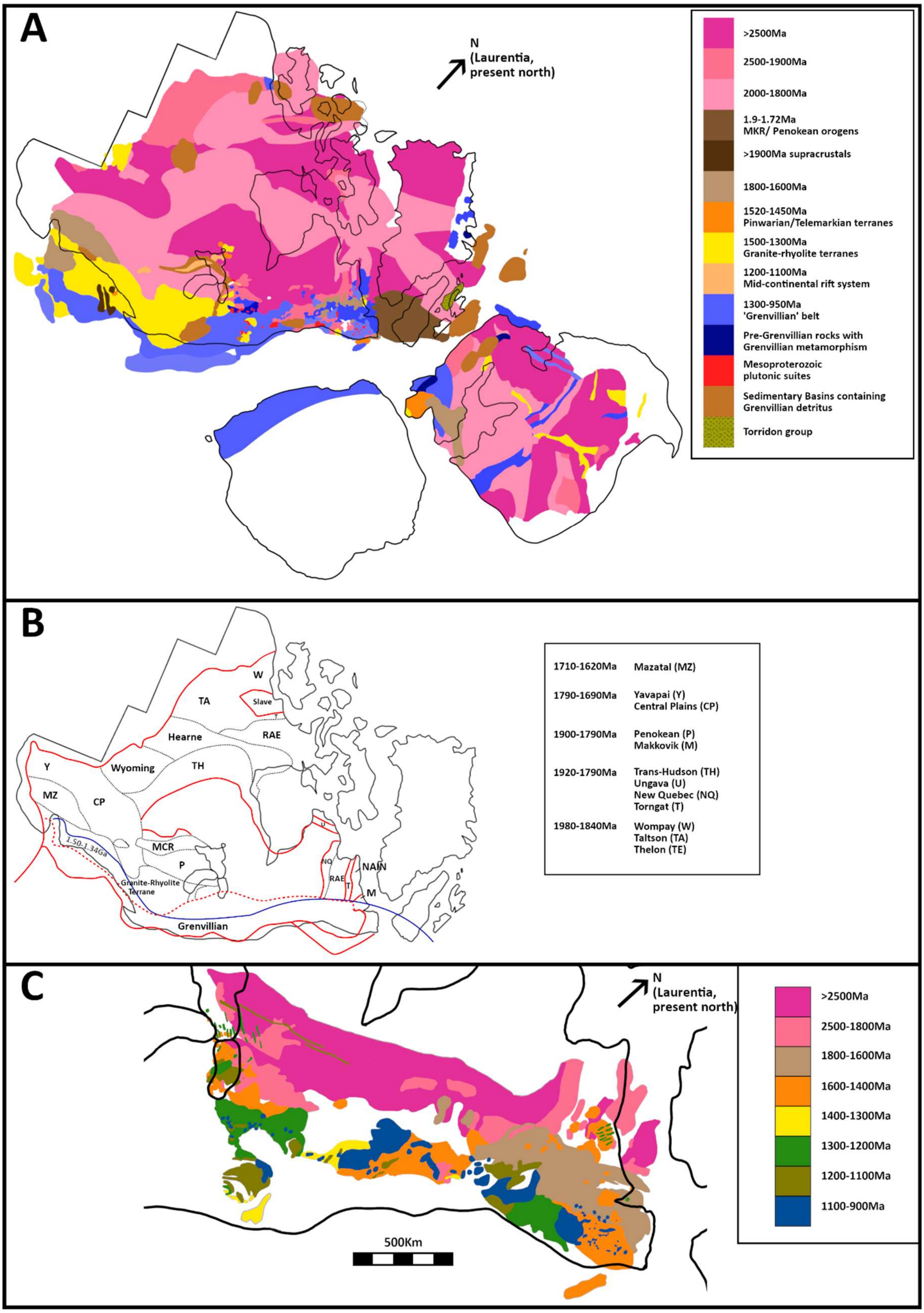

Figure 8: A) Basement rock ages in Laurentia and Baltica. B) Orogens in Laurentia, C) Basement rock ages in East Canada. A) After (Rivers, 1997; Pisarevsky *et al.*, 2003; Li *et al.*, 2008; Cawood *et al.*, 2010; Krabbendam *et al.*, 2017), Basement and terrane ages in Laurentia and Baltica highlighting possible source areas for the Applecross detrital zircon suite. The location of the Torridon Group is highlighted adjacent to Baltica and Greenland. The approximate location of the Rockall Plateau is displayed northwest of the Torridon Group, between Greenland, Baltica and Laurentia B) After (Rivers, 1997). Major Terranes and orogens of Laurentia likely to have affected pan continental river systems. C) After (Rivers, 1997). Basement ages in the Canadian sector of the Grenville Orogen.

The Grenville Orogen occurred between 1080-950Ma across eastern Canada, the USA (present positions), Baltica (Sveconorwegian Orogen), and possibly Amazonia (Sunsas Orogen) (Figure 8 Pisarevsky *et al.*, 2003; Bingen *et al.*, 2008; Li *et al.*, 2008; Cawood *et al.*, 2010; Krabbendam *et al.*, 2017; Rainbird *et al.*, 2017). Numerous protolith suites are incorporated into the Grenville Orogen. These are outlined in Figure 8C (after Rivers, 1997; Krabbendam *et al.*, 2017). Rocks from the MKR (1820-1720Ma), trans-Labrador, and Matazal (1700-1600Ma), Pinwarian and granite-rhyolite province (1520-1380Ma), AMCG plutonic suite (1400-1300Ma), Elzevirian (1300-1200Ma), Shawingan and Adironian (1200-1100Ma) are incorporated into the proximal Grenville Orogen in eastern Canada (Rivers, 1997; Krabbendam *et al.*, 2017) along with some Archean material. As a result of this, it is possible for these protolith ages to appear in detrital zircon suites derived directly from the Grenville Orogen as only the core of the orogen is likely to reset or generate new zircon ages; an 'orogenic lid' preserves older material (Krabbendam *et al.*, 2017).

Cawood *et al.* (2007) note that prior to the final formation of Rodinia (~1200-1000Ma), Laurentian sedimentary basin fill is likely to be dominated by detritus from ongoing arc magmatism, adding that the final stages of collision (continent-continent) will see more detritus derived from reworking of older material. This may contribute to the presence of sandstone pebbles containing detrital zircon of Grenvillian age within the Applecross Formation (Rogers *et al.*, 1990; Williams and Foden, 2011). Pebbles from the Applecross Formation also yield detrital zircon ages of 2875-2628Ma, 1662-1625Ma, and 1193-1088Ma (Rogers *et al.*, 1990; Williams and Foden, 2011), which are consistent with the peak ages from this study for the Applecross Formation itself. Moorbath *et al.* (1967) offer further K-Ar and Rb-Sr ages for pebbles from the Applecross Formation, with K-Ar fuschite-schist ages from 1654-1798Ma and various pebbles with Rb-Sr ages between 1524±50ma, 1516±40Ma, 1358±35ma, and 1275±40Ma. The varied pebble suite supports reworking of source material for the Applecross Formation. The similarity between Applecross pebble detrital zircon ages and detrital zircon ages from the sediment itself suggests similar sources or reworking of an older sedimentary formation directly related to the Applecross Formation- perhaps fluvial deposits lain down and later removed during the Sleat-Applecross unconformity.

During the construction of Rodinia a number of orogenic events occurred, creating relief across Laurentia. This topography creates an additional constraint on possible courses for fluvial systems during the Grenville Orogen and deposition of the Torridonian. Rivers (1997) outlines late Palaeoproterozoic collisional and accretionary orogenic fronts in Laurentia (see Figure 8B). The youngest of these fronts formed at least 600Ma prior to deposition of the Torridonian. The mid-continental rift system (MCR) in central Laurentia provides a possible western boundary more contemporary with the Torridon Group (1100-1090Ma, Rivers 1997)(Figure 8B), potentially constraining any orogen axial river system supplying the Torridonian to the eastern Grenvillian foreland (east Canada, present position). Beyond Laurentia, Baltica is undergoing rotation and collision with Rodinia during this period (Cawood *et al.*, 2010) (Figure 7). This movement led to an accretionary event coeval with the end of, but disparate from, the Grenville/Sveconorwegian Orogen known as the Valhalla Orogen focussed around an ocean known as the Asgard sea between Laurentia, Baltica, and Amazonia (Cawood *et al.*, 2010). Sedimentary successions within the Valhalla Orogen are approximately coeval with Torridonian deposition, occurring between 1030-980Ma and 910-870Ma (Cawood *et al.*, 2010).

1.6.1 Rockall Plateau

The Rockall Plateau is a microcontinent isolated during the opening of the Iapetus and Atlantic oceans (Roberts *et al.*, 1970; Roberts, Ardus and Dearnley, 1973) (Figure 8A). Intermediate granulites of Grenvillian age (987±5Ma) (Miller, Matthews and Roberts, 1973) and Precambrian acid granulites (Roberts, Ardus and Dearnley, 1973) have been recovered from Rockall Bank, indicating a continuation of Lewisian lithologies beyond the Outer Hebrides and extension of Grenvillian metamorphism as far as southern Rockall.

A number of early Neoproterozoic deposits containing Grenvillian detritus are highlighted in Figure 8B (after Krabbendam *et al.*, 2017). These deposits provide evidence for large scale continental river systems, such as those discussed by Rainbird *et al.* (1997, 2017); Rainbird, Hamilton and Young (2001); Krabbendam, Prave and Cheer (2008); Krabbendam *et al.* (2017). Rainbird *et al.* (1997, 2017) interpret these fluvial systems to transport material to the northwest across Laurentia with proximal deposits in the Middle Run basin and further east in the central Laurentian MCR. Subsequently the southeasterly Applecross palaeocurrents require a change in vector in fluvial systems in eastern Laurentia compared to those in western Laurentia, either by a change in direction or by presence of a disparate fluvial system in the Canadian sector of the Grenville Orogen, perhaps separated by the MCR.

Potential source areas of Grenvillian age incorporating older lithologies can also be found in the Sveconorwegian sector in Baltica (Figure 8A); sourcing the Applecross from this area however would require flow directions at 180° to those observed (approximately southeast in the Applecross Formation, see Gracie and Stewart, 1967; Nicholson, 1993; Williams and Foden, 2011; Owen and Santos, 2014; Ielpi *et al.*, 2017). In summary, the Sveconorwegian sector can be ruled out as a direct source.

1.7 Palaeocurrents and sedimentology

The Applecross Formation consists of largely homogenous arkoses with occasional mud clasts and a varied pebble suite (see Williams, 1966; Williams, 2001). Soft sediment deformation is seen throughout the formation, indicating a high sediment influx combined with a high water table (see Figure 24 section 3.2.2, Owen, 1995; Owen and Santos, 2014). Cross bedding has been observed in a variety of orientations (see Figure 25, section 3.2.2) and in many cases can be characterised as lateral accretion of bar deposits (Nicholson, 1993; Ghinassi and Ielpi, 2017). Sandstones are typically channelised. Structures and lithologies indicate a fluvial system with high, possibly seasonal discharge and frequent avulsion typical of braidplain systems within the broader temporal framework of the Torridon Group.

1.7.1 Torridon Group setting

The Torridon Group coarsens upwards from locally derived fan and lacustrine deposits in the Diabaig Formation into higher energy braidplain and megafan deposits within the Applecross and Aultbea Formations, prior to an eventual reduction in energy and sediment supply within the Cailleach Head Formation (See Figure 3, section 1.2). This may reflect an increase in sediment influx between the Diabaig and Applecross Formations (Stewart, 2002) as a result of increased relief or denundation of the source area.

Initial Applecross deposition occurs around 977±32Ma (Turnbull, Whitehouse and Moorbath, 1996), coeval with the later stages of the Grenville Orogen. This would create relief in suitable source areas to provide a high influx of sediment to the Torridon if a distal source is accepted. Extension related to an extensional phase of the Grenville Orogen along the Minch basin may also provide relative relief for a proximal source (Williams, 2001; Williams and Foden, 2011). Krabbendam and Rainbird (2012) note a lack of direct evidence for movement of this age along the Minch Fault; however this does not strictly preclude the possibility as later movements are likely to have obscured such evidence. Further work on the early movements of the Minch basin is required to clarify this argument. The settings and variations in style of each Torridon Group formation is discussed in further detail.

1.7.2 Diabaig Formation

The Diabaig Formation at the base of the Torridon Group is characterised by locally derived sandstones and breccias filling Lewisian palaeovalleys (Park *et al.*, 2002; Stewart, 2002). Breccias within the formation have been interpreted as wedges filling the valley sides, with shales forming in lacustrine settings on the valley floors (Park *et al.*, 2002). The upper section of the formation is characterised by sandstones displaying eastward palaeocurrents, taken to indicate the presence of Applecross style rivers (Park *et al.*, 2002; Santos and Owen, 2016).

1.7.3 Applecross Formation

The Applecross Formation comprises up to 4500m thickness of coarse sandstones, generally interpreted to represent braided fluvial deposits (Selley, 1965; Rainbird, Hamilton and Young, 2001; Williams, 2001; Stewart, 2002; Williams and Foden, 2011; Krabbendam *et al.*, 2017; Rainbird *et al.*, 2017). Palaeocurrents within the Applecross Formation dominantly support flow to the southeast (Gracie and Stewart, 1967; Nicholson, 1993; Williams, 2001; Owen and Santos, 2014; Ielpi *et al.*, 2017). The 450m thick Cape Wrath member supports this regional flow direction; the member has been interpreted as a megafan ~50km wide with an apex ~30km west of the Scottish mainland as opposed to the more distal braidplain facies seen further south in the formation (Williams, 2001; Williams and Foden, 2011). The Applecross Formation therefore shows multiple outcrop-lateral fluvial facies along its extensive outcrop. Williams and Foden (2011) suggest that the outcrop exposed today represents a diagonal transect of the original basin, interpreting the Cape Wrath member in the north to be proximal to the source (or basin edge) with braidplain deposits further south representing distal elements of the same system. In contrast to this interpretation of fans in the Applecross Formation Krabbendam and Rainbird (2012) argue that the Cape Wrath member represents an individual fan, facilitated by a localised obstacle. Eventual burial caused fan formation to cease. Palaeosols and weathering profiles within the Cape Wrath member suggest a warm, arid environment during deposition (Williams, 2001; Williams and Foden, 2011)

1.7.4 Aultbea Formation

The Aultbea Formation conformably overlies the Applecross Formation and similarly consists of arkosic sandstones with some grey shales (Williams and Foden, 2011). Some workers consider the separation of the Applecross and Aultbea Formations to be a misclassification, preferring them to be considered a single formation (Stewart, 2002). Palaeocurrents indicate that transport within the Aultbea Formation is similar to that within the Applecross Formation.

1.7.5 Cailleach Head Formation

The Cailleach Head Formation lies at the top of the Torridon Group. The formation consists of upward coarsening cyclothems including grey shales and red sandstones (Stewart, 2002) indicative of fluvial and lacustrine processes (van de Kamp and Leake, 1997).

Chapter 2 Methodology

2.1 Preliminary fieldwork and sample collection

2.1.1 Study area

This study focuses on the Applecross Peninsula, south of Loch Torridon. Sampling was undertaken entirely within the Applecross Formation, along a transect of ~12.5km between Loch Kishorn and Applecross Bay (see Appendix 1).

The sample area was selected on the basis of its proximity to the Moine Thrust, extensive outcrop of a single formation, and accessibility. Additionally information on local lithology pertinent to the study was reviewed from the literature (see Thomson *et al.*, 1999; Piper and Darabi, 2005; Persano *et al.*, 2007; Hudson, 2011; Ellis *et al.*, 2012; Krabbendam *et al.*, 2017). In the field, a stratigraphic log was constructed to provide further context to the area.

2.1.2 Sampling regime

Sampling outcrops were chosen on the basis of field observations and scatter along the transect. Ideal sampling localities contain coarse immature sandstones that include cross bedding structures or heavy mineral laminae. At localities where no such outcrop exists an increased sample size of finer, more mature rock was collected to increase the probability of finding suitable apatite and zircon crystals. Samples were collected in-situ from outcrop only.

When collecting samples, the outcrop was first photographed; key features were noted including hand specimen descriptions and measurements. Localities were numbered in order of visit, with both OS grid references and latitude/longitude noted. Additionally GPS systems were used to mark localities and create a map of ground covered for reference. Collected samples were labelled according to locality of collection and whole rocks cleaned prior to processing.

2.2 Laboratory protocol

2.2.1 Mineral separation

2.2.1.1 Crushing

Samples were initially described in hand specimen prior to being broken up by percussion and with a hydraulic rock splitter. Samples were next passed through coarse then fine jaw crushers until only sand remains. All equipment was cleaned thoroughly between samples to prevent contamination.

2.2.1.2 Washing

Crushed samples were washed to remove clay and other light minerals. Each sample was placed in a bucket with clean water. The sample was agitated until the lightest minerals become suspended in the water column. Water was carefully poured off and the process repeated until light minerals cease to become suspended.

Washed samples were placed in labelled trays in a low temperature oven to dry overnight. Dry samples were taken for sieving.

2.2.1.3 Sieving

Single grains of apatite and zircon were required for analysis; as such each sample was sieved to separate a sub 500 μm fraction. Remaining coarse material was labelled and stored, or crushed and washed again if too small a fraction was recovered. Between samples sieves were carefully cleaned to remove all lodged grains from the gauze.

2.2.1.4 Magnetic separation

As apatite and zircon were non-magnetic, magnetic minerals were removed from the samples. Magnetic separation was performed in two stages to prevent apparatus from clogging.

Vertical magnetic separation: Samples were first placed into a vertical Frantz magnetic separator calibrated to divide material into two streams of magnetic and non-magnetic material. Efficient separation was achieved by adjustment of magnet strength and distance of the sample from the magnet. Samples were stored in a hopper at the top of the equipment and a stream of material moved past the magnet by gravity (see Figure 9A). The non-magnetic material falls under the influence of gravity and lands in a container below the hopper. Magnetic material was pulled towards the magnet as it falls, creating the second stream of material, landing in a collection pot below the magnet. The magnetic material was labelled and stored. Non-magnetic material was labelled and sent for horizontal magnetic separation.

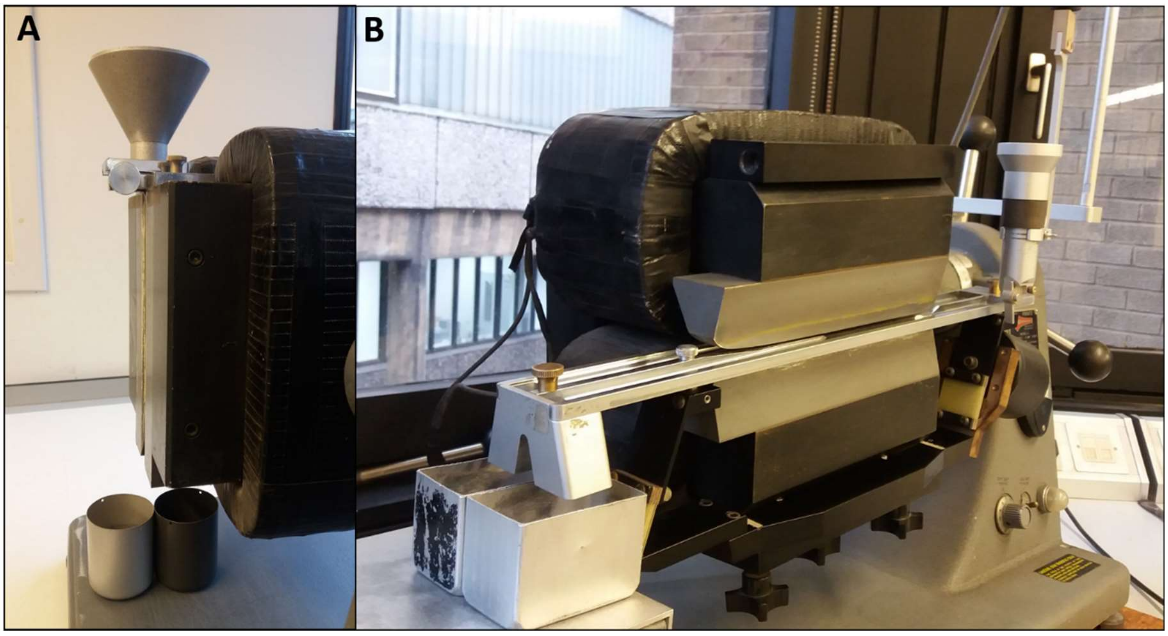

Figure 9: Frantz magnetic separators. A) Vertical magnetic separator. Samples were stored in the hopper visible at the top of the equipment. Samples fall past the magnet and were separated into two streams; magnetic material was pulled towards the magnet and was collected in the black container. Non-magnetic material simply falls under the influence of gravity and was collected in the grey container.

Horizontal magnetic separation: Vertical separation removes only the most magnetic grains, such as magnetite, due to the high rate of flow. The remainder of the magnetic material was removed by passing the sample through a horizontal Frantz magnetic separator. Samples were placed in a hopper that releases a steady stream of material into the separation track, which runs through the magnet and was separated, along its length, into two parts by a ridge (see Figure 9B). The track was tilted at a shallow angle so that gravity counteracts the magnetic force. Magnet strength and track angle must be calibrated for each sample. The magnetic material was attracted by the magnet and therefore was directed into the section of the track nearer to the magnet; the non-magnetic material was pulled down the slope to the lower track, further from the magnet, by the influence of gravity. Each fraction was collected in a container at the end of the track; magnetic material was labelled and stored. Non-magnetic material was sent for density separation.

2.2.1.5 Density separation

Remaining samples contain a small amount of zircon and apatite compared to a large bulk of quartz and other light minerals. Zircon and apatite are heavy minerals (~3.93-4.73 g/ml and ~3.16-3.23 g/ml respectively) in comparison to quartz (2.65 g/ml). Lithium heteropolytungstates (LST) separating fluid has a density of 2.8±0.02g/ml, falling between the heavy and light mineral groups present in the samples. Each sample was placed into a separating funnel and suspended in LST. Samples were stirred gently for 30 minutes to allow light and heavy grains to move past one another and to avoid flocculation. Samples were next allowed to settle until a clear divide was seen between the heavy and light sections. Heavy minerals were then poured out of the funnel, filtered from the LST and cleaned using deionised water. Light minerals were poured out separately for filtration and cleaning. Light minerals were labelled and stored. Heavy minerals were placed into sample vials and labelled for assessment of apatite and zircon content.

2.2.1.6 Sample assessment, picking, and mounting

The remaining sample fractions contain a relatively pure separate of zircon and apatite. To confirm this each sample was assessed for zircon and apatite abundance under a reflected light picking microscope. Zircons are typically recognised by their rectangular cross section and overall cuboid shape, with prismatic tips on intact crystals. Apatites are typically recognised by their hexagonal cross section and flat tips, giving them a “barrel like” appearance. Additionally, zircons have a high relief while apatites possess a lower relief; subsequently zircon can appear to have a sharper border when viewed under the picking microscope. Relief was used to assist identification where grains were damaged and therefore difficult to distinguish through morphology. During this phase different populations of zircon and apatite were identified; each population must be sampled to ensure accurate interpretation of data.

Grains were picked directly onto mounting slides. A strip of double-sided adhesive tape was applied to a glass slide, and washers applied to this tape. Grains were picked from the sample and applied directly to the adhesive tape within the washers, a method developed at the University of Glasgow (Figure 10). Grains were arranged in a grid pattern where possible to improve ease of location during analysis.

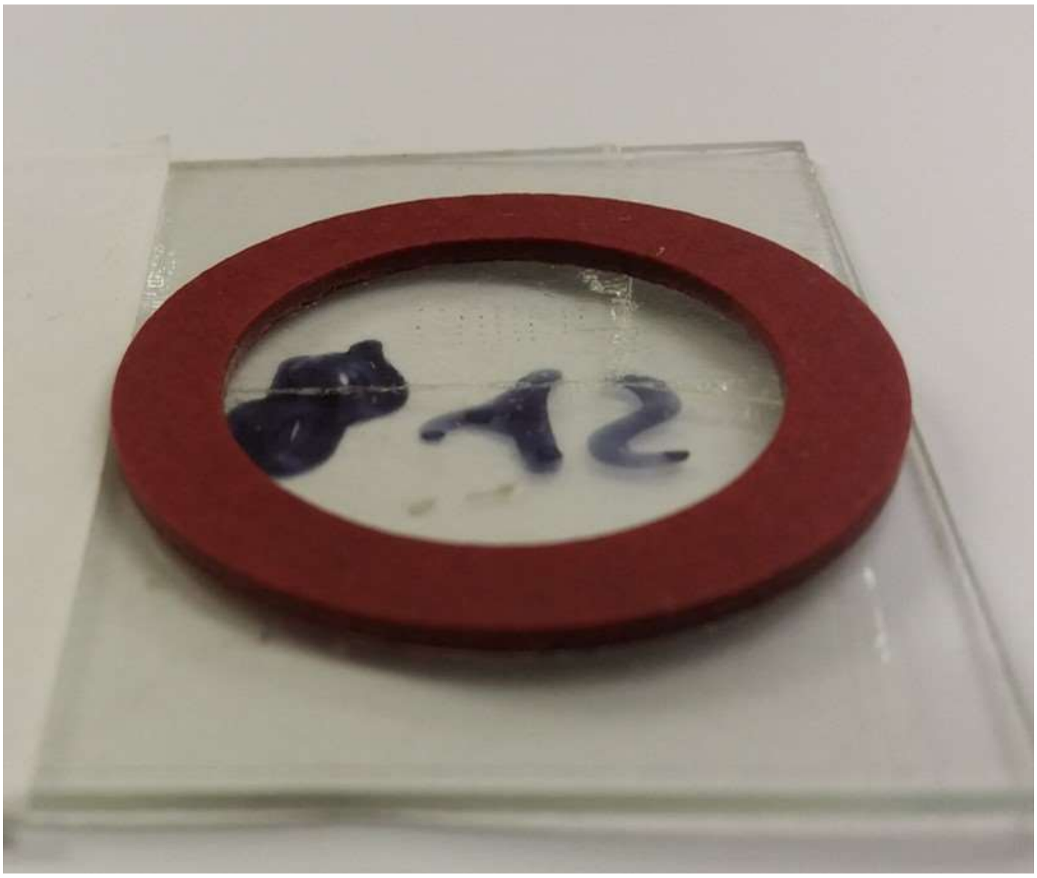

Figure 10: Grain mount preparation. In preparation for grain mounting double-sided adhesive tape was applied to a glass slide. The adhesive tape serves a dual purpose; firstly it allows the washer to be attached to the slide to contain resin later in the preparation of the sample mount. Secondly, the adhesive tape allows picked grains to be arranged in an ordered grid without risk of any grain becoming dislodged or loose. Grains in this sample are small; however the grid can be made out within the far portion of the washer.

Once slides have been filled with a given set of grains a two part epoxy resin was mixed. The resin must be mixed well in equal parts to ensure a clear glass-like finish. The epoxy was stirred gently to prevent the inclusion of gas during mixing, as any bubbles will tend to stick to grains. This leads to loss of grains during polishing as the resin will not adequately hold them. Once mixed the resin was poured into the washers. A sheet of plastic was placed over the washers to prevent adhesion and a glass plate placed on top. Weight was applied to the top of the plate to compress the resin into the washers and prevent the formation of bubbles.

Once the resin has set (after ~2-3 days) the washers were removed from the glass slides. The washer was cut away from the resin disk containing the grains. The disk and grains were polished incrementally with p1200, p2500, and p4000 grinding paper. p800 paper was unnecessarily coarse and causes loss of grains from the disk face. Disks were finished with a 1μm and 0.3μm aluminium oxide solution providing a suitable surface for SEM imaging and laser ablation.

Between and after each stage of polishing, disks were washed in and ultrasonic bath for 30 seconds to remove any residual grit or aluminium oxide. Additionally the grinding paper was cleaned with distilled water between polishing to remove any loose grains. Once polishing was complete reference points *A*, *B*, and *C* were marked on three corners of the grid to orient the disk when viewing grains (Figure 11).

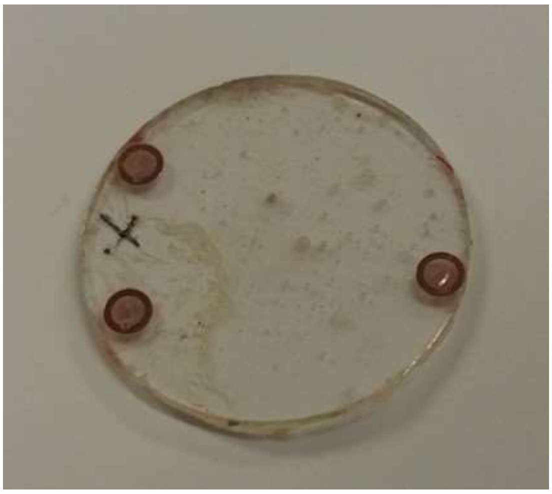

Figure 11: Completed grain mount. Polished and grain mount for SA10. The copper disks visible are labelled *A*, *B*, and *C.* Each disk includes a grid with the respective letter at the centre, and a larger letter on the rim. The letters and grids can be used to orient the grain mount and were used as reference points when producing spot coordinates for analysis.

2.2.2 Analysis

2.2.2.1 SEM cathodoluminescence and secondary electron imaging

Once polished, each sample disk was cleaned in an ultrasonic wash and methanol to remove all excess polishing powder and fingerprints. Cleaned samples were carbon coated to improve electron flow during imaging with the scanning electron microscope (SEM).

Imaging was undertaken at the Imaging Spectroscopy and Analysis Centre (ISAAC) at the University of Glasgow utilising the FEI Quanta 200F environmental SEM.

Samples were imaged using both a panchromatic cathodoluminescence detector and secondary electron detectors. This allowed analysis of zoning, inclusions, and the topography of the polished sample to ensure suitable ablation sites can be selected for LA-ICP-MS analysis (see Figure 12). Samples SA2, SA3.1, SA4, SA5, SA7, SA8, SA10 and SA21 were selected for analysis on the basis of sample size and geographic spread across the study transect. 50-100 zircons from each sample were imaged.

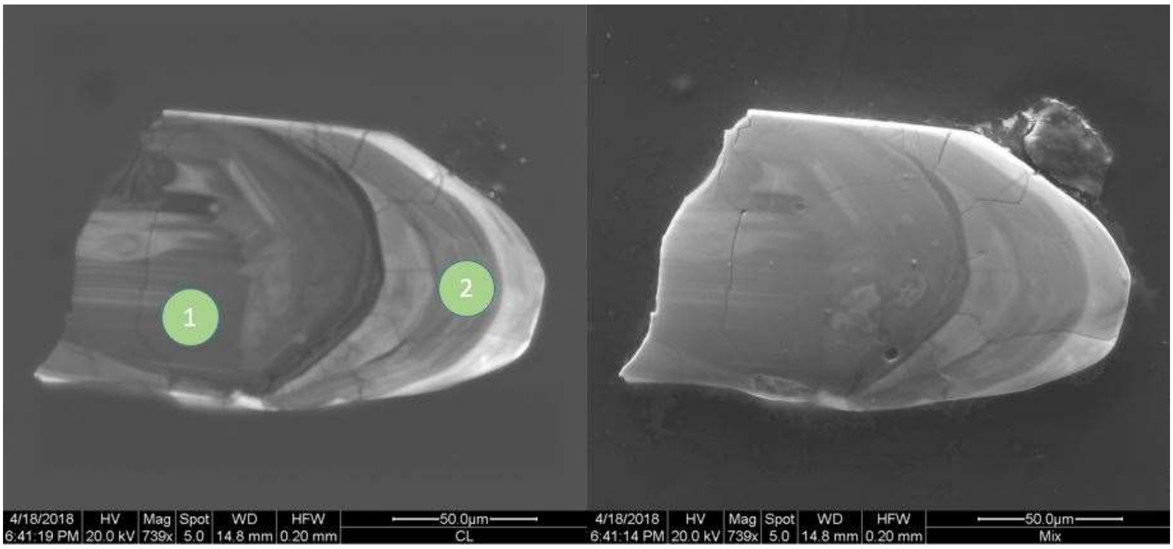

Figure 12: CL (Cathodoluminescence) and SE (Secondary Electron) images, sample SA_10_0915. Zircon SA10_0915 cathodoluminescence (CL) image with composite CL and secondary electron image (mix). 20µm spots 1 and 2 were marked for laser ablation analysis in distinct compositional zones. Ideally a third spot would be placed in the bright rim of the crystal at the right of the image, however the zone was too small. Radial fractures in the crystal suggest a greater concentration of uranium in the crystal rim.

Cathodoluminescence images show the internal structure of zircon (Figure 12). Assessment of the internal structure of each zircon to be analysed were made in order to choose sites for analysis which would not be contaminated by inclusions, radiation damage, or ablation of multiple zones.

2.2.2.2 Sample mapping

The locations of laser targets selected in section 2.2.2.1 were mapped to provide targeting coordinates for the laser. Sample mounts were fixed to a glass slide and placed under a Zeiss Axioplan 2 imaging microscope. The microscope stage was controlled by a joystick and spots were logged using FTStage software. Reference points at *A*, *B*, and *C* were marked first for future alignment of the grain mount (see 2.2.1.6). Ablation points were then marked in numerical order. Spot labels and numbers were entered into a database created to contain the data (see Appendix 2). The database was used to verify that spot numbers provided by the FTStage application were in the correct sequence. Completed coordinate files were saved in .CSV format to be imported into the laser control software.

2.2.3 Laser Ablation-Inductively Coupled Plasma-Mass Spectrometry (LA-ICP-MS)

LA-ICP-MS analysis combines laser ablation (LA) systems with inductively coupled plasma-mass spectrometry (ICP-MS) to enable sampling and analysis of individual zones within individual crystals using spots or time resolved transects of multiple zones by ablating along a line (Figure 13). Material ablated from the sample by the laser was transported to the mass spectrometer by a carrier gas. Analysis was undertaken using a RESOlution SE laser ablation system in combination with the iCAP RQ ICP-MS system.

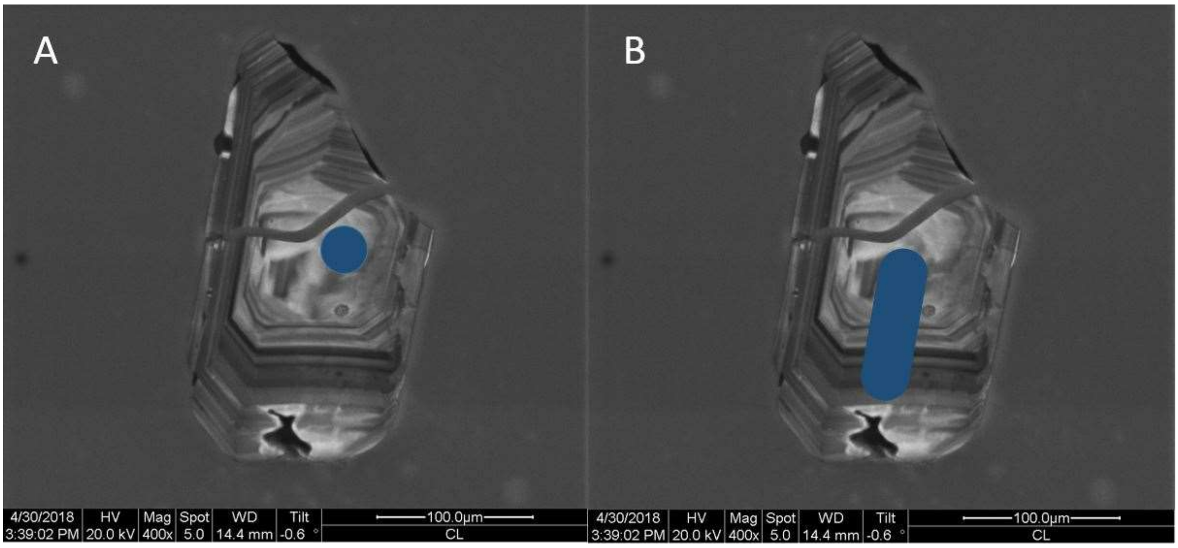

Figure 13 Cathodoluminescence image of zircon SA2_0004 (this study). A) 30μm spot targeting a single zone at the core of the zircon. When analysing single spots corrections for downhole fractionation are required. B) 30μm wide line to analyse multiple zones continuously. This method was applied where spatial variations in composition were of interest.

2.2.3.1 Laser setup

Samples for analysis were mounted in a holder (Figure 14) with Plesovice Zircon standards and NIST 610 glass (see section 2.2.3.3). Samples were adjusted to ensure consistent orientation and height in the holder. A scanned image of the sample holder was created for reference during analysis.

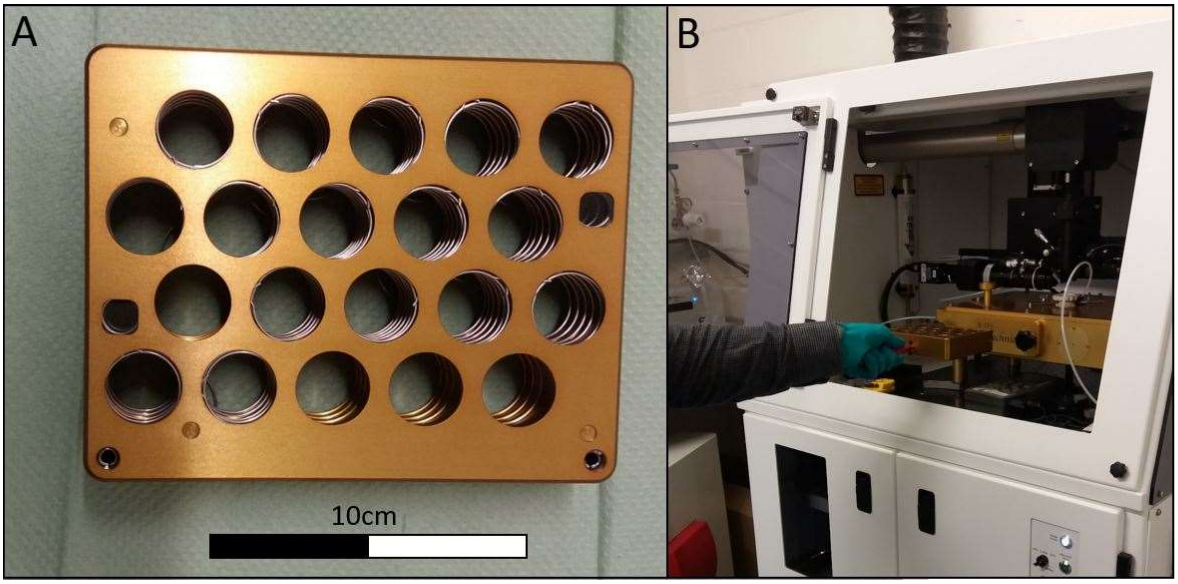

Figure 14: (A) Sample holder for use in LA-ICP. (B) Sample loading procedure for LA-ICP. (A) Samples were mounted in each of the holes visible in the holder, which was then scanned using a conventional scanner to produce a reference image containing the location of each sample. (B) Once the sample holder has been prepared it was loaded into the ICP-MS ablation chamber for analysis.

Once the samples were mounted in the holder, the sample exchange sequence was begun. The sample chamber was drained of carrier gas and the subsequent vacuum re-pressurised. The sample holder was mounted in the sample chamber and the hatch sealed. The vacuum within the chamber was re-established and the chamber backfilled with carrier gasses. The scanned image of the sample holder was aligned with the live microscope feed allowing easy location of individual disks.

Analysis sequences for the laser were created by importing previously prepared .CSV files for each sample (2.2.2.2). Additional laser spots were added to each sequence for NIST and Plesovice standards at the beginning and end of each analysis, with one measurement of each for every five samples.

Single spot analysis with a 30µm spot diameter was used to target individual zones while minimising downhole fractionation effects (Diwakar *et al.*, 2014). A fluence of 4.5J.cm^{-2} was found to effectively ablate sampled zircon with a 3.0Hz repetition rate.

2.2.3.2 ICP-MS setup

During analysis the ICP-MS receives material ablated by the LA system and measures a pre-selected set of atomic weights relating to the isotopes required.

^{204}Pb (common lead) was measured to correct for any non-radiogenic lead in the sample. ^{198}Hg was measured to correct for interference, to verify that there was no magnesium in the sample and therefore any 204 isotopes found are ^{204}Pb.

*^{206}Pb and ^{238}U, *^{207}Pb and ^{235U,} *^{208}Pb and ^{232}Th ('*' indicates radiogenic origin) are the parent-daughter end members of their respective radioactive decay chains and all were measured to provide accurate U-Pb ages from the analysis.

2.2.3.3 Standards

Appropriate standards were vital to monitor the production of accurate and reliable data for analysis. The use of multiple standard materials improves integrity as internal standards of known composition can be used to calibrate analysis, and natural zircon standards of known age can be used to test the accuracy of the analysis.

The LA-ICP-MS system was tuned using NIST 610 glass standards (*NIST - SRM 610 Trace Elements in Glass*, accessed 24/07/2018). NIST 610 was used throughout analysis to track background variations and convert the CPS (counts per second) provided by the ICP-MS for each isotope into concentrations in ppm.

Plesovice zircon standards were used alongside NIST 610 to track variations during analysis and to determine the accuracy of each analysis. Plesovice Zircon standards have a ^{206}Pb/^{238}U age of 337.13±0.37Ma using the ID-TIMS method, with U concentration ranging between 465-3084ppm (Sláma *et al.*, 2008). Plesovice standards were analysed prior to unknowns to prove analysis was reliable and reproducible. Once the accuracy of the age calculations was determined, samples of unknown age were analysed. Additional Plesovice standards in each analysis sequence monitor the reliability of each run.

2.2.4 Data reduction

Due to the small zone widths in the zircons sampled there was little leeway for error in targeting. Subsequently all ablated spots were assessed under an optical microscope prior to data reduction to determine whether spots have crossed zones or uncovered inclusions leading to inaccurate isotope measurements (Figure 15).

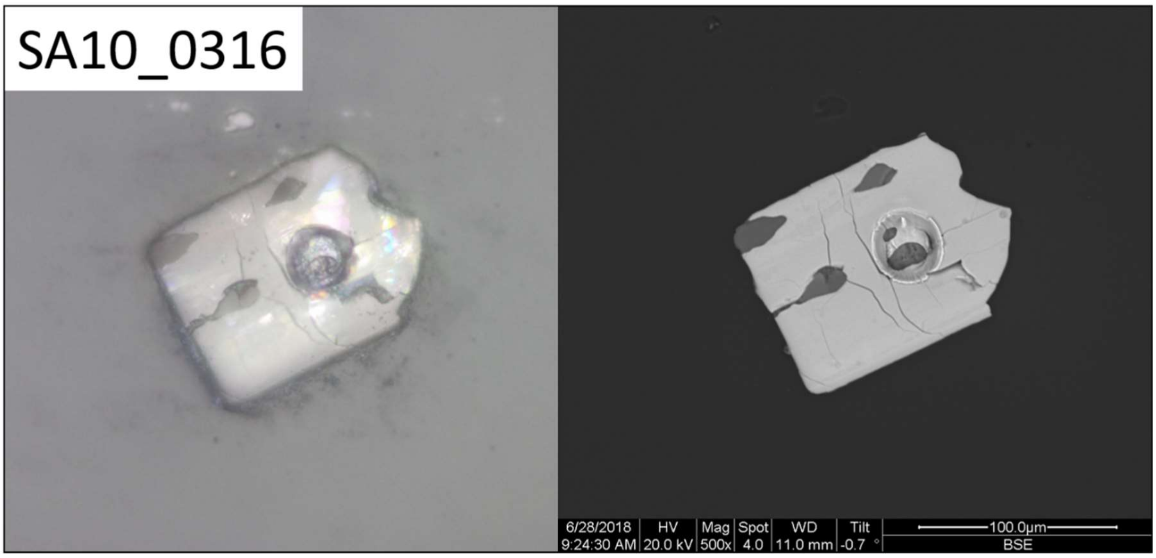

Figure 15:reflected light and secondary electron images of grain SA10_0316. Spot SA10_0316_1 was visible in the centre of the grain. Although no inclusion was visible prior to analysis, a subsurface inclusion has been cut and can be seen in both reflected light and SEM secondary electron imagery.

Data tables were produced using Igor pro v6.37 data reduction software (available from *Iolite Software*, 2018). Plesovice Zircon standard deviation was calculated based on the final $^{206}Pb/^{238}U$ ages of all Plesovice analysis in this study. The accuracy of the Plesovice standards was calculated by comparing calculated age to true age (Equation 1). Precision was be calculated by dividing standard deviation by average calculated age (Equation 2).

Equation 1

$$\frac{true\ age}{average\ calculated\ age} = \%\ accuracy$$

Equation 2

$$\frac{Standard\ deviation}{average\ calculated\ age} = \%\ precision$$

Any calculated Plesovice ages lying more than 2σ (σ = standard deviation of calculated ages) above or below the true age (337.13±0.37Ma, Sláma *et al.*, 2008b) were removed. The sample from which each age was removed and the total number of ages removed were recorded. Standard deviation was recalculated with the remaining ages and the process repeated until precision and accuracy start to drop.

Once the standard age was determined, the reduction of sample data was begun. The reliability of measurements in a given sample was estimated based on the number of Plesovice standard ages measured that had to be removed calculate the accurate standard age. If, within the same run of ten determined Plesovice standard ages four of them need to be removed, then there has been a problem with that particular LA-ICP-MS analysis session, or with the data reduction. The sample ages will not be as reliable as a separate sample in which all Plesovice standard ages were accurate.

2.2.4.1 Kernel density estimates and probability density plots

Probability density plots (PDP's) have in the past proven to be a popular tool for data visualisation in geochronology. However, this method has been found to provide misleading displays when working with precise measurements (Vermeesch, 2012).

In geochronology, PDP frequency distribution was based on the age of each data point in combination with its analytical uncertainty. This method produces clusters of peaks in densely populated areas; however as the overlap was based on analytical uncertainties rather than age deviation these clusters cannot reliably be assumed to display the true distribution of probable age (Vermeesch, 2012).

In response to this issue, kernel density estimates (KDE's) have been proposed as a scientifically grounded alternative. KDE plots were calculated using the age of each data point in combination with the standard deviation of that data point (as ±x Ma) as Gaussian bell curves. The overlap of these bells was then stacked to produce the KDE. As overlap was generated by age standard deviations, an accurate representation of data distribution was be created. This method was detailed in full by (Vermeesch, 2012).

Figure 16 plots both KDE and PDP's for samples SA10, SA3.1, and SA2 (this study). The KDE for SA10 displays a trimodal distribution, with the bandwidth defined by the maximum standard deviation (in Ma) for that dataset. The PDP plotted alongside instead displays a number of disparate spikes, with clustering around the three major peaks of the KDE. In a dataset such as this, the clusters are discernible, however the KDE is clearer and makes outliers easier to discern, as it accounts for age deviation.

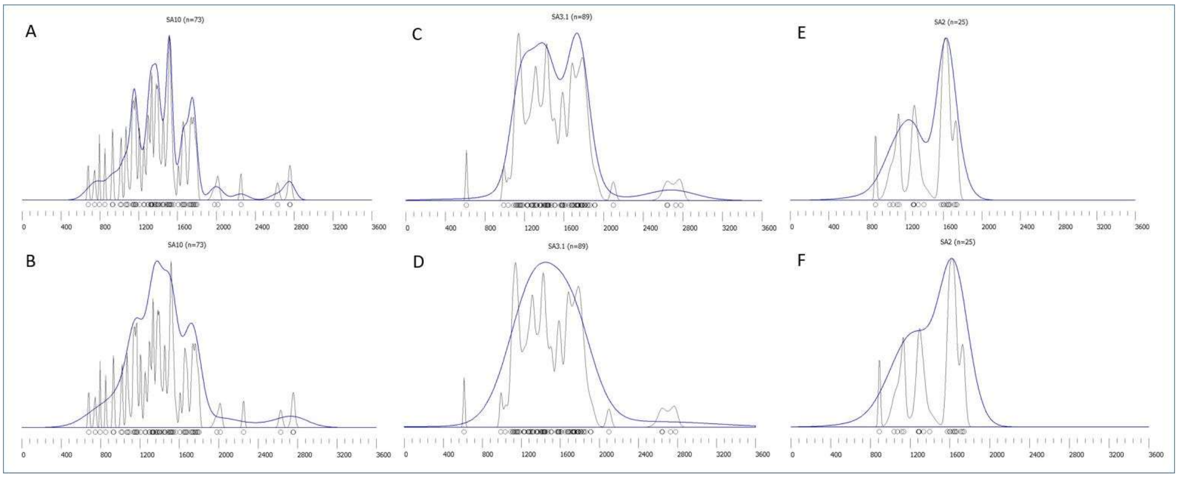

Figure 16: Comparison of PDPs and KDEs. Kernel density estimates (KDE, thick blue curve) and probability density plots (PDP, thin black peaks) for samples from this study. Plots were created using 'density plotter' software (Vermeesch, 2012). A, C, and E have a bandwidth = σ (standard deviation in Ma). B, D, and E have a bandwidth = 2σ. KDE's in A, C, E display age trends within the dataset clearly, whilst PDP's in the same graphs display a large number of sharp spikes which are difficult to interpret in samples with a large number of data points (SA10) and comparatively easy to interpret in a sample with few data points (SA2). This is not a beneficial trait in data analysis. By altering the bandwidth to 2σ in B, D, E, we see a significant change in resolution of the KDE, however the PDP remains unchanged. This is because PDP's do not consider age deviation and instead rely on analytical uncertainty.

This study utilises KDE's for data visualisation. For ease of comparison all plots cover a standard time axis of 0-3600Ma. Plots were constructed using 'Density Plotter' (Vermeesch, 2012) available from (http://www.ucl.ac.uk/~ucfbpve/densityplotter/), a java based KDE and PDP platform. 'Density plotter' provides an 'adaptive distribution' feature which determines bandwidth across a plot based on the local density of data to provide ideal resolution in both dense and sparse areas of the plot. In this study the adaptive distribution model led to oversmoothing of plots (see Figure 17A).

Subsequently each bandwidth was defined by the maximum standard deviation in the dataset for that sample (Figure 17B). Bandwidths lower than this definition would lead to undersmoothing of the plot. Exceptions to this rule were made in sample SA21 as the maximum standard deviation of 460Ma was indicative of poor data quality, subsequently the sample was re-analysed. Data from the subsequent reliable analysis of SA21 was labelled SA21_C.

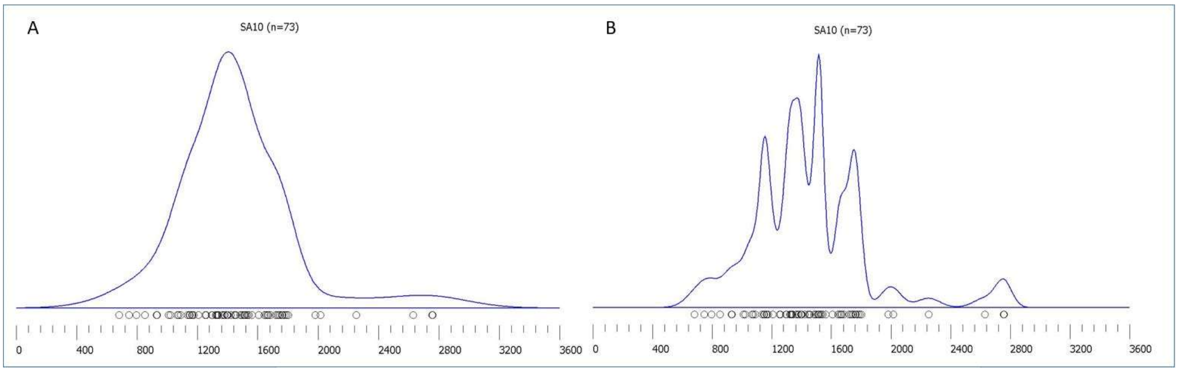

Figure 17: KDE bandwidth comparison. A) The KDE produced using 'adaptive distribution' for sample SA10. The entire dataset is smoothed into a unimodal peak spanning ~1000Ma. Compare to B) the KDE produced using a bandwidth of σ (standard deviation in Ma) for the same sample. This is the maximum viable resolution as lower bandwidths would cease to represent the data accurately. The KDE now displays a generally trimodal distribution and more clearly displays outlying data.

Chapter 3 Results

3.1.1 Zircon textures in Cathodoluminescence

3.1.1.1 Zoning

Zones in zircon represent different phases of crystal growth and may vary in composition dependant upon composition of the source melt for each zone. In CL imagery variations in zone composition are highlighted by variations in colour between zones (see
Figure 18, SA4_0800, SA8_0409, SA8_0501). Zone colouration in CL is primarily controlled by variations in U and Hf concentration (Hanchar and Hoskin, 2003). Oscillatory zoning is present in some grains (
Figure 18, SA10_0011). Analysis was targeted at individual zones to provide ages for distinct zircon forming events. Where multiple zones were ablated the age produced was dismissed as unreliable as a combination of the ages of each zone.

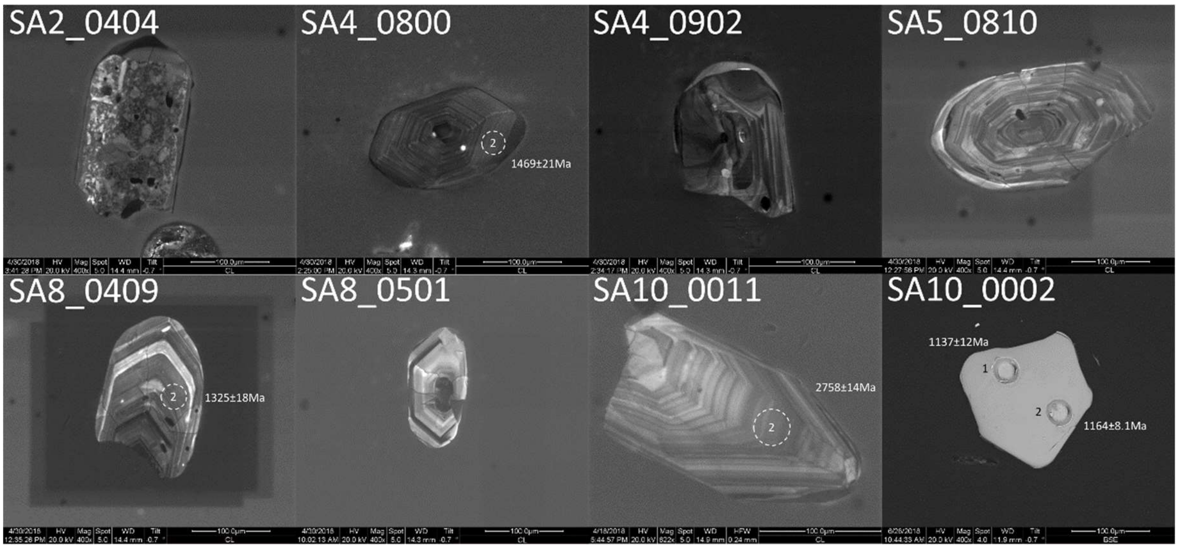

Figure 18: CL and BSE images of zircon texture and ablation pits. SA2_0404: Zircon metamiction in **CL. SA4_0800**: Euhedral zircon displaying oscillatory zoning and minor inclusions visible as bright spots. **SA4_0902**: Relict zircon containing fractures and inclusions displaying bright overgrowth zone on rim. **SA5_0810**: Zircon displaying oscillatory zoning, minor inclusions, and radial fractures. Overgrowth present on crystal rim. **SA8_0409**: Euhedral crystal displaying variations in zone composition highlighted in CL images by zone brightness. Minor inclusions visible as dark and bright spots throughout. Radial fracturing is visible in some zones. **SA8_0501**: Euhedral zircon formed around an included core. Radial fractures are present around the zircon core. **SA10_0011**: Euhedral zircon displaying a high degree of oscillatory zoning. **SA10_0002**: SE image displaying ablated pits in zircon. Pits are typically steep sided with a flat base.

3.1.1.2 Metamorphic overgrowths

Regional metamorphic events may lead to conditions suitable for the formation of metamorphic zircon. Metamorphic zircon forming on the rim of a pre-existing crystal create thin zones known as overgrowths (see

Figure 18, SA4_0902, SA5_0810). Where analysis was possible metamorphic overgrowths provide important insight into the timing of orogenic and other metamorphic processes to have affected the zircon, however overgrowths were not typically large enough for analysis.

3.1.1.3 Metamictization

Radioactive decay of uranium isotopes in zircon causes decay of the crystal lattice leading to a total loss of structure and zoning within the crystal as seen in Figure 18 (SA2_0404). This process is known as metamictization. Loss of original zoning in metamict crystals renders them unsuitable for LA-ICP-MS analysis.

3.1.1.4 Fracturing

Radial fracturing occurs in zircon due to radioactive decay of uranium isotopes. Where uranium is more highly concentrated in the rim of a crystal radial fractures are seen in the rim (
Figure 18, SA5_0810, SA8_0409, SA8_0501). Where uranium concentration is greater in the crystal core radiation induced fractures are more likely to be seen in the core. Some fractures may be related to regional stress and strain or transport of the crystal. Where high degrees of radiation damage and fracturing are present it is likely that ages produced from the area are unreliable. Areas of dense fracturing were avoided during analysis.

3.1.1.5 Inclusions

Fluid and mineral inclusions are often found in zircon. In CL images inclusions typically appear as either dark or bright areas depending upon their composition (see
Figure 18, SA4_0800, SA4_0902, SA5_0810, SA8_0409, SA8_0501). Inclusions will generate unreliable ages in targeted during analysis. In zircon with minor inclusions or sparse larger inclusions spots are positioned to avoid inclusions. Where inclusions lay near to or on a major fracture the entire fracture was avoided during analysis.

3.1.1.6 Ablation pit morphology

Ablation pits were imaged using SE imaging to provide topographic information on the ablation site. Pits typically were typically steep sided with level bases (
Figure 18, SA10_0002). Plesovice Zircon standard mean ages are presented prior to discussion of unknown ages.

3.1.2 Plesovice Zircon standards

3.1.2.1 Standards data

Plesovice Zircon standards have a $^{206}Pb/^{238}U$ age of 337.13±0.37Ma (see section 2.2.3.3). Plesovice Zircon is measured prior to and during analysis of unknowns to ensure consistently accurate results. Total mean age for Plesovice Zircon in this study is 337.46Ma with two standard deviations of 11.67Ma, providing a mean accuracy of 99.90% and precision of 1.07%. Mean ages for standard measurements taken during analysis of unknowns vary (see Table 1).

	Mean Age	Standard Deviation	2 Standard Deviations	Accuracy (% correct age)	Precision (% variation)
Total	336.781	3.60	7.19	99.90%	1.07%
Standalone	337.375	2.38	4.75	99.93%	0.70%
SA2	337.271	4.60	9.20	99.96%	1.36%
SA3.1	337.635	6.64	13.28	99.85%	1.97%
SA4	337.027	2.12	4.24	99.97%	0.63%
SA5	339.471	14.50	29.01	99.31%	4.27%
SA7	337.060	2.95	5.90	99.98%	0.88%
SA8	336.996	2.17	4.33	99.96%	0.64%
SA10	337.091	0.27	0.55	99.99%	0.08%
SA21C	336.969	1.55	3.10	99.99%	0.46%

Table 1: Mean standards data by sample. Mean standard ages for Plesovice standards measured during analysis of each sample. Accuracy is calculated as a percentage of the correct age, higher %accuracy indicates greater concordance with published ages. Precision is calculated as the percentage of variation between ages in a given sample, lower %precision indicates lower variability. Sample SA21C displays the highest accuracy and precision, whilst SA3.1 and SA5 display the lowest indicating measurements of poorer quality.

Standard ages are typically above 99.93% accuracy (within 0.07% of published Plesovice ages). Notable exceptions to this are SA3.1 Plesovice measurements (see Table 1) which has an accuracy of 99.85% (within 0.15% of published ages) and SA5 which has an accuracy of 99.31% (within 0.69% of published ages). The highest quality Plesovice data obtained during analysis of unknowns was from sample SA10 with an accuracy of 99.99% (within 0.01% of published ages).

Unknown zircon ages are presented using visual representations of the larger dataset.

3.2 LA-ICP-MS ages: Applecross Peninsula

3.2.1 Kernel Density Estimates (KDE)

Results are here visualised using KDE plots. KDEs are preferred over probability density plots (PDPs) as they provide a more realistic interpretation of the possible age spectrum in the sample (see Methodology, section 2.2.4.1). KDEs are plotted using 'Density Plotter' (Vermeesch, 2012) software available at 'http://www.ucl.ac.uk/~ucfbpve/densityplotter/'.

KDEs are plotted on a standard timeline of 0-3600Ma for ease of comparison. Bandwidth is defined by the maximum 2σ value of all ages within that sample. Within each sample, cores are plotted separately as they determine the maximum age of each grain.

3.2.1.1 SA2 – SA 3.1

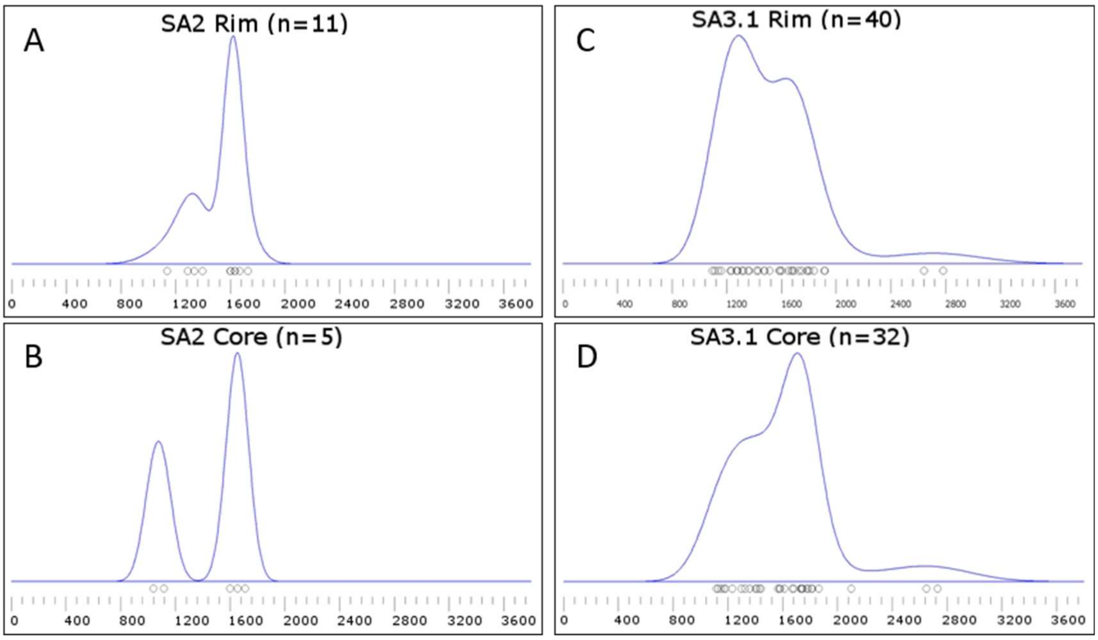

Figure 19: KDE; SA2-SA3.1. KDE plots displaying data for samples SA2 (A, B) and SA3_1 (C, D) with grain cores and grain rims, plotted separately. SA2 is plotted at a bandwidth of 58Ma, SA3_1 is plotted with a bandwidth of 73Ma (2σ)

Although the number of analyses is limited, sample SA2 rims display a bimodal trend (Figure 19A); a minor peak is positioned around 1322Ma with a more prominent peak occurring later, at around 1620Ma. Figure 19B displays a bimodal trend for grain cores in SA2 with a pronounced peak at 1076Ma and second at 1657Ma, coinciding with the larger peak displayed by rims in the same sample.

Sample SA3_1 is slightly oversmoothed due to a high maximum 2σ value for the sample. The KDE is broadly unimodal, although two clusters can be discerned in Figure 19C (grain rims); a major peak occurs around 1287Ma, with a poorly defined older peak around 1630Ma. Figure 19D (grain cores) displays the inverse for cores of the same sample, with a major peak around 1710Ma and a poorly defined hummock between 1120-1360Ma. Four grains in Sample SA3_1 (two core ages and two rims) give ages in excess of 2600Ma: SA3_1_0302_1 provides a core age of 2730±30Ma from a rounded grain with minimal fracturing and brown tint; SA3_1_0608_1 provides a core age of 2648±66Ma in a larger grain containing a defined core. SA3_1_0306_1 has a $^{206}Pb/^{238}U$ age of 2780±30Ma from a clearly defined zone near the rim; some red spots indicative of radiation damage are present in the grain, but are avoided during the analysis. SA3_1_0908_2 has a $^{206}Pb/^{238}U$ age of 2640±36Ma from an area of oscillatory zoning, just outside the grain core.

3.2.1.2 SA4 - SA7

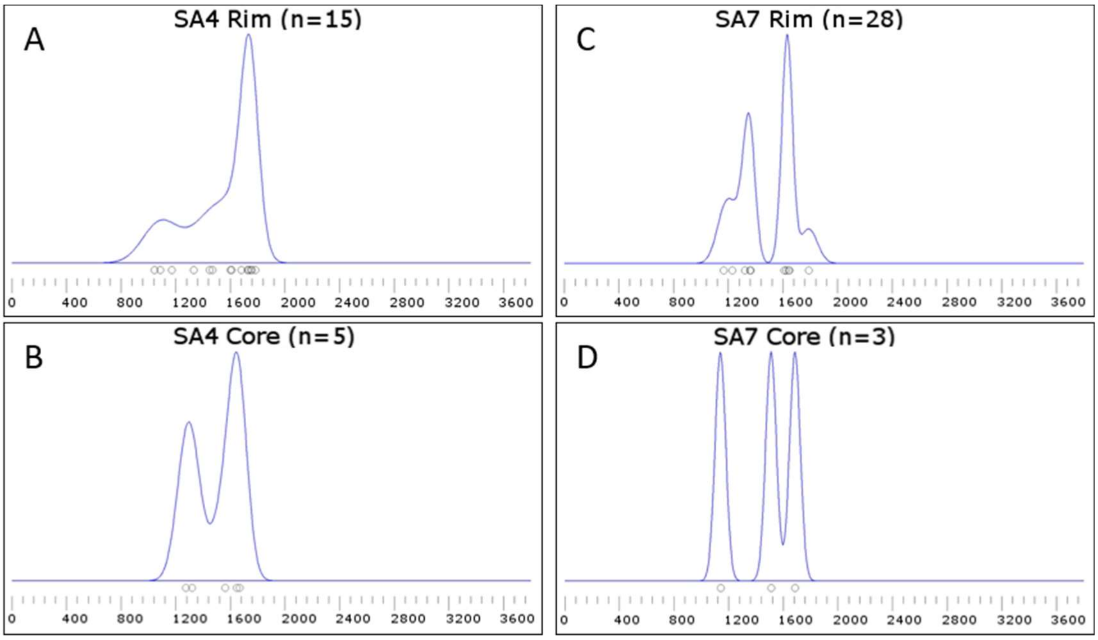

Figure 20: KDE; SA4-SA7. KDE plots displaying data for sample SA4 (A, B) and SA7 (C, D). SA4 is plotted with a bandwidth of 41Ma, SA7 is plotted with a bandwidth of 32Ma (2ϑ).

Rims in sample SA4 (Figure 20A) show a low peak at 1111Ma, followed by a gradual increase in age density from 1300-1600Ma, with a major peak at 1733Ma. Only a small number of cores are measured in SA4 (Figure 20 B), producing peaks at 1295Ma and 1610Ma. Due to the low volume of core data in this sample, any core interpretations must be taken as provisional.

Rim analysis in SA7 (Figure 20C) shows a bimodal trend. The youngest peak has a small component peaking at 1206Ma before a main peak at 1348Ma. The older major peak in the sample lies at 1630Ma with a tight cluster of four grains. A single grain rim provides an age of 1789±21Ma. Core analysis of SA7 (Figure 20D) includes only three grains, which do not cluster at the bandwidth used. Spot SA7_0001_2 has a $^{206}Pb/^{238}U$ age of 1140±29Ma. Spot SA7_0306_1 has a $^{206}Pb/^{238}U$ age of 1686±29Ma. Spot SA7_0402_1 has a $^{206}Pb/^{238}U$ age of 1511±17Ma. Grains SA7_0306_1 and SA7_0402_1 begin to coalesce, however as the points do not cluster strongly they should be taken as single grain ages and not KDE peaks.

3.2.1.3 SA5

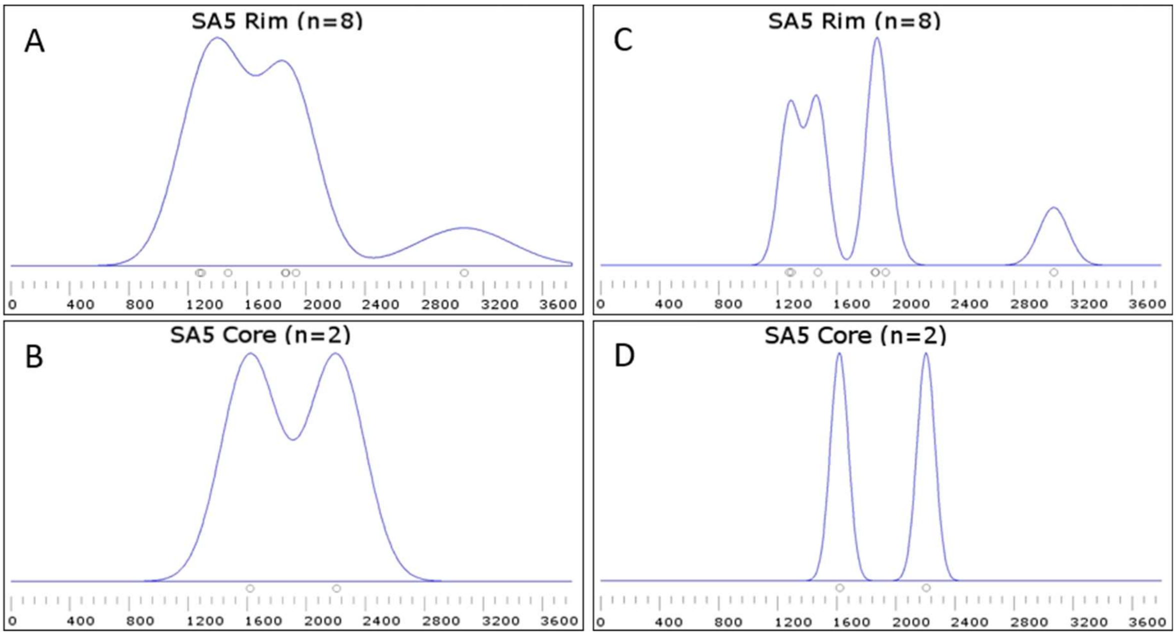

Figure 21: KDE; SA5. KDE plots showing data from sample SA5. Plots A, B have a bandwidth of maximum 2ϑ within the sample. Plots C, D have a bandwidth of maximum 1σ within the sample.

Spot targeting was poor during analysis of SA5 due to ablation of multiple zones, inclusions, or resin as desired ablation sites were missed. This lead to a depleted dataset. Post-analysis assessment of ablated spots provided some usable data, however as a result of the poor quality of the analysis the KDE plots are oversmoothed, with bandwidth based on maximum 2σ. To better understand the distribution of smoothed peaks, a second pair of KDEs based on a 1σ bandwidth are plotted; however these peaks should be interpreted with caution.

Rims in SA5 (Figure 21A) display a broadly bimodal trend at 1398Ma and 1836Ma respectively. The peaks in Figure 21A are of similar magnitude and with no defined divide; by comparison, in Figure 21C (KDE at 1σ), the relationship between the two peaks is clearer. A divide exists in the dataset between ~1650Ma – 1720Ma. As the dataset for this sample is limited and of low quality it is likely that this gap is an artefact of analysis.

Spot SA5_0707_2 provides a maximum age of 3071±36Ma. The analysed spot is located in a clearly defined zone between the rim and core of the grain. Although some discolouration is present, it is focused around the tip of the grain furthest from the ablation site.

SA5 core analyses provide two ages. SA5_0603_1 has a $^{206}Pb/^{238}U$ age of 2205±94Ma, SA5_0706_2 has a $^{206}Pb/^{238}U$ age of 1618±61Ma. Due to the low number of data, points SA5 core ages are interpreted as single ages.

3.2.1.4 SA8

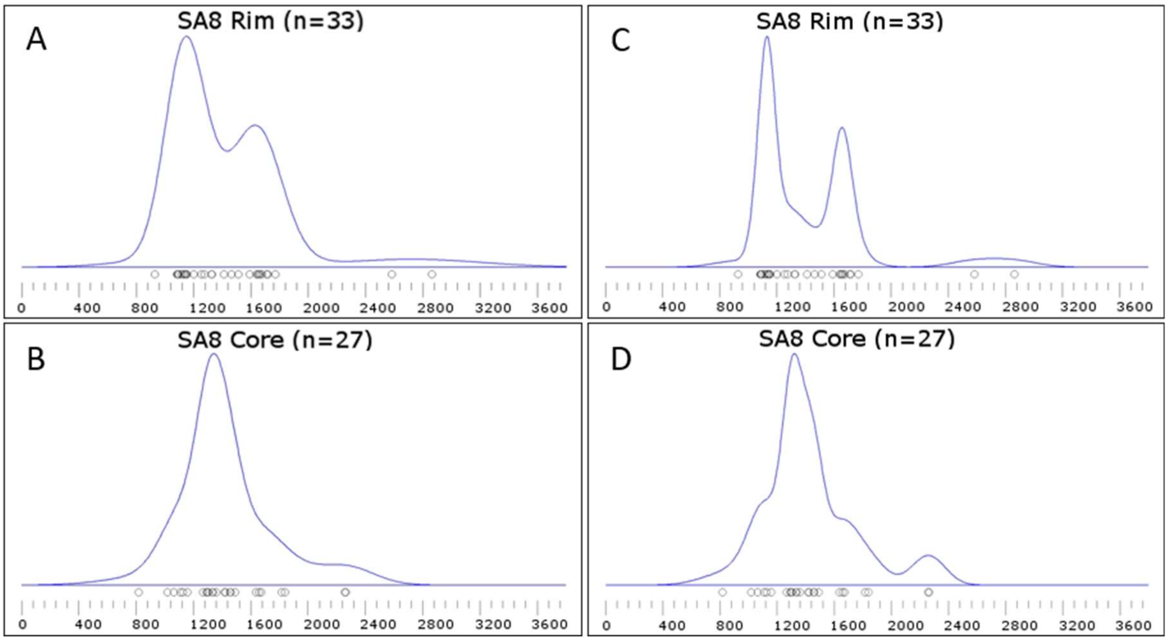

Figure 22: KDE; SA8. KDE plots showing data from sample SA8. Plots A, B have a bandwidth of 86Ma (2σ). Plots C, D have a bandwidth of 43Ma (1σ).

KDEs based on 2σ bandwidth for SA8 are reliable, however a second plot at 1σ (Figure 22) provides a higher resolution to assess broad clusters within the KDE.

Rims in SA8 show a bimodal trend (Figure 22 A) with peaks at 1148Ma and 1628Ma. Two grains provide ages in excess of 2400Ma; SA8_0203_2 has a $^{206}Pb/^{238}U$ age of 2581±61Ma. SA8_0312_1 has a $^{206}Pb/^{238}U$ age of 2863±86Ma from a fragment.

Figure 22B shows a broadly unimodal trend in SA8 core data, with a peak at 1343Ma. A single grain (SA8_0204_1) has a $^{206}Pb/^{238}U$ age of 2263±49Ma. Figure 22 D has a bandwidth of 1σ providing higher KDE resolution. Higher 2σ uncertainties are related to grains over 2Ga in age, therefore this level of smoothing is more appropriate for the main peak in the KDE. Increased resolution shows two additional clusters in the sample which do not stand apart from the unimodal trend. Two clusters are present, one between 1060Ma-1150Ma and the other between 1600Ma-1680Ma.

3.2.1.5 SA10 - SA21C

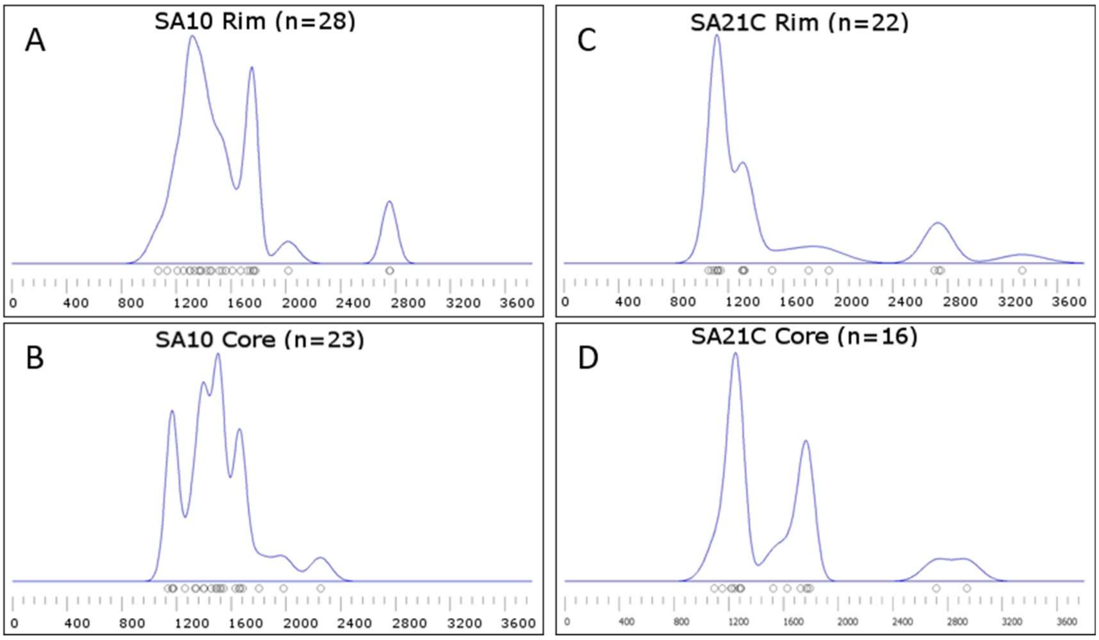

Figure 23: KDEs; SA10-SA21C. KDE plots displaying data for samples SA10 (A, B) and SA21C (C, D). SA10 is plotted with a bandwidth of 26Ma (2σ). SA21C is plotted with a bandwidth of 43Ma (2σ).

Figure 23A shows a trimodal trend for rim ages in sample SA10. Dominant peaks are present at 1317Ma and 1752Ma. An older a peak at 2758Ma consists of two grain rims. SA10_0011_2 has a $^{206}Pb/^{238}U$ age of 2758±14Ma from an area of oscillatory zoning near the crystal tip; some brown colouration is present nearby but is avoided by the spot. SA10_0405_2 has a $^{206}Pb/^{238}U$ age of 2755±21Ma from a broad, clear zone between the core and rim of the grain.

Core data in sample SA10 display a trimodal distribution of data (Figure 23,B) with outlying single grains. A defined peak is present at 1166Ma. Two similar peaks at 1396Ma and 1504Ma are interpreted as phases of a single event. A final major peak occurs at 1657Ma, followed by an individual grain (SA10_0109_2) with an age of 1980±26Ma. A maximum core age is defined by SA10_0407_1 with an age of 2252±11Ma.

Sample SA21C grain rims (Figure 23C) show a bimodal trend with minor interstitial elements. A tight cluster of ages provides a major peak at 1116Ma, followed by a minor peak at 1304Ma. The second major cluster is found at 2728Ma, with a small number of single grain ages between the two main clusters. A single grain (SA21C_0202_1) has a $^{206}Pb/^{238}U$ age of 3346±43Ma. Grain SA21C_0202 has an even, faint red hue throughout the crystal, however CL (cathodoluminescence) imagery indicates that zones in the ablation area are intact, despite the fact that the spot is adjacent to a fracture.

Grain cores in SA21C (Figure 23D) display a trimodal distribution of ages. The first major peak occurs at 1248Ma with the second peak at 1762Ma. The third cluster shown in the KDE consists of two data points ~600Ma apart and are treated as single grain ages. SA21C_0005_1 has a $^{206}Pb/^{238}U$ age of 2942±42Ma, SA21C_0206_1 has a $^{206}Pb/^{238}U$ age of 2716±28Ma.

General trends within each sample are presented above, it is also important to consider the variations between each sample in a stratigraphic context.

3.2.2 Stratigraphic succession

Samples are taken entirely within the Applecross Formation, from various stratigraphic levels. Sedimentary features include heavy mineral laminae, cross bedding (various), laminations, granules from 1mm upwards, soft sediment deformation, and some accretions. The context log (Figure 24) provides important detail on the sedimentary succession of the Applecross Formation, however no samples taken directly from the logging area were analysed. Stratigraphic relationships between analysed samples are determined using local geological maps (available online at https://www.bgs.ac.uk/data/maps/maps.cfc?method=viewRecord&mapId=10903, Geikie *et al.*, 1973). By placing KDEs in relative stratigraphic positions, variations in detrital zircon U-Pb age over time can be assessed (see Figure 26, Figure 27).

184 m of Applecross sandstone are logged for geological context (Figure 24) on the southeast face of Sgurr a'Chaorachain (GPS 57.40762). The entirety of the logged succession is quartzo-feldspathic sandstone of varying coarseness, with rare localised mud clasts. Granules are found in a number of units with varying coarseness and abundance. The lithology is mature and homogenous (see Table 2), suggesting that sediment has been transported from a distal source. Grains are often angular to sub rounded (Table 2), indicating that although the degree of sorting is high, high levels of rounding have not been achieved. This could be related to the resistance of bulk minerals to erosion. The structures present (coarse cross bedding, heavy mineral laminae, soft sediment deformations) indicate a high sediment influx and rate of flow within a fluvial regime at the time of deposition.

Structures favouring heavy mineral deposition (cross bedding, heavy mineral laminae, story surfaces, etc.) are preferentially sampled to improve zircon yield for analysis. Whilst depositional processes can lead to a natural bias in ages, this is difficult to quantify and is likely to be outweighed by analytical biases (Sláma *et al.*, 2008).

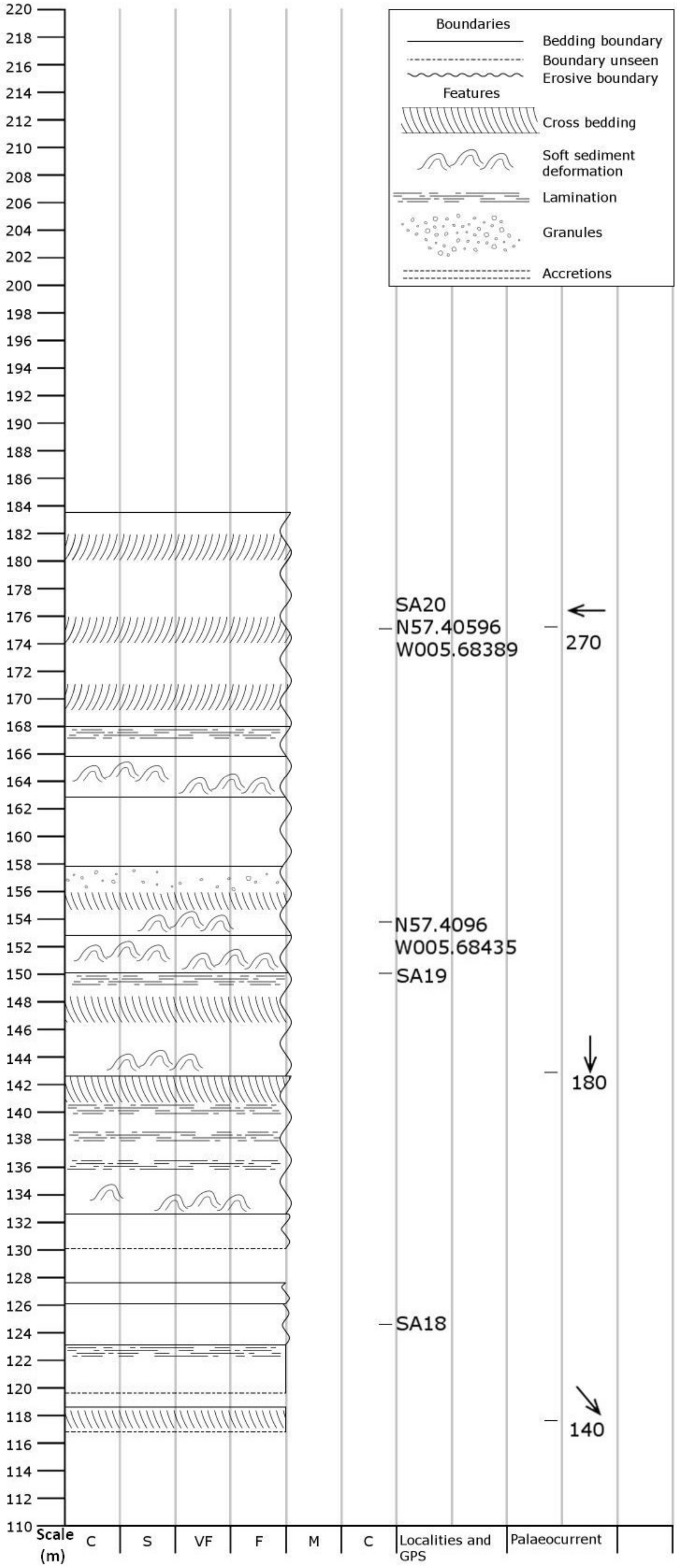

Boundaries
Bedding boundary
Boundary unseen
Erosive boundary
Features
Cross bedding
Soft sediment deformation
Lamination
Granules
Accretions
SA20
N57.40596
W005.68389
270
N57.4096
W005.68435
SA19
180
SA18
140
220
218
216
214
212
210
208
206
204
202
200
198
196
194
192
190
188
186
184
182
180
178
176
174
172
170
168
166
164
162
160
158
156
154
152
150
148
146
144
142
140
138
136
134
132
130
128
126
124
122
120
118
116
114
112
110
Scale (m)
C
S
VF
F
M
C
Localities and GPS
Palaeocurrent

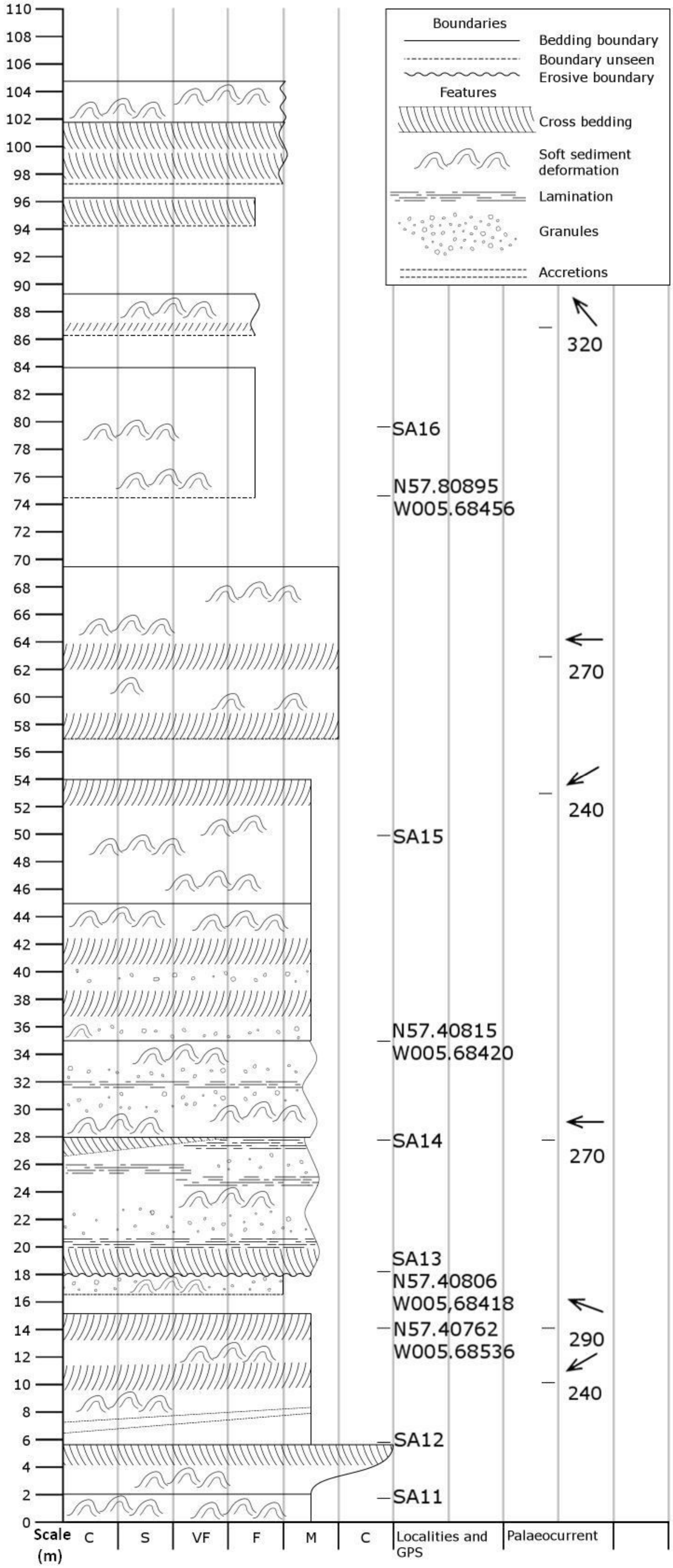
Boundaries
Bedding boundary
Boundary unseen
Erosive boundary
Features
Cross bedding
Soft sediment deformation
Lamination
Granules
Accretions
SA16
N57.80895
W005.68456
SA15
N57.40815
W005.68420
SA14
SA13
N57.40806
W005,68418
N57.40762
W005.68536
SA12
SA11
320
270
240
270
290
240
Scale (m)
C
S
VF
F
M
C
Localities and GPS
Palaeocurrent

Figure 24: Applecross context log. Context log taken approximately midway along the sample transect including palaeocurrent directions and sedimentary features of the succession. GPS positions and sampling locations within the logging area are included. Lithology is feldspathic sandstone throughout with silt present in localised laminations.

The primary focus of this study is the U-Pb dating of the Applecross Formation, however a small sample of paleocurrent data were collected to indicate the direction of the sediment source (Figure 25). Palaeocurrents taken from the log section plus two additional measurements from sampling localities 21 and 24 indicate a broadly west and southwest flow regime. This could be interpreted as indicating a source area to the northeast; it is noteworthy however, that the palaeocurrent measurements were taken individually across several sample locations and may not be characteristic of the outcrops at which they were observed. Palaeocurrents within the Applecross Formation are typically to the south east indicating a source to the north west (Gracie and Stewart, 1967; Nicholson, 1993; Williams, 2001; Owen and Santos, 2014).

Sample depths given below estimated using structure contours, with depths stated relative to sample SA10. A graphical representation can be found in Figure 26.

Sample SA10 is the lowest stratigraphic sample analysed and provides a comparative base to the sample succession (Figure 26). Sample SA8 occurs approximately 677m stratigraphically above SA10, and is roughly level with the top of the context log (670m). SA7 and SA5 are found approximately 870m and 894m stratigraphically above SA10, respectively. SA4 and SA21C form a similarly close pair approximately 990m and 1004m above SA10. SA2 and SA3.1 form the uppermost set of samples approximately 1869m and 1898m stratigraphically above SA10. The age variation between zircon populations in these samples is discussed below.

3.2.2.1 Age variation through stratigraphy

Age clusters from individual samples must be considered in a stratigraphic context. Core analyses (Figure 26, Figure 27: left column) typically include a clustered component of varying precision around 1680Ma. In the lower to middle sections of the sequence (SA10 and SA8) grain cores also display clusters around 1150Ma, with single grains and pairs of grains around 2250Ma. A greater portion of grain cores clustering around 1000-1100Ma are present in SA8 (~677m, top of context log).

Sample	Colour	Cement	Grain Size (µm)	Sorting	Sphericity	Rounding	Support	Consolidation	Lithology	Notes
SA1	Pink	Fine white cement	1000	Poorly sorted	Low	Rounded-angular	Grain supported	Good	Quartzo-feldspathic sandstone	Pebbles and granules up to 4mm.
SA2	Pink-grey	None/ Interlocking grains	500-750	Poorly sorted	Low	Angular- some sub rounded pebbles	Grain supported	Good	Quartzo-feldspathic sandstone	Small pebbles and granules up to 3mm.
SA3.1	Pink	None/ interlocking grains	375-750	Poorly sorted	Moderate-low	Sub rounded	Grain supported	Good	Quartzo-feldspathic sandstone	Granules and pebbles up to 10mm. Sample includes a large 'blob' of coarse material, possibly a clast.
SA3.2	Dark pink	Fine white cement	500-750	Moderately sorted	Moderate-low	Angular	Grain supported	Good	Quartzo-feldspathic sandstone	Granules up to 2mm.
SA4	Pink-grey	Fine white cement	500-1000	Moderately sorted	Moderate-high	Sub rounded- occasionally well rounded	Grain supported	Good	Quartzo-feldspathic sandstone	Granules present, comprised of K-feldspar and quartz.
SA5	Dark pink	Fine white cement	187-375	Well Sorted	Moderate-low	Sub angular	Grain supported	Good	Quartzo-feldspathic sandstone	Contains occasional granules.
SA6	Dark pink	Fine white cement	187-250	Well Sorted	Moderate	Sub angular	Grain supported	Good	Quartzo-feldspathic sandstone	Mica is up to 750µm in some coarser bands of up to 2cm thickness.
SA7	Pink	None/ interlocking grains	187	Very well sorted	Low	Sub angular- sub rounded	Grain supported	Good	Quartzo-feldspathic sandstone	
SA8	Dark Pink	None/ interlocking grains	187-250	Well Sorted	Low	Sub rounded	Grain supported	Good	Quartzo-feldspathic sandstone	Muscovites tend to be localised and of greater grain size (up to 500µm).
SA21	Pink	Fine white cement	250-375	Poorly sorted	Low	Angular	Grain supported	Good	Quartzo-feldspathic sandstone	Some grains up to 750µm.
SA23	Pink	None/ interlocking grains	250	Well sorted	Low	Sub angular	Grain supported	Good	Quartzo-feldspathic sandstone	
SA24	Pink	None/ interlocking grains	187	Very well sorted	Low	Very angular	Grain supported	Good	Quartzo-feldspathic sandstone	

Table 2: Hand specimen descriptions. Hand specimen descriptions for samples from which grains have been analysed.

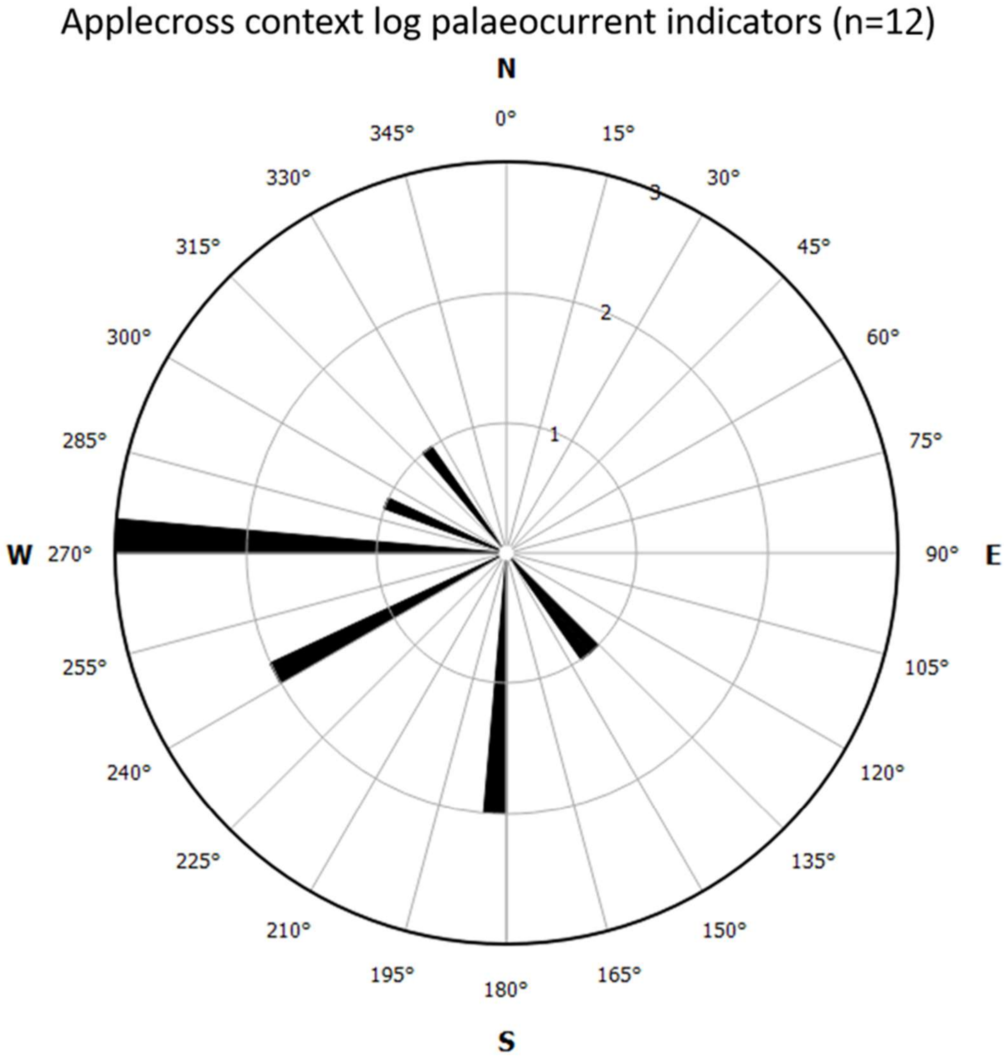

Figure 25: Applecross context log palaeocurrent indicators. Rose diagram displaying palaeocurrent measurements taken in this study. Notice that the sample size is small and therefore could only refer to locally defined flows. Flow indicators (cross bedding) have a mean flow direction of 233.75°

Samples SA7and SA5 are stratigraphically close (~24m) and lie ~2.7km apart geographically. SA7 has a depleted core dataset with only three ages: 1140±29Ma, 1511±17Ma, and 1686±29Ma. SA5 is similarly depleted in core data providing ages of 2205±94Ma and 1618±61Ma. Viewed together, three grains from SA7 and SA5 are clustered between 1500Ma-1700Ma, in line with clusters around 1680Ma seen in the lower stratigraphy. The oldest core from SA5 correlates approximately with oldest single grains in SA10 and SA8.

.

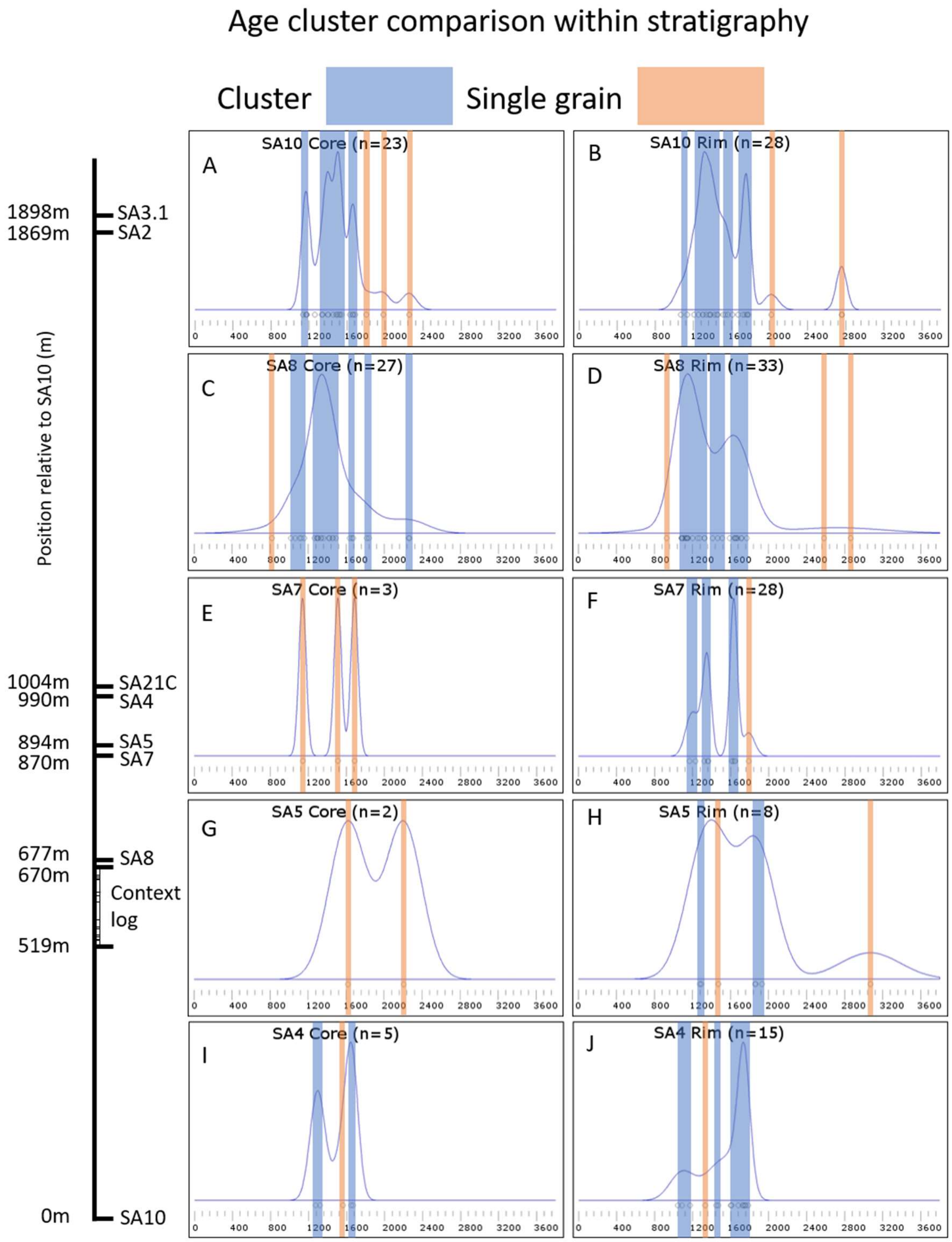

Figure 26: KDE peak changes over stratigraphy upper. KDEs for samples SA10 (A, B), SA8 (C, D), SA7 (E, F), SA5 (G, H), and SA4 (I, J), with stratigraphic position relative to SA10 (uppermost analysed sample) on the left.

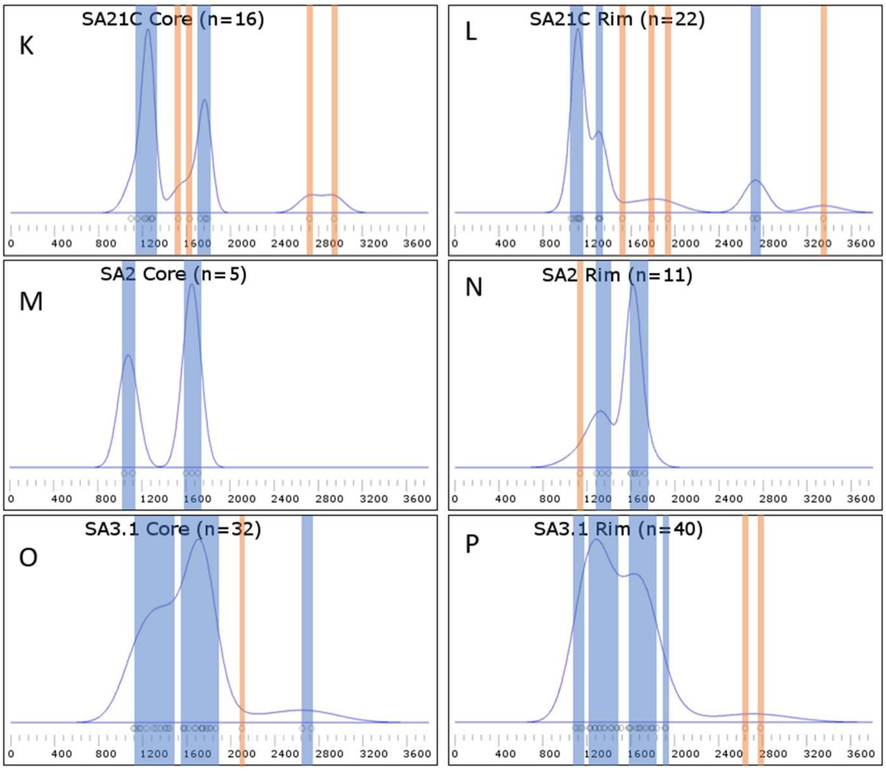

Figure 27: KDE peak changes over stratigraphy lower. KDEs for samples SA21C (K, L), SA2 (M, N), and SA3.1 (O, P) in stratigraphic order. For relative stratigraphic position see Figure 26.

SA4 and SA21C are approximately halfway through the sampled stratigraphy (~990m and 1004m above SA10). Single grain cores are present which correlate to the large clusters around 1680Ma present near the base of the sequence. This component is still present, however it represents a lower proportion of grain ages. SA4 and SA21C core ages are dominated by clusters around 1120Ma-1280Ma with an additional cluster around 1760Ma displayed in SA21C. SA21C cores have maximum single grain ages of 2716±44Ma and 2942±421Ma

SA2 and SA3.1 represent the uppermost sampled stratigraphy (~1869m and 1898m above SA10). Core age clusters are split between a primary cluster of 1600Ma-1700Ma cores correlating with clusters in the lowermost stratigraphy, and a secondary cluster in SA 3.1 between ~1120Ma-1440Ma. SA2 has a youngest core age of 1039±47Ma. SA3.1 includes maximum core ages of 2648±66Ma and 2730±39Ma.

Rim analyses of samples SA10 and SA8 (lowermost and log-correlated samples) again show age clusters between 1600Ma-1720Ma matching the core analysis clusters around 1680Ma in the same samples. SA8 displays a minimum single grain age of 1083±29Ma from rim analysis compared to a minimum single grain age of 1018±14Ma from core analysis. SA10 and SA8 each contain single grain rim ages in excess of core ages, 2755±21Ma from SA10, 2581±61Ma and 2863±86Ma from SA8.

SA7 and SA5 (middle of stratigraphy) rim analyses display small clusters and single grain ages which are in general agreement with the lowermost samples, including a small cluster around 1880Ma in SA5 correlating to a single grain from SA10. SA5 provides a maximum single grain rim age of 3071±36Ma. SA7 rims display two small clusters around 1200Ma and 1300Ma, correlating with a single core of similar age, as well as the youngest clusters in SA8.

SA4 and SA21C (middle of stratigraphy) rim analyses show clusters equivalent to core analyses of the same samples, however core clusters in the range of 1120Ma-1280Ma are replaced by clusters between 1040Ma-1150Ma. SA21C rim analysis includes a cluster around ~2720Ma correlating with single grain cores of similar age. SA21C rim analysis gives a maximum single grain (rim) age for all samples of 3346±43Ma (SA21C_0202_1).

SA2 (uppermost sampled stratigraphy) rim analysis display similar oldest age clusters to core analysis of the same sample, however only a single grain rim is equivalent to the youngest core age cluster. An older cluster around 1280Ma-1400Ma is present in place of the core cluster and is consistent with rim ages in other samples. SA3.1 (uppermost sampled stratigraphy) rim analysis displays clusters of similar age to core analysis in the same sample. Where core analysis shows a trend towards older ages, rim analysis displays and inverse set of peaks with a trend towards younger grain ages.

3.2.2.2 Age variation through stratigraphy summary

The lowermost sampled stratigraphy is shown to contain predominantly Mesoproterozoic population with a significant Palaeoproterozoic component. Rim analysis of the lowermost stratigraphy continues to show predominantly Mesoproterozoic populations with a slightly greater proportion of Palaeoproterozoic ages compared to core analysis of the same samples. Additionally rim analysis provide evidence of an Archaean zircon population in the lower part of the sample stratigraphy otherwise unseen in core analysis of the same samples.

The middle of the sampled stratigraphy is here shown to have a younger bulk of core ages, with greater maximum core ages. Rim analyses show a weaker trend towards younger ages. Archean components of the core analysis are reinforced by rim analysis, however it is shown that the lower stratigraphy also includes a component of Archean zircon.

The uppermost stratigraphy is shown to have similar core ages to the lowermost stratigraphy, with a greater density of ages present in younger clusters than the uppermost stratigraphy. Oldest single cores are similar in age to those found in the middle of the sequence (Palaeoproterozoic- Archean). Rim analysis reinforces the trend towards younger ages in the uppermost sampled stratigraphy seen in core analysis

3.3 Ablation spots

3.3.1 Ablation sites

Ablation sites are positioned within individual core or rim zones of grains (see methodology, sections 2.2.2- 2.2.3) as in Figure 28. During ablation of samples laser targeting was out by up to 40μm in some instances. The position of spots in CL images are corrected post-ablation to show where actual ablation occurred and not sites at which it was intended to occur. Subsequently a number of data points are rejected from the analysis based on crystal texture at the site of ablation, see Figure 28, Figure 29, Figure 30, Appendix 2.

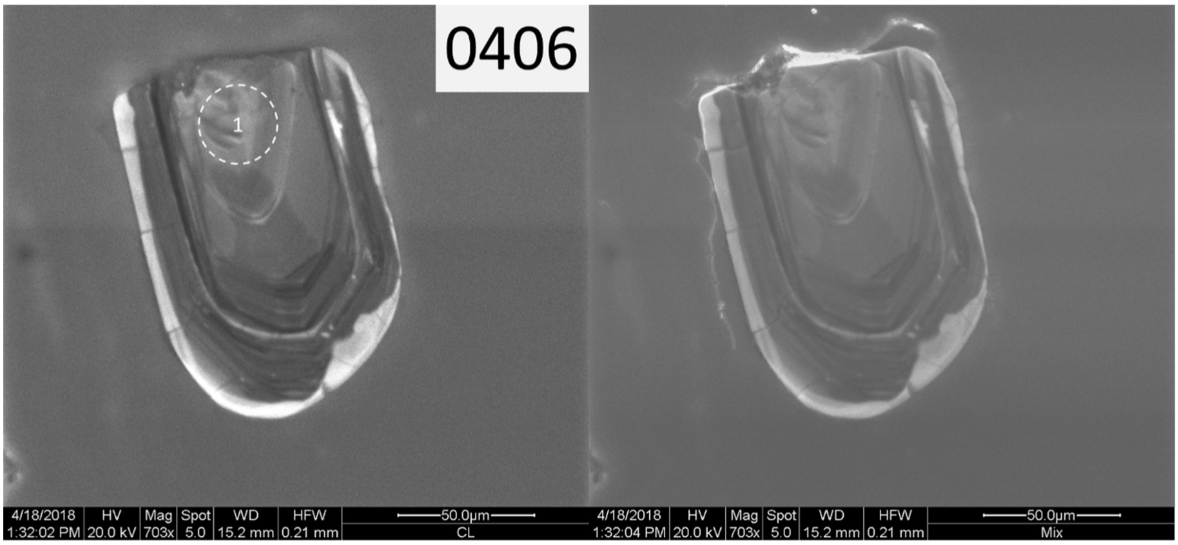

Figure 28: CL and SE images, SA3.1_0406. Grain SA3.1_0406 CL (cathodoluminescence, left) with combined CL and secondary electron (right) imagery. Spot 1 (SA3.1_0406_1) is positioned within the core of the grain clearly visible in the CL image.

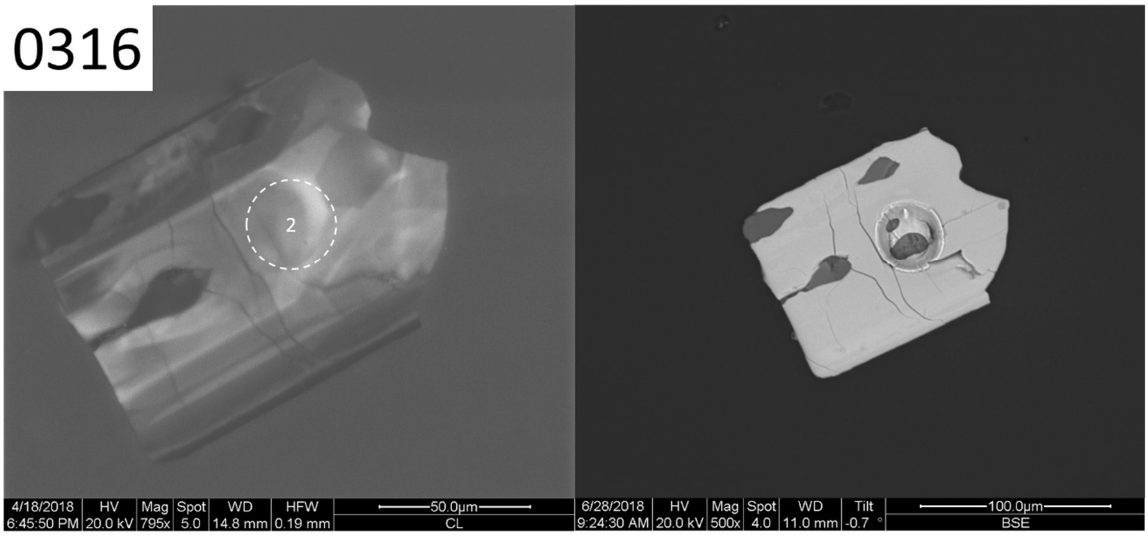

Figure 29: Pre-ablation CL and post-ablation SE images, SA10_0316. Grain SA10_0316 in Cl (cathodoluminescence, left) pre-ablation and secondary electron post-ablation image. Spot SA10_0316_2 is marked on the left and ablated on the right. Although no inclusion is visible in the CL image (left) subsurface inclusions have clearly been cut in the post-ablation image (right).

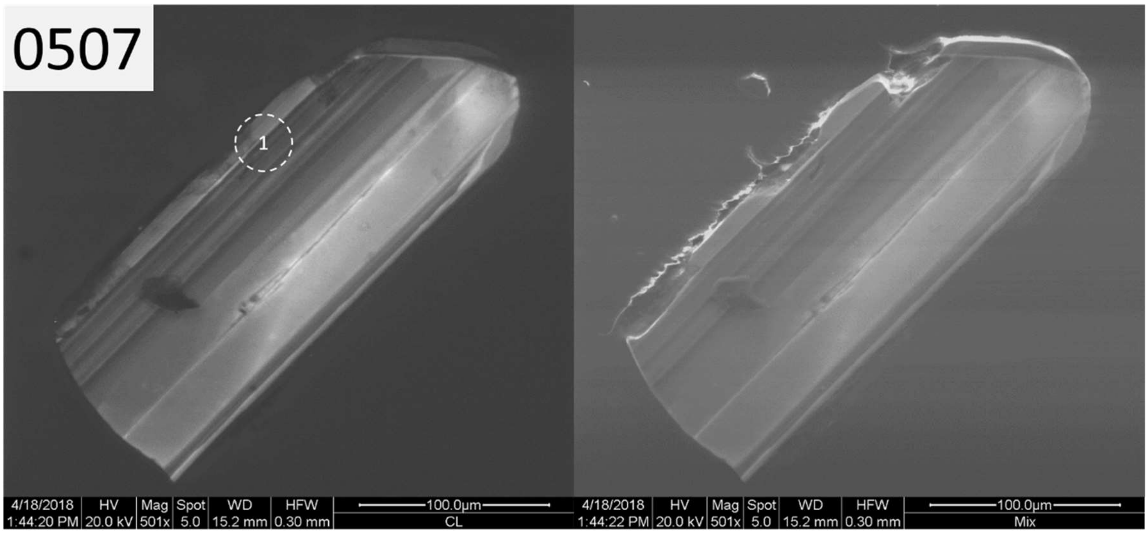

Figure 30: CL and SE images, SA3.1_0507. Grain SA3.1_0507 in CL (cathodoluminescence, left) with combined CL and secondary electron image (right). Spot SA3.1_0507_1 is marked on the CL image and has been corrected to show the site of ablation. The spot was originally intended to be entirely with the zone in which its right half sits and has shifted by ~20µm to the left due to poor adjustment of laser targeting prior to analysis. As the spot not only crosses multiple zones, but also cuts the resin in which the grain is mounted it must be rejected from the analysis.

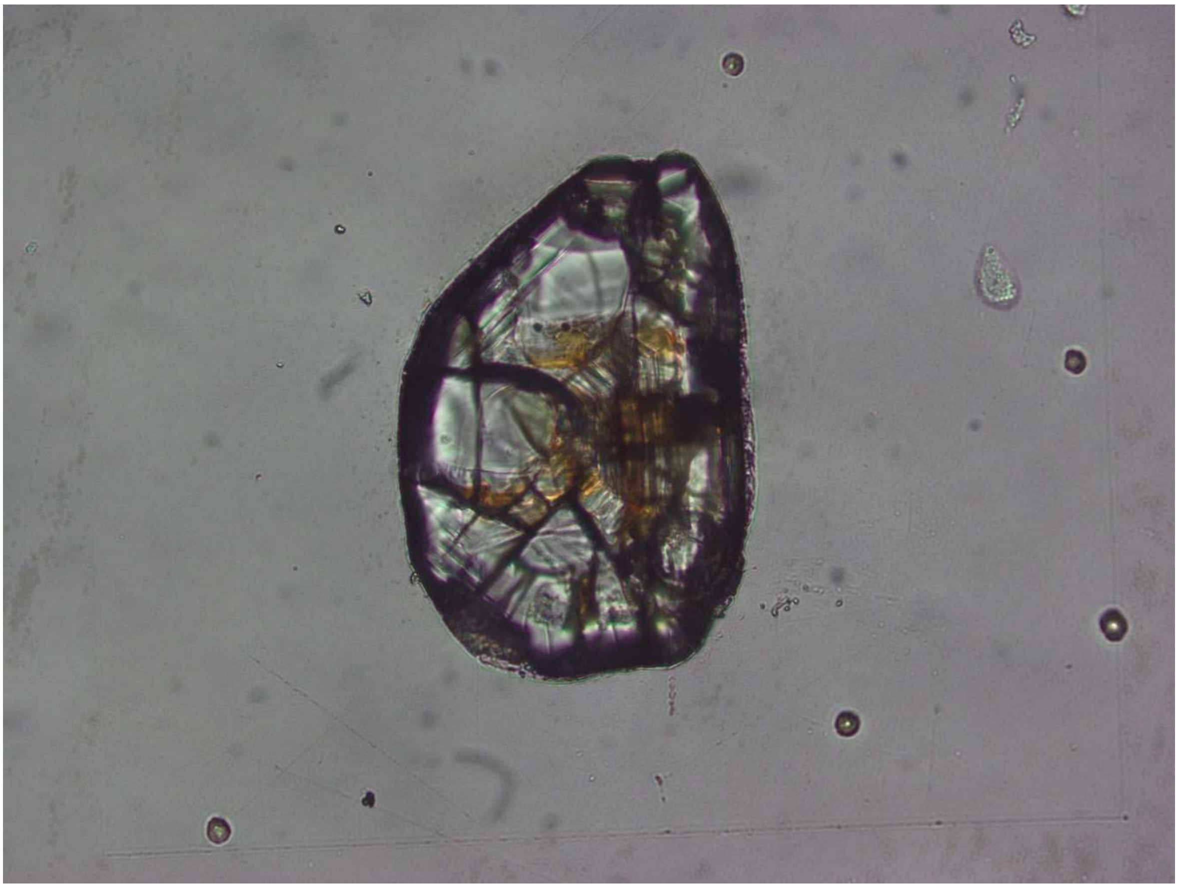

Figure 31: Transmitted light image, SA8_0309. Plain light image of grain SA8_0309 showing discolouration in the area of ablation indicative of radiation damage.

3.3.2 Table of ablated spots

During data reduction, a number of ablated spots are rejected from the data set due to poor quality. Data points are not rejected on the basis of non-concordance or undesirable fit. Rejection criteria are based around poor crystal or spot quality and include spots which have (due to errors in laser targeting) missed the crystal entirely, missed the planned ablation site and crossed clearly defined zones, missed the crystal site and hit resin, or struck areas of crystal with strong evidence of radiation damage, metamictization, or other undesirable textures. Reasons for exclusion are given in Appendix 2. As it is likely that a number of non-ideal ablation sites will be present in a large dataset it is necessary to verify the quality of analysis after data has been obtained.

3.3.3 Analysis quality

The KDE for SA8 displayed in shows a minor peak later than any seen elsewhere in the study. This peak relates to two grains of young age (later ages than the accepted depositional age of the Applecross Formation) included here to demonstrate some of the criteria for exclusion of grains and analysed spots from final interpretation. It should be noted that the ages produced during analysis are not considered valid grounds for exclusion.

Sample SA8_0309_1 provides a $^{206}Pb/^{238}U$ age of 927+-14Ma, ~53Ma later than deposition of the Applecross Formation. SEM CL (Cathodoluminescence) imagery (Figure 32A) display some alteration and inclusions within the grain, however a zone within the grain appeared viable for analysis and a spot was included. Transmitted light images (Figure 32B) taken post-ablation reveal radiation damage (visible as a brown/orange tint) in the region of the ablated spot. This damage is less visible in the CL images and is likely to have affected the results.

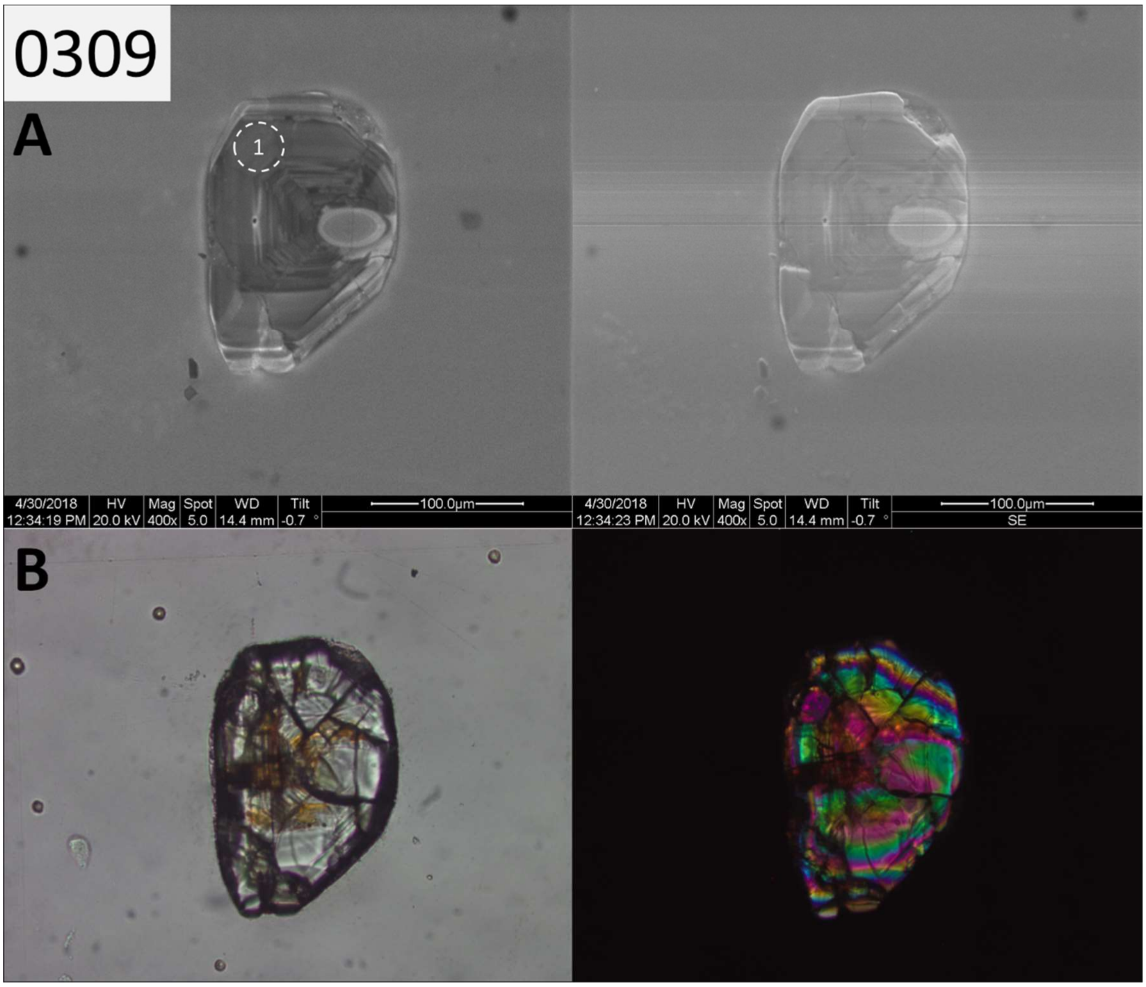

Figure 32: Cathodoluminescence (CL) and transmitted light images of sample SA8_0309. A) CL and secondary electron composite images display several areas of alteration visible as lighter grey areas and inclusions visible as dark spots, often with associate alteration. B) PPL and XPL transmitted light images. The PPL displays a clear brown tint associated with radiation damage in the grain, more visible here than in the CL image. XPL is here used to assess the ablation pit (top left of grain. As the grain has been polished thin there is a risk of cutting through to the grain mount, particularly where ablation is sited near the rim. In small grains birefringence is clearly visible as displayed here and can be used to determine whether a spot has cut through the grain entirely as the resin remains dark; if the ablation pit hits resin this would be visible by a lack of colour.

Sample SA8_0505_1 provided a $^{206}Pb/^{238}U$ age of 814+-14Ma, ~164Ma later than deposition of the Applecross Formation. CL images (Figure 33A) display clear zoning, however areas of alteration are visible around the core zones. An effort was made to analyse a clear area of the grain core, however it is clear from the position of the ablated spot (Figure 33B) that an area of alteration adjacent to the inclusion visible above the spot in both images was ablated during analysis and is likely responsible for the ages calculated.

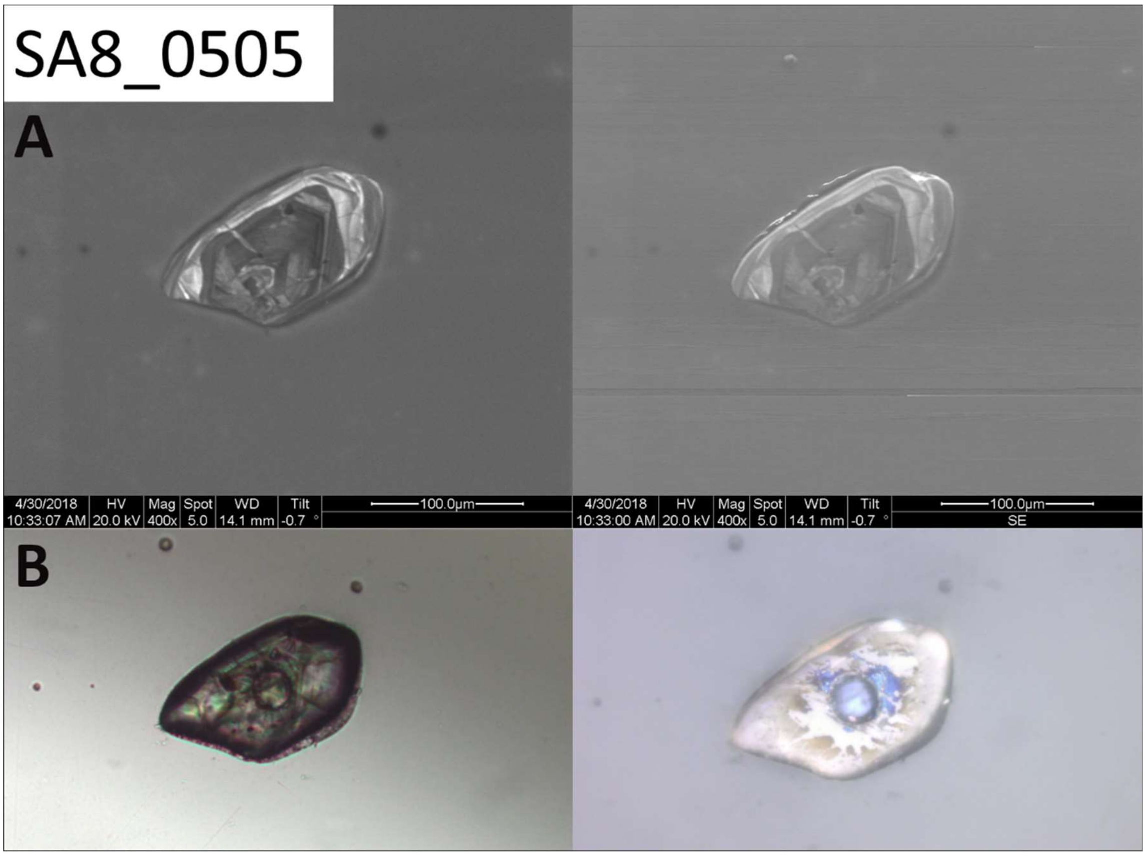

Figure 33: Cathodoluminescence (CL) and transmitted light images of sample SA8_0505. A) CL and secondary electron composite images highlight alteration within the crystal core. Alteration is here visible as lighter areas. Small inclusions are visible as dark spots; note the inclusion in the upper-middle part of the grain. This inclusion has an area of alteration extending around and below it as a light grey smudge. B) Transmitted light and reflected light images showing the final location of the ablation pit. Note the proximity of the pit to areas of ablation visible and described in the CL imagery.

As these analyses are deemed unreliable they are not included in further discussions or KDEs.

Chapter 4 Discussion

4.1 Detrital zircon age data

Kernel density estimates (KDEs) for samples from this study are replotted with a standard bandwidth of 50Ma for ease of comparison (Figure 34). See Chapter 3 for overview of KDEs. Samples are arranged in stratigraphic order to highlight development of and changes in source ages over 1900m of the 4500m succession. Figure 34A compares KDE’s combining both core and rim values for all samples as per the methodology of Zimmermann *et al.* (2018). The comparison highlights the breadth of detrital ages present, with localities typically showing major Palaeo-Mesoproterozoic peaks with additional Archean components, though these are of lower abundance and do not appear in some low quantity samples (see Figure 27, section 3.2.2). The breadth of ages suggests diverse sources for the Applecross Formation. Some reworking is evident from the pebble suite (Williams, 2001; Stewart, 2002), which may account for part of this diversity. Multiple sources suggest that the source area was a large catchment. Figure 34B displays a visualisation of peak age variations within the Mesoproterozoic, Palaeoproterozoic, and Archean. Earliest deposition (SA10) displays a high influx of Proterozoic zircon, dominantly of early Mesoproterozoic age. A number of late-Palaeoproterozoic grains are also present, with a minor peak in the early-Palaeoproterozoic and individual Archean grains.

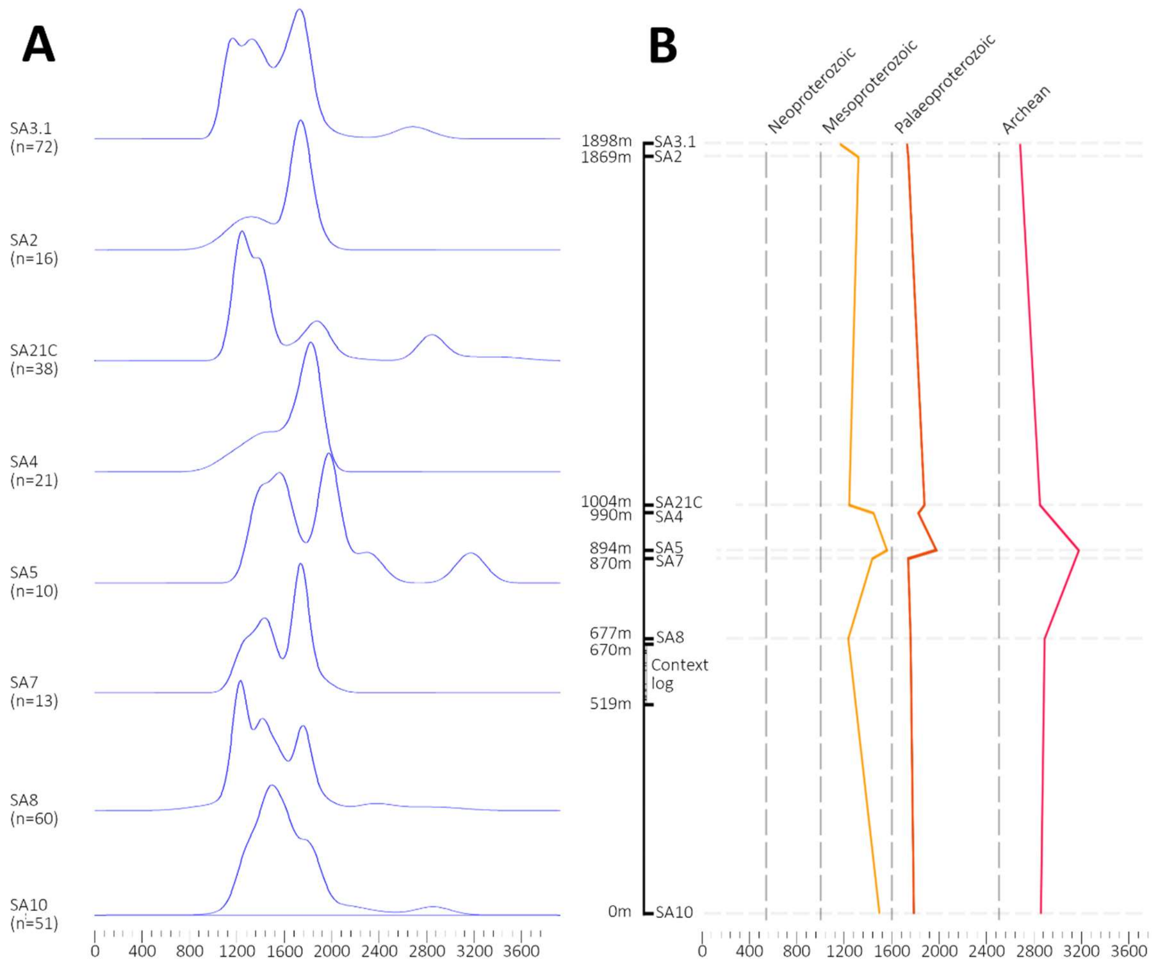

Figure 34:KDE (kernel density estimate) variation through stratigraphy. A) U-Pb detrital zircon KDEs for the Applecross Formation in stratigraphic order. B) Comparative schematic of stratigraphic relationships between samples and variations in dominant peak ages through stratigraphy. See text for full discussion.

~677m stratigraphically above this level a sample of similar size (SA8) shows a consistent influx of late-Palaeoproterozoic age; however the primary Mesoproterozoic peak shifts towards the mid-Mesoproterozoic (~1128Ma)- Figure 34A. Early-Mesoproterozoic grains are present, but no longer dominant. This subtle change may relate to incision of the river system into magmatic rocks. Minor early-Palaeoproterozoic and Archean grains remain present.

Above SA8 the succession includes a greater ratio of older detrital zircon. SA7 (870m) and SA5 (894m) display early-Mesoproterozoic peaks similar to the base of the sequence. The late-Palaeoproterozoic peaks of these samples are dominant and a distinct gap is present between them. SA5 has a Palaeoproterozoic peak at ~1874 Ma which aligns with a paucity of similar ages in SA7. The inferred gap between these samples is likely to relate to the low sample size from the locality. The Archean component of SA5 is older than that seen at the base of the sequence with a peak at ~3069 Ma.

Samples SA4 and SA21C (~100m stratigraphically above) display the reverse trend, with peaks rapidly shifting towards younger ages in each period. SA4 (~990m) contains a comparatively small proportion of Mesoproterozoic detritus with ages spread across the era, a primary peak occurring at ~1715 Ma, in the mid-late Palaeoproterozoic. No Archean grains are present in this sample. SA21C (1004m), conversely, displays a major mid-Mesoproterozoic peak at ~1128 Ma, with a 'shoulder' at ~1260 Ma. A Palaeoproterozoic peak at 1763 Ma is similar in age to the Palaeoproterozoic peak in SA4. An early Archean peak is present at 2731 Ma, similar to Archean peaks seen in SA8 and SA10. One Archean grain with an age of 3346±43Ma is present. If the increase in population ages in SA5 and SA7 relate to incision of the channel into older material in the source area then it is likely that the abrupt decrease in population ages between SA4 and SA21C represent a more dramatic event in the source area, such as channel adjustment by faulting.

Within the uppermost stratigraphy -samples SA2 (~1869m) and SA3.1 (~1898m)- the dominant detrital zircon ages display late-Palaeoproterozoic peaks, with a more even spread between the late-Palaeoproterozoic and mid-late Mesoproterozoic occurring in the larger sample size of SA3.1.

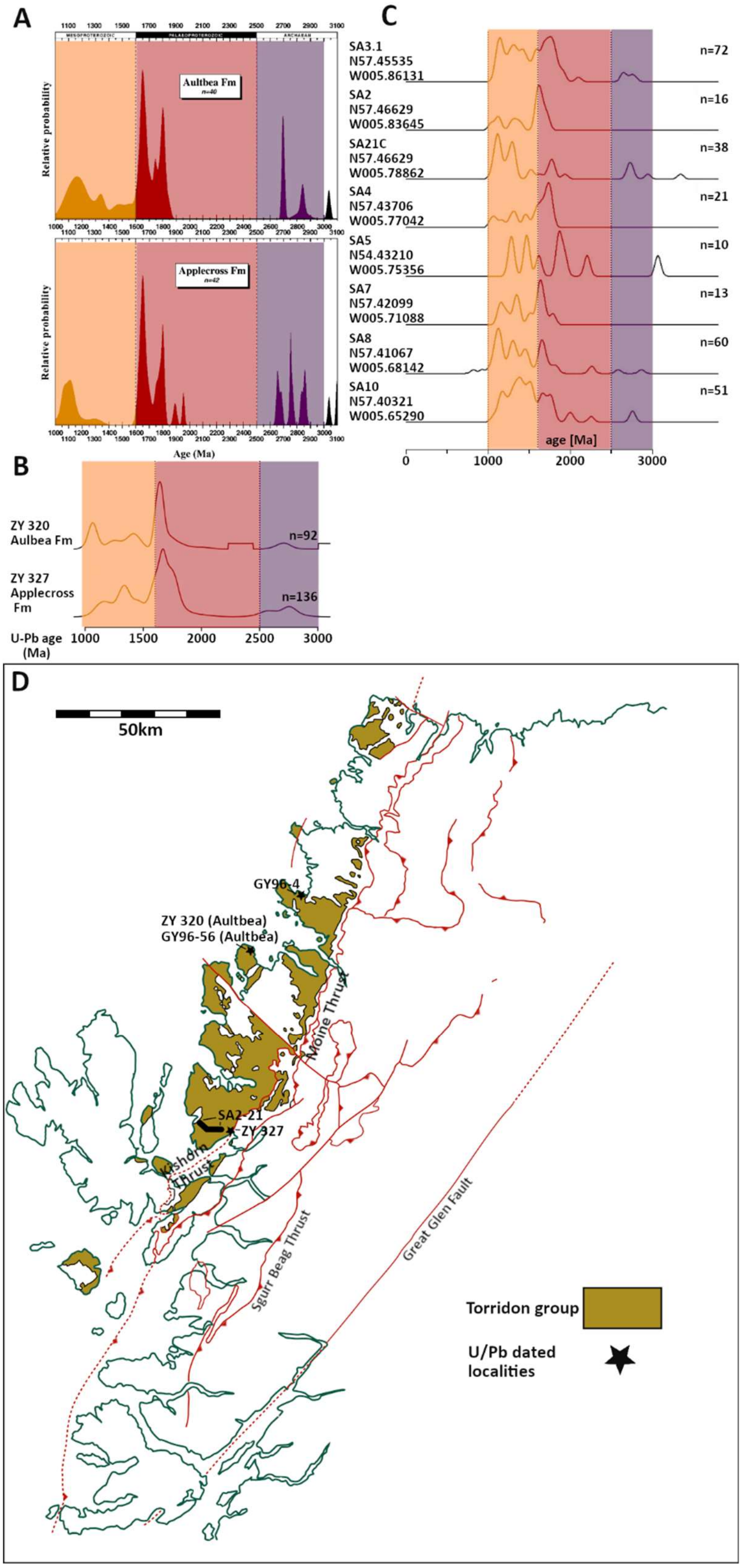

Figure 35: Comparison of detrital zircon suites from localities in the Applecross and Aultbea Formations.. After (Rainbird, Hamilton and Young, 2001; Krabbendam *et al.*, 2017). A) U-Pb detrital zircon PDPs (probability density plot) for the Applecross and Aultbea Formations after (Rainbird, Hamilton and Young, 2001). B) U-Pb detrital zircon KDEs (kernel density estimate) for the Applecross and Aultbea Formations after (Krabbendam *et al.*, 2017). C) U-Pb detrital zircon KDEs for the Applecross Formation (this study). D) Map of the Torridon Group after (Krabbendam *et al.*, 2017) displaying sample localities for plots in A, B, C. Localities are within the Applecross Formation unless otherwise stated. Localities after (Rainbird, Hamilton and Young, 2001; Krabbendam *et al.*, 2017). Comparison of plots shows similar peaks across all areas of the Applecross and Aultbea Formation sampled supporting a single sediment input into the system.

KDE peaks and data throughout samples from this study are similar to those of Rainbird, Hamilton and Young (2001), and of Krabbendam *et al.* (2017) for Applecross and Aultbea samples (Figure 35) taken from Enard Bay and Guinard Bay respectively (Figure 35D),supporting a single well mixed input of detrital zircon into these areas of the Torridon Group. This may have been facilitated by a broad source area with detritus undergoing mixing during prolonged transport in a distal fluvial system.

Figure 36A (multi-dimensional scaling plot/MDS) displays the closest detrital zircon population relationships between samples from this study (within the Applecross Formation). Solid lines indicating nearest neighbours show that position within the stratigraphy is not the key factor determining population similarity; samples SA7 and SA2 are similar in the MDS, but relatively distant stratigraphically. It is likely that small sample size for some localities has influenced population similarity by excluding or exaggerating low abundance detrital zircon populations.

Figure 36B (cumulative distribution function/CDF) is intended to display subtle variations in sample peak ages through the stratigraphy. Krabbendam *et al.* (2017) display a clear younging trend for Palaeoproterozoic peaks through the regional stratigraphy (Loch na Dal fm.- Beinn na Seamraig fm.- Kinloch fm.- Applecross fm.- Aultbea fm.). Samples at a local stratigraphy scale (Figure 36B, this study) do not show such a trend; CDF trends overlap throughout the stratigraphy in no discernable pattern. This trend reinforces consistency in the Applecross source area over the course of deposition and thorough mixing of detrital zircon signatures prior to distribution of sediment within the sampled Applecross sandstones. Applecross Formation CDFs show a similar trend of consistently present Mesoproterozoic peaks with subordinate Palaeoproterozoic peaks and minor Archean populations to that seen in Krabbendam *et al.* (2017), figure 9b, p78.

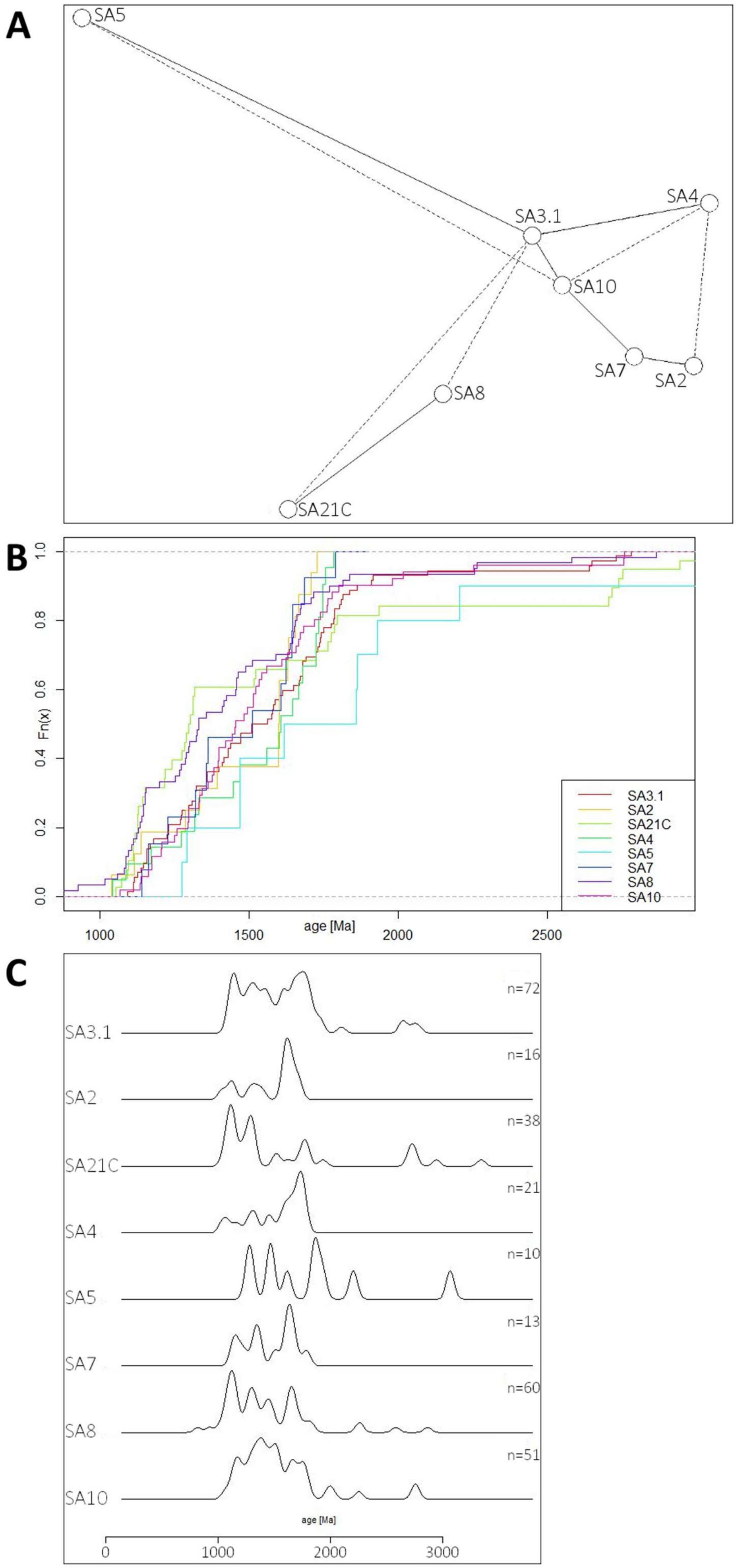
A
SA5
SA4
SA3.1
SA10
SA7
SA2
SA8
SA21C
B
1.0
0.8
0.6
0.4
0.2
0.0
Fn(x)
1000
1500
age [Ma]
2000
2500
SA3.1
SA2
SA21C
SA4
SA5
SA7
SA8
SA10
C
n=72
SA3.1
n=16
SA2
n=38
SA21C
n=21
SA4
n=10
SA5
n=13
SA7
n=60
SA8
n=51
SA10
age [Ma]
0
1000
2000
3000

Figure 36: A) MDS (multi-dimensional scaling) plot, B) CDF (cumulative distribution function) plot, C) KDEs (kernel density estimate) for comparison with Krabbendam *et al.*(2017) p78, fig 9a,b,c. A) solid lines display greater similarity between samples, dashed lines show less similarity. B) CDF displays samples from this study in stratigraphic order. C) KDEs plotted using 'provenance' software, see (Vermeesch, 2012). A, B, and C display only data collected in this study.

Figure 36C displays a replot of sample KDEs in stratigraphic order using the 'provenance' software package specifically for comparison with Krabbendam *et al.* (2017), figure 9c, p 78. See 'Results' sections 3.2.1-3.2.2 (this paper) and associated text for discussion of KDE trends in this study alone. Applecross and Aultbea KDEs from Krabbendam *et al.* (2017) display strong late-mid Palaeoproterozoic peaks, with peaks present across the majority of the Mesoproterozoic. The Applecross Formation displays a minor Archean peak. With the exception of a small number of early-Palaeoproterozoic peaks present in this study, the data presented is in close agreement with the detrital zircon data of Krabbendam *et al.* (2017).

Assessment of detrital zircon populations from the Applecross Formation provides insight into possible source areas of sediment in the Applecross Formation.

4.2 Source areas

Detrital zircon ages from this study and others (see Rainbird, Hamilton and Young, 2001; Cawood *et al.*, 2007; Krabbendam *et al.*, 2017) suggest extensive source areas for detrital zircon in the Applecross Formation distal enough to facilitate thorough mixing of the detrital zircon signal. Transport and deposition may have been directly from a Grenville Orogen axial trunk river system (Nicholson, 1993; Rainbird, Hamilton and Young, 2001; Krabbendam *et al.*, 2017) or via prior deposition in consolidated sediments/metasediments more proximal to the Applecross Formation.

As discussed in **Error! Reference source not found.**1.7.3 (this paper) palaeocurrents and stratigraphy support transport of sediments from the northwest (Gracie and Stewart, 1967; Nicholson, 1993; Williams, 2001; Owen and Santos, 2014; Ielpi and Ghinassi, 2015) with distributive fan formation at Cape Wrath (Williams and Foden, 2011). Braidplain deposits in the southwest of the Applecross Formation (Ielpi and Ghinassi, 2015) may represent the distal deposits of alluvial fans further west (Williams and Foden, 2011). It is necessary to consider all available terranes in order to determine the most likely source area of the Applecross Formation.

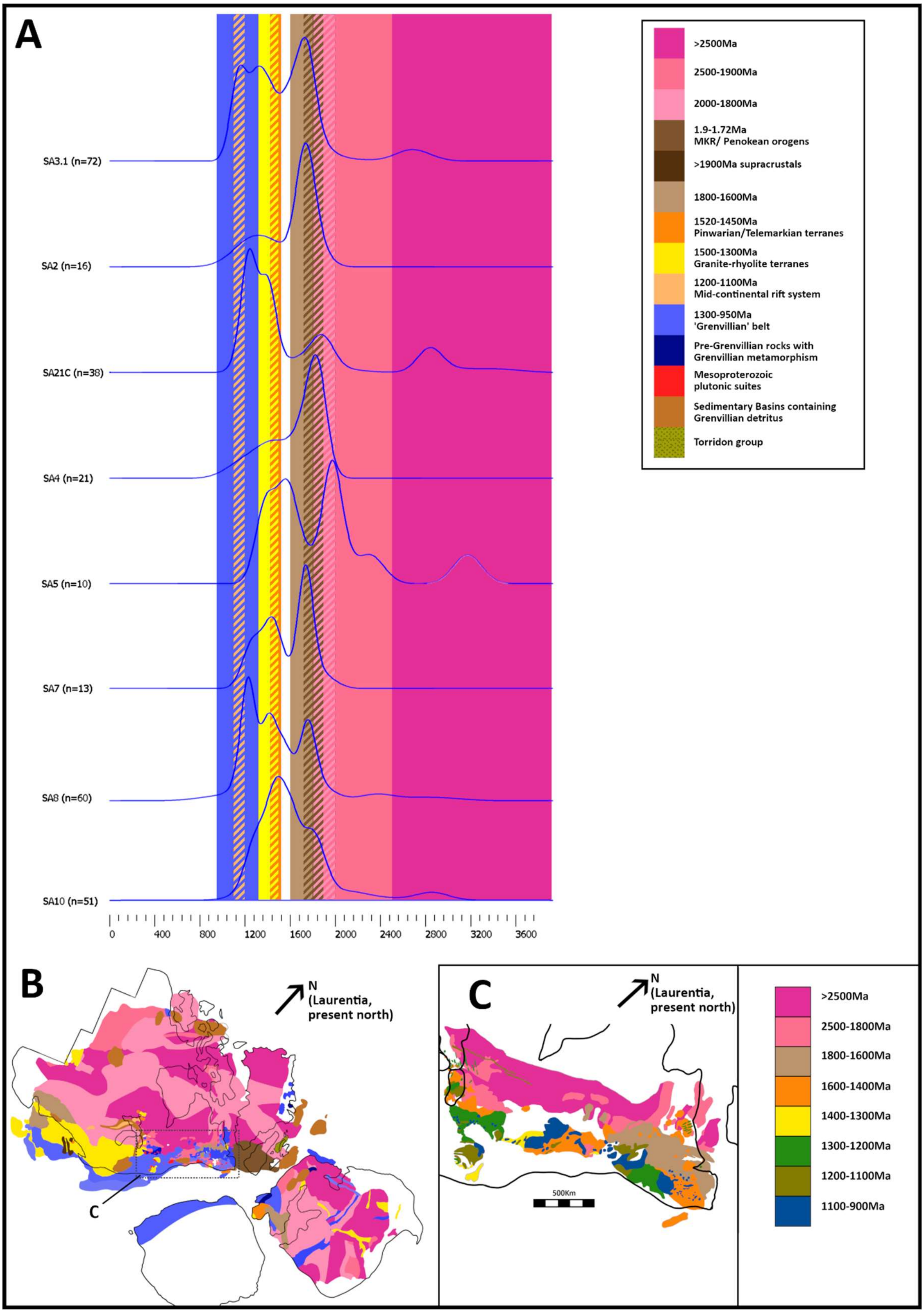

Figure 37: A) Comparison of Applecross detrital zircon ages to Laurentian basement ages. B) Basement ages in Laurentia and Baltica. C) Basement ages in the Canadian sector of the Grenville Orogeny. Correlation of Applecross KDEs (this study) with basement ages in Laurentia.

Potential source areas for the majority of peaks can be found in magmatic and metamorphic basement rocks. A notable gap in magmatism occurs between 1420-1500Ma in Laurentia, peaks in this gap may have been sourced from supracrustal sequences in Laurentia. B) After (Rivers, 1997; Pisarevsky *et al.*, 2003; Li *et al.*, 2008; Cawood *et al.*, 2010; Krabbendam *et al.*, 2017; Rainbird *et al.*, 2017). C) After.(Rivers, 1997).

Terranes suitable to provide sections of the Applecross Formation detrital zircon suite are discussed in detail prior to the construction of a depositional model.

4.2.1 Archean-early Palaeoproterozoic

Archean cratonic rocks are found across Rodinia (see Figure 37B), particularly around the core of the continent away from later accretionary and collisional zones. The Superior craton of Laurentia and the North Atlantic Craton of southern Greenland (Rivers, 1997; Rainbird, Hamilton and Young, 2001) may have contributed Archean detrital zircon to a Laurentian trunk river system supplying the Torridon. The North Atlantic Craton (Greenland) may also have been within the catchment of a more proximal Torridonian source area.

4.2.2 Palaeoproterozoic

Early-mid Palaeoproterozoic orogens provide zircon ages from 2500-2000Ma from Laurentia, Greenland, and are inferred on the Rockall Plateau (Rivers, 1997; Li *et al.*, 2008).

2000-1800Ma cratonic rocks related to final assembly of fragments around Archean nuclei (Cawood *et al.*, 2007) are exposed in central and western Laurentia, Greenland, and the Canadian sectors of the Grenville Orogen. The new Quebec and Torngat Orogens (1920-1790Ma) also occur in the Canadian sector of the Grenville Orogen (Rivers, 1997), providing a more likely source for the low quantities of mid-late Proterozoic zircon than the more substantial suites further west.

Age densities from this study begin to increase at ~1890Ma, around the onset of the 1900-1720Ma Makkovik and Penokean accretions (Rivers, 1997) in Canada and Greenland. Later orogens include the Matazal (1700-1600Ma) terranes in Labrador and more distally in the southwestern sector of Laurentia (Krabbendam *et al.*, 2017; Rainbird *et al.*, 2017). A high concentration of detrital zircon from the Applecross Formation falls within this period and was most likely derived from the more proximal block in the Canadian sector of the Grenville province.

4.2.3 Early Mesoproterozoic age gap

The early Mesoproterozoic in Laurentia is dominated by a gap in magmatism from ~1.6-1.5Ga (Karlstrom *et al.*, 2001) during which few Laurentian zircon sources are formed. This implies a non-Laurentian provenance for detrital zircon of this age in Laurentian basins (Doe *et al.*, 2013) and subsequently it is likely that zircon of this age in the Torridon is derived from recycled sediments sourced from an area of active magmatism outside Laurentia. This is supported by a lull, but not absence, of detrital zircon ages for this period from the Applecross Formation Figure 37A.

Sedimentary successions containing detrital zircon of 1600-1490Ma age include the Purcell Supergroup in the northern Laurentia (Doe *et al.*, 2013) and the Hess Canyon Group of southern Arizona. Deposits more proximal to the western Grenville province include the Yankee Joe and Blackjack Formations deposited around 1488±9Ma (Doe *et al.*, 2012). The Missouri line (Van Schmus *et al.*, 1993) represents a 1500Ma accretionary province in the granite-rhyolite terrane; however no zircon has been dated from the subcrop to fill the magmatic gap (Doe *et al.*, 2012, after (Van Schmus *et al.*, 1993).

4.2.4 Mid-late Mesoproterozoic

Pinwarian (1495-1445Ma, Cawood *et al.*, 2007) terranes in eastern Laurentia (Cawood *et al.*, 2007; Krabbendam *et al.*, 2017) may have contributed to major Mesoproterozoic detrital zircon peaks in the Applecross Formation. The granite-rhyolite terrane of central Laurentia (~1500-1300Ma, Rivers, 1997; Krabbendam *et al.*, 2017; Rainbird *et al.*, 2017) extends along the later Grenville front offering a distal source for detrital zircon of this age.

The period 1300-1100Ma includes a number of terranes forming protoliths to the Grenville Orogen. Elzevirian (1300-1200Ma) rocks include localised intrusions in the Canadian sector, along with the 1100-1200Ma Shawingan terrane (Rivers, 1997; Krabbendam *et al.*, 2017). Further west the 1200-1100Ma midcontinent rift (MCR) in central Laurentia is a possible distal site for reworking of the associated basin sediments (Rivers, 1997; Krabbendam *et al.*, 2017; Rainbird *et al.*, 2017) to be incorporated into the Applecross Formation from a distal source.

4.2.5 Grenville Orogen (1200-900Ma)

Individual zircon forming events of appropriate age such as the Grenville Orogen must also be discussed as they may provide zircon of a given age across a broad geographic area.

Accretion and collision associated with the Grenville-Sunsas-Sveconorwegian Orogens occurred from ~1200-900Ma (Rivers, 1997; Cawood *et al.*, 2007; Krabbendam *et al.*, 2017). The Grenvillian sector represents an abundant source for late Mesoproterozoic-early Neoproterozoic detrital zircon in the Applecross Formation. Final collisional events may have uplifted older protolith terranes, generating a greater potential for denundation of those areas.

4.2.6 Summary

Combined with reconstructions of the supercontinent Rodinia (see section 1.5, this paper) and the Grenvillian setting (see section 1.6, this paper) the sedimentary data (see section 1.7, this paper) indicate transport of detrital zircon from Laurentia, in the west. Figure 37A highlights basement rocks likely to provide detrital zircon to the river systems of Laurentia. Figure 37A overlays the time periods covered by each potential source with KDEs from the Applecross Formation (this study) in stratigraphic order. It is evident from peaks and point clusters that the zircon suite of the Applecross Formation is broad and likely sourced from a number of terranes. Abundant detrital zircon is sourced from terranes with ages between 1800-1600Ma and 1500-1100Ma including the 1500-1300Ma granite-rhyolite terranes (Davidson, 2008), 1200-1100Ma MCR and Mesoproterozoic AMCG plutonic suites (Rivers, 1997). The 1200-900Ma Grenville Orogen (Van Kranendonk and Kirkland, 2013; Krabbendam *et al.*, 2017) provides a portion of detrital zircon of this age alongside older material uplifted as an ‘orogenic lid’ (see Krabbendam *et al.*, 2017). Palaeoproterozoic events including the 1900-1720Ma Penokean-Makkovik accretions (Rivers, 1997) may account for a portion of older detrital zircon peaks.

4.3 Palaeogeographic reconstructions

A number of transport and depositional regimes have been proposed to explain the sedimentology and detrital zircon suite of the Torridonian. Proposals include deposition of the Applecross Formation as proximal fan deposits relating to tectonic movement along the western boundary of the Minch basin (Williams, 2001; Williams and Foden, 2011) and deposition as part of an orogen axial Grenville foreland trunk river system extending from distal sources across Laurentia (Rainbird, Hamilton and Young, 2001; Krabbendam *et al.*, 2017).

Previous models are discussed in the context of new and existing evidence, a revised depositional model for the Applecross Formation is proposed.

4.3.1 Proximal fan deposits

The Torridonian as exposed today is truncated by the Moine Thrust in the east and the Minch Fault in the west. Williams and Foden (2011) suggest a western boundary of deposition along the Outer Hebrides Fault Zone (OHFZ), facilitated by a half-graben basin downthrown on the Minch side of the OHFZ. Ongoing tectonics during deposition are supported by the presence of dilational sand dykes throughout the Applecross Formation and by sediment transport perpendicular to the OHFZ with variable coarseness through the succession, representing periodic reactivation of faults (Williams and Foden, 2011). The tectonic setting for the formation of a half graben at the time of Applecross deposition may be facilitated by periods of extension during the Grenville Orogeny (Rivers, 1997; Cawood *et al.*, 2007). The Cape Wrath Megafan indicates a distributional apex ~30km west of mainland Scotland, in the region of the OHFZ (Williams and Foden, 2011).

Williams and Foden (2011) suggest general fining in the southern Applecross Formation, compared to the Cape Wrath member in the north, indicating that the Applecross, as exposed today, represents an oblique transect of the original basin. In this proposal Cape Wrath represents zones proximal to faulting and the southern Applecross Formation represents areas more distal from fan apexes.

Based on the composition of the Applecross sedimentary rocks and pebble suite (see Moorbath *et al.*, 1967) Williams and Foden (2011) propose a supracrustal source area overlying the Lewisian beyond the OHFZ, noting that proximal drainage in this style (see Figure 38) would require a catchment of at least 10^4km^2.

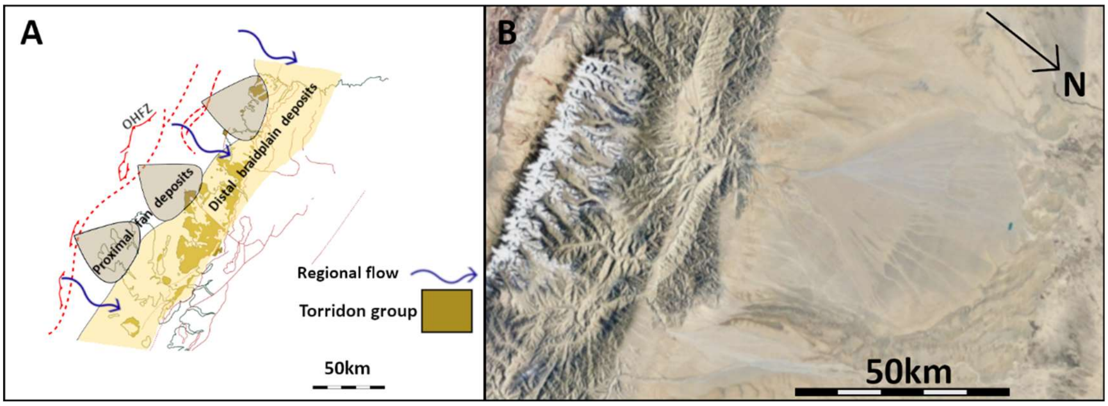

Figure 38: A) Schematic diagram displaying fan and braided deposits laterally filling the Applecross basin. B) Satellite image of fans of similar scale to the Cape Wrath member in the Tarim Basin, China. A) After (Williams, 2001; Williams and Foden, 2011). Williams and Foden (2011) propose a proximal source for the Torridon Group beyond the Minch Fault and Outer Hebrides Fault Zone (OHFZ). Sediment from the relatively uplifted source area form alluvial fan deposits proximally with braidplains forming beyond the fans. B) After (Google Earth V 9.2.71.3, 2018). Displays a fan similar in scale to the proposed Cape Wrath Megafan, however it is relatively isolated with braidplain facies occurring alongside the extant fan. Extant examples such as this lend weight to the proposal of Williams and Foden (2011). A proximal source requires a supracrustal series, for which there is as yet no evidence, to provide the Applecross Formation detrital zircon suite and sediment composition.

Flaws in this proposal include a lack of extant evidence for the supracrustal series, noted by Krabbendam and Rainbird (2012). KDEs for detrital zircon in different areas of the Applecross Formation display similar populations, suggesting that either a previously deposited sediments forming the supracrustal series were highly homogenous, or that mixing of populations was able to occur during transport to a single fan apex. Basement sources are unlikely to be proximal as a greater disparity or lower diversity of detrital zircon ages would be expected, and few basement sources of Grenvillian age are available proximally to generate the detrital zircon peaks seen.

4.3.2 Grenvillian foreland trunk river system

Alternative datasets have lead to the significantly different proposal of a distal source area largely precluding deposition in multiple large scale fan deposits.

The detrital zircon suite of the Applecross Formation (see Results, section 3.2.1) spans an interval of ~1100Ma, between ~1000-2100Ma, indicating an extensive source area. Several authors have identified the Grenville Orogen as a potential source (notably Rainbird, Hamilton and Young, 2001; Krabbendam *et al.*, 2017), suggesting an orogen axial trunk river system in the foreland of the orogen (Figure 39). The presence of pan-continental river systems in Laurentia is well established (Rainbird *et al.*, 1997, 2017). Basement lithologies in the Grenville foreland provide potential sources for almost the entire Applecross detrital zircon suite, with the exception of the ~1600-1520ma gap in Laurentian magmatism (Karlstrom *et al.*, 2001), which may have been provided by reworking of previous basin deposits in the foreland (see section 4.2.3, this paper). Krabbendam *et al.* (2017) suggests a number of terranes in the Canadian sector of the Grenville Orogen as sources.

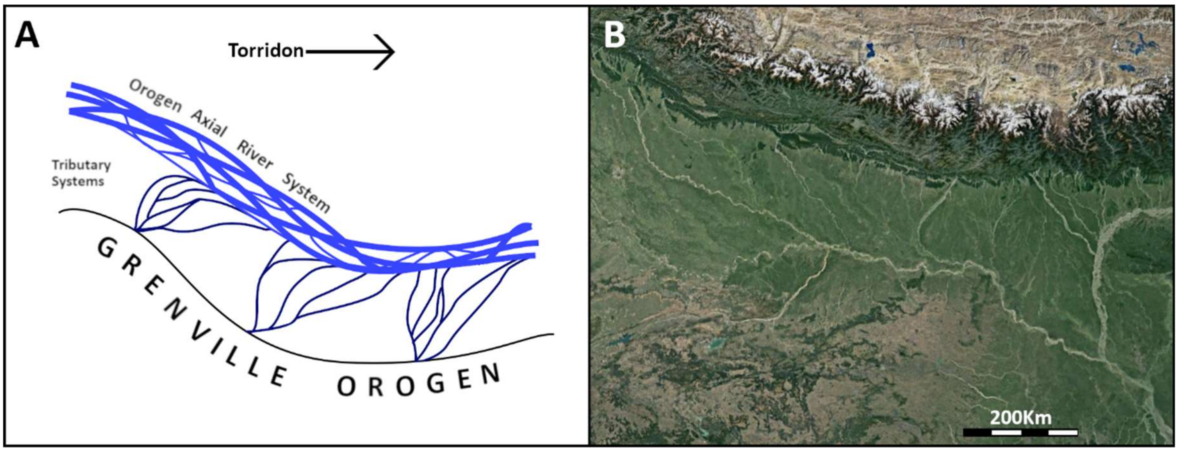

Figure 39: A) Schematic diagram displaying fluvial regime for distal transport of sediment from the Grenville Orogen. B) Modern analogue of (A); satellite image of the Gaghara River, India. A) Small distributary fans fill the Grenvillian foreland basin laterally. Orogen axial drainage occurs when channels reach the forebulge preventing further drainage away from the orogenic front. The fluvial regime of the orogen axial system is unknown as little is preserved in the rock record. B) After (Google Earth V 9.2.71.3, 2015a). Image is oriented to North. Distributary and distributary channels are visible flowing south from the Himalayas into the Gaghara river. Additional channels supply some sediment from the forebulge south of the river.

Krabbendam *et al.* (2017) propose several stages of development in the Grenvillian foreland basin, initiating with a narrow basin during deposition of the upper Sleat underlying the southern Torridon Group. The basin is interpreted to widen by the time of Applecross deposition, accommodating the broader extent of this formation (Krabbendam *et al.*, 2017). This model of transport provides clear, extant sources for the Applecross detrital zircon suite, combined with sufficient transport to provide an evenly distributed signal across the Applecross Formation.

Palaeocurrents within the Applecross Formation flow to the southeast. The model of Krabbendam *et al.* (2017) conversely implies transport to the northeast, although there is scope within the model to accommodate both possibilities. The key issue with this proposal lies in comparative widths of the Applecross Formation (~200km) and proposed orogen axial channel. In order to produce the brainplain facies and alluvial fans of the Applecross Formation the channel would need to supply sediment to the full ~200km width of the formation whilst maintaining flow perpendicular to the exposed outcrop (Figure 40). No provision is made in the model of Krabbendam *et al.* (2017) for a switch from a distal trunk system to the distributive systems required to generate this width of outcrop with similar detrital zircon signatures across the exposure.

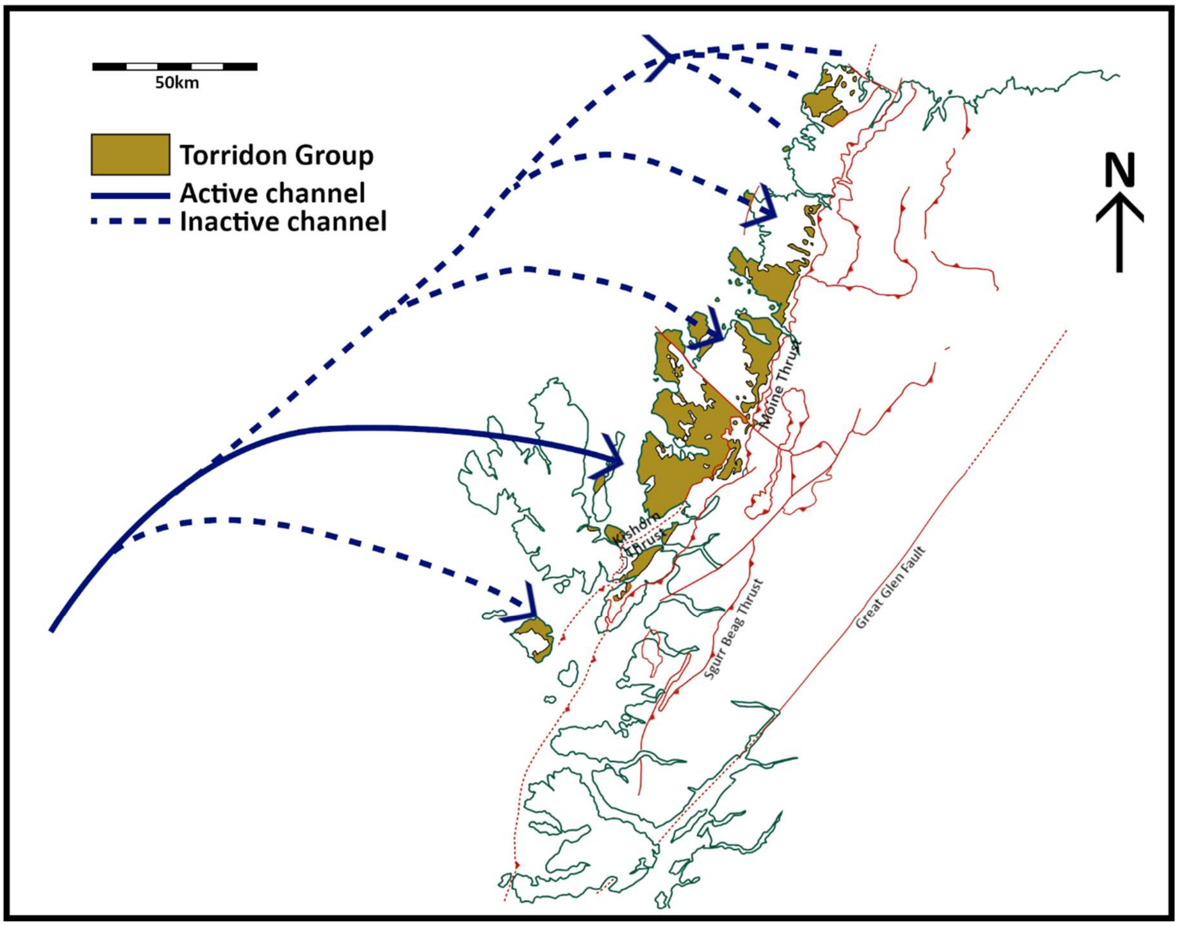

Figure 40: Distribution of trunk river to supply the Applecross Formation. Initial trunk river flow direction after (Krabbendam *et al.*, 2017). Flow from the source area in the Krabbendam *et al.* (2017) model brings sediment from the southwest, perpendicular to observed palaeocurrents in the Applecross Formation. A possible solution is migration of the trunk system over time to deposit the full width of the Applecross Formation as braidplain facies.

4.3.3 Distally sourced distributive system

The key issue in determining the provenance of the Applecross Formation lies in the difficulty of reconciling the sedimentology and the detrital zircon geochronology. The sedimentology suggests a proximal source (Williams, 2001; Williams and Foden, 2011), whereas detrital zircon provenance studies indicate distal transport across Laurentia (Nicholson, 1993; Rainbird, Hamilton and Young, 2001; Owen and Santos, 2014; Krabbendam *et al.*, 2017). Unifying the proposals outlined in the previous sections requires conversion of an established foreland basin river system into a broad distributive system at its distal end. This scenario is initially considered unlikely, as it requires loss of confinement from the foreland basin to enable a distributive system to form.

An extant example of a similar system exists in northwestern Botswana (Figure 41). The Okavango Delta (a large scale alluvial fan) represents a ~150-200km wide inland distributive system fed by a trunk river system sourced from the Angolan Highlands (Hutchins, 1976). The Okavango Delta lies in a region underlain by Archean granitoid gneisses, quartz-feldspar porphyry (Kgwebe Formation), quartzites, shales, and limestones. The structure itself is underlain by fluvial sands and windblown deposits (Hutchins, 1976).

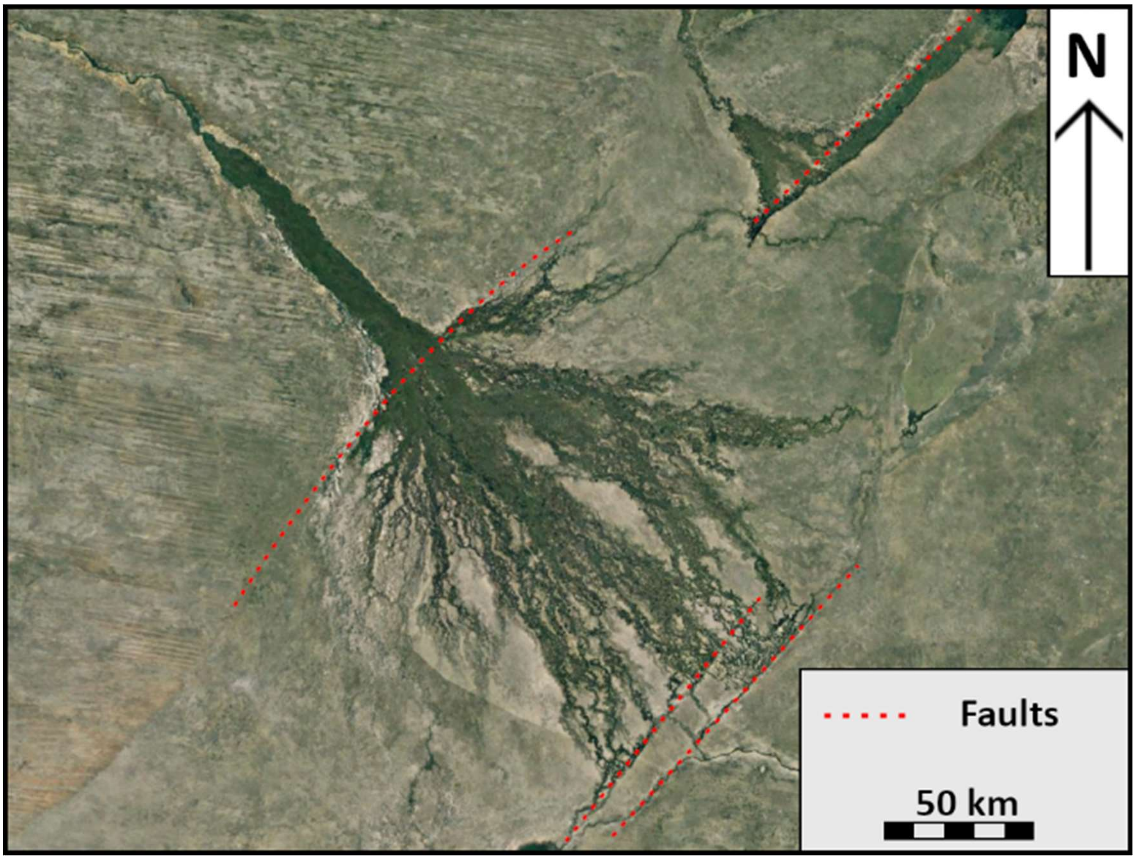

Figure 41: Satellite image of the Okavango Delta, Botswana. Annotations after (McCarthy *et al.*, 1997;image after Google Earth V 9.2.71.3, 2015b). The ‘Panhandle’ and alluvial fan areas of the Okavango Delta, Botswana. Distribution at the distal end of a trunk river system occurs due to change in slope related to extensional tectonics (see (Pike, 1970; Hutchins, 1976; McCarthy, Stanistreet and Cairncross, 1991; McCarthy *et al.*, 1997).

Channel morphology above the delta apex is meandering and bedload dominated, with minimal suspended load and channel width progressively narrowing down the delta (McCarthy, Stanistreet and Cairncross, 1991). Drainage leaks through defined channel levees due to a lack of suspended load to clog the peat which forms the levees (McCarthy, Stanistreet and Cairncross, 1991) to supply the perennial swamps present across the delta, draining overland at right angles to the main channels (Hutchins, 1976; McCarthy, Stanistreet and Cairncross, 1991; McCarthy *et al.*, 1997).

The Okavango Delta distributary system occurs due to a loss of confinement at the apex, with slope variations across the fan determined primarily by bedload and local tectonics (Hutchins, 1976; McCarthy *et al.*, 1997). Several faults alter the reach of seasonal flooding on the delta; seismic evidence indicate that the lower delta may have developed on an an arm of the East Africa rift system (Scholz, 1975; Hutchins, 1976). Although direct evidence is difficult to acquire due to the remote location of the delta and near total superficial cover, gravity surveys suggest some faults may have up to 1000m throw (Hutchins, 1976). The influence of tectonics on local drainage is highlighted by anecdotal reports of the Boro channel becoming a major distributary after an earthquake in 1952 (see Pike, 1970; Wilson, 1973) and by coincidence of slope changes in the delta with major fault lines, including a change in gradient from 1:5570 to 1:3400 at the delta apex where the Gumare Fault facilitates a loss of channel confinement (McCarthy *et al.*, 1997).

Fluvial style in the Okavango is not a perfect match for the high energy braided channels of the Applecross and Aultbea Formations; however a number of similarities can be drawn with the model of Applecross fluvial dynamics proposed by Owen and Santos (2014). A scarcity of mud lenses in the Applecross likely lead to increased permeability (Owen and Santos, 2014). Although clay beds are present underlying the sediments of the Okavango Delta (McCarthy, Stanistreet and Cairncross, 1991) suspended load is minimal, preventing peat levees in the system from becoming clogged and allowing leakage from channel bodies (McCarthy, Stanistreet and Cairncross, 1991). The Applecross Formation contains abundant soft sediment deformation not associated directly with flood events, having likely formed in areas of the system that remained waterlogged while inactive (Owen and Santos, 2014), a setting facilitated by high water tables and seen in the perennial swamps in interchannel areas of the Okavango Delta (Hutchins, 1976; McCarthy, Stanistreet and Cairncross, 1991; McCarthy *et al.*, 1997).

In the Okavango Delta loss of discharge due to evaporation and transpiration allow only 2% of input flow at the apex to leave the fan edge (Nichols and Fisher, 2007). Transpiration is unlikely to have influenced the pre-vegetation Torridonian river systems, however rates of evaporation would not have been hindered by shade and groundcover from plants. Considering the similarities of sediments in the Okavango Delta and the Applecross Formation, it is possible that a similarly high degree of flow loss would occur in a Mesoproterozoic fan similar to the Okavango and subsequently a closed basin setting may not prohibit a terrestrial system.

The differences in morphology can be attributed to a number of possible influences, including the stabilising effect of modern vegetation and greater abundance of clays in the Okavango Delta (McCarthy, Stanistreet and Cairncross, 1991; McCarthy *et al.*, 1997), local climate, and slope angle relating to local tectonics. Although not an ideal sedimentological match for the Applecross, the Okavango Delta demonstrates the viability of a distally sourced, confined trunk river system forming a fan with radius great enough to provide sediment to the entire width of a group such as the Torridonian- extent of Torridonian ~200km (Sutton and Watson, 1964; Williams and Foden, 2011), width of Okavango Delta ~150km (Nichols and Fisher, 2007)-in an extensional tectonic setting (Pike, 1970; Scholz, 1975; Hutchins, 1976; McCarthy, Stanistreet and Cairncross, 1991; McCarthy *et al.*, 1997).

Alluvial fans in the Tarim basin may provide an alternative modern analogue to the Cape Wrath member; fans up to ~50km across contain conglomerates and sands in braided stream deposits (Wei *et al.*, 2013). Proximal fluvial systems similar to those supplying fans in the Tarim basin are unlikely to provide zircon suites as diverse or evenly distributed as those seen in the Applecross Formation without a source area at least $10^4 km^2$ (see Williams and Foden, 2011) distributing from a single apex; fans emanating from multiple apexes would likely show greater variations than present. The aridity of the Tarim basin precludes the waterlogging required to facilitate soft sediment deformation such as that seen in the Applecross Formation.

A mode of deposition similar to that of the Okavango Delta fits the extensional half-graben setting proposed for the Applecross by Williams and Foden (2011) and the well-mixed detrital zircon record of the formation (this study, Rainbird, Hamilton and Young, 2001; Cawood *et al.*, 2007; Krabbendam *et al.*, 2017). The possibility of Applecross deposition in an extensional basin is further supported by periods of extension between Baltica and Laurentia in the period 1000-950Ma (Cawood *et al.*, 2004, 2007), coeval with deposition of the Torridonian. Extension in this period may have led to unconfinement of the orogen axial channel and formation of an alluvial fan on the scale of the Okavango Delta (Figure 42).

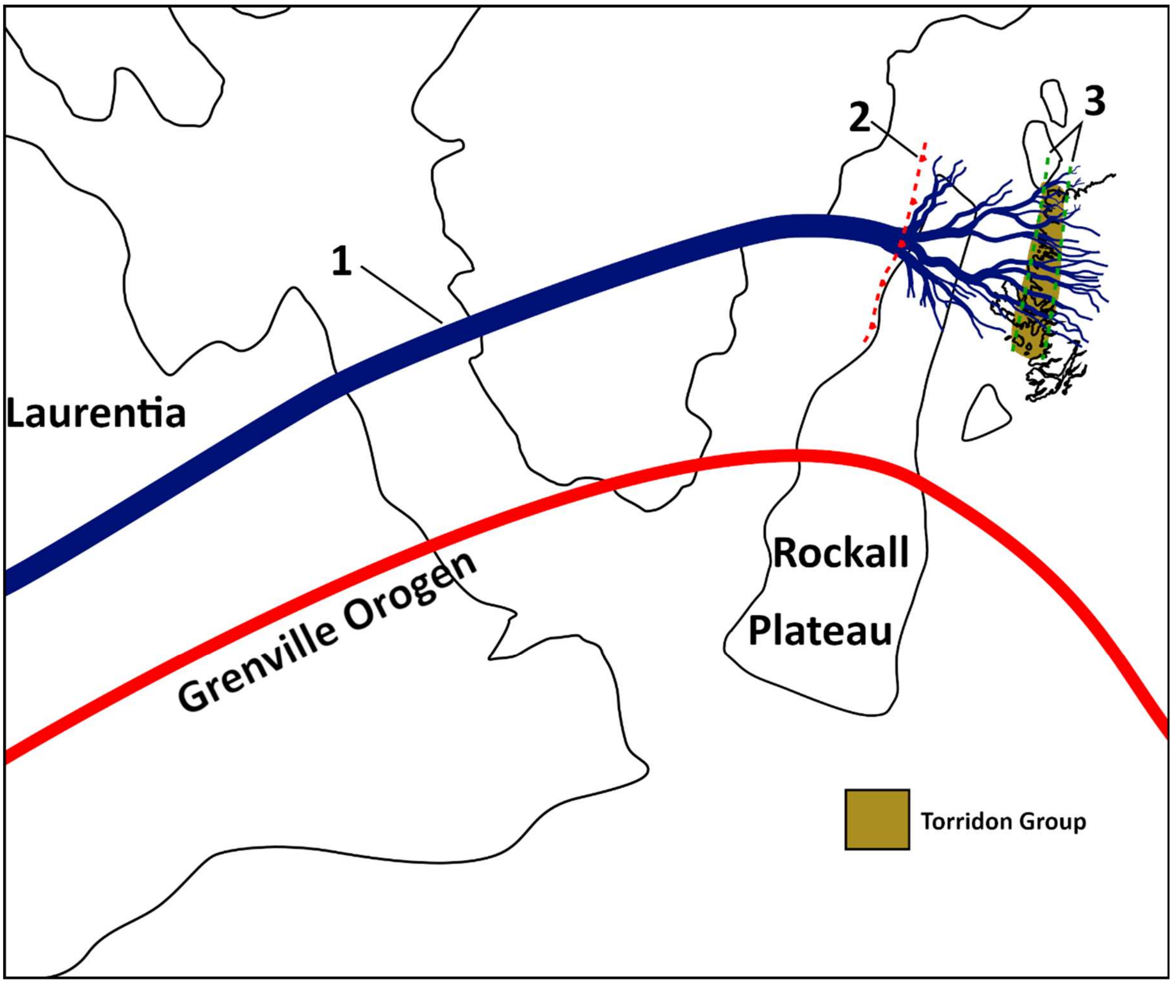

Figure 42: Proposed distributive fluvial regime for deposition of the Applecross Formation. 1) Detrital zircon geochronology supports an extensive Laurentian source area with transport occurring along a Grenvillian foreland basin in a trunk river system. 2) Palaeocurrents and sedimentology in the Applecross Formation support a local distributive system. Extensional faulting may have facilitated formation of a large alluvial fan similar in scale to the Okavango Delta, Botswana. 3) The apparent difference between distributive facies in the northern Applecross Formation and braidplain facies in the southern part of the formation may be an artefact of the

preserved outcrop and the scale of the original fan. A transect across the schematic fan may preserve parallel streams in the south whilst indicating a smaller fan similar to the Cape Wrath member further north. The fan schematic displayed is traced from satellite imagery of the Okavango Delta.

Chapter 5 Conclusions

5.1 Work done

In this study $^{206}Pb/^{238}U$ analysis of detrital zircon from the Applecross Formation is combined with sedimentological context to further elucidate the provenance and depositional style of the sediments. Sampling is undertaken on the Applecross Peninsula, along an east-west transect incorporating ~2000m of Applecross stratigraphy.

Detrital zircon ages display dominant clusters in the early-mid Mesoproterozoic (~1128-1397Ma) and late Palaeoproterozoic (~1630-1873Ma) with minor early Palaeoproterozoic (~2191Ma) and Archean (~2691-3069Ma) clusters. The oldest detrital zircon from sample SA21C has a $^{206}Pb/^{238}U$ age of 3346±43Ma. The youngest detrital zircon from sample SA8 has a $^{206}Pb/^{238}U$ age of 1018±14Ma. Detrital age peaks indicate that ages cover a ~1100Ma interval, from 1000-2100Ma with a lull between 1600-1500Ma, coincident with a major gap in magmatism in Laurentia.

Palaeocurrents and sedimentology within the Applecross Formation support a source to the west or northwest, possibly as part of a distributive system. On this basis Baltica is ruled out as a source, whilst Laurentia, Greenland, and the Rockall Plateau are considered geographically viable in models of continental configuration at the time of deposition.

Viable primary sources for detrital zircon suitable to generate the signature seen in the Applecross Formation are found along the extent of the Grenville Orogen foreland, particularly in the Canadian sector. Supracrustal formations such as the Yankee Joe and Blackjack Formations are suitable to provide reworked zircon within the 1600-1500Ma magmatic gap in Laurentia. Other workers propose a totally removed proximal supracrustal series as the source for the Applecross Formation (see Williams and Foden, 2011). A distal system transporting sediment from the Grenville foreland is preferred, combining elements from multiple previous models.

5.2 Palaeogeographic reconstructions

5.2.1 Previous work

Two primary transport and depositional regimes have been proposed for the Applecross Formation supported by different datasets;

1. Sourcing from proximal supracrustal or removed basement rocks west of the Minch prior to deposition as a series of alluvial fan and braidplain facies is supported by palaeocurrent and sedimentological evidence from the Applecross Formation itself (see Nicholson, 1993; Williams, 2001; Williams and Foden, 2011). This proposal suffers from a lack of evidence for the proposed supracrustal series, which would have been at least 10^4km^2 (Williams and Foden, 2011) to have supplied the volume of sediment required to produce the Applecross Formation.

2. The detrital zircon suite of the Applecross Formation (this study and others, see Rainbird, Hamilton and Young, 2001; Cawood *et al.*, 2007; Krabbendam *et al.*, 2017) supports distal source areas in the foreland of the Grenville Orogen. This extensive source area has the potential to provide the entire observed detrital zircon suite from basement and supracrustal rocks along its length. As yet most authors have not attempted to justify the proposed trunk river system with the distributive fans and broad braidplain facies of the Applecross exposure (see section 4.2 this study). Similar detrital zircon signatures throughout the Applecross support a single source or apex for these channels.

5.2.2 Distally sourced distributive model

On the basis of detrital zircon provenance analysis, evidence for distributive facies in the Applecross Formation, and extensional phases of Grenville tectonics coeval with deposition of the Applecross Formation, a Grenville foreland source area is supported. Transport of sediment occurred in an orogen axial trunk river system, providing thorough mixing of material from various terranes. Deposition occurred during extensional tectonics relating to the rotation of Baltica around Laurentia, which lead to loss of channel confinement to the west or northwest of the Minch Fault and Outer Hebrides Fault Zone (OHFZ) facilitating the formation of a large distributive fan similar in structure to the Okavango Delta, Botswana, or that proposed by Owen and Santos (2014), see Figure 41, Figure 42 section 4.3.3.

5.3 Further work

Further work is required to confirm current models of Applecross deposition:

1. Additional detrital zircon studies within areas of the formation not yet represented are required to determine the validity of a single apex or channel supplying the entire depositional system. Although current datasets support this, only a small number of localities are sampled (Applecross Peninsula- this study, Enard Bay- Rainbird, Hamilton and Young, 2001, Guinard Bay- Krabbendam *et al.*, 2017) see Figure 35, 4.1.

2. Further classification of palaeocurrents from the Applecross Formation as a whole is required to determine the validity of interpretation as a distributive feature. Comparative work on modern sedimentary flow indicators in the Okavango Delta may be beneficial in understanding the evidence seen in the limited (~40km X 200km) outcrop of the Applecross Formation.

3. reassessment of current detrital zircon U-Pb datasets using concordia ages following the methodology of Zimmermann *et al.* (2018) may improve the accuracy of analysis and subsequently provide further insight into potential source areas and sediment flux over the course of deposition.

List of References

Bingen, B. *et al.* (2008) *The Mesoproterozoic in the Nordic countries Evolution of the VMS-bearing Skellefte District View project Mesozoic magmatism in Scania View project*. Available at: https://www.researchgate.net/publication/242751046 (Accessed: 19 September 2018).

Bond, G. C., Nickeson, P. A. and Kominz, M. A. (1984) 'Breakup of a supercontinent between 625 Ma and 555 Ma: new evidence and implications for continental histories', *Earth and Planetary Science Letters*. Elsevier, 70(2), pp. 325–345. doi: 10.1016/0012-821X(84)90017-7.

Cawood, P. A. *et al.* (2004) 'Laurentian provenance and an intracratonic tectonic setting for the Moine Supergroup, Scotland, constrained by detrital zircons from the Loch Eil and Glen Urquhart successions', *Journal of the Geological Society*. Geological Society of London, 161(5), pp. 861–874. doi: 10.1144/16-764903-117.

Cawood, P. A. *et al.* (2007) 'Sedimentary basin and detrital zircon record along East Laurentia and Baltica during assembly and breakup of Rodinia', *Journal of the Geological Society*. Geological Society of London, 164(2), pp. 257–275. doi: 10.1144/0016-76492006-115.

Cawood, P. A. *et al.* (2010) 'Neoproterozoic orogeny along the margin of Rodinia: Valhalla Orogen, North Atlantic', *Geology*. GeoScienceWorld, 38(2), pp. 99–102. doi: 10.1130/G30450.1.

Dalziel, I. W. D., Mosher, S. and Gahagan, L. M. (2000) 'Laurentia-Kalahari Collision and the Assembly of Rodinia', *Source: The Journal of Geology*, 108(5), pp. 499–513. doi: 10.1086/314418.

Davidson, A. (2008) 'Late Paleoproterozoic to mid-Neoproterozoic history of northern Laurentia: An overview of central Rodinia', *Precambrian Research*, 160, pp. 5–22. doi: 10.1016/j.precamres.2007.04.023.

Diwakar, P. K. *et al.* (2014) ‘Ultrafast laser ablation ICP-MS: role of spot size, laser fluence, and repetition rate in signal intensity and elemental fractionation’, *J. Anal. At. Spectrom.*, 29(2), pp. 339–346. doi: 10.1039/C3JA50315A.

Doe, M. F. *et al.* (2012) ‘Basin formation near the end of the 1.60–1.45 Ga tectonic gap in southern Laurentia: Mesoproterozoic Hess Canyon Group of Arizona and implications for ca. 1.5 Ga supercontinent configurations’, *Lithosphere*. GeoScienceWorld, 4(1), pp. 77–88. doi: 10.1130/L160.1.

Doe, M. F. *et al.* (2013) ‘Using detrital zircon ages and Hf isotopes to identify 1.48–1.45 Ga sedimentary basins and fingerprint sources of exotic 1.6–1.5 Ga grains in southwestern Laurentia’, *Precambrian Research*. Elsevier, 231, pp. 409–421. doi: 10.1016/J.PRECAMRES.2013.03.002.

Ellis, M. A. *et al.* (2012) ‘Fracture development and diagenesis of Torridon Group Applecross Formation, near An Teallach, NW Scotland: millennia of brittle deformation resilience?’, *Journal of the Geological Society*, 169(3), pp. 297–310. doi: 10.1144/0016-76492011-086.

Geikie, A. *et al.* (1973) ‘Applecross Solid and Drift 1:63000. British Geological Survey (BGS)’, *1896, reprinted 1954, 1973*. Geological Survey of Scotland, Ordnance Survey. Available at: http://www.bgs.ac.uk/data/maps/maps.cfc?method=viewRecord&mapId=10902 (Accessed: 26 November 2018).

Ghinassi, M. and Ielpi, A. (2017) ‘Precambrian snapshots: Morphodynamics of Torridonian fluvial braid bars revealed by three-dimensional photogrammetry and outcrop sedimentology’, *Sedimentology*. doi: 10.1111/sed.12389.

Google Earth V 9.2.71.3 (2015a) *Gaghara River, India. 26°17’27‘N 78°44’47’E, Eye alt 1574km*. DigitalGlobe. Available at: https://earth.google.com/web/ (Accessed: 14 November 2018).

Google Earth V 9.2.71.3 (2015b) *Okavango Delta, Botswana. 19°34’40‘S 21°00’20’E, Eye alt 526km*. DigitalGlobe. Available at:

https://earth.google.com/web/@0.00000136,-5.6794643,-29.6682112a,22251782.71003962d,35y,0h,0t,0r (Accessed: 14 November 2018).

Google Earth V 9.2.71.3 (no date) *Alluvial fan, Tarim basin, China. 36°45'26'N 83°31'53'E, Eye alt. 223km*. DigitalGlobe. Available at: https://earth.google.com/web/@37.74767479,85.24465251,1811.15238161a,1410652.07237989d,35y,0.0431333h,0t,0r (Accessed: 14 November 2018).

Gracie, A. J. and Stewart, A. D. (1967) 'Torridonian sediments at Enard Bay, Ross-shire', *Scottish Journal of Geology*. Geological Society of London, 3(2), pp. 181–194. doi: 10.1144/sjg03020181.

Hudson, J. D. (2011) 'Discussion on "Multiple post-Caledonian exhumation episodes across NW Scotland revealed by apatite fission-track analysis": Journal, Vol. 167, 675-694', *Journal of the Geological Society*, 168(5), pp. 1225–1226. doi: 10.1144/0016-76492011-030.

Hutchins, D. G. (1976) 'A Summary of the geology, seismicity, geomorphology, and hydrogeology of the Okavango Delta'. Available at: https://books.google.co.za/books?id=AWtPAQAAIAAJ.

Ielpi, A. *et al*. (2017) 'Morphometric convergence between Proterozoic and post-vegetation rivers', *Nature Communications*, 8, p. 15250. doi: 10.1038/ncomms15250.

Ielpi, A. and Ghinassi, M. (2015) 'Planview style and palaeodrainage of Torridonian channel belts: Applecross Formation, Stoer Peninsula, Scotland', *Sedimentary Geology*, 325, pp. 1–16. doi: 10.1016/j.sedgeo.2015.05.002.

Iolite Software | See your data. Know your data (2018). Available at: https://iolite-software.com/ (Accessed: 25 July 2018).

van de Kamp, P. C. and Leake, B. E. (1997) 'Mineralogy, geochemistry, provenance and sodium metasomatism of Torridonian rift basin clastic rocks, NW Scotland', *Scottish Journal of Geology*. Geological Society of London, 33(2), pp. 105–124. doi: 10.1144/sjg33020105.

Karlstrom, K. E. *et al*. (2001) 'Long-lived (1.8–1.0 Ga) convergent orogen in southern Laurentia, its extensions to Australia and Baltica, and implications for refining Rodinia', *Precambrian Research*. Elsevier, 111(1–4), pp. 5–30. doi: 10.1016/S0301-9268(01)00154-1.

Kinnaird, T. C. *et al*. (2007) 'The late Mesoproterozoic-early Neoproterozoic tectonostratigraphic evolution of NW Scotland: the Torridonian revisited', *Journal of the Geological Society*. Geological Society of London, 164(3), pp. 541–551. doi: 10.1144/0016-76492005-096.

Krabbendam, M. *et al*. (2017) 'Tracking the evolution of the Grenvillian foreland basin: Constraints from sedimentology and detrital zircon and rutile in the Sleat and Torridon Groups, Scotland'. doi: 10.1016/j.precamres.2017.04.027.

Krabbendam, M., Prave, T. and Cheer, D. (2008) 'A fluvial origin for the Neoproterozoic Morar Group, NW Scotland; implications for Torridon-Morar Group correlation and the Grenville Orogen foreland basin', *Journal of the Geological Society*, 165(1), pp. 379–394. doi: 10.1144/0016-76492007-076.

Krabbendam, M. and Rainbird, R. H. (2012) 'Discussion: A unifying model for the Torridon Group (early Neoproterozoic), NW Scotland: Product of post-Grenvillian extensional collapse, by GE Williams and J Foden', *Earth-Science Reviews*, 111(1–2), pp. 82–85. doi: 10.1016/j.earscirev.2011.12.003.

Van Kranendonk, M. J. and Kirkland, C. L. (2013) 'Orogenic climax of Earth: The 1.2-1.1 Ga Grenvillian superevent', *Geology*. GeoScienceWorld, 41(7), pp. 735–738. doi: 10.1130/G34243.1.

Li, Z. X. *et al*. (2008) 'Assembly, configuration, and break-up history of Rodinia: A synthesis', *Precambrian Research*, 160, pp. 179–210. doi: 10.1016/j.precamres.2007.04.021.

McCarthy, T. S. *et al*. (1997) 'The gradient of the Okavango fan, Botswana, and its sedimentological and tectonic implications', *Journal of African Earth Sciences*, 24(1–2), pp. 65–78. doi: http://dx.doi.org/10.1016/S0899-5362(97)00027-4.

McCarthy, T. S., Stanistreet, I. G. and Cairncross, B. (1991) ‘The sedimentary dynamics of active fluvial channels on the Okavango fan, Botswana’, *Sedimentology*. Wiley/Blackwell (10.1111), 38(3), pp. 471–487. doi: 10.1111/j.1365-3091.1991.tb00362.x.

Miller, J. A., Matthews, D. H. and Roberts, D. G. (1973) ‘Rock of Grenville Age from Rockall Bank’, *Nature Physical Science*. Nature Publishing Group, 246(152), pp. 61–61. doi: 10.1038/physci246061a0.

Moorbath, S. *et al.* (1967) ‘Geochronological studies on the Torridonian sediments of northwest Scotland’, *Scott. J. Geol.*, 3, pp. 389–412. doi: 10.1144/sjg03030389.

Moorbath, S. (1969) ‘Evidence for the age of deposition of the Torridonian sediments of north-west Scotland’, *Scottish Journal of Geology*. Geological Society of London, 5(2), pp. 154–170. doi: 10.1144/sjg05020154.

Nichols, G. J. and Fisher, J. A. (2007) ‘Processes, facies and architecture of fluvial distributary system deposits’, *Sedimentary Geology*. Elsevier, 195(1–2), pp. 75–90. doi: 10.1016/J.SEDGEO.2006.07.004.

Nicholson, P. G. (1993) ‘A Basin Reappraisal of the Proterozoic Torridon Group, Northwest Scotland’, in *Tectonic Controls and Signatures in Sedimentary Successions*. Oxford, UK: Blackwell Publishing Ltd., pp. 183–202. doi: 10.1002/9781444304053.ch11.

NIST - SRM 610 Trace Elements in Glass (no date). Available at: https://www-s.nist.gov/srmors/view_cert.cfm?srm=610 (Accessed: 24 July 2018).

Owen, G. (1995) ‘Soft-sediment deformation in upper Proterozoic Torridonian sandstones (Applecross Formation) at Torridon, Northwest Scotland.’, *Journal of Sedimentary Research Section A Sedimentary Petrology and Processes*, 65(3), pp. 495–504. doi: 10.1306/D4268108-2B26-11D7-8648000102C1865D.

Owen, G. and Santos, M. G. M. (2014) ‘Soft-sediment deformation in a pre-vegetation river system: The Neoproterozoic Torridonian of NW Scotland’, *Proceedings of the Geologists' Association*, 125(5–6), pp. 511–523. doi: 10.1016/j.pgeola.2014.08.005.

Park, R. G. *et al*. (2002) 'The Hebridean terrane', *The Geology of Scotland. Geological Society, London*, 45, p. 80.

Persano, C. *et al*. (2007) 'Constraints on early Cenozoic underplating-driven uplift and denudation of western Scotland from low temperature thermochronometry', *Earth and Planetary Science Letters*. Elsevier, 263(3–4), pp. 404–419. doi: 10.1016/j.epsl.2007.09.016.

Pike, J. G. (1970) 'Interim technical notes on the hydrology and water resources of the Okavango River system'. FAO/UNDP. Available at: http://agris.fao.org/agris-search/search.do?recordID=XF2017001807 (Accessed: 30 October 2018).

Piper, J. D. A. and Darabi, M. H. (2005) 'Palaeomagnetic study of the (late Mesoproterozoic) Torridon Group, NW Scotland: Age, magnetostratigraphy, tectonic setting and partial magnetic overprinting by Caledonian Orogeny', *Precambrian Research*. Elsevier, 142(1–2), pp. 45–81. doi: 10.1016/j.precamres.2005.09.008.

Pisarevsky, S. A. *et al*. (2003) 'Models of Rodinia assembly and fragmentation', *Geological Society, London, Special Publications*, 206(1), pp. 35–55. doi: 10.1144/GSL.SP.2003.206.01.04.

Rainbird, R. H. *et al*. (1997) 'Pan-Continental River System Draining Grenville Orogen Recorded by U-Pb and Sm-Nd Geochronology of Neoproterozoic Quartzarenites and Mudrocks, Northwestern Canada', *The Journal of Geology*, 105(1), pp. 1–17. doi: 10.1086/606144.

Rainbird, R. H. *et al*. (2017) 'Zircon provenance data record the lateral extent of pancontinental, early Neoproterozoic rivers and erosional unroofing history of the Grenville Orogen', *GSA Bulletin*. GeoScienceWorld, 129(11–12), pp. 1408–1423. doi: 10.1130/B31695.1.

Rainbird, R. H., Hamilton, M. A. and Young, G. M. (2001) 'Detrital zircon geochronology and provenance of the Torridonian, NW Scotland', *Journal of the Geological Society*, 158, pp. 15–27. Available at: http://jgs.lyellcollection.org/content/jgs/158/1/15.full.pdf (Accessed: 6 March 2018).

Rivers, T. (1997) 'Lithotectonic elements of the Grenville Province: review and tectonic implications', *Precambrian Research*, 86(3–4), pp. 117–154. doi: 10.1016/S0301-9268(97)00038-7.

Roberts, D. G. *et al*. (1970) 'New Sedimentary Basin on Rockall Plateau', *Nature*. Nature Publishing Group, 225(5228), pp. 170–172. doi: 10.1038/225170b0.

Roberts, D. G., Ardus, D. A. and Dearnley, R. (1973) 'Precambrian Rocks drilled on the Rockall Bank', *Nature Physical Science*. Nature Publishing Group, 244(132), pp. 21–23. doi: 10.1038/physci244021a0.

Rogers, G. *et al*. (1990) 'Provenance ages of the Torridonian sandstone of NW Scotland using single grain U-Pb zircon analysis'. Available at: https://inis.iaea.org/search/search.aspx?orig_q=RN:22071159 (Accessed: 1 November 2018).

Santos, M. G. M. and Owen, G. (2016) 'Heterolithic meandering-channel deposits from the Neoproterozoic of NW Scotland: Implications for palaeogeographic reconstructions of Precambrian sedimentary environments', *Precambrian Research*. Elsevier, 272, pp. 226–243. doi: 10.1016/J.PRECAMRES.2015.11.003.

Van Schmus, W. R. *et al*. (1993) 'Transcontinental Proterozoic provinces', in Reed, J.C., J. et al. (eds) *Precambrian: Conterminous U.S.* Boulder, Colorado, pp. 171–334.

Scholz, C. H. (1975) 'Seismicity, tectonics and seismic hazard of the Okavango Delta, Botswana'. (np). Available at: http://agris.fao.org/agris-search/search.do?recordID=XF2016071444 (Accessed: 30 October 2018).

Selley, R. C. (1965) 'Diagnostic characters of fluviatile sediments of the

Torridonian Formation {(Precambrian)} of northwest Scotland', *Journal of Sedimentary Research*. JUNE, 35(2), pp. 366–380. doi: 10.1306/74D7127B-2B21-11D7-8648000102C1865D.

Sláma, J. *et al*. (2008) 'Plešovice zircon — A new natural reference material for U–Pb and Hf isotopic microanalysis', *Chemical Geology*. Elsevier, 249(1–2), pp. 1–35. doi: 10.1016/J.CHEMGEO.2007.11.005.

Stewart, A. D. (2002) *The Later Proterozoic Torridonian Rocks of Scotland: their Sedimentology, Geochemistry, and Origin*. London : Elsevier. doi: 10.1144/GSL.MEM.2002.024.

Stewart, A. D. and Donnellan, N. C. B. (1992) 'Geochemistry and provenance of red sandstones in the Upper Proterozoic Torridon Group in Scotland', *Scottish Journal of Geology*. Geological Society of London, 28(2), pp. 143–153. doi: 10.1144/sjg28020143.

Sutton, J. and Watson, J. (1964) 'Some aspects of Torridonian stratigraphy in Skye', *Proceedings of the Geologists' Association*. Elsevier, 75(3), p. 251–IN1. doi: 10.1016/S0016-7878(64)80033-X.

Thomson, K. *et al*. (1999) 'Evidence from apatite fission track analysis for the post-Devonian burial and exhumation history of the northern Highlands, Scotland', *Marine and Petroleum Geology*, 16(1), pp. 27–39. doi: 10.1016/S0264-8172(98)00064-6.

Turnbull, M. J. M., Whitehouse, M. J. and Moorbath, S. (1996) 'New isotopic age determinations for the Torridonian, NW Scotland', *Journal of the Geological Society*. Geological Society of London, 153(6), pp. 955–964. doi: 10.1144/gsjgs.153.6.0955.

Vermeesch, P. (2012) 'On the visualisation of detrital age distributions', *Chemical Geology*. Elsevier, 312–313, pp. 190–194. doi: 10.1016/J.CHEMGEO.2012.04.021.

Vervoort, J. D. *et al*. (2007) 'The magmatic evolution of the Midcontinent rift:

New geochronologic and geochemical evidence from felsic magmatism', *Precambrian Research*. Elsevier, 157(1–4), pp. 235–268. doi: 10.1016/J.PRECAMRES.2007.02.019.

Wei, H.-H. *et al*. (2013) 'Tertiary evolution of the western Tarim basin, northwest China: A tectono-sedimentary response to northward indentation of the Pamir salient', *Tectonics*. Wiley-Blackwell, 32(3), pp. 558–575. doi: 10.1002/tect.20046.

Williams, G. E. (1966) 'Palaeogeography of the Torridonian Applecross Group', *Nature*, (209), pp. 1303–1306.

Williams, G. E. (1969) 'Petrography and Origin of Pebbles from Torridonian Strata (Late Precambrian), Northwest Scotland: Chapter 44: Northwestern Border of the Orogenic Belt'. AAPG Special Volumes, 106, pp. 609–629. Available at: http://archives.datapages.com/data/specpubs/history3/data/a106/a106/0001/0600/0609.htm (Accessed: 5 August 2018).

Williams, G. E. (2001) 'Neoproterozoic (Torridonian) alluvial fan succession, northwest Scotland, and its tectonic setting and provenance', *Geological Magazine*. Cambridge University Press, 138(2), pp. 161–184. doi: 10.1017/S0016756801005064.

Williams, G. E. and Foden, J. (2011) 'A unifying model for the Torridon Group (early Neoproterozoic), NW Scotland: Product of post-Grenvillian extensional collapse', *Earth-Science Reviews*, 108(1–2), pp. 34–49. doi: 10.1016/j.earscirev.2011.05.004.

Wilson, B. H. (1973) 'Some natural and man-made changes in the channels of the Okavango Delta', *Botswana Notes and Records*, 5, pp. 132–153. Available at: https://www-jstor-org.ezproxy.lib.gla.ac.uk/stable/40979388?pq-origsite=summon&seq=1#metadata_info_tab_contents (Accessed: 31 October 2018).

Zimmermann, S. *et al*. (2018) 'Maximising data and precision from detrital zircon

U-Pb analysis by LA-ICPMS: The use of core-rim ages and the single-analysis concordia age', *Sedimentary Geology*. Elsevier, 375, pp. 5–13. doi: 10.1016/J.SEDGEO.2017.12.020.

Chapter 6 Appendices

6.1 Appendix 1

6.1.1 Map of sample localities.

Holmes, Samuel, "Sample localities, Applecross" [PNG map], Scale 1:50000, DiGMapGB-50, [geospatial data], Updated: November 2018, Version 8, British Geological Survey (BGS), UK, Using: EDINA Geology Digimap Service, <http://digimap.edina.ac.uk/>, Created: November 2018

Sampling was undertaken on the Applecross Peninsula, Northwest Scotland (see Figure 35 section 4.1). Natural relief in the chosen study area allows collection of data and samples from a variety of stratigraphic levels. To achieve this a transect of the peninsula is sampled along the main road. Areas of alluvium displayed on the map contain bedrock outcrops and do not preclude sampling in the area, however additional care must be taken to ensure that sampled rocks are in situ where cover is abundant.

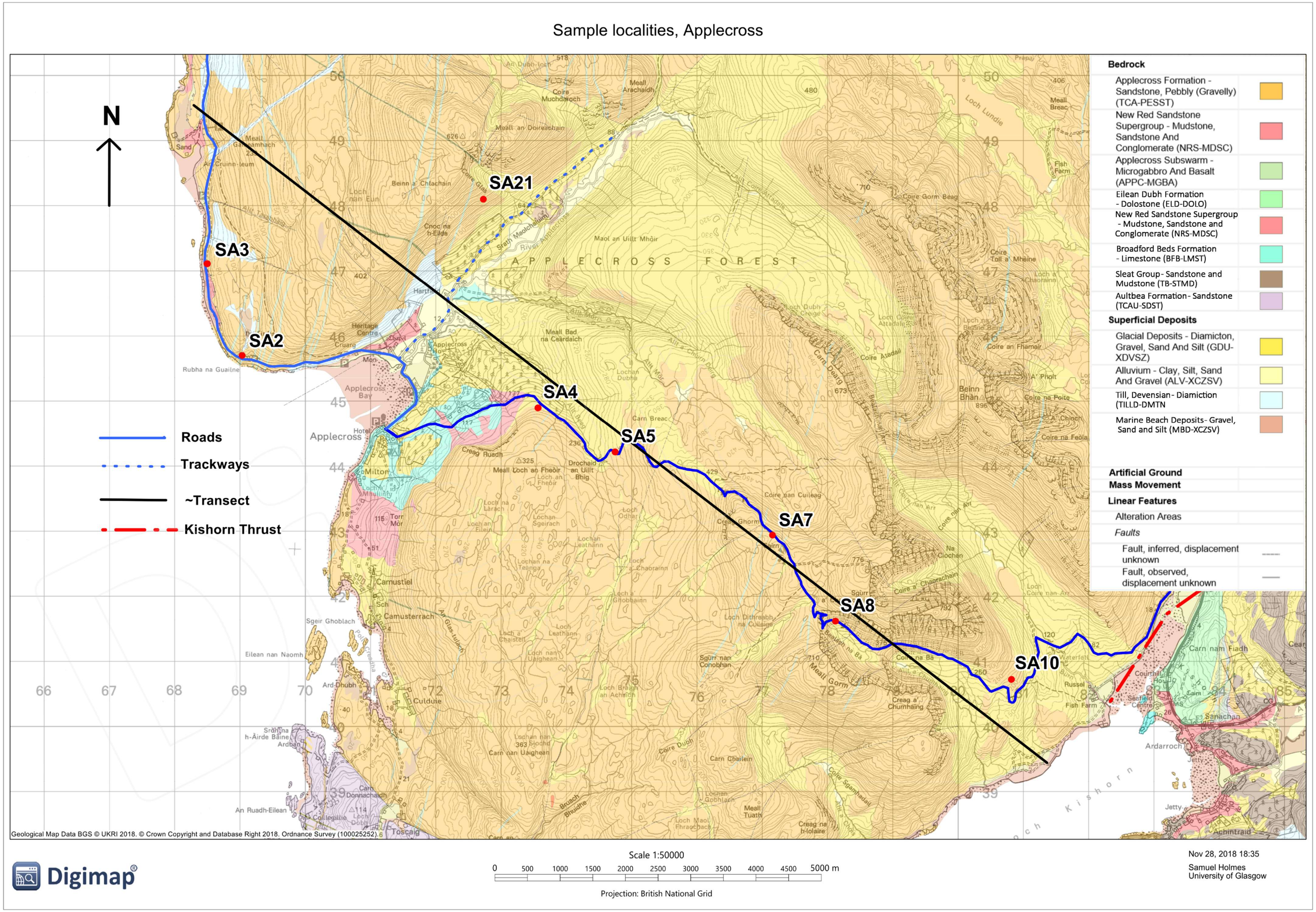

Sample localities, Applecross
N
SA21
SA3
SA2
SA4
SA5
SA7
SA8
SA10
Roads
Trackways
~Transect
Kishorn Thrust
Bedrock
Applecross Formation - Sandstone, Pebbly (Gravelly) (TCA-PESST)
New Red Sandstone Supergroup - Mudstone, Sandstone And Conglomerate (NRS-MDSC)
Applecross Subswarm - Microgabbro And Basalt (APPC-MGBA)
Eilean Dubh Formation - Dolostone (ELD-DOLO)
New Red Sandstone Supergroup - Mudstone, Sandstone and Conglomerate (NRS-MDSC)
Broadford Beds Formation - Limestone (BFB-LMST)
Sleat Group- Sandstone and Mudstone (TB-STMD)
Aultbea Formation- Sandstone (TCAU-SDST)
Superficial Deposits
Glacial Deposits - Diamicton, Gravel, Sand And Silt (GDU-XDVSZ)
Alluvium - Clay, Silt, Sand And Gravel (ALV-XCZSV)
Till, Devensian- Diamiction (TILLD-DMTN)
Marine Beach Deposits- Gravel, Sand and Silt (MBD-XCZSV)
Artificial Ground
Mass Movement
Linear Features
Alteration Areas
Faults
Fault, inferred, displacement unknown
Fault, observed, displacement unknown
APPLECROSS FOREST
Applecross
Geological Map Data BGS © UKRI 2018. © Crown Copyright and Database Right 2018. Ordnance Survey (100025252).
Scale 1:50000
0 500 1000 1500 2000 2500 3000 3500 4000 4500 5000 m
Projection: British National Grid
Nov 28, 2018 18:35
Samuel Holmes
University of Glasgow
Digimap

6.2 Appendix 2

6.2.1 LA-ICP-MS data tables

LA-ICP-MS U/Pb data table for detrital zircon containing, from left to right;

- Sample ID structured as <sample number><_grain number>_<spot number>.
- U/Pb, U/Th, and Pb/Pb isotope ratios corrected for background and gas blank. Ratios and errors for $^{206}Pb/^{238}U$, $^{207}Pb/^{235}U$, and $^{207}Pb/^{206}Pb$ are included.
- Calculated ages and deviation for $^{206}Pb/^{238}U$, $^{207}Pb/^{235}U$, and $^{207}Pb/^{206}Pb$.
- U, Th, and Pb concentrations in PPM.
- U/Pb final ages.
- % Discordance between $^{206}Pb/^{238}U$, and $^{207}Pb/^{206}Pb$ ages. In a closed system both ages should be the same- or concordant- discordance is a measure of similarity, the nearer discordance is to zero the more reliable the ages are likely to be. Percentage discordance alone is only an indicator of reliability and further investigations are made into highly discordant grains.
- Column 'X' contains information on the location of each analysed spot within either the core or rim of the grain. Spots marked 'C' are in the grain core, whilst spots marked 'R' are in the outer zones of the grain.
- The Notes column contains information on the quality of each grain or spot. Notes are brief and refer primarily to reasons for exclusion of a grain from further analysis or interpretation.

Spot name	206 /238	206 /238 2SE	207 /235	207 /235 2SE	207 /206	207 /206 2SE	U/Th Ratio	U/Th 2SE	206/204 Pb ratio	206 /204 2SE	U PPM	U PPM 2SE	Th PPM	Th PPM 2SE	Pb PPM	Pb PPM 2SE	206 /238 Age	206 /238 Age 2SE	207 /235 Age	207 /235 Age 2SE	207 /206 Age	207 /206 Age 2SE	% Discord-ance	X	Notes
SA2_0000_1	0.2928	0.0042	3.99	0.15	0.0956	0.0037	2.41	0.03	42000	25000	283.3	3.2	116.5	1.5	246.4	9.3	1654	21	1614	31	1476	76	-12.06	C	
SA2_0001_1	0.2187	0.0037	3.6	0.15	0.117	0.0049	0.913	0.011	106000	26000	276.6	3	297.5	3.7	399	10	1274	19	1532	34	1825	82	30.19		Cuts zones
SA2_0003_1	0.244	0.011	2.93	0.46	0.085	0.014	1.296	0.033	75000	19000	25.63	0.49	19.4	0.46	35.8	3.1	1395	57	960	160	430	340	-224.42	R	
SA2_0004_1	0.2816	0.0046	4.74	0.19	0.119	0.0049	1.209	0.015	261000	52000	224.9	2.8	180.5	2.6	383	13	1598	23	1753	33	1873	75	14.68		Cuts zones

SA2_0004_2	0.282	0.0053	4.24	0.19	0.106	0.0048	0.97	0.013	153000	41000	163.2	3.4	164.1	4.1	300	13	1599	27	1660	38	1660	91	3.67	R	
SA2_0005_1											0.253	0.074	-0.058	0.082	405	21									metamictization
SA2_0006_1	0.191	0.011	1.66	0.58	0.067	0.026	1.323	0.035	12400	5800	24.79	0.68	19.26	0.57	43.4	5.2	1115	58	1230	150	-830	650	234.34	C	
SA2_0006_2	0.171	0.013	-0.1	1.2	0.014	0.092	1.09	0.049	-730	780	10.7	0.25	10.44	0.39	15.9	4.3	1002	69	1300	220	-5800	1800	117.28		Cuts resin
SA2_0008_1	0.304	0.005	4.41	0.18	0.1028	0.0044	3.722	0.057	-76000	26000	129.4	1.9	35.97	0.61	134.1	7	1709	25	1693	34	1584	85	-7.89	C	
SA2_0100_1	0.1931	0.0028	2.21	0.1	0.08	0.0036	2.083	0.023	30000	25000	239.8	2.6	119.6	1.6	239.8	9.1	1137	15	1165	32	1115	91	-1.97	R	
SA2_0100_2	0.1894	0.0039	2.46	0.16	0.0928	0.0062	0.5975	0.0083	-29000	16000	130.1	3.6	222.6	4.8	332	15	1117	21	1248	47	1350	130	17.26		Cuts zones
SA2_0105_1	0.2907	0.004	4.05	0.16	0.0983	0.0038	3.511	0.046	-105000	46000	224.8	5.4	65.6	1.9	225.5	9.6	1646	20	1624	32	1513	75	-8.79		Radiation damage
SA2_0106_2	0.2304	0.0045	2.94	0.16	0.0912	0.005	2.326	0.032	-54000	22000	135.3	1.7	58.41	0.91	149.9	7.2	1335	24	1362	43	1290	120	-3.49	R	
SA2_0107_1	0.2749	0.004	4.05	0.17	0.105	0.0045	1.821	0.021	460000	240000	203.7	2.1	110.5	1.3	296	11	1564	20	1624	34	1626	83	3.81		Cuts resin
SA2_0108_1	0.2823	0.0051	3.97	0.18	0.1002	0.0049	3.002	0.047	30000	22000	150.9	1.8	49.31	0.75	145.2	7.2	1601	26	1610	39	1529	92	-4.71	R	
SA2_0108_2	0.2882	0.005	4.26	0.19	0.1047	0.0046	1.75	0.019	30000	34000	169.4	2.5	93.7	1.4	308	12	1631	25	1656	37	1622	86	-0.55	R	
SA2_0201_1	0.2775	0.0047	3.94	0.22	0.1003	0.0057	1.998	0.033	-600000	220000	127.7	2.8	63	1.9	178.9	9	1577	24	1585	47	1490	120	-5.84		Fracture, metamictization
SA2_0201_2	0.2821	0.0045	4.01	0.18	0.1012	0.0046	2.167	0.028	97000	57000	154.9	1.8	70.7	1	235.9	9.7	1600	23	1620	37	1550	92	-3.23	R	
SA2_0204_1	0.2216	0.0069	1.72	0.37	0.056	0.013	0.4662	0.0073	-80000	31000	34.31	0.53	73.49	0.84	208.5	9.2	1286	36	890	170	-260	390	594.62	R	
SA2_0205_1											0.625	0.088	1.76	0.11	14	4.7									Readings too low to calculate age
SA2_0206_1	0.1792	0.0026	3.314	0.06	0.1311	0.0026	1.191	0.012	640000	600000	865	10	755	12	1915	36	1062	14	1482	14	2094	35	49.28		Cuts zones
SA2_0206_2	0.249	0.0043	4.11	0.14	0.1166	0.0038	2.417	0.034	380000	160000	276.7	9	118.9	3.1	373	15	1432	22	1639	28	1858	61	22.93		Cuts resin
SA2_0207_1	0.2226	0.004	2.72	0.14	0.087	0.0047	1.258	0.013	216000	93000	196.7	3	165	2.8	354	13	1294	21	1305	42	1200	120	-7.83		Radiation damage
SA2_0208_1	0.2693	0.0037	4.03	0.13	0.1053	0.0033	1.408	0.032	-1310000	660000	471.3	5	364	10	531	15	1536	19	1625	26	1692	55	9.22		Cuts resin
SA2_0301_1	0.3075	0.0044	4.67	0.15	0.1068	0.0034	1.937	0.02	-7000000	2200000	335.7	3.5	184	2.1	374	10	1727	21	1746	27	1703	64	-1.41	R	
SA2_0301_2	0.3106	0.0045	4.86	0.16	0.1109	0.0038	1.58	0.018	2240000	750000	314.6	3.3	203.9	2.4	322	11	1742	22	1785	28	1776	62	1.91		Cuts zones
SA2_0303_1	0.2208	0.0054	3.06	0.29	0.098	0.0095	1.262	0.017	91000	59000	101	1.3	79.8	1.1	155	8.1	1284	29	1342	80	1180	230	-8.81		Cuts resin

SA2_0305_1	0.1266	0.002	2.683	0.086	0.1506	0.005	3.528	0.081	62000	87000	648	9.8	185.5	6.4	798	19	768	11	1314	24	2306	59	66.70		Cuts resin
SA2_0306_1											-0.315	0.076	-0.178	0.089	-11	3.5									Cuts resin
SA2_0306_2											-0.083	0.08	-0.01	0.11	-4.3	4									Cuts resin
SA2_0307_1	0.2379	0.0037	3.94	0.15	0.1174	0.0046	0.837	0.013	99000	95000	253.4	5.4	294.4	4.4	392	15	1374	19	1608	31	1860	72	26.13		Cuts resin
SA2_0308_1	0.3228	0.0044	5.16	0.17	0.1131	0.0035	1.573	0.027	-250000	170000	288.8	3.2	183.3	2.9	491	12	1802	22	1829	28	1808	57	0.33		Cuts resin
SA2_0401_1	0.224	0.012	0.89	0.78	0.021	0.025	1.346	0.04	-18100	8800	21.33	0.43	16.23	0.42	30.8	4.9	1292	60	1510	150	-2480	820	152.10		Metamictization
SA2_0406_1	0.208	0.024	5.4	3.1	0.05	0.77	13.2	7.2	-38000	53000	7.24	0.29	1.52	0.19	20.6	5	1160	130	2430	240	-14400	9300	108.06		Cuts resin
SA2_0406_2											0.029	0.09	-0.19	0.11	-4.5	4.2									Cuts resin
SA2_0407_1	0.1889	0.0027	2.917	0.094	0.1094	0.0034	3.476	0.056	-380000	150000	531.2	5.5	157.7	3.3	437	14	1116	15	1376	24	1757	59	36.48		Cuts resin
SA2_0408_1	0.2209	0.0049	2.66	0.17	0.0867	0.0055	1.291	0.02	-111000	47000	167.6	2	131	1.7	187.2	7.6	1284	26	1281	49	1150	130	-11.65		Cuts inclusion
SA2_0409_2	0.5	0.12	15.2	9.6	0.49	0.58	0.87	0.11	-3600	3000	2.96	0.23	3.62	0.25	15.5	5.5	2320	490	3330	230	-4100	5300	156.59		Cuts resin
SA2_0500_2	0.2908	0.0042	4.6	0.18	0.1127	0.0043	1.501	0.015	-123000	62000	238.5	2.7	153.7	1.8	340	13	1647	22	1727	32	1785	69	7.73		Cuts resin
SA2_0500_3	0.2129	0.004	3.86	0.17	0.1275	0.0051	0.815	0.016	-80000	51000	262.9	9.9	310	13	443	20	1243	21	1590	35	2028	74	38.71		Cuts resin
SA2_0501_1	0.2989	0.0055	4.63	0.21	0.1106	0.0051	2.825	0.043	220000	85000	152.3	1.7	52.23	0.79	161.8	7.9	1683	27	1728	38	1716	89	1.92		Cuts resin
SA2_0503_1	0.2956	0.0055	4.26	0.21	0.1015	0.0051	1.395	0.018	-19000	29000	153.4	1.6	107.6	1.3	218.8	9.9	1667	27	1657	43	1583	98	-5.31	R	
SA2_0503_2	0.2839	0.0054	4.54	0.22	0.1141	0.0053	1.387	0.022	-700000	300000	144.6	2.2	104.2	2.1	175.8	8.5	1609	27	1710	41	1785	87	9.86		Cuts resin
SA2_0505_1											-0.0696	0.0017	0.08849	0.0006	6	1.3									Cuts resin
SA2_0506_1	0.1842	0.004	2.09	0.14	0.0802	0.0052	2.007	0.033	103000	31000	157	2.3	80.6	1	115.6	6.2	1088	22	1098	47	990	150	-9.90		Cuts resin
SA2_0506_3	0.1932	0.0033	2.137	0.097	0.0789	0.0035	2.253	0.031	163000	49000	280.6	2.9	130.5	1.9	208.4	7.9	1138	18	1146	33	1072	96	-6.16		Cuts zones
SA2_0508_1	0.185	0.0037	4.06	0.16	0.1595	0.0067	1.019	0.019	78000	24000	187.4	5.2	190.1	3.7	320	13	1093	20	1635	34	2401	73	54.48		Cuts resin
SA2_0509_1	0.2878	0.0047	4.07	0.15	0.1	0.0036	1.385	0.015	996000	230000	244.9	2.9	181.8	2.1	467	11	1629	24	1630	29	1565	68	-4.09	R	
SA2_0509_2	0.1426	0.002	3.7	0.088	0.1844	0.0045	0.6136	0.0054	196000	43000	683	9.3	1130	18	1328	29	859	11	1563	20	2671	41	67.84		Cuts resin
SA2_0602_1	0.338	0.014	4.65	0.53	0.1	0.012	1.571	0.058	25500	7600	26.1	1.6	17.4	1.1	38.8	4	1865	65	1470	140	1050	270	-77.62		Cuts resin
SA2_0604_1	0.2297	0.0036	4.71	0.16	0.1455	0.0051	0.9819	0.0097	162000	43000	287.2	4.2	290.5	3.9	547	14	1332	19	1750	29	2248	63	40.75		Cuts resin
SA2_0605_1	0.2819	0.0052	4.3	0.15	0.11	0.0041	1.12	0.013	140000	40000	197.2	2.7	175.7	2.3	461	13	1598	26	1682	30	1736	69	7.95	C	

SA2_0605_2	0.2058	0.0035	3.47	0.14	0.1194	0.0047	1.091	0.014	119000	27000	268.4	3.1	248.4	3.9	535	15	1205	19	1506	31	1896	72	36.45		Cuts resin
SA2_0606_1											-0.0186861	0.0000079	-0.022691	0.000071	2.1	1.2									Cuts resin
SA2_0608_1	0.3837	0.008	18.47	0.62	0.3404	0.0093	1.46	0.028	53000	13000	130.7	2.5	92.4	3	1420	63	2089	37	2995	33	3646	42	42.70		Cuts resin
SA2_0701_1	0.1483	0.0018	2.798	0.067	0.1338	0.0029	5.32	0.12	303000	71000	1685	19	344	10	1366	56	891	10	1348	18	2125	39	58.07		Radiation damage
SA2_0702_1	0.1824	0.0074	1.8	0.23	0.0735	0.0097	4.32	0.13	8100	3600	53.42	0.88	13.51	0.43	19	2.6	1074	40	882	90	430	260	-149.77		metamictization
SA2_0702_2	0.178	0.0061	1.55	0.2	0.0648	0.0089	1.765	0.038	17200	4900	54.93	0.88	33.82	0.71	46.1	3.9	1056	33	803	92	210	260	-402.86		Cuts resin
SA2_0704_1	0.1753	0.0085	1.94	0.29	0.085	0.014	0.919	0.021	6600	2200	38.22	0.82	45.4	1	44.5	3.9	1039	47	870	110	440	320	-136.14	C	
SA2_0704_2											0.055	0.023	0.004	0.016	-0.37	0.72									Cuts resin
SA2_0705_1	0.27	0.005	3.88	0.17	0.1027	0.0045	1.029	0.015	80000	22000	194.2	2.5	189.6	3.2	340	11	1539	25	1581	38	1570	92	1.97		Cuts resin
SA3_1_0001_1	0.325	0.0078	4.55	0.24	0.1044	0.006	0.933	0.013	34000	12000	81	1.7	86.8	1.8	206.7	8.5	1809	38	1716	47	1560	110	-15.96	C	
SA3_1_0006_1	0.2528	0.0035	4.386	0.092	0.1255	0.0025	1.101	0.02	222000	56000	600.1	6.3	548	12	1009	19	1452	18	1703	17	2016	36	27.98		Cuts zones
SA3_1_0008_1	0.2016	0.0029	3.624	0.099	0.1307	0.0035	0.3935	0.0071	99000	26000	423	16	1046	26	942	36	1183	16	1545	21	2077	50	43.04		Cuts resin
SA3_1_0008_2	0.1747	0.0039	3.82	0.18	0.1598	0.0075	0.1675	0.0033	27600	9000	163.4	7.1	943	27	425	16	1037	21	1573	38	2367	85	56.19		Fracture, radiation damage
SA3_1_0103_1	0.3182	0.0061	4.55	0.18	0.1048	0.0041	0.7573	0.0078	49000	17000	159.6	2.5	206.4	3.2	603	14	1778	30	1723	34	1643	77	-8.22		Metamictization
SA3_1_0103_2	0.3461	0.0078	4.9	0.25	0.1031	0.0052	1.139	0.015	18700	9100	89.8	1.2	77.5	1.2	237.3	8.8	1911	37	1776	44	1580	100	-20.95	R	
SA3_1_0104_1	0.296	0.0046	4.89	0.12	0.1202	0.0031	1.133	0.038	114000	35000	390.8	6.1	356	12	635	21	1670	23	1795	21	1942	46	14.01	C	
SA3_1_0105_1	0.1992	0.0039	2.07	0.12	0.0766	0.0047	1.056	0.012	34000	10000	157	2.4	147.4	2.2	289	9	1170	21	1100	44	910	140	-28.57	C	
SA3_1_0106_1	0.2777	0.005	4.11	0.13	0.1085	0.0039	0.6837	0.0069	65000	19000	184.4	3.6	269.9	5.9	440	12	1577	25	1647	27	1721	69	8.37	C	
SA3_1_0107_1	0.2192	0.0076	2.26	0.23	0.076	0.0079	1.701	0.032	12800	4200	52.47	0.82	31.19	0.62	60.5	3.8	1277	39	1071	81	660	220	-93.48	R	
SA3_1_0107_2	0.2152	0.0043	2.25	0.12	0.0761	0.004	0.6752	0.0091	68000	17000	172.3	3.1	260.5	6.4	504	14	1255	23	1169	39	950	110	-32.11		Cuts zones
SA3_1_0201_1	0.296	0.0051	4.2	0.15	0.1038	0.004	1.045	0.012	74000	29000	195.9	3.5	191.6	4.1	484	13	1669	25	1664	31	1634	76	-2.14	R	
SA3_1_0202_1	0.298	0.005	4.05	0.14	0.0996	0.0034	2.613	0.029	93000	41000	277.7	4.3	108.2	1.8	274.5	9.1	1679	25	1641	27	1586	63	-5.86	R	
SA3_1_0203_1	0.3095	0.0066	4.27	0.23	0.1005	0.0055	2.056	0.031	45000	15000	100.5	1.4	49.76	0.86	130.6	5.7	1735	33	1657	48	1520	120	-14.14	C	
SA3_1_0204_1	0.203	0.014	1.78	0.42	0.089	0.028	1.233	0.047	2600	1100	12.01	0.34	10.28	0.35	16.7	2.1	1181	73	600	160	-390	400	402.82	C	

SA3_1_0205_1	0.1553	0.0026	2.189	0.089	0.1024	0.0039	1.139	0.013	69000	19000	325.3	4.7	287.6	4	363	11	930	15	1160	28	1598	73	41.80		Cuts resin
SA3_1_0206_1	0.3358	0.0076	4.59	0.24	0.101	0.0056	1.295	0.021	12800	7200	68.45	0.89	53.32	0.84	163	6.2	1862	37	1721	45	1510	110	-23.31	C	
SA3_1_0207_1	0.2463	0.0047	2.94	0.15	0.0859	0.0043	2.335	0.039	37000	11000	141.6	1.9	61.1	1.2	118.1	6.1	1417	24	1358	40	1220	110	-16.15		Cuts resin
SA3_1_0208_1	0.3131	0.0088	4.58	0.33	0.1068	0.0078	3.382	0.085	12400	4300	46.82	0.65	14.07	0.31	44.3	3.5	1749	43	1682	63	1530	150	-14.31	R	
SA3_1_0209_1	0.2783	0.0053	3.49	0.15	0.092	0.004	1.486	0.019	28000	10000	122.4	2	82.4	1.5	230.5	8.3	1580	27	1502	35	1384	91	-14.16	C	
SA3_1_0300_2	0.2373	0.0042	2.74	0.14	0.085	0.0043	1.584	0.024	42000	12000	166.1	6	105.8	4.9	263	12	1373	22	1317	37	1180	110	-16.36		Cuts zones
SA3_1_0301_1	0.2631	0.0044	3.26	0.13	0.0904	0.0035	2.359	0.027	23000	13000	182.5	2.7	76.7	1.1	190.7	7.2	1504	22	1454	30	1358	77	-10.75		Fracture, radiation damage
SA3_1_0302_1	0.5284	0.0091	16.25	0.37	0.2237	0.0041	1.334	0.027	157000	36000	222	3	167.5	3.8	383	20	2730	39	2883	22	2997	30	8.91	C	
SA3_1_0303_1	0.2114	0.0069	2.15	0.21	0.0762	0.0081	1.172	0.02	8500	3100	43.71	0.76	37.07	0.7	78.5	4.7	1232	36	1062	76	680	210	-81.18	C	
SA3_1_0305_2	0.2502	0.0068	2.65	0.23	0.0792	0.0071	1.177	0.021	16700	5200	56.08	0.77	47.61	0.77	116.1	5.4	1439	36	1217	75	810	190	-77.65	C	
SA3_1_0306_1	0.5392	0.0072	13.87	0.26	0.1874	0.003	1.122	0.01	251000	74000	298.6	5.3	264.6	5.3	1300	26	2780	30	2734	18	2708	27	-2.66	R	
SA3_1_0307_1	0.3319	0.0053	5.13	0.2	0.1132	0.0046	2.994	0.066	55000	21000	132.1	1.9	44.32	0.76	129.1	5.9	1845	26	1815	35	1778	79	-3.77		Cuts inclusion
SA3_1_0307_2	0.3469	0.0087	5.1	0.32	0.1087	0.0069	1.895	0.078	24800	8400	49.38	0.72	27.39	0.93	69.1	4.4	1914	42	1785	58	1590	140	-20.38	R	
SA3_1_0307_3	0.2497	0.0035	4.493	0.094	0.1316	0.0027	1.201	0.011	322000	67000	620	12	513	11	920	19	1436	18	1723	17	2098	37	31.55		Cuts zones
SA3_1_0308_2	0.2486	0.0047	2.95	0.17	0.0862	0.0051	1.7	0.023	45000	15000	120	1.7	70.2	1.3	159.2	6.5	1429	25	1356	45	1170	130	-22.14	C	
SA3_1_0308_3	0.2527	0.0066	3.06	0.22	0.0882	0.0063	1.662	0.027	30000	9900	86.1	1.3	51.71	0.87	108.5	5.8	1456	35	1375	56	1180	150	-23.39		Cuts zones
SA3_1_0400_1	0.2277	0.0043	2.81	0.12	0.0913	0.0042	1.463	0.023	52000	20000	191.7	2.6	132.3	3.2	204.6	7.8	1321	22	1336	33	1346	90	1.86	R	
SA3_1_0400_2	0.245	0.0056	3.32	0.17	0.1005	0.0055	1.427	0.024	50000	15000	139.8	2.1	98.6	2.1	157.7	7	1410	29	1457	41	1490	110	5.37	C	
SA3_1_0401_1	0.1973	0.0054	2.02	0.16	0.077	0.0061	1.331	0.019	15100	6900	81.6	1.3	61.41	0.94	89.8	4.4	1158	29	1069	58	830	170	-39.52	R	
SA3_1_0402_1	0.3103	0.005	4.5	0.15	0.1061	0.0035	3.183	0.043	123000	32000	239	2.6	75.6	1.1	183.9	6.5	1740	25	1721	27	1696	63	-2.59	C	
SA3_1_0402_2	0.2641	0.0034	4.43	0.11	0.1222	0.0027	1.234	0.012	259000	65000	631	10	519	11	628	14	1510	17	1709	21	1967	41	23.23	R	
SA3_1_0404_1	0.1887	0.0037	1.86	0.11	0.0726	0.0043	1.734	0.022	38000	14000	176.6	2.3	103.7	1.6	132.7	6	1113	20	1034	39	820	130	-35.73	R	
SA3_1_0405_1	0.3087	0.0073	4.55	0.25	0.1085	0.0061	0.7663	0.0098	31000	11000	92.3	1.5	123	2	246.4	8.6	1730	36	1700	49	1640	110	-5.49	C	
SA3_1_0406_1	0.3106	0.0049	4.56	0.14	0.1076	0.0034	2.094	0.022	105000	42000	324.8	4.4	159.1	2.3	336.6	9.1	1742	24	1726	26	1716	56	-1.52	C	

SA3_1_0407_2	0.1851	0.0033	2.24	0.1	0.0888	0.0042	0.9512	0.0091	61000	21000	264.6	3.6	286	4.1	272.1	7.9	1094	18	1180	32	1307	97	16.30	R	
SA3_1_0408_1	0.1895	0.0051	1.91	0.17	0.0745	0.0067	0.6847	0.0093	22300	7600	100.2	1.4	149.6	2.3	196	6.8	1116	28	1005	63	690	190	-61.74	C	
SA3_1_0500_1	0.3206	0.0045	5.25	0.13	0.1202	0.0027	1.735	0.021	311000	77000	644.9	9.6	379.2	7.4	557	13	1791	22	1854	21	1935	40	7.44		Cuts zones
SA3_1_0501_2	0.2382	0.0042	3.27	0.13	0.1015	0.0043	0.6585	0.0085	59000	21000	231	2.7	355.5	5.5	453	13	1376	22	1456	32	1569	83	12.30		Cuts zones
SA3_1_0502_1	0.3194	0.0051	4.56	0.13	0.1052	0.003	2.087	0.024	108000	40000	319.9	4.4	153.6	2.4	378.4	9.9	1785	25	1741	23	1689	53	-5.68	C	
SA3_1_0503_1	0.2509	0.0054	3.35	0.18	0.0981	0.0053	0.974	0.012	29000	12000	129.2	3.6	131.7	3.3	253	10	1441	28	1457	44	1460	110	1.30		Cuts inclusion
SA3_1_0503_2	0.2787	0.006	3.52	0.2	0.0928	0.0053	1.544	0.023	24700	8600	93.8	1.3	59.49	0.87	151.1	6.1	1582	30	1486	46	1310	120	-20.76	R	
SA3_1_0504_1	0.2345	0.0053	2.61	0.17	0.0821	0.0056	2.501	0.039	18100	7100	96.4	1.2	37.6	0.66	83.1	4.7	1356	28	1253	50	1030	150	-31.65	R	
SA3_1_0505_1	0.282	0.0044	4.25	0.15	0.1109	0.0039	0.556	0.008	63000	17000	194.1	2.9	340.8	8.2	918	17	1600	22	1668	29	1756	67	8.88	R	
SA3_1_0506_1	0.1892	0.003	2.074	0.078	0.081	0.0032	1.293	0.012	65000	17000	279.7	5	208.6	4.1	371	11	1116	16	1125	26	1158	79	3.63		Cuts zones
SA3_1_0507_1	0.2169	0.0055	2.41	0.16	0.081	0.0055	1.088	0.015	12600	5100	77.4	1.1	68.8	1	150.7	6.5	1269	30	1202	52	1030	150	-23.20		Cuts resin
SA3_1_0508_1	0.2459	0.0032	3.266	0.079	0.0974	0.0022	4.31	0.11	143000	49000	671	11	160.3	6.3	357	12	1416	16	1465	19	1548	43	8.53	R	
SA3_1_0508_2	0.2678	0.005	3.45	0.14	0.095	0.0039	2.683	0.055	63000	17000	193.9	2.3	74	1.9	84.9	4.8	1527	25	1495	33	1437	86	-6.26		Cuts zones
SA3_1_0509_1	0.3177	0.0075	4.76	0.27	0.1102	0.0058	1.716	0.032	33300	9900	101.9	1.8	61.22	0.89	156	9.6	1774	36	1739	48	1670	100	-6.23	C	
SA3_1_0600_1	0.2647	0.0065	3.04	0.19	0.0858	0.0054	0.944	0.012	25900	7400	83.9	1.3	94.1	1.6	175.1	6.7	1510	33	1378	50	1130	130	-33.63	R	
SA3_1_0601_3	0.2433	0.0057	3.22	0.19	0.0976	0.0056	0.946	0.015	38000	11000	118.2	3.9	135.3	3.6	154.4	7.6	1401	30	1434	45	1450	120	3.38		Cuts zones
SA3_1_0602_1	0.2487	0.0046	2.85	0.14	0.0848	0.0043	1.473	0.02	68000	17000	174.4	2.5	136.8	2.3	185.8	7.2	1430	24	1350	38	1200	100	-19.17	R	
SA3_1_0603_1	0.1	0.0015	3.281	0.058	0.2417	0.0043	1.0141	0.0073	45000	6000	1714	27	1935	27	2638	44	614	8.5	1472	14	3121	28	80.33		Fracture
SA3_1_0604_1	0.2846	0.0056	4.2	0.18	0.1093	0.005	0.7734	0.0092	55000	19000	143.4	3	210.3	5	277	10	1612	28	1651	36	1693	91	4.78	C	
SA3_1_0604_2	0.3259	0.0076	4.58	0.23	0.1046	0.0057	1.177	0.017	34000	15000	104.4	1.4	98.2	1.6	166.4	6.5	1814	37	1716	43	1580	110	-14.81		Cuts inclusion
SA3_1_0605_1	0.298	0.0044	4.05	0.14	0.1006	0.0038	0.875	0.011	126000	36000	250.7	2.8	308.4	4.1	520	12	1680	22	1626	30	1563	75	-7.49	C	
SA3_1_0606_1	0.192	0.007	2.24	0.27	0.085	0.01	1.063	0.022	16200	5100	53.18	0.86	50.39	0.85	34.2	3	1127	38	1026	92	730	250	-54.38	C	
SA3_1_0607_1	0.2743	0.0055	3.37	0.19	0.0913	0.0052	1.317	0.016	69000	21000	153	1.7	115.8	1.4	181.8	6.7	1563	28	1473	46	1340	110	-16.64	C	
SA3_1_0607_2	0.257	0.011	3.43	0.41	0.104	0.014	0.994	0.067	6000	3500	32.3	0.73	38.4	2.6	22.1	2.4	1473	56	1310	110	990	270	-48.79	R	

SA3_1_0608_1	0.511	0.016	11.39	0.69	0.168	0.011	0.648	0.014	34800	8200	35.24	0.6	53.95	0.9	151	5.8	2648	66	2499	61	2370	120	-11.73	C	
SA3_1_0608_2	0.534	0.015	12.78	0.85	0.178	0.012	0.614	0.013	20700	6800	28.73	0.57	46.5	1	141.5	6.3	2745	63	2584	68	2480	120	-10.69		Cuts zones
SA3_1_0609_1	0.2232	0.0048	2.57	0.15	0.0853	0.005	1.157	0.017	35000	13000	138.9	4.3	118.4	3.5	207.1	8.4	1297	25	1250	45	1130	130	-14.78	C	
SA3_1_0700_1	0.193	0.0028	2.052	0.072	0.0787	0.0027	1.574	0.013	115000	38000	471.8	8.2	295.5	5.3	460	12	1137	15	1126	24	1091	73	-4.22	R	
SA3_1_0700_2	0.1952	0.0037	2.03	0.098	0.0775	0.0038	1.45	0.015	28000	14000	192.2	2.8	130.9	1.9	215.3	7.1	1148	20	1112	34	1020	100	-12.55	C	
SA3_1_0702_1	0.1885	0.0025	1.948	0.075	0.0756	0.0028	2.014	0.022	97000	24000	314.8	4.3	154.9	2.6	265.5	8.6	1112	14	1083	26	1037	78	-7.23	R	
SA3_1_0702_2	0.1933	0.0047	2.15	0.16	0.0827	0.0062	1.74	0.022	22100	6900	92.3	1.6	52.52	0.88	95.5	4.6	1137	25	1130	52	1000	160	-13.70		Cuts inclusion
SA3_1_0703_1	0.1974	0.0057	1.97	0.18	0.0745	0.0069	1.76	0.036	13800	4200	54.61	0.83	31.04	0.76	52.2	3.4	1158	30	1039	67	730	190	-58.63	R	
SA3_1_0703_3	0.1967	0.0056	1.98	0.19	0.0771	0.0076	0.917	0.014	17500	4100	52.67	0.93	56.79	0.86	102	5.4	1158	31	1030	73	750	210	-54.40	R	
SA3_1_0705_2	0.3072	0.0048	4.27	0.14	0.1025	0.0032	1.561	0.015	101000	29000	252.1	3	159.2	1.9	513	12	1725	24	1674	28	1631	58	-5.76	R	
SA3_1_0706_1	0.3239	0.0079	4.29	0.29	0.0997	0.007	2.159	0.043	18100	5000	42.34	0.74	19.43	0.44	59.6	4.3	1804	39	1628	61	1370	150	-31.68	R	
SA3_1_0707_1	0.3033	0.006	4.11	0.17	0.1001	0.0042	1.638	0.021	47000	16000	129.9	2	78	1.4	255	8.1	1705	29	1634	34	1550	81	-10.00		Cuts inclusion
SA3_1_0708_1	0.3247	0.0048	4.74	0.13	0.1087	0.003	2.186	0.03	129000	37000	315.9	3.2	142.8	2	311	10	1814	23	1768	23	1745	50	-3.95	C	
SA3_1_0708_2	0.32	0.0052	4.68	0.16	0.1089	0.0041	3.266	0.045	65000	20000	177.1	2.1	53.53	0.79	165.4	6.3	1787	25	1751	30	1730	74	-3.29	R	
SA3_1_0708_3	0.3187	0.0048	4.66	0.14	0.108	0.0034	3	0.042	114000	24000	226.6	2.6	75	1.2	215.1	8	1784	24	1745	27	1714	59	-4.08	R	
SA3_1_0804_1	0.254	0.014	2.76	0.51	0.079	0.016	3.85	0.23	1730	730	9.94	0.26	2.83	0.15	5.3	1.2	1451	74	810	170	40	380	-3527.50		Cuts zones
SA3_1_0804_2	0.2278	0.005	2.72	0.13	0.0892	0.004	0.9003	0.0093	37000	12000	171.1	1.9	191.3	2.2	287.9	8.8	1321	26	1317	35	1314	95	-0.53	R	
SA3_1_0805_1	0.1663	0.0023	4.238	0.079	0.1884	0.0032	0.5623	0.0052	39900	5700	1080	15	1981	21	2530	31	991	13	1676	15	2715	28	63.50		Cuts zones
SA3_1_0808_2	0.228	0.0037	2.7	0.13	0.0872	0.0041	1.146	0.029	54000	16000	217	8.4	209	13	309	17	1323	19	1306	35	1260	100	-5.00	C	
SA3_1_0900_1	0.3001	0.0047	4.01	0.14	0.0991	0.0036	1.07	0.011	72000	21000	210.6	3.2	206.3	3.4	378	11	1690	23	1628	29	1559	71	-8.40	R	
SA3_1_0900_2	0.3097	0.005	4.22	0.17	0.1017	0.0042	1.271	0.018	65000	20000	196.7	2.4	162.8	2.9	208	7.3	1740	24	1659	33	1572	80	-10.69		Cuts inclusion
SA3_1_0900_3	0.2444	0.0035	4.16	0.12	0.1263	0.0038	0.3595	0.0036	165000	40000	451.3	6.8	1319	22	1647	28	1408	18	1659	24	2016	53	30.16		Cuts inclusion
SA3_1_0903_1	0.2186	0.0036	2.92	0.11	0.0987	0.0035	1.878	0.038	178000	43000	401	6.5	227.1	7.5	273	12	1273	19	1372	30	1541	71	17.39	R	
SA3_1_0904_1	0.2209	0.0053	2.52	0.16	0.0849	0.0056	0.983	0.013	43000	16000	133.8	2.1	140.2	2	175.3	6.5	1284	28	1237	47	1120	140	-14.64		Radiation damage

SA3_1_0904_2	0.236	0.012	2.65	0.41	0.087	0.014	1.325	0.042	7600	2900	24.29	0.51	19.36	0.61	21.2	2.2	1361	65	990	130	490	320	-177.76	R	
SA3_1_0908_2	0.507	0.0084	12.21	0.32	0.178	0.0045	0.924	0.013	185000	54000	186.2	5.3	206.3	7.7	602	22	2640	36	2611	24	2619	44	-0.80	R	
SA3_1_1000_1	0.2349	0.0041	2.97	0.12	0.0939	0.0041	0.7596	0.0079	119000	29000	211.8	3	280.5	4	414	10	1359	21	1378	33	1406	89	3.34	C	
SA3_1_1001_2	0.2568	0.0041	3.21	0.11	0.0928	0.0033	2.075	0.026	114000	37000	293.7	4.3	140.8	2.8	232.6	7.4	1472	21	1446	28	1438	67	-2.36	R	
SA3_1_1002_2	0.3302	0.0059	4.82	0.15	0.1092	0.0035	3.351	0.046	114000	37000	236.4	3.5	70.1	1.3	181.3	6.6	1836	29	1779	28	1738	61	-5.64	R	
SA3_1_1003_1	0.22	0.011	2.67	0.46	0.096	0.017	2.83	0.14	4600	1400	12.74	0.25	4.8	0.24	6.8	1.3	1271	59	940	150	410	370	-210.00	R	
SA3_1_1003_2	0.1923	0.0034	2.15	0.11	0.0839	0.0045	1.366	0.016	46000	14000	165.8	1.9	120.3	1.3	190.7	7	1135	18	1143	36	1140	110	0.44		Cuts resin
SA3_1_1004_1											-0.00112457	0.0000009	-0.00116167	0.00000087	0.56	0.63									Cuts inclusion
SA3_1_1006_2	0.222	0.0031	3.989	0.095	0.1331	0.0031	0.4297	0.0041	128000	29000	352.4	4.1	819	8.3	1729	25	1291	16	1626	19	2122	40	39.16		Cuts zones
SA3_1_1007_1	0.2983	0.0058	4.11	0.18	0.1023	0.0044	0.8049	0.0089	45000	12000	94.5	1.1	117.3	1.5	403	11	1680	29	1634	35	1577	82	-6.53	C	
SA3_1_1008_1	0.2255	0.0033	2.77	0.076	0.0916	0.0025	1.997	0.022	89000	28000	297.2	3.8	148.9	1.8	362.1	9.7	1310	17	1338	21	1424	53	8.01	R	
SA3_1_1100_1	0.3851	0.005	11	0.17	0.2119	0.0028	0.6122	0.005	233000	50000	403.8	6.3	660.8	9.4	1653	23	2098	23	2518	14	2915	21	28.03	C	
SA3_1_1103_1	0.2481	0.0068	2.79	0.19	0.0859	0.0061	2.113	0.039	17500	4400	46.58	0.73	22.27	0.46	70.2	4.1	1424	35	1319	52	1120	150	-27.14		Cuts inclusion
SA3_1_1103_2	0.2428	0.005	2.89	0.17	0.0878	0.0049	2.07	0.031	18800	7000	74.8	2.3	36.5	1.1	107.2	5.3	1399	26	1344	47	1250	120	-11.92	C	
SA3_1_1104_1	0.2793	0.004	4.43	0.13	0.118	0.0034	0.868	0.019	106000	26000	237.2	5	285	11	636	17	1586	20	1705	24	1890	52	16.08	R	
SA3_1_1104_2	0.2949	0.0048	5.55	0.26	0.1378	0.0055	1.043	0.021	135000	28000	264.6	6.3	254.7	7.7	954	40	1664	24	1872	41	2128	73	21.80		Cuts zones
SA3_1_1105_1	0.2918	0.0049	4.24	0.16	0.1077	0.0039	2.139	0.071	62000	17000	138.2	2	67.1	1.8	145.5	6.1	1649	24	1660	32	1695	72	2.71	R	
SA3_1_1106_1	0.2104	0.0075	2.39	0.23	0.087	0.0091	1.572	0.034	12200	3100	34.93	0.56	22.78	0.43	40.3	3.5	1230	40	1145	80	930	220	-32.26	R	
SA3_1_1106_2	0.2097	0.0047	2.3	0.13	0.0823	0.0051	1.811	0.028	35000	10000	108.1	1.5	60.7	1	108.6	5.1	1225	25	1177	43	1070	130	-14.49		Cuts inclusion
SA3_1_1107_2	0.2098	0.0048	2.18	0.15	0.0775	0.0053	1.81	0.027	26500	8300	94.6	1.2	52.81	0.78	90.6	4.4	1225	26	1134	50	930	140	-31.72	R	
SA3_1_1108_1	0.1965	0.0038	2.17	0.13	0.0828	0.005	1.226	0.016	50000	11000	133.1	2.7	109.8	2.7	186.5	8	1155	21	1133	43	1070	130	-7.94		Radiation damage
SA4_0005_1											0.838	0.07	2.73	0.15	11.6	1.5									Readings too low to calculate age

SA4_0007_1	0.2954	0.0056	4.03	0.18	0.1046	0.005	1.779	0.023	44000	10000	120.4	1.6	67.8	1.1	143.3	5.2	1666	28	1622	38	1621	96	-2.78	C	
SA4_0008_3	0.2974	0.0065	3.73	0.19	0.0955	0.0048	1.434	0.02	43800	9500	106.2	1.3	74.2	1	159.6	5.6	1679	31	1549	42	1442	94	-16.44	R	
SA4_0104_1	0.2845	0.0081	3.71	0.27	0.1015	0.0076	1.781	0.038	20800	4600	52.92	0.78	29.92	0.48	65.7	3.9	1608	41	1506	63	1370	170	-17.37	R	
SA4_0104_2	0.2862	0.0076	3.84	0.28	0.1023	0.0075	1.737	0.034	21500	4500	50.01	0.69	28.94	0.49	60.5	3.7	1618	38	1547	62	1460	150	-10.82		Cuts zones
SA4_0105_1	0.71	0.091	58.7	8.5	0.76	0.15	0.522	0.047	1510	480	1.477	0.091	2.98	0.13	45.4	3	3210	320	4130	140	3820	630	15.97		Not a zircon
SA4_0108_1	0.1834	0.0066	2.15	0.16	0.0924	0.0066	1.454	0.052	27300	6500	110.8	9.2	71.2	4.8	74.8	5.8	1081	36	1128	49	1260	150	14.21		Cuts resin
SA4_0108_2	0.2276	0.005	2.5	0.17	0.0833	0.0055	2.027	0.029	41600	8800	117.5	1.3	58.88	0.8	109.3	4.8	1319	26	1218	51	1050	150	-25.62	C	
SA4_0200_2	0.2798	0.004	3.92	0.12	0.1064	0.0034	2.147	0.049	67000	18000	213.7	2.7	101.7	2	134.6	5.5	1589	20	1607	25	1700	60	6.53		Cuts resin
SA4_0207_1											-0.0025115 6	0.0000002 9	-0.0012723	0.0000000 58	-0.4	0.45									Cuts resin
SA4_0300_1	0.2184	0.004	2.6	0.12	0.0908	0.0044	1.197	0.014	53000	12000	167.6	2.3	144.4	2.7	196.5	6.6	1272	21	1275	35	1333	97	4.58	C	
SA4_0301_1	0.2281	0.0047	3.21	0.16	0.1072	0.0053	0.93	0.02	38900	9100	126.8	2.2	140.8	2.2	143.8	5.4	1322	24	1435	38	1654	98	20.07		Cuts resin
SA4_0301_2	0.3074	0.0061	4.32	0.2	0.1066	0.0048	1.809	0.028	47900	9400	95.5	1.3	54.55	0.84	131.8	5.3	1725	30	1675	41	1665	92	-3.60	R	
SA4_0302_1	0.274	0.004	3.9	0.12	0.1084	0.0033	1.818	0.032	128000	27000	314.4	3.6	179.3	2.9	232.3	6.8	1560	21	1602	26	1728	60	9.72	C	
SA4_0302_2	0.2156	0.0042	3.22	0.13	0.113	0.0044	3.16	0.044	88000	18000	269	4.4	87.5	1.8	155.2	5.5	1257	22	1446	31	1793	75	29.89		Cuts zones
SA4_0303_1	0.2257	0.0053	2.89	0.18	0.098	0.0062	0.903	0.014	31600	6600	95.2	1.6	106.1	1.5	193.8	6.8	1313	27	1340	49	1420	130	7.54		Cuts inclusion
SA4_0303_2	0.2303	0.0063	2.78	0.19	0.0923	0.0063	2.342	0.047	22400	5000	70.4	1.1	30.77	0.6	54.9	3.4	1332	33	1301	54	1250	150	-6.56	R	
SA4_0304_2	0.23	0.01	2.54	0.34	0.086	0.012	2.75	0.1	6500	1500	19.94	0.38	7.51	0.24	14.5	1.8	1326	53	1060	120	700	290	-89.43		metamictiz ation
SA4_0305_1	0.293	0.01	4.16	0.35	0.114	0.01	2.009	0.047	11200	2900	33.55	0.59	16.96	0.38	39.7	2.5	1646	51	1605	69	1450	190	-13.52		metamictiz ation
SA4_0306_1	0.2916	0.0063	3.98	0.22	0.1045	0.006	0.861	0.011	39300	8200	96.1	1.3	111.5	1.5	253.2	7.6	1646	31	1588	47	1540	120	-6.88	C	
SA4_0307_2	0.1551	0.0026	1.776	0.077	0.0869	0.0039	1.317	0.016	60000	15000	360.7	3.8	274.3	4.1	251.4	7.7	929	15	1025	30	1270	93	26.85		Cuts inclusion
SA4_0308_1	0.2702	0.0049	3.64	0.16	0.1026	0.0048	2.209	0.072	56000	12000	149.4	2.7	68.9	1.7	104.7	5.2	1540	25	1533	37	1569	87	1.85		Cuts resin
SA4_0401_1	0.1975	0.0041	2.99	0.1	0.1143	0.0038	2.135	0.028	101000	19000	334.2	4.3	156.9	2.5	218.2	7.2	1160	22	1389	26	1813	62	36.02		Cuts inclusion
SA4_0401_2	0.3119	0.0051	4.33	0.15	0.1042	0.0034	3.858	0.054	79000	19000	213.5	3.4	55.6	1.1	133.9	5.3	1748	25	1684	28	1652	63	-5.81	R	
SA4_0402_1	0.2229	0.004	2.98	0.12	0.1011	0.0043	1.117	0.017	68000	15000	239	4.5	215.2	2.8	287	9	1296	21	1386	31	1573	82	17.61		Cuts inclusion
SA4_0403_2	0.3191	0.0058	4.79	0.2	0.1143	0.005	2.669	0.037	61000	14000	158.1	1.7	60.41	0.89	147.7	5.6	1783	28	1762	37	1797	81	0.78	R	

SA4_0404_1	0.1823	0.0061	1.83	0.21	0.0786	0.0093	1.317	0.029	11300	2600	48.11	0.76	37.55	0.75	54.9	3.3	1076	33	927	86	620	240	-73.55		Cuts resin
SA4_0404_2	0.1841	0.0051	1.97	0.16	0.0823	0.0072	1.91	0.036	17400	4100	74.7	1.1	40.25	0.69	62.1	3.8	1087	27	1034	62	890	190	-22.13	R	
SA4_0405_1	0.2606	0.0069	3.88	0.25	0.1128	0.0074	1.345	0.029	23600	5200	66.6	1.2	52	1.6	69.6	4.4	1489	35	1555	54	1680	130	11.37		Cuts resin
SA4_0405_3	0.3071	0.0047	4.3	0.15	0.1057	0.0038	2.084	0.025	90000	19000	203.7	2.3	100.9	1.4	235.3	8.1	1724	23	1683	29	1674	69	-2.99	R	
SA4_0407_1											0.086	0.022	0.41	0.053	16.3	2									Cuts resin
SA4_0407_2	0.3085	0.0045	4.35	0.13	0.1054	0.0032	1.752	0.019	107000	23000	243.9	3.3	144.4	2.2	323.5	9.2	1732	22	1691	26	1691	58	-2.42	R	
SA4_0407_3	0.3137	0.0061	4.47	0.19	0.108	0.0047	2.263	0.037	26000	8400	96.7	1.4	44.38	0.73	115.1	5.1	1756	30	1700	37	1667	84	-5.34	R	
SA4_0408_3	0.1875	0.0043	2.03	0.14	0.0828	0.0058	2.162	0.03	21300	5400	103.6	1.4	49.64	0.7	73.9	4.2	1106	23	1083	49	1020	150	-8.43		Cuts resin
SA4_0500_1	0.2402	0.0087	3.58	0.24	0.1141	0.0078	0.804	0.018	23500	5400	73.3	2.1	95.6	4.2	139.8	5.8	1380	45	1488	58	1650	150	16.36		Cuts resin
SA4_0500_3	0.3176	0.0058	4.98	0.19	0.1176	0.0047	1.049	0.012	39000	10000	134.7	1.9	132.1	1.8	330	7.8	1775	28	1793	33	1850	73	4.05		Cuts zones
SA4_0501_2	0.301	0.0042	4.53	0.14	0.1129	0.0035	1.686	0.026	122000	27000	305.4	4	186	2	359	9.3	1695	21	1721	26	1802	58	5.94		Cuts resin
SA4_0503_1	0.1894	0.0078	1.99	0.23	0.085	0.011	3.21	0.22	10200	2100	36.1	1.4	12.47	0.62	11.8	2	1112	42	973	91	730	260	-52.33		Cuts resin
SA4_0503_2	0.2526	0.006	3.21	0.2	0.0952	0.006	1.437	0.021	24900	6200	86.7	1.1	61.44	0.91	126.9	5.4	1448	31	1406	51	1340	130	-8.06	R	
SA4_0504_1	0.2825	0.0055	3.85	0.21	0.1025	0.0056	0.7276	0.0098	33400	7100	88.2	1.2	122.8	1.4	274.5	8.6	1601	28	1575	44	1590	100	-0.69	R	
SA4_0505_2	0.1675	0.0026	2.108	0.066	0.0956	0.0032	1.397	0.013	96000	19000	426.5	4.1	303.8	3.1	338	9.7	998	14	1152	23	1496	62	33.29		Cuts zones, fracture, inclusion
SA4_0506_1	0.23	0.03	2.8	1.2	0.209	0.063	1.37	0.12	480	170	2.64	0.14	2.16	0.13	2.53	0.93	1270	150	230	530	-1140	650	211.40		metamictization
SA4_0600_1	0.4236	0.0086	10.94	0.29	0.1943	0.0045	2.046	0.029	87000	20000	177.1	2.3	85.5	1.5	269.3	7.7	2272	39	2508	24	2756	39	17.56		Cuts zones
SA4_0601_1	0.1285	0.0024	1.907	0.066	0.1109	0.0038	2.11	0.024	97000	21000	656.5	6.5	304.8	3.8	374	11	779	14	1072	23	1759	66	55.71		Cuts resin
SA4_0602_1	0.2588	0.0076	3.41	0.29	0.1011	0.0089	1.137	0.028	15100	3600	51	1	44.1	1.5	77.9	4.6	1479	39	1397	76	1240	190	-19.27		Cuts resin
SA4_0604_1	0.2278	0.0032	2.698	0.098	0.0883	0.0032	2.311	0.041	100000	21000	364	4.9	152.7	2.8	234.6	7.9	1322	17	1312	27	1321	73	-0.08		Cuts resin
SA4_0606_1	0.286	0.012	3.45	0.45	0.095	0.013	2.92	0.11	6800	1600	21.26	0.42	7.35	0.23	17.5	2.3	1618	59	1230	130	800	290	-102.25		Not zircon
SA4_0608_1	0.1794	0.0038	2.05	0.11	0.0865	0.0049	0.947	0.013	38800	8100	179.1	3.6	184.9	4.4	175.8	7.4	1062	21	1107	38	1180	120	10.00		Cuts resin
SA4_0608_2	0.2272	0.0049	2.63	0.17	0.0873	0.0057	1.929	0.026	32700	7400	126.7	1.4	64.41	0.91	99.5	4.8	1318	25	1257	50	1120	140	-17.68		Cuts zones
SA4_0700_1	0.183	0.0035	2.99	0.15	0.1209	0.006	3.739	0.06	36700	8300	181.1	3.2	48.7	1.1	73.2	4.5	1085	20	1381	40	1878	98	42.23		Cuts resin
SA4_0700_2	0.5313	0.0079	13.37	0.29	0.1872	0.0038	1.414	0.014	140000	34000	249.4	2.9	176.9	2.2	667	13	2743	34	2697	21	2704	34	-1.44		Cuts zones
SA4_0702_1	0.2907	0.0088	3.88	0.27	0.1009	0.007	2.403	0.048	26600	4500	55.37	0.79	23.33	0.42	54.9	3.7	1639	43	1569	58	1460	140	-12.26		Cuts inclusion

SA4_0702_2	0.2792	0.0078	3.48	0.26	0.0935	0.0074	1.816	0.041	17400	3600	49.49	0.73	27.99	0.54	44.2	3.3	1582	39	1457	61	1200	170	-31.83		Fracture, radiation damage
SA4_0705_1	0.58	0.72	35	60	-4.1	8.6	0.36	0.17	900	1500	0.885	0.07	3.11	0.17	14.1	1.9	2200	2100	4100	1400	-190000	380000	101.16		Cuts inclusion
SA4_0707_2	0.1952	0.0039	2.44	0.13	0.0925	0.0048	2.034	0.04	52000	11000	199.1	2.6	101.9	2.1	167.4	7.5	1148	21	1223	38	1360	110	15.59		Cuts resin
SA4_0707_3	0.2723	0.0054	3.66	0.15	0.1002	0.0042	1.271	0.019	60000	12000	162.6	1.8	131.5	2	278.6	7.8	1550	27	1543	33	1552	81	0.13		Cuts resin
SA4_0800_2	0.2562	0.0041	3.153	0.098	0.0925	0.003	2.207	0.023	89000	23000	337.8	4.5	156.6	2.3	322	10	1469	21	1438	25	1420	63	-3.45	R	
SA4_0806_1											-0.00132148	0.00000023	-0.00088568	0.00000011	1.75	0.88									Cuts resin
SA4_0808_1	0.2743	0.004	4.09	0.12	0.1108	0.0031	2.152	0.03	140000	28000	374.8	3.4	178	2.5	269.5	7.4	1561	20	1641	23	1778	52	12.20		Cuts resin
SA4_0808_2	0.3119	0.0063	4.44	0.24	0.1051	0.0053	2.813	0.051	40200	8800	103	1.6	37.25	0.83	92.7	4.7	1747	31	1682	45	1620	100	-7.84	R	
SA4_0900_1	0.1785	0.0052	1.95	0.16	0.0823	0.007	0.6392	0.0084	14000	3700	78	1.1	122.5	1.5	181.4	6.5	1056	28	1033	60	920	180	-14.78		Cuts zones
SA4_0900_2	0.1764	0.0062	1.72	0.19	0.0727	0.0081	0.946	0.015	13900	3000	57.54	0.87	61.3	1.1	91.1	5.1	1043	34	918	76	610	230	-70.98	R	
SA4_0902_1	0.2637	0.0055	3.85	0.17	0.1083	0.0046	2.177	0.052	69000	13000	171.1	6.3	78.2	3	93.2	5.1	1506	28	1574	37	1696	86	11.20		Cuts resin
SA4_0902_3	0.3015	0.0055	4.3	0.19	0.1063	0.0048	2.519	0.034	71000	15000	177.5	2.7	70.5	1.2	151.6	6.5	1696	27	1677	36	1671	83	-1.50		Cuts zones, inclusion
SA4_0903_1	0.2541	0.0044	3.47	0.14	0.1019	0.0044	1.573	0.02	52000	12000	179	4.7	113	2.9	172.3	6.8	1458	23	1503	33	1570	83	7.13		Cuts zones
SA4_0903_2	0.1999	0.0059	2.07	0.19	0.0756	0.007	1.59	0.03	15600	3500	62.65	0.94	39.24	0.62	63.1	4.2	1171	32	1049	69	750	200	-56.13	R	
SA4_0905_2	0.0944	0.0015	1.4	0.044	0.1095	0.0032	0.9508	0.0079	88000	21000	891	13	927	12	442	13	581	9.1	884	18	1766	53	67.10		Cuts zones
SA4_0906_1	0.316	0.0053	4.52	0.17	0.1056	0.004	2.522	0.035	69000	14000	161.5	2.2	64	1.2	170.2	6.8	1768	26	1718	33	1671	75	-5.80		Cuts inclusion
SA4_0908_1	0.209	0.0051	2.52	0.18	0.0907	0.0068	1.35	0.028	23400	4600	77.9	1.1	58.1	1.4	87	4.5	1221	27	1237	51	1230	150	0.73		Cuts resin
SA4_0908_2	0.231	0.0069	2.5	0.24	0.0803	0.0079	1.589	0.034	11800	2800	44.81	0.91	28.26	0.68	49.6	3.4	1335	36	1152	82	780	220	-71.15		Cuts inclusion
SA5_0004_2	0.431	0.044	59.5	6.7	0.98	0.17	0.944	0.069	-1170	260	25	1.4	29	1.5	506	46	2230	200	3950	120	4800	1200	53.54		zone cutter
SA5_0005_2	0.231	0.026	2.3	0.94	0.174	0.061	1.81	0.25	50600	5600	37.5	2	25.9	1.6	82	19	1310	140	170	220	-830	490	257.83		zone cutter
SA5_0005_3	0.226	0.016	2.48	0.61	0.085	0.023	1.761	0.088	57800	4600	94	3	56.7	2.3	100	20	1299	83	570	180	-400	410	424.75		Cuts resin
SA5_0006_1	0.129	0.017	1.5	0.71	0.174	0.046	0.845	0.08	13300	1800	41.6	2.1	59.5	4.7	37	13	751	95	10	190	-400	520	287.75		Cuts resin
SA5_0006_2	0.1879	0.0092	2.06	0.33	0.074	0.012	1.691	0.063	104800	6400	197.1	5.2	118.1	4.4	205	25	1101	50	850	130	210	320	-424.29		Cuts zones

SA5_0008_1	0.2235	0.0087	3.26	0.33	0.107	0.012	1.548	0.048	126600	5400	300.5	7.9	188.1	5.4	365	35	1293	46	1300	100	1200	260	-7.75		Cuts resin
SA5_0008_2	0.191	0.0066	3.51	0.29	0.139	0.013	1.246	0.027	112100	7600	453	13	340	12	649	48	1126	36	1412	79	1740	210	35.29		Cuts resin
SA5_0009_1	0.224	0.018	1.49	0.6	0.066	0.029	1.64	0.11	17300	1400	67	2.7	41.6	2.2	57	12	1274	94	120	180	-1410	410	190.35		Cuts resin
SA5_0101_1											-0.0345683	0.000000079	-0.05301	0.00011	1.1	4									Cuts resin
SA5_0101_2	0.263	0.016	2.76	0.66	0.082	0.02	1.424	0.066	150600	9800	97.2	3	64.1	2.6	105	14	1490	84	670	190	-270	410	651.85		Radiation damage
SA5_0104_1	0.209	0.019	2.26	0.66	0.153	0.051	2.79	0.24	23100	2300	62.9	2.9	24.2	1.7	29.5	8.5	1220	110	510	180	-530	470	330.19		Cuts zones
SA5_0104_2	0.218	0.013	2.82	0.42	0.122	0.021	1.889	0.085	35600	2500	144.5	4.4	72.7	2.9	92	15	1256	69	1060	140	780	360	-61.03		Cuts zones
SA5_0106_1											-0.030047	0.000013	0.0874	0.00068	0.2	4.1									Cuts resin
SA5_0108_2	0.263	0.025	2.49	0.71	0.117	0.039	2.2	0.2	14600	1400	53	2.5	26.1	1.6	40	10	1470	130	470	190	-540	470	372.22	R	
SA5_0200_1											0.78	0.25	1.03	0.31	-8.7166	0.0063									Cuts resin
SA5_0201_1	0.338	0.024	2.91	0.64	0.076	0.019	1.146	0.062	21600	1500	64.2	2.5	57.9	2.6	96	13	1830	110	710	190	-240	410	862.50		Cuts resin
SA5_0203_1	0.075	0.009	0.2	0.23	0.187	0.063	0.752	0.031	7190	940	71.2	2.9	95	3.8	54	11	456	53	-115	90	-1350	550	133.78		zone cutter
SA5_0204_1	0.34	0.017	4.1	0.65	0.1	0.017	2.44	0.13	68400	5000	95.8	4	41.6	2.2	82	12	1863	82	1210	160	620	340	-200.48	R	
SA5_0205_1	0.1887	0.0086	2.36	0.34	0.101	0.015	1.274	0.051	87400	5800	226.8	9.5	184.6	9.7	218	21	1107	46	1000	120	810	320	-36.67		Cuts zones
SA5_0205_2	0.245	0.01	2.98	0.33	0.102	0.012	1.991	0.07	133700	5400	200.2	5	101.8	3.4	142	15	1401	53	1220	100	1050	260	-33.43		Cuts resin
SA5_0206_2											2.27	0.41	2.97	0.62	5	4.1									Cuts resin
SA5_0300_2	0.191	0.01	1.78	0.29	0.081	0.013	1.812	0.063	53600	3000	159.4	6.8	88.7	4.4	97	14	1115	55	820	120	310	330	-259.68		Cuts resin
SA5_0303_1	0.292	0.019	3.58	0.7	0.123	0.03	1.88	0.11	37800	2500	71.4	2.4	40.5	2.1	54	11	1619	95	900	190	180	410	-799.44		Cuts resin
SA5_0303_2	0.1037	0.0059	1.5	0.23	0.12	0.02	0.757	0.031	46300	3200	266.7	9.3	351	15	137	16	632	34	765	99	900	360	29.78		Cuts resin
SA5_0308_1	0.149	0.029	0.79	0.85	0.313	0.069	0.902	0.08	3090	570	19.1	1.2	23.4	1.3	26.4	7.1	830	150	-310	250	510	660	-62.75		Cuts resin
SA5_0308_2	0.223	0.026	1.55	0.78	0.196	0.066	1.23	0.12	23600	2600	25.7	1.3	23.5	1.6	29.9	7.2	1240	130	-250	250	-950	540	230.53		Cuts resin
SA5_0406_2	0.368	0.016	6.22	0.71	0.122	0.014	5.61	0.34	91800	4200	137.1	3.9	25.9	1.5	64	11	2000	73	1720	140	1350	270	-48.15		Cuts resin
SA5_0500_1	0.339	0.018	4.6	0.65	0.099	0.014	1.81	0.08	54900	3600	125.1	5	67.4	3.1	153	17	1860	83	1360	160	790	310	-135.44	R	
SA5_0500_2	0.316	0.014	4.35	0.58	0.096	0.013	1.916	0.081	68600	3700	140.6	4.4	71.5	3.1	169	18	1763	68	1360	140	810	300	-117.65		Cuts zones
SA5_0501_1	0.2	0.011	2.71	0.42	0.094	0.015	2.46	0.11	49800	3300	155.8	5	60.8	2.8	72	12	1161	59	1000	140	590	340	-96.78		Cuts resin

SA5_0501_2	0.301	0.058	4.1	2.8	0.2	0.12	-5	11	6800	1200	11	1.9	7.9	1.3	3.7	4.1	1600	270	190	550	-870	890	283.91		Cuts resin
SA5_0508_2	0.267	0.026	3.8	1.1	0.149	0.04	2.38	0.31	10050	970	44.7	2.5	21.4	1.6	41	10	1470	130	480	260	-400	490	467.50	R	
SA5_0508_3	0.26	0.031	3.4	1.2	0.174	0.051	1.67	0.17	7900	870	27	1.2	17.1	1.3	57	10	1430	160	250	270	-640	530	323.44		Cuts inclusion
SA5_0509_1	0.228	0.018	2.84	0.74	0.114	0.04	2.5	0.17	14700	1200	74.3	3.2	28.9	1.8	39.4	8.8	1292	94	540	190	-430	480	400.47	R	
SA5_0600_2	0.206	0.032	2.1	1.3	0.249	0.079	0.9	2.3	5500	850	19.7	1.4	11.1	1.1	13.7	5.5	1150	170	-200	400	-390	740	394.87		zone cutter
SA5_0601_1	0.27	0.067	0.6	1.8	-0.2	0.92	0.94	0.16	3640	960	13.8	1.1	16.3	1.1	31.9	8.4	1420	320	-780	730	-21000	40000	106.76		zone cutter
SA5_0603_1	0.412	0.02	7.7	1	0.135	0.019	2.11	0.11	24400	1800	85.5	4	39.2	2.1	140	18	2205	94	1740	180	1280	330	-72.27	C	
SA5_0608_1	0.078	0.014	0.51	0.47	0.166	0.038	0.586	0.037	2820	500	36.2	2.3	60.9	3.8	26.7	7.9	488	84	-230	79	-150	560	425.33		Cuts resin
SA5_0700_2	0.234	0.025	6.3	1.3	-0.02	0.41	1.163	0.081	8240	960	39.9	2.5	35.7	2.3	125	16	1330	130	1220	240	-12000	18000	111.08		Cuts resin
SA5_0703_1	0.192	0.016	2.42	0.64	0.147	0.054	1.92	0.13	11290	930	60	2.5	33.9	1.9	30	7.7	1109	85	560	180	-450	470	346.44		Cuts resin
SA5_0704_1	0.18	0.012	2.07	0.51	0.132	0.052	1.89	0.1	11270	870	78.9	2.5	42.8	1.8	55	10	1050	66	620	160	-260	430	503.85		Cuts resin
SA5_0704_2	0.264	0.013	2.95	0.47	0.085	0.015	2.46	0.1	36900	2300	119.5	4.3	48.6	2.2	104	14	1496	64	1020	150	390	330	-283.59		Cuts inclusion, radiation damage
SA5_0706_1	0.162	0.02	2.97	0.94	0.265	0.064	1.32	0.1	4480	610	30.5	1.3	25	1.4	50.5	8.8	920	110	320	220	50	560	-1740.00		Cuts resin
SA5_0706_2	0.288	0.012	3.91	0.47	0.1	0.013	3.98	0.19	43300	2500	145.2	4.6	37.1	1.9	89	13	1618	61	1350	120	980	280	-65.10	C	
SA5_0707_1	0.538	0.031	13.8	1.4	0.199	0.02	-150	130	42300	2700	74.1	3.4	9.5	0.86	67	11	2730	130	2570	120	2260	240	-20.80		Cuts resin
SA5_0707_2	0.6103	0.0089	17.1	0.43	0.2025	0.0048	54.3	3.5	743000	19000	1024	27	20.2	1.2	109	15	3071	36	2928	24	2826	40	-8.67	R	
SA5_0708_1											0.38	0.17	0.94	0.37	0.6	2.8									Cuts resin
SA5_0800_1											-0.0118672	0.0000026	0.012341	0.000054	2.5	3.1									Cuts resin
SA5_0800_2	0.0454	0.0075	0.03	0.14	0.214	0.053	0.807	0.041	4040	650	64.9	5.3	78.8	6.5	26.5	6.1	280	45	-98	53	-80	570	450.00		Cuts resin
SA5_0801_1	0.297	0.017	5.1	0.7	0.142	0.022	1.84	0.1	33400	2600	83.9	3.9	46.2	2.9	115	16	1658	88	1440	160	1190	350	-39.33		Cuts resin
SA5_0802_1	0.39	0.021	6.93	0.82	0.14	0.017	1.252	0.055	54500	3400	88.5	2.9	68.8	2.5	109	13	2091	94	1770	150	1480	290	-41.28		Cuts resin
SA5_0804_1											-0.0104846	0.0000023	-0.00957	0.00002	-3.6936	0.0042									Cuts resin
SA5_0804_2	0.356	0.022	4.4	0.74	0.102	0.019	2.98	0.19	29700	2200	70.6	3.3	24.2	1.5	65.7	9.2	1930	100	1130	180	490	370	-293.88	R	

SA5_0804_3	0.319	0.015	4.49	0.52	0.108	0.013	2.79	0.15	56600	3300	101.6	2.6	37.2	1.7	79	10	1778	75	1450	130	1100	280	-61.64		Cuts zones
SA5_0805_1	0.056	0.012	-0.18	0.24	0.435	0.067	0.672	0.042	3020	580	25.3	1.2	36.5	1.6	16.5	5.9	336	70	-613	58	1040	650	67.69		Cuts resin
SA5_0806_1	0.073	0.014	-0.37	0.3	0.67	0.11	1.45	0.18	3270	590	22.7	1.3	19.2	1.4	2.7	3.1	435	79	-950	150	1220	770	64.34		Cuts resin
SA5_0808_1	0.224	0.031	2.5	1.4	-0.68	0.86	1.73	0.19	8200	1000	15.8	1.1	10.63	0.85	18.6	5.7	1310	170	-120	320	-40000	38000	103.28		Cuts inclusion
SA5_0810_1	0.388	0.02	9.58	0.84	0.198	0.018	1.065	0.037	62500	4400	114.8	5.6	107.6	5	277	22	2097	92	2346	77	2640	150	20.57		Cuts zones
SA5_0810_2	0.52	0.023	12.4	1.1	0.189	0.018	1.332	0.051	69200	3600	83.1	2.2	64.5	2.1	223	19	2667	98	2538	85	2450	180	-8.86		Cuts inclusions and fractures
SA5_0900_1	0.317	0.027	3.9	1	0.105	0.029	1.009	0.081	20100	1800	36.1	2.3	40.6	2.9	59	11	1720	130	770	220	-290	440	693.10		Cuts resin
SA5_0900_2	0.385	0.028	4.72	0.89	0.116	0.025	1.59	0.1	34600	2500	42.5	1.9	32.8	1.8	88	12	2050	130	1040	210	360	410	-469.44		Cuts inclusion
SA5_0901_1	0.2	0.028	1.69	0.9	0.255	0.061	0.838	0.071	5610	750	18.34	0.97	29.7	1.8	32	8.1	1100	140	-100	220	-60	560	1933.33		Cuts resin
SA5_0905_1	0.2201	0.0093	3.28	0.33	0.112	0.011	2.146	0.069	112600	7400	296	14	168	9	257	24	1275	48	1338	93	1350	230	5.56	R	
SA5_0910_1	0.243	0.038	0.94	0.79	0.192	0.074	0.995	0.095	11100	1500	19.9	1.3	27	1.6	32.3	8.5	1320	190	-340	290	-1000	640	232.00		zone cutter
SA5_0910_2	0.171	0.015	1.82	0.61	0.136	0.05	1.95	0.14	16500	1500	51.8	2.7	33.9	2.1	34.7	8.1	994	83	400	180	-810	460	222.72		Cuts zones
SA7_0001_2	0.1941	0.0054	2.4	0.15	0.0931	0.006	0.793	0.013	26000	18000	162.5	4.8	207.3	5.2	261.1	8.8	1140	29	1208	45	1280	130	10.94	C	
SA7_0003_1	0.176	0.0022	2.274	0.064	0.095	0.0025	1.24	0.012	245000	84000	834.7	9.2	681.9	9	731	17	1044	12	1202	20	1494	52	30.12		Cut zones, radiation damage
SA7_0003_2	0.2346	0.0029	2.868	0.081	0.0899	0.0026	2.082	0.021	97000	74000	571.1	7.5	276.2	3.7	491	13	1358	15	1363	22	1391	55	2.37	R	
SA7_0005_1	0.2102	0.0033	2.49	0.11	0.0865	0.0035	1.545	0.018	67000	31000	278.8	4.2	181.3	3.4	221.7	8.5	1229	18	1249	32	1276	86	3.68	R	
SA7_0005_2	0.1498	0.0026	1.944	0.076	0.0954	0.0038	0.778	0.012	73000	36000	470	11	603	14	383	14	899	15	1081	26	1458	79	38.34		Inclusion and zone cutter
SA7_0101_1	0.1977	0.0043	2.23	0.14	0.0833	0.0055	2.027	0.035	29000	14000	143.3	1.9	70.5	1.2	120.7	6.7	1164	24	1155	47	1070	140	-8.79		Cuts zones
SA7_0101_2	0.1983	0.0044	2.32	0.14	0.0866	0.0055	2.312	0.036	18000	14000	136.4	1.8	58.46	0.99	101.4	6.1	1164	24	1182	46	1130	140	-3.01	R	
SA7_0101_3	0.2011	0.0043	2.24	0.14	0.0804	0.0051	3.181	0.057	16000	13000	133.2	2.4	41.61	0.85	75	4.8	1180	23	1154	46	1010	140	-16.83		Cuts zones
SA7_0104_1	0.2379	0.0034	2.976	0.093	0.0903	0.0029	2.567	0.028	110000	50000	419.1	4.7	161.7	2.3	340	11	1375	18	1397	25	1382	64	0.51		Cuts zones
SA7_0104_2	0.2359	0.0038	3.03	0.12	0.0919	0.0036	1.554	0.02	47000	41000	342.5	7.6	215.6	3.5	412	13	1364	20	1401	29	1387	79	1.66		Cuts inclusion
SA7_0105_1	0.5384	0.006	16.18	0.21	0.211	0.0026	4.15	0.22	590000	280000	963	41	289	28	1330	120	2774	25	2886	12	2907	19	4.58		Cuts resin
SA7_0106_1	0.5488	0.007	16.18	0.32	0.207	0.0038	3.31	0.054	125000	87000	291.5	3.3	88	1.5	426	13	2817	29	2880	19	2867	30	1.74		Cuts zones

SA7_0202_2	0.1584	0.0024	3.329	0.075	0.1484	0.0037	0.813	0.0085	174000	46000	702.3	7.4	855.4	9.3	1357	26	947	14	1481	18	2304	43	58.90		Cuts zones
SA7_0203_1	0.2278	0.0031	2.726	0.097	0.0847	0.003	2.076	0.023	103000	56000	448.8	5.1	214.1	3.4	431	12	1322	16	1323	27	1238	70	-6.79	R	
SA7_0204_1											0.037	0.015	0.09	0.026	13	2.7									Cuts resin
SA7_0205_1	0.1481	0.004	2.266	0.084	0.1108	0.0033	0.533	0.0094	89000	49000	628	28	1188	60	734	20	891	23	1193	27	1780	55	49.94		Cuts inclusion
SA7_0208_1	0.2354	0.0035	3.44	0.1	0.1065	0.003	1.467	0.02	166000	73000	538.8	8.5	361.5	3.8	601	16	1362	18	1504	23	1702	55	19.98	R	
SA7_0301_2	0.278	0.0061	3.66	0.21	0.0992	0.0061	1.456	0.021	26000	18000	100.9	1.4	68.5	1.2	169.7	7	1578	30	1533	45	1440	120	-9.58		Radiation damage
SA7_0303_1	0.1695	0.004	2.079	0.081	0.0916	0.0032	0.7885	0.0089	129000	55000	527.4	7.9	658	11	738	17	1007	22	1129	27	1407	68	28.43		Radiation damage
SA7_0304_1	0.1024	0.0014	1.883	0.041	0.1384	0.003	1.46	0.013	437000	94000	1665	18	1116	15	1517	24	628.3	8.3	1072	14	2188	38	71.28		Radiation damage
SA7_0304_2	0.2911	0.0035	4.09	0.11	0.1071	0.0029	2.906	0.038	220000	100000	510.5	7.1	172.5	3.6	162.7	7.3	1646	18	1641	23	1711	51	3.80	R	
SA7_0306_1	0.2994	0.0058	4.15	0.16	0.1067	0.0045	1.05	0.011	91000	35000	160.8	2.5	149.7	2.7	407	12	1686	29	1645	33	1670	79	-0.96	C	
SA7_0401_1	0.284	0.0064	3.98	0.22	0.1077	0.0063	1.008	0.014	22000	17000	86.6	1.3	84	1.2	220.1	8.7	1608	32	1594	47	1630	120	1.35	R	
SA7_0401_2	0.2842	0.0058	3.78	0.2	0.101	0.0055	0.999	0.012	56000	26000	122.1	1.8	119.6	1.7	307.9	9.5	1609	29	1550	46	1490	120	-7.99		Cuts zones
SA7_0401_3	0.2294	0.0036	3.08	0.12	0.1017	0.0039	1.095	0.011	71000	43000	262.2	3.5	233.9	3.2	461	12	1330	19	1410	30	1613	69	17.54		Cuts zones
SA7_0402_1	0.2644	0.0034	3.67	0.097	0.1024	0.0028	1.94	0.018	260000	110000	554.8	6.3	279.8	3.9	579	15	1511	17	1555	21	1639	48	7.81	C	
SA7_0403_1	0.1685	0.0026	2.506	0.072	0.1088	0.0031	0.976	0.018	189000	86000	677	12	693	21	1032	24	1003	14	1264	21	1744	51	42.49		Cuts zones
SA7_0404_1	0.287	0.0046	3.95	0.14	0.1009	0.0039	1.207	0.013	121000	49000	226.7	3.6	183.8	2.6	389	12	1624	23	1613	29	1570	75	-3.44	R	
SA7_0404_2	0.2879	0.0042	3.99	0.12	0.0995	0.003	1.331	0.016	130000	87000	400.2	5	295.2	5.3	686	15	1630	21	1625	24	1586	57	-2.77		Cuts zones
SA7_0405_1	0.07368	0.00094	1.184	0.03	0.1147	0.0029	1.97	0.016	329000	67000	1687	21	839	13	957	17	458.2	5.6	789	14	1843	46	75.14		Cuts resin
SA7_0504_1	0.3203	0.0042	4.85	0.12	0.1069	0.0026	4.115	0.049	166000	90000	423.9	4.6	101.1	1.3	270.1	8.7	1789	21	1786	21	1716	46	-4.25	R	
SA7_0505_1	0.2207	0.003	2.883	0.085	0.092	0.0027	0.7946	0.0098	137000	64000	441.8	4	547.6	7.8	545	13	1285	16	1369	22	1430	58	10.14		Cuts inclusion
SA7_0506_1	0.2176	0.0029	2.668	0.072	0.0869	0.0023	1.793	0.017	145000	78000	558.4	7.4	306.6	4.6	556	12	1268	16	1311	20	1324	52	4.23		Cuts inclusion
SA7_0506_2	0.2075	0.0027	2.826	0.082	0.0964	0.0028	1.822	0.023	212000	77000	640.8	7.7	346.5	4.4	535	20	1215	14	1355	21	1524	54	20.28		Cuts inclusion
SA7_0701_1	0.1988	0.0036	2.18	0.11	0.0778	0.0042	0.842	0.022	34000	18000	160.5	1.9	193.1	4.8	264.8	8.3	1170	20	1144	39	990	120	-18.18		Cuts resin
SA7_0804_1	0.2909	0.0045	4.37	0.14	0.1073	0.0036	1.33	0.013	92000	43000	257.8	2.8	192.7	2.1	289.4	9.6	1644	22	1693	27	1709	64	3.80	R	
SA8_0000_1	0.23	0.013	2.46	0.47	0.084	0.017	1.029	0.035	3300	5600	13.6	0.31	13.57	0.36	27.3	2.8	1334	71	810	160	170	380	-684.71		Cuts resin
SA8_0001_1	0.2471	0.0042	3.26	0.12	0.0977	0.0037	0.953	0.01	110000	110000	262.9	5	276.7	6.6	459	15	1424	22	1454	28	1505	73	5.38	C	
SA8_0003_2	0.2152	0.0059	2.65	0.21	0.0923	0.0072	0.873	0.016	-20000	28000	71.7	1.2	82.2	1.2	123.7	6.6	1253	31	1273	56	1160	170	-8.02		Cuts zones

SA8_0004_1	0.2217	0.0039	2.75	0.12	0.0912	0.0038	1.365	0.016	500000	120000	279.6	5	205	3.9	305	11	1289	21	1319	33	1356	89	4.94	C	
SA8_0004_2	0.2465	0.0047	2.86	0.11	0.0862	0.0034	1.839	0.02	-300000	130000	262.9	3.2	142.9	1.9	297	10	1418	24	1362	28	1284	76	-10.44		Radiation damage
SA8_0005_1	0.2918	0.0066	3.83	0.22	0.0995	0.0061	2.002	0.035	24000	70000	102.8	1.7	51.4	0.96	127.7	6.5	1647	33	1572	47	1440	120	-14.38	R	
SA8_0009_1	0.2926	0.0055	4.06	0.15	0.1029	0.0041	2.534	0.034	100000	180000	243.2	3.9	95.7	1.5	227.1	8.2	1652	28	1626	31	1592	77	-3.77	R	
SA8_0013_1	0.1966	0.0039	2.06	0.11	0.0781	0.0041	1.991	0.027	120000	110000	216.1	2.6	108.3	1.4	179.9	7.8	1156	21	1111	37	1010	110	-14.46	C	
SA8_0015_1	0.175	0.0027	2.164	0.063	0.091	0.0027	0.9933	0.0093	610000	300000	648	13	650	14	827	22	1039	15	1163	21	1410	59	26.31		Cuts zones
SA8_0100_1	0.2922	0.0064	4.3	0.25	0.11	0.0064	0.958	0.018	150000	100000	118.1	1.4	123.5	2.6	327	15	1649	32	1660	48	1640	120	-0.55		Cuts resin
SA8_0100_2	0.2716	0.007	3.73	0.26	0.102	0.0073	0.6614	0.0095	64000	84000	85.9	1.6	128.4	1.8	290	11	1545	35	1512	60	1400	160	-10.36		Cuts resin
SA8_0101_1	0.2533	0.004	3.13	0.13	0.0896	0.0035	1.476	0.02	350000	360000	349.2	6.2	235.7	6.3	513	19	1456	20	1422	32	1352	83	-7.69	C	
SA8_0103_1	0.268	0.0099	3.17	0.31	0.0921	0.0093	0.948	0.03	20000	51000	45.2	1.5	47.35	0.92	105.5	6.8	1528	51	1334	94	1000	230	-52.80		Cuts inclusion
SA8_0104_1	0.2416	0.0038	3.5	0.1	0.1064	0.0033	1.672	0.022	310000	610000	569.6	6.4	338.2	4.6	582	17	1394	20	1516	23	1690	58	17.51		Cuts zones
SA8_0104_2	0.3059	0.0063	4.11	0.21	0.0993	0.005	1.785	0.028	600000	250000	177.7	2.8	98.6	1.8	256	12	1717	31	1623	43	1500	100	-14.47	R	
SA8_0105_1	0.2341	0.0046	3.06	0.12	0.0957	0.0036	1.78	0.021	560000	680000	495	26	274	14	557	28	1354	24	1405	28	1469	71	7.83		Cuts resin
SA8_0105_2	0.2234	0.0036	2.82	0.087	0.0924	0.0027	2.314	0.056	1100000	1100000	803	15	346.2	4.8	564	18	1298	19	1352	24	1431	59	9.29	C	
SA8_0109_2	0.1877	0.0035	1.88	0.09	0.0723	0.0033	1.081	0.012	480000	420000	349	4.4	320.8	4.1	533	17	1108	19	1056	31	906	98	-22.30	C	
SA8_0112_1	0.2458	0.004	3.01	0.12	0.0886	0.0034	2.004	0.023	780000	590000	349	4.4	173.5	2.5	377	13	1416	21	1397	31	1331	82	-6.39	C	
SA8_0113_1	0.1917	0.0046	2.26	0.18	0.0856	0.0067	1.488	0.026	270000	170000	131.3	1.8	87.8	1.4	151.9	8.7	1129	25	1123	63	1010	180	-11.78	R	
SA8_0115_1	0.2965	0.0046	4.33	0.13	0.1059	0.0029	1.262	0.013	1300000	1100000	569	7.2	450.1	6.3	860	20	1672	23	1689	24	1697	51	1.47	C	
SA8_0200_1	0.2646	0.0057	3.2	0.18	0.0891	0.0052	1.004	0.013	600000	290000	162.7	2.4	161.7	2.3	374	13	1510	29	1430	46	1240	120	-21.77		Cuts resin
SA8_0200_2	0.2544	0.0071	2.96	0.24	0.0864	0.0071	0.5225	0.0087	800000	130000	79.3	1.1	152.4	2.5	332	12	1457	36	1342	62	1020	180	-42.84	C	
SA8_0201_1	0.1835	0.0052	1.89	0.18	0.0764	0.0074	1.534	0.026	0	130000	117.7	1.9	76.8	1.4	133.3	7.7	1083	29	989	70	700	210	-54.71	R	
SA8_0203_2	0.494	0.014	13.51	0.59	0.199	0.0079	0.642	0.013	-200000	170000	58	1	91.1	1.9	333	12	2581	61	2688	41	2776	65	7.02	R	
SA8_0204_1	0.422	0.011	10.09	0.48	0.1756	0.0084	0.857	0.015	220000	230000	106.9	1.7	125.1	2.5	394	18	2263	49	2409	45	2520	81	10.20	C	
SA8_0205_1	0.296	0.0056	4.17	0.17	0.1021	0.0042	0.852	0.01	240000	320000	224.8	3.1	263.7	4.2	648	18	1669	28	1645	34	1575	84	-5.97		Fracture, radiation damage
SA8_0209_2	0.2867	0.0045	3.99	0.13	0.1003	0.0028	2.422	0.038	-390000	770000	605.1	9.9	252.3	6.6	473	15	1626	23	1618	26	1591	54	-2.20		Cuts resin
SA8_0212_1	0.1711	0.0026	2.388	0.074	0.1012	0.003	1.348	0.019	920000	650000	933	19	699	19	651	20	1018	14	1231	23	1599	58	36.34	C	

SA8_0215_2	0.2052	0.0053	2.4	0.16	0.0855	0.0058	1.079	0.016	150000	130000	153.5	1.9	142.6	1.9	205.4	9.9	1200	29	1198	50	1110	140	-8.11	R	Radiation damage
SA8_0301_1	0.2322	0.005	2.81	0.15	0.0877	0.0048	1.511	0.021	110000	160000	189.3	3.2	125	2.2	256	11	1347	27	1325	42	1230	120	-9.51		Cuts inclusion
SA8_0302_1	0.2196	0.0028	3.44	0.082	0.1132	0.0025	1.228	0.01	1400000	710000	1075	11	870.6	8.6	1582	33	1279	15	1508	19	1831	39	30.15		Cuts resin
SA8_0302_2	0.2919	0.0046	4.09	0.12	0.101	0.0028	1.072	0.011	530000	490000	541.5	6.9	502.9	7.5	1082	26	1649	23	1643	24	1617	55	-1.98	R	
SA8_0303_1	0.3037	0.0049	4.68	0.15	0.1118	0.0036	1.387	0.015	270000	380000	420.2	7.3	301.6	5.8	698	18	1708	24	1747	28	1772	65	3.61	R	
SA8_0303_2	0.3164	0.0052	4.62	0.14	0.1055	0.0033	2.501	0.027	110000	390000	443.4	5.3	176.1	2.4	455	14	1770	26	1739	26	1692	60	-4.61	R	
SA8_0304_1	0.1918	0.0052	2.04	0.16	0.0767	0.0064	1.011	0.016	23000	54000	108.1	1.8	106	2.1	164.7	7.6	1128	28	1053	61	800	180	-41.00		Cuts inclusion
SA8_0304_2	0.1548	0.0026	1.753	0.063	0.0816	0.0031	0.6313	0.0051	350000	270000	744	11	1160	21	1532	30	927	14	1019	24	1174	80	21.04	R	
SA8_0305_1	0.2447	0.0039	3.22	0.13	0.0948	0.0038	1.229	0.014	260000	200000	351.3	4.6	280.7	3.5	544	16	1410	20	1441	32	1433	81	1.61	R	
SA8_0309_1	0.1251	0.0023	2.004	0.058	0.1154	0.0032	1.699	0.021	1040000	320000	1255	27	725	12	996	24	761	13	1108	20	1859	50	59.06		Fracture, radiation damage
SA8_0311_1	0.2536	0.004	3.5	0.14	0.0994	0.0038	0.82	0.012	190000	140000	244.1	6.3	298	11	551	24	1456	21	1505	32	1550	73	6.06		Cuts resin
SA8_0311_2	0.2548	0.0053	3.49	0.12	0.0992	0.0033	0.891	0.019	330000	240000	451	14	520	28	1003	37	1461	27	1512	26	1564	64	6.59		Fracture, radiation damage
SA8_0312_1	0.565	0.021	16.6	1.1	0.216	0.014	2.82	0.12	23000	21000	18.05	0.44	6.67	0.28	29.2	3.1	2863	86	2846	67	2800	130	-2.25	R	
SA8_0315_1	0.2609	0.0077	3.78	0.29	0.1076	0.0087	1.116	0.021	24000	30000	57.9	1.1	51.6	1.1	73.8	5.1	1489	39	1529	64	1480	170	-0.61	C	
SA8_0402_1	0.2899	0.007	4.04	0.23	0.1024	0.006	1.852	0.03	85000	58000	96.5	1.5	52.03	0.96	125.7	5.7	1637	35	1598	49	1500	120	-9.13	R	
SA8_0402_2	0.2977	0.0078	4.12	0.26	0.1012	0.0062	2.166	0.039	43000	43000	75.1	1.3	34.84	0.69	83.4	4.6	1675	38	1610	52	1450	130	-15.52	R	
SA8_0404_1	0.205	0.0052	2.42	0.15	0.0866	0.0055	1.294	0.021	27000	41000	112.5	2.1	89.1	2.1	156.6	7.1	1199	28	1208	48	1130	140	-6.11		Cuts resin
SA8_0405_1	0.2546	0.0041	3.68	0.12	0.1041	0.0033	0.8478	0.0082	230000	160000	329.6	5.1	401	7.1	730	17	1463	21	1559	25	1664	57	12.08	R	
SA8_0405_2	0.2509	0.0041	3.66	0.1	0.1051	0.0028	0.6051	0.0072	140000	180000	390.9	9.7	679	22	1297	35	1442	21	1556	23	1702	49	15.28		Cuts inclusion, radiation damage
SA8_0409_1	0.2235	0.0038	2.784	0.083	0.0901	0.0027	1.598	0.016	140000	150000	373.5	6.3	245.8	4.1	439	12	1299	20	1340	23	1380	61	5.87		Cuts zones
SA8_0409_2	0.2284	0.0035	2.844	0.088	0.0902	0.0029	1.532	0.015	170000	150000	385.3	4.1	266.1	2.8	449	11	1325	18	1360	24	1379	64	3.92	R	
SA8_0409_3	0.0892	0.0013	1.4	0.037	0.1131	0.0029	0.638	0.011	890000	180000	1603	17	2678	51	1246	21	550.4	7.9	884	15	1816	47	69.69		Radiation damage
SA8_0411_1	0.2731	0.0054	3.86	0.16	0.1029	0.0045	1.052	0.01	98000	73000	176.6	2.4	175.8	2.4	401	12	1554	27	1586	35	1582	87	1.77		Cuts inclusion
SA8_0412_1	0.2283	0.0044	2.71	0.13	0.0865	0.0042	1.475	0.017	75000	58000	179.9	3.6	127	3.1	242.2	9.1	1324	23	1307	38	1220	100	-8.52	R	

SA8_0412_2	0.235	0.0048	2.71	0.14	0.084	0.0045	1.645	0.022	62000	42000	134.3	3.6	84.2	2.5	163.5	7.5	1359	25	1303	41	1150	110	-18.17		Cuts zones
SA8_0414_1	0.2296	0.0044	2.73	0.14	0.0865	0.0046	1.867	0.023	11000	55000	196.4	2.6	106.6	1.6	193.7	8.1	1331	23	1310	40	1200	110	-10.92	C	
SA8_0415_1	0.1888	0.0031	1.999	0.094	0.0766	0.0037	0.785 2	0.007 5	80000	56000	267.1	2.9	336.5	3.6	547	14	1114	17	1104	33	1031	98	-8.05		Cuts inclusion
SA8_0415_2	0.1946	0.0034	2.134	0.094	0.0789	0.0034	2.057	0.031	72000	66000	318	3.3	153.6	2.5	248	10	1147	18	1142	31	1089	91	-5.33	R	
SA8_0501_1	0.2062	0.0055	2.63	0.17	0.0942	0.0065	0.442 7	0.006 7	32000	27000	126.3	3.2	284.9	9.6	454	15	1206	30	1263	49	1270	140	5.04		Cuts zones
SA8_0502_1	0.2042	0.003	3.17	0.077	0.1115	0.0026	4.264	0.052	440000	160000	826	12	191.5	3.3	257.8	9.9	1197	16	1442	19	1805	44	33.68		Cuts resin
SA8_0502_2	0.4196	0.0066	10.69	0.24	0.183	0.0039	0.601 1	0.008 2	140000	130000	306.4	4.2	506	9.4	1568	43	2256	30	2489	21	2668	36	15.44	C	
SA8_0505_1	0.1354	0.0024	1.97	0.065	0.1038	0.0034	1.037	0.015	147000	86000	696.4	8.8	668.2	7.9	1513	29	818	14	1094	22	1662	60	50.78	C	
SA8_0509_2	0.3303	0.0051	5.2	0.13	0.1137	0.003	0.997 7	0.009 1	200000	140000	469.9	5.3	469.3	5.1	1314	27	1838	25	1844	23	1831	47	-0.38	C	
SA8_0511_1	0.2104	0.0042	2.89	0.12	0.1003	0.0046	2.06	0.044	113000	58000	315.1	7.3	156.5	5.6	339	18	1229	22	1357	33	1519	95	19.09		Cuts resin
SA8_0513_1	0.1913	0.0044	2.03	0.14	0.0766	0.0054	0.589 8	0.009 7	40000	29000	168.5	2.1	286.5	4.4	485	15	1127	24	1084	48	880	150	-28.07		Cuts inclusion
SA8_0515_2	0.1941	0.0049	2.26	0.15	0.0834	0.0056	1.539	0.024	41000	25000	144.7	1.9	94.2	1.5	135.8	7.2	1141	26	1147	51	1050	150	-8.67	R	
SA8_0515_3	0.1959	0.0044	2.27	0.14	0.0836	0.0052	2.387	0.041	-10000	24000	158.9	2.4	66.9	1.3	118.8	7.4	1152	24	1163	44	1080	130	-6.67	R	
SA8_0600_1	0.2216	0.0049	2.67	0.15	0.0865	0.0049	1.313	0.018	50000	31000	169.8	2	129.3	1.6	264	10	1288	26	1283	42	1190	120	-8.24	C	
SA8_0600_2	0.2237	0.0047	2.43	0.14	0.0785	0.0044	1.49	0.021	50000	31000	161.8	2.5	108.7	1.9	210.1	8.9	1299	25	1229	43	1030	120	-26.12		Cuts resin
SA8_0602_1	0.202	0.0037	2.35	0.1	0.0841	0.0038	1.958	0.026	74000	55000	333	4.2	169.6	2.2	210	11	1185	20	1214	31	1227	90	3.42		Cuts zones
SA8_0602_2	0.2148	0.0041	2.45	0.14	0.0821	0.0048	1.619	0.023	69000	38000	215.4	2.9	132.4	1.7	232.4	9.6	1252	22	1229	41	1100	120	-13.82	R	
SA8_0603_1	0.2975	0.0053	4.06	0.15	0.0987	0.0038	0.958	0.011	111000	69000	277.7	3.6	286.5	3.3	717	20	1676	26	1631	30	1547	72	-8.34		Cuts resin
SA8_0609_1	0.1663	0.0048	1.87	0.17	0.0802	0.0076	1.117	0.022	17000	14000	104	2.4	92.5	2.2	123.8	7.2	989	27	977	68	810	210	-22.10		Miss
SA8_0609_2	0.1462	0.0019	1.625	0.056	0.08	0.0028	0.719 8	0.005 5	320000	110000	906.8	9.4	1242	14	1322	26	879	11	969	22	1139	72	22.83		
SA8_0611_1	0.1322	0.0057	1.71	0.22	0.094	0.012	0.619	0.014	8300	6900	62.9	2.2	103.3	4.5	101.3	6.3	797	32	858	91	800	290	0.38		Cuts resin
SA8_0613_2	0.189	0.0043	2.06	0.12	0.079	0.0048	0.976	0.012	47000	30000	184.1	2.5	186.7	2.5	295	11	1114	23	1100	44	970	130	-14.85	R	
SA8_0614_1	0.1841	0.0036	2.58	0.13	0.0998	0.0049	0.672 9	0.008 9	112000	45000	277.1	5.6	414	11	730	18	1088	20	1263	39	1519	96	28.37	R	
SA8_0614_2	0.1752	0.0031	1.897	0.092	0.0775	0.0036	0.569 1	0.005 3	107000	47000	294.1	4.6	517	8.5	793	19	1040	17	1056	33	1030	100	-0.97		Cuts zones
SA8_0615_2	0.1909	0.0033	2.013	0.086	0.0759	0.0033	1.622	0.026	55000	46000	265.1	3.9	166.1	4	280	12	1125	18	1102	29	987	89	-13.98	C	
SA8_0700_2	0.2892	0.0054	3.98	0.18	0.0994	0.0045	0.973	0.011	48000	48000	172.7	2.4	179.2	2.7	469	13	1635	27	1609	37	1520	90	-7.57	C	
SA8_0702_1	0.2932	0.0059	4.42	0.22	0.1089	0.0054	1.844	0.028	67000	38000	130.7	2	72.1	1.3	200	8.4	1655	29	1691	39	1680	92	1.49	C	

SA8_0703_1	0.2238	0.0064	2.68	0.2	0.0872	0.0065	1.231	0.02	13000	16000	72	1.2	59.8	1.1	124.5	6.6	1302	34	1285	57	1150	150	-13.22	C	
SA8_0703_2	0.2292	0.0046	2.7	0.15	0.0842	0.0047	1.941	0.029	24000	40000	168.8	2.9	89	2	186.8	8.3	1329	24	1295	42	1150	120	-15.57		Cuts inclusion
SA8_0704_1	0.2185	0.0045	2.64	0.13	0.088	0.0046	1.909	0.026	46000	34000	152.8	2.3	81.7	1.7	146.2	6.7	1272	24	1284	39	1230	110	-3.41	R	
SA8_0709_1	0.2172	0.0036	2.825	0.076	0.0937	0.0025	1.879	0.042	300000	140000	652.2	9.9	361	11	358	13	1266	19	1356	20	1462	52	13.41	C	
SA8_0711_1	0.179	0.0027	1.905	0.079	0.0766	0.0031	3.717	0.042	113000	83000	458.8	8	124.8	2	166.4	7.3	1061	15	1066	28	1011	88	-4.95	C	
SA8_0711_2	0.181	0.0037	1.82	0.11	0.0724	0.0045	6.67	0.13	77000	38000	210	2.6	32.04	0.71	55.4	4.5	1071	20	1021	42	820	130	-30.61		Cuts inclusion
SA8_0712_2	0.253	0.0044	3.71	0.14	0.1055	0.0038	0.4025	0.0044	191000	76000	295.3	3.8	733	11	1634	30	1452	22	1555	30	1662	72	12.64		Cuts zones
SA8_0712_3	0.2797	0.0044	4.07	0.13	0.1046	0.0031	0.4954	0.0046	130000	100000	381.9	4.8	768	11	1892	33	1588	22	1638	25	1660	57	4.34		Cuts zones
SA8_0713_1	0.1838	0.0033	1.952	0.088	0.0766	0.0035	0.8933	0.0087	82000	58000	324.6	4.5	360.1	5.2	593	16	1087	18	1082	31	997	96	-9.03	R	
SA8_0713_2	0.1872	0.0076	2.09	0.25	0.084	0.011	0.658	0.011	12900	6600	35.22	0.57	53.06	0.85	94.8	5.8	1101	41	977	98	710	270	-55.07		cuts inclusion
SA8_0714_1	0.2288	0.004	2.78	0.11	0.0869	0.0035	1.995	0.023	87000	71000	331.3	5	164	3.2	321	13	1327	21	1335	31	1293	83	-2.63		Radiation damage
SA8_0800_1	0.2084	0.0038	2.27	0.11	0.0791	0.004	1.334	0.017	93000	49000	252.7	2.9	186.9	2.4	358	15	1219	20	1181	36	1040	110	-17.21		Cuts zones
SA8_0800_2	0.2153	0.0043	2.45	0.13	0.0823	0.0046	1.632	0.02	65000	37000	193.5	2.7	117.2	1.8	233.2	9.7	1255	23	1226	41	1090	120	-15.14		Cuts zones
SA8_0801_1	0.195	0.0038	2.118	0.098	0.0787	0.0038	2.277	0.024	30000	61000	358.9	4.7	155.9	2.2	292	12	1147	21	1135	33	1050	100	-9.24	R	
SA8_0801_2	0.1928	0.0044	2.52	0.17	0.096	0.0066	2.379	0.042	56000	25000	151.3	2	63.3	1.1	158.7	8.9	1135	24	1236	51	1300	140	12.69		Cuts inclusion
SA8_0803_1	0.2939	0.0077	4.27	0.29	0.105	0.0074	0.764	0.013	22000	17000	67.3	1.6	88	2.6	235	12	1656	38	1631	61	1480	150	-11.89		Cuts zones
SA8_0803_2	0.296	0.012	3.58	0.38	0.0907	0.0098	1.217	0.03	11000	9200	37.93	0.87	31.21	0.73	85.8	5.9	1662	57	1380	100	930	230	-78.71		Cuts inclusion, cuts zones
SA8_0804_1	0.17	0.0022	2.629	0.069	0.1109	0.0028	0.5871	0.0057	450000	130000	952	16	1619	30	1070	25	1011	12	1301	19	1791	48	43.55		Cuts resin
SA8_0804_2	0.2942	0.0043	4.14	0.15	0.1015	0.0037	1.627	0.019	178000	78000	303.4	4.6	185.4	3.1	480	15	1661	22	1647	29	1592	67	-4.33	R	
SA8_0805_1	0.1895	0.0059	2.15	0.19	0.0818	0.0073	1.715	0.036	15000	13000	80.8	1.3	47.14	0.95	81.1	5.3	1115	32	1085	69	910	190	-22.53		Radiation damage
SA8_0805_2	0.1964	0.0061	2.17	0.22	0.0806	0.0086	2.697	0.068	21000	11000	67	1	25.02	0.55	48.6	4.4	1152	33	1060	79	760	220	-51.58	R	
SA8_0809_1	0.325	0.0062	6.09	0.25	0.1349	0.0055	1.231	0.016	177000	58000	215.4	2.8	174.2	2.2	659	26	1815	31	1971	38	2099	75	13.53	C	
SA8_0900_1	0.2542	0.0047	3.21	0.14	0.0913	0.0039	1.587	0.018	75000	52000	246.1	4.4	154.8	3	330	12	1458	24	1442	34	1382	83	-5.50	C	
SA8_0900_2	0.2199	0.0038	3.092	0.094	0.1017	0.0034	1.0829	0.0098	166000	82000	435.2	7.7	401.6	7.1	745	19	1280	20	1419	23	1596	63	19.80		Cuts zones
SA8_0901_1	0.0803	0.0016	1.366	0.035	0.1227	0.0029	0.2849	0.0033	530000	110000	2153	42	7570	190	3276	51	497.8	9.5	871	15	1967	44	74.69		Fracture, cuts resin

SA8_0901_2	0.097	0.0015	1.42	0.048	0.1051	0.0037	0.245	0.0031	178000	65000	858	10	3510	43	795	19	596.7	9	888	20	1658	67	64.01		Cuts zones
SA8_0902_1	0.1792	0.0039	1.97	0.12	0.0797	0.0054	1.312	0.02	27000	23000	169.3	3.1	129	2.2	186.5	8.4	1061	21	1078	44	1010	140	-5.05		Cuts resin
SA8_0902_2	0.1858	0.0053	1.97	0.15	0.078	0.0063	1.639	0.028	31000	16000	111.8	1.8	68.3	1.2	114.9	6.1	1096	29	1051	56	860	170	-27.44	R	
SA8_0903_1	0.1101	0.0019	1.701	0.058	0.1105	0.0036	0.756	0.016	200000	64000	812	15	1084	29	494	14	673	11	998	22	1764	63	61.85		Cuts resin
SA8_0903_2	0.2309	0.0082	2.7	0.27	0.0863	0.0088	1.218	0.027	7300	8400	49.1	0.88	40.02	0.76	79.2	6.1	1333	42	1197	91	900	220	-48.11	C	
SA8_0904_1	0.2798	0.0053	3.95	0.2	0.1023	0.0053	0.97	0.011	31000	34000	174.7	2.3	177.3	2.7	373	12	1591	27	1598	41	1550	100	-2.65	R	
SA8_0904_2	0.2813	0.0073	3.98	0.17	0.1029	0.0044	0.815	0.016	114000	53000	264.2	8.1	330	16	736	26	1593	37	1611	37	1600	80	0.44		Cuts inclusion
SA8_0909_1	0.2645	0.0046	3.8	0.16	0.1036	0.0044	2.014	0.029	94000	47000	246.8	3	121.1	2	160.4	8.2	1511	24	1575	34	1628	76	7.19	R	
SA8_0911_2	0.1521	0.0028	1.936	0.094	0.0912	0.0042	0.7321	0.0088	93000	41000	382.9	5.5	514.8	7.1	625	15	912	15	1075	31	1351	89	32.49		Cuts inclusion
SA8_0911_4	0.1931	0.0045	2.1	0.14	0.0781	0.0054	1.143	0.014	49000	21000	147.4	2.1	127.3	2.1	196.6	8.2	1136	24	1096	50	910	150	-24.84	R	
SA8_0915_2	0.2348	0.0047	2.83	0.14	0.0872	0.0044	1.019	0.012	72000	36000	214.2	5.9	208.8	6.3	419	17	1358	25	1341	38	1270	100	-6.93	C	
SA8_0915_3	0.2281	0.0045	2.86	0.16	0.0915	0.0052	1.023	0.014	70000	28000	166.6	3	161.9	2.7	289	11	1323	24	1344	42	1290	120	-2.56		Cuts resin
SA10_0000_1	0.2975	0.0015	4.261	0.045	0.1073	0.0012	1.8064	0.0078			453.2	4.6	253.5	2.4	459.4	4.7	1678.7	7.5	1683	8.8	1740	20	3.52		Cuts resin
SA10_0000_2	0.32	0.0023	4.534	0.08	0.1062	0.0019	2.7	0.023			161	3.1	61	1.5	144.2	3.3	1789	11	1729	15	1712	34	-4.50		Cuts inclusion
SA10_0001_2	0.2295	0.0014	2.705	0.042	0.0885	0.0015	1.82	0.01			292.2	4.2	162	2.3	245.4	4.2	1331.7	7.3	1326	12	1370	31	2.80	R	
SA10_0002_1	0.1931	0.0023	2.012	0.085	0.0787	0.0034	2.708	0.026			62.62	0.4	23.43	0.22	33.5	1.2	1137	12	1084	30	947	96	-20.06	C	
SA10_0002_2	0.198	0.0015	2.063	0.045	0.0781	0.0018	2.621	0.015			175.3	1.7	67.39	0.75	104.7	2.2	1164	8.1	1126	15	1083	48	-7.48	C	
SA10_0003_2	0.3099	0.0018	4.582	0.057	0.1105	0.0014	0.9718	0.0084			262.8	2.7	272.2	4.1	346.3	4.6	1739.7	9	1743	10	1794	24	3.03	R	
SA10_0004_2	0.13128	0.00078	1.578	0.016	0.08988	0.00091	1.948	0.013			1229	10	632	6.1	623	6.8	795	4.4	960.1	6.4	1413	19	43.74		Fracture, metamictization
SA10_0006_1	0.2317	0.0018	2.828	0.048	0.0911	0.0015	2.043	0.021			257.4	1.2	127.4	1.4	210.2	3.3	1342.6	9.4	1355	13	1422	32	5.58	C	
SA10_0009_1	0.182	0.0018	2.321	0.092	0.0951	0.0036	1.276	0.019			91.4	1.2	73	1.4	132.1	4.6	1077	10	1199	29	1396	78	22.85		Cuts inclusion, radiation damage
SA10_0011_2	0.5344	0.0034	13.66	0.14	0.1902	0.0019	1.837	0.011			181.8	2.9	98.7	1.4	395.4	4.8	2758	14	2722.7	9.6	2734	17	-0.88	R	
SA10_0012_1	0.1801	0.0011	2.726	0.032	0.1127	0.0012	1.4665	0.0069			687.6	7.4	469.5	5.8	553.9	5.3	1067	6.1	1333.4	8.6	1831	20	41.73	R	
SA10_0012_2	0.3224	0.0021	4.662	0.069	0.1072	0.0015	3.036	0.018			188.7	2.7	62.3	1	161.4	2.8	1801	10	1755	12	1735	27	-3.80	C	

SA10_0013_1	0.2144	0.0017	2.58	0.058	0.0892	0.0021	1.448	0.017	154.8	1.1	107.09	0.79	128.1	2.4	1251.7	8.9	1284	17	1355	48	7.62	R	
SA10_0013_2	0.2391	0.0015	2.849	0.048	0.0888	0.0015	1.931	0.012	253	3.1	131.7	2.2	244.1	3.7	1381.8	8	1363	13	1373	34	-0.64		Cuts zones
SA10_0014_1	0.2513	0.0024	3.67	0.047	0.1086	0.0011	1.7074	0.008	631.5	3.6	369.6	2.4	696.4	6.2	1445	13	1561	10	1767	18	18.22	R	
SA10_0014_2	0.2952	0.0018	4.258	0.051	0.1078	0.0013	2.189	0.013	383.9	6.1	176.3	3.4	391.8	5.8	1666.8	9	1682	10	1747	23	4.59		Cuts resin
SA10_0015_1	0.2879	0.0023	3.857	0.085	0.0996	0.0022	0.7115	0.0037	104.4	1.2	146.4	1.7	346	4.5	1630	12	1592	18	1576	44	-3.43	C	
SA10_0015_2	0.2931	0.0022	4.039	0.072	0.1026	0.0019	0.7755	0.0059	146.1	2.8	190.5	4.8	455.8	9.8	1656	11	1632	15	1645	35	-0.67	C	
SA10_0016_1	0.2427	0.0015	2.839	0.047	0.0875	0.0015	1.7473	0.0079	262.1	3.5	149.2	2	299.9	4.4	1400.3	7.6	1358	12	1339	34	-4.58	C	
SA10_0017_1	0.2865	0.0019	4.025	0.066	0.1057	0.0018	0.8973	0.0038	195.8	3	216.9	3.4	513.9	6.4	1623.4	9.5	1634	13	1699	31	4.45		Cuts resin
SA10_0100_1	0.1997	0.0036	2.25	0.13	0.086	0.0052	2.41	0.04	25.91	0.56	11.05	0.36	21.5	1.3	1174	20	1157	42	990	130	-18.59	C	
SA10_0100_2	0.2004	0.0036	2.24	0.12	0.085	0.0048	3.418	0.049	26.6	0.43	7.84	0.16	14.22	0.86	1175	19	1147	40	990	130	-18.69	C	
SA10_0101_2	0.2534	0.0017	3.642	0.048	0.108	0.0014	1.2529	0.0049	360.9	3.4	285.1	2.7	548.5	5.2	1455.3	8.9	1555	10	1752	23	16.93	R	
SA10_0101_3	0.2389	0.0017	3.28	0.039	0.1034	0.0012	1.251	0.01	499.7	6.9	400.6	8.3	741.5	8.7	1380.5	8.7	1473.1	9	1673	21	17.48		Cuts zones
SA10_0103_2	0.2701	0.0015	3.813	0.056	0.1062	0.0015	0.814	0.0045	344.6	3.9	418.1	4.4	869.1	6.8	1541.3	7.5	1590	12	1716	25	10.18	C	
SA10_0104_1	0.265	0.0017	3.724	0.06	0.1053	0.0016	1.0465	0.0049	220.3	3.4	208.1	3.4	429.8	6.6	1515.7	8.7	1570	13	1702	30	10.95		Cuts inclusion
SA10_0104_2	0.1698	0.0014	2.306	0.028	0.1023	0.001	1.415	0.022	939	27	696	31	820	29	1010.3	7.9	1210.6	8.5	1657	18	39.03		Metamictization
SA10_0105_1	0.1925	0.0012	2.325	0.034	0.0907	0.0014	1.0993	0.006	425.8	6.4	380.9	4.8	506.9	5.4	1134.5	6.7	1215	10	1422	29	20.22	R	
SA10_0105_2	0.2024	0.0017	2.364	0.044	0.088	0.0016	1.315	0.018	261.6	2.1	198.1	3.1	267.7	3.7	1187.8	9.1	1224	13	1348	36	11.88		Cuts resin
SA10_0106_1	0.2477	0.0016	3.102	0.051	0.0946	0.0016	0.9635	0.004	224.9	1.1	229.1	1.2	466.8	5.1	1426.3	8.2	1428	12	1490	32	4.28		Cuts zones
SA10_0106_2	0.237	0.0018	3.02	0.055	0.0963	0.0018	1.325	0.011	179.9	1.3	133.9	1.6	239.2	4.4	1370.5	9.2	1408	14	1522	36	9.95		Cuts zones
SA10_0108_1	0.3143	0.002	4.465	0.068	0.107	0.0016	2.6	0.015	194.7	2.2	73.7	1	200.6	3.1	1762.1	9.7	1718	13	1729	28	-1.91	R	
SA10_0109_2	0.3607	0.0056	6.21	0.27	0.1307	0.0054	0.7503	0.0071	26.24	0.3	34.46	0.46	110.2	3	1980	26	1951	34	1977	74	-0.15	C	
SA10_0110_1	0.2984	0.0019	4.049	0.059	0.1022	0.0015	1.5428	0.009	207.3	3	131.3	1.5	336.8	4.4	1683.5	9.4	1639	12	1644	27	-2.40	C	
SA10_0111_1	0.5043	0.004	14	0.16	0.2086	0.0019	1.567	0.023	195.7	2.8	127.6	3.9	429.7	5.6	2630	17	2746	10	2888	15	8.93		Fracture, radiation damage
SA10_0112_1	0.1987	0.001	3.007	0.028	0.1135	0.0011	0.878	0.014	637.5	5.1	721.4	7	731.7	5.8	1168.1	5.5	1407	7.2	1852	17	36.93		Radiation damage

SA10_0112_2	0.2061	0.0011	2.873	0.032	0.1047	0.0012	3.09	0.018	503.7	3.5	160.5	1.3	356.6	4.4	1207.9	5.6	1371.4	8.4	1693	21	28.65	R	
SA10_0113_1	0.3148	0.0017	4.508	0.049	0.1074	0.0011	1.7591	0.0073	381.7	5	213.4	3.1	572	6.3	1764	8.2	1729.3	9.1	1749	20	-0.86	R	
SA10_0115_1	0.2976	0.002	4.055	0.058	0.102	0.0015	0.8236	0.0058	210.8	4.3	255.1	6.4	647	14	1678.7	9.9	1640	12	1642	28	-2.24		Cuts zones
SA10_0115_2	0.3057	0.0023	4.255	0.086	0.1041	0.0022	1.3994	0.009	100.3	1.3	70.9	1	187.6	3.1	1719	12	1673	17	1664	39	-3.31	R	
SA10_0116_1	0.2513	0.0017	3.34	0.052	0.0996	0.0015	1.681	0.011	201.3	2.2	118.7	1.3	255.7	3.4	1445.8	8.9	1486	12	1594	29	9.30		Cuts resin
SA10_0116_2	0.2425	0.0023	3.201	0.066	0.099	0.0019	0.634	0.0061	168.5	3.4	263.3	5.4	518	14	1398	12	1446	16	1568	37	10.84	C	
SA10_0117_2	0.193	0.0039	2.2	0.12	0.0865	0.0051	0.935	0.029	26.12	0.27	29.85	0.88	40.1	1.4	1136	21	1137	40	1000	130	-13.60		Cuts resin
SA10_0200_1	0.1952	0.0013	2.062	0.041	0.0791	0.0016	2.057	0.011	224.4	2.1	108.48	0.84	172.1	2.9	1149	6.9	1130	14	1139	40	-0.88		Cuts inclusion
SA10_0201_1	0.12929	0.0008	1.672	0.023	0.0966	0.0013	1.321	0.017	703.1	8.4	532.7	4.7	408.4	5.3	783.7	4.5	994.8	8.9	1542	27	49.18		Cuts zones
SA10_0201_2	0.1718	0.0011	1.866	0.039	0.0809	0.0017	0.759	0.011	318.3	5	433	11	607	13	1021.7	6.1	1060	14	1168	42	12.53		Cuts zones
SA10_0202_1	0.308	0.0018	4.338	0.062	0.1051	0.0015	1.2476	0.0087	220.6	2.4	176.1	1.3	415	4.7	1730.2	8.7	1694	12	1693	26	-2.20		Cuts zones
SA10_0205_2	0.1849	0.0048	1.87	0.18	0.0792	0.0081	1.078	0.014	12.5	0.18	11.7	0.18	18.07	0.93	1089	26	832	83	440	210	-147.50		Metamictization
SA10_0206_2	0.2649	0.002	3.689	0.069	0.1033	0.002	1.438	0.015	161.12	0.81	113.8	1.3	227.4	3.3	1514	10	1558	15	1643	36	7.85	R	
SA10_0207_1	0.2634	0.0024	3.603	0.051	0.101	0.0012	1.551	0.014	399.6	6.2	262.9	5.6	520	4.9	1506	12	1545	11	1631	22	7.66		Cuts inclusion
SA10_0207_2	0.2959	0.002	4.091	0.061	0.1019	0.0016	1.4388	0.0068	210.9	3.4	148.2	2.6	359	5.5	1670	10	1645	12	1635	29	-2.14	R	
SA10_0209_1	0.2531	0.002	3.197	0.073	0.0925	0.0022	1.512	0.0093	115.1	1.3	77	1	166.5	3.7	1453	10	1447	18	1433	48	-1.40	C	
SA10_0209_2	0.2356	0.0013	2.933	0.039	0.0913	0.0013	2.663	0.016	406.7	3.6	154.7	1.9	306.9	4.3	1363.5	6.8	1387	10	1434	27	4.92	R	
SA10_0210_2	0.2928	0.0016	4.15	0.059	0.1032	0.0015	0.6314	0.0057	261.2	5.3	426	12	1012	23	1655.8	8	1660	12	1669	26	0.79		Cuts inclusion
SA10_0211_2	0.2864	0.0032	4.07	0.12	0.104	0.0031	1.223	0.011	56.25	0.91	46.71	0.87	100.4	2.7	1622	16	1621	25	1597	60	-1.57		Cuts resin
SA10_0213_1	0.2828	0.0017	3.917	0.05	0.1006	0.0014	4.124	0.029	269.1	2.4	65.76	0.43	150.2	2.5	1605.1	8.4	1614	10	1614	26	0.55		Cuts resin
SA10_0214_1	0.3178	0.0019	4.683	0.071	0.1069	0.0017	1.9255	0.0097	208.6	1.6	109.17	0.75	281.8	3.5	1778.3	9.1	1757	13	1726	29	-3.03	R	
SA10_0214_2	0.2916	0.0015	4.299	0.041	0.10653	0.00099	2.46	0.011	547.3	5.7	224.5	2.8	458.9	4.6	1649.7	7.4	1690.8	8	1733	18	4.81		Cuts resin
SA10_0215_1	0.2288	0.0026	2.744	0.051	0.087	0.0014	1.641	0.028	302	12	201	11	327	13	1327	14	1336	14	1331	33	0.30		Cuts inclusion, radiation damage

SA10_0217_1	0.1977	0.0031	2.5	0.12	0.0926	0.0042	1.282	0.019	56.5	1	44.44	0.85	65.6	2.5	1161	17	1247	29	1316	84	11.78		Cuts resin
SA10_0217_3	0.2234	0.0024	2.609	0.086	0.0846	0.0029	1.646	0.013	69.36	0.79	42.3	0.43	78.2	1.8	1299	13	1285	24	1208	69	-7.53	R	
SA10_0300_2	0.2699	0.002	3.809	0.077	0.1022	0.0022	1.1497	0.006	126.7	2.4	110.5	2.1	227.7	4.9	1540	10	1584	16	1624	40	5.17		Cuts resin
SA10_0301_1	0.1952	0.0023	2.801	0.041	0.1038	0.0011	0.884	0.008	743	19	864	29	1129	19	1148	13	1350	11	1683	19	31.79		Cuts inclusion, radiation damage
SA10_0301_2	0.269	0.0028	3.783	0.077	0.1022	0.002	1.231	0.02	149.5	2.6	127.6	4.3	214.8	3.3	1534	14	1577	17	1638	36	6.35	R	
SA10_0302_1	0.2062	0.0025	2.308	0.085	0.0826	0.0032	1.924	0.017	55.79	0.83	28.97	0.4	51.7	1.5	1207	13	1187	27	1078	85	-11.97	R	
SA10_0303_1	0.1113	0.0014	1.472	0.022	0.0965	0.0011	3.801	0.021	1351	22	354.1	5.3	583.9	6.2	680.1	7.9	915	8.9	1542	22	55.89		Cuts zones, nearby fractures
SA10_0303_2	0.2667	0.0027	3.327	0.09	0.0916	0.0025	1.443	0.013	78.25	0.88	54.12	0.44	116.9	2.6	1524	14	1477	22	1404	56	-8.55	C	
SA10_0304_1	0.2157	0.0022	2.478	0.068	0.0843	0.0023	1.477	0.012	101.6	2	69.3	1.7	124.9	3.2	1259	12	1250	20	1229	55	-2.44	C	
SA10_0305_1	0.2835	0.0017	3.862	0.051	0.1014	0.0014	2.389	0.014	298.8	1.2	123.85	0.64	228.6	3	1608.5	8.3	1602	11	1633	25	1.50	R	
SA10_0305_2	0.2806	0.0017	3.857	0.06	0.1026	0.0016	1.653	0.01	210.7	2.6	126.2	1.5	255.8	4.5	1593.9	8.7	1598	13	1649	29	3.34		Cuts resin
SA10_0309_1	0.2301	0.0014	2.647	0.039	0.0865	0.0013	1.4864	0.0061	321.5	4.8	213.3	3	370.9	5.2	1334.4	7.4	1309	11	1322	30	-0.94	C	
SA10_0309_2	0.2297	0.0014	2.62	0.039	0.0857	0.0013	2.2407	0.0097	395.5	4.3	174	2	314.5	4.4	1332.6	7.3	1302	11	1310	30	-1.73		Cuts resin
SA10_0313_1	0.2615	0.0029	3.699	0.052	0.1069	0.0011	2.096	0.035	610	10	298	8.4	556	16	1496	15	1567	11	1738	19	13.92	C	
SA10_0314_1	0.2229	0.0017	2.434	0.053	0.083	0.0018	1.92	0.011	173.1	2.2	88.8	1.3	152.4	2.9	1296.7	9.1	1246	16	1230	44	-5.42	R	
SA10_0315_1	0.267	0.0016	3.635	0.045	0.1034	0.0013	1.4067	0.0091	357	2.8	250.5	2.9	258.1	3.3	1525.3	8.2	1553	10	1670	24	8.66		Fracture, cuts zones, cuts inclusion
SA10_0315_2	0.2592	0.0028	3.671	0.095	0.1079	0.0028	0.997	0.0076	84.02	0.81	82.19	0.8	144.2	3.2	1484	14	1550	21	1705	52	12.96	C	
SA10_0316_2	0.302	0.0027	4.419	0.071	0.1119	0.0015	1.873	0.03	353	12	194.8	8.6	393	12	1700	13	1712	13	1811	24	6.13		Cuts inclusion
SA10_0317_1	0.2232	0.0027	2.411	0.088	0.0831	0.0031	1.919	0.016	66.8	0.81	34.29	0.49	58	1.6	1297	14	1221	26	1126	78	-15.19	R	
SA10_0317_2	0.2202	0.0038	2.94	0.2	0.1005	0.0057	1.284	0.015	49.81	0.55	38.64	0.73	78.2	5.8	1282	20	1306	43	1400	110	8.43		Cuts resin
SA10_0401_1	0.2467	0.0019	3.011	0.062	0.0926	0.0019	2.384	0.014	167.7	1.5	69.19	0.64	128.2	2.3	1421.4	9.8	1400	16	1434	40	0.88	R	

SA10_0402_1	0.2835	0.0053	4.02	0.2	0.1099	0.0058	2.554	0.043			20.67	0.17	8.11	0.12	16.49	0.9	1604	27	1575	42	1530	110	-4.84		Cuts resin
SA10_0403_2	0.2741	0.0029	3.76	0.11	0.1033	0.003	0.6762	0.0044			72.78	0.69	106.7	1.1	215	3.4	1560	14	1565	23	1603	56	2.68	R	
SA10_0405_2	0.5339	0.0049	14.53	0.23	0.203	0.0033	1.68	0.014			60.65	0.87	35.72	0.5	129.8	2.4	2755	21	2775	15	2829	28	2.62	R	
SA10_0406_1	0.2951	0.003	4.29	0.11	0.1084	0.0029	2.775	0.034			75.6	1.5	27.51	0.71	64.3	2.3	1665	15	1675	22	1720	51	3.20	C	
SA10_0407_1	0.4184	0.0023	10.749	0.082	0.1891	0.0014	1.371	0.012			495	6.4	362.9	7.2	644	16	2252	11	2500.3	7.2	2729	12	17.48	C	
SA10_0408_1	0.2469	0.002	3.499	0.071	0.1042	0.0022	0.767	0.018			163.9	2.3	232.1	8.9	329.5	5	1422	10	1518	16	1666	39	14.65		Cuts zones
SA10_0410_1	0.2285	0.0044	3.317	0.072	0.1067	0.0019	0.8414	0.0064			242.4	4.5	285.8	4	535.5	8.1	1322	24	1471	17	1719	33	23.09		Cuts inclusion, radiation damage
SA10_0411_1	0.1551	0.0015	1.615	0.036	0.0756	0.0018	2.578	0.066			254.1	2.9	105.1	2.3	121.4	2.8	929.1	8.1	970	14	1009	52	7.92		Cuts resin
SA10_0412_1	0.2648	0.002	3.981	0.047	0.1062	0.001	1.615	0.016			629	16	399	14	733	13	1514	10	1626.7	9.5	1725	18	12.23	C	
SA10_0415_1	0.3677	0.0032	9.3	0.11	0.1771	0.0014	2.215	0.02			428.9	2	197	2.4	460.4	4.7	2017	15	2363	10	2619	13	22.99	R	
SA10_0415_2	0.3114	0.0018	8.082	0.065	0.1808	0.0013	1.098	0.022			798	11	794	29	690.4	6	1747.3	8.7	2237.7	7.2	2655	12	34.19		Cuts inclusion, radiation damage
SA10_0417_1	0.1416	0.001	1.557	0.037	0.0765	0.0019	0.5026	0.0026			250	3.2	510.1	7.8	553.7	7.5	853.2	5.7	946	15	1038	51	17.80		Cuts incllusion
SA10_0501_1	0.2392	0.0017	3.541	0.063	0.1021	0.0019	1.976	0.011			214.7	1.8	111.5	1.1	196	2.9	1381.8	8.8	1528	14	1625	35	14.97	R	
SA10_0501_2	0.238	0.0015	3.545	0.053	0.1022	0.0016	2.187	0.011			297.8	3.3	140.2	1.6	247	3.4	1375.7	7.8	1533	12	1650	29	16.62	R	
SA10_0502_1	0.2419	0.0015	3.695	0.05	0.1042	0.0014	1.8344	0.0094			346.2	4.4	194.5	2.2	346.4	4.1	1396.3	7.7	1566	11	1684	25	17.08	C	
SA10_0503_1	0.1228	0.0017	1.595	0.063	0.0886	0.0036	1.434	0.012			105.9	1.1	77	1.2	59	1.6	745.9	9.8	941	25	1211	86	38.41		Fracture, radiation damage
SA10_0503_2	0.156	0.0013	2.036	0.049	0.0887	0.0022	1.72	0.011			202.2	1	122.4	1	114.5	2.3	933.9	7.5	1116	16	1334	49	29.99		Fracture, radiation damage
SA21C_0002_1	0.3152	0.0044	4.36	0.12	0.1008	0.0025	3.005	0.028	121000	42000	188.4	2.6	58.67	0.87	199.6	5.9	1764	22	1696	22	1612	48	-9.43	C	
SA21C_0003_1	0.1943	0.0034	2.005	0.083	0.0754	0.0031	1.551	0.015	32000	14000	113.3	1.7	67.2	1	158.4	4.7	1143	18	1100	29	973	92	-17.47	R	
SA21C_0004_1	0.2086	0.0033	2.269	0.079	0.0797	0.0028	1.477	0.018	43000	20000	166.5	2.3	103.3	1.4	196.8	5	1220	18	1192	25	1122	72	-8.73	C	
SA21C_0005_1	0.58	0.01	19.76	0.49	0.2487	0.0059	1.734	0.056	31000	15000	47.72	0.86	25.76	0.88	153.6	5	2942	42	3068	24	3155	38	6.75	C	

SA21C_0007_1	0.3506	0.006	8.01	0.18	0.1662	0.0029	1.535	0.018	109000	40000	202.6	3.1	121.8	2	349.5	8.3	1934	29	2223	20	2504	30	22.76	R	
SA21C_0008_1	0.1914	0.0045	1.99	0.13	0.0777	0.0054	1.466	0.019	9900	4100	52.19	0.81	33.92	0.56	74.6	3	1127	24	1076	48	880	150	-28.07	R	
SA21C_0100_1	0.2192	0.0049	2.44	0.16	0.0828	0.0056	1.078	0.014	10500	3700	42.52	0.72	38.2	0.7	88.5	3.4	1275	26	1217	48	1030	140	-23.79	C	
SA21C_0101_1	0.1849	0.0026	1.818	0.044	0.0714	0.0017	2.248	0.016	84000	38000	554.3	8.8	241.1	4.1	442.6	9.5	1093	14	1048	16	936	49	-16.77	C	
SA21C_0101_2	0.178	0.0039	2.23	0.15	0.0918	0.0059	1.666	0.038	15400	6200	91.2	1.3	55.2	1.7	110	10	1054	22	1148	47	1220	140	13.61		Cuts inclusion
SA21C_0102_1	0.1857	0.0043	1.86	0.12	0.074	0.005	0.7331	0.0078	16100	4900	61.73	0.97	84.8	1.3	137.8	4.6	1096	24	1040	45	790	150	-38.73	R	
SA21C_0104_1	0.2657	0.0037	3.719	0.081	0.1017	0.0021	1.1923	0.0096	157000	47000	466.3	6.6	405.4	5.2	696	13	1518	19	1570	18	1630	40	6.87	R	
SA21C_0105_1	0.5335	0.0085	13.46	0.3	0.1825	0.0041	1.239	0.014	50000	15000	79	1.2	66.6	1	223.7	5.6	2751	36	2702	21	2659	37	-3.46	R	
SA21C_0106_1	0.2896	0.004	3.882	0.099	0.0966	0.0023	0.9802	0.0083	89000	34000	335.1	4.9	357.9	5.8	680	13	1640	20	1600	20	1532	44	-7.05		Fracture, cuts inclusion
SA21C_0107_1	0.1819	0.0046	1.76	0.15	0.0698	0.0059	0.994	0.014	10400	4100	60.1	1	63.1	1.2	78	3.4	1075	25	954	57	590	180	-82.20	R	
SA21C_0108_1	0.3194	0.0044	4.71	0.1	0.1069	0.0023	2.569	0.024	152000	51000	384.5	7.9	155.1	3.2	320.3	8.3	1785	22	1765	18	1719	41	-3.84	R	
SA21C_0109_1	0.5295	0.0074	13.49	0.27	0.1839	0.0033	1.613	0.014	98000	42000	203.3	2.8	128.3	1.9	402.5	8.8	2736	31	2705	19	2672	30	-2.40	R	
SA21C_0200_1	0.2211	0.0062	2.44	0.21	0.0814	0.0071	0.6356	0.0085	9500	3600	37.35	0.67	59.2	1	84.9	3.2	1284	33	1147	73	850	200	-51.06	C	
SA21C_0201_1	0.2878	0.0047	3.79	0.14	0.0954	0.0035	2.297	0.026	56000	20000	159.9	2.2	70.1	1.2	124.2	4.5	1628	23	1576	30	1488	68	-9.41	C	
SA21C_0202_1	0.681	0.011	29.76	0.57	0.3148	0.0047	1.015	0.011	202000	54000	155	2.8	152.6	3	466.3	9.9	3346	43	3472	19	3535	23	5.35	R	
SA21C_0203_1	0.2248	0.0043	2.44	0.11	0.0792	0.0037	1.498	0.016	69000	18000	149.2	2.2	99.3	1.5	142.2	5	1305	23	1239	33	1065	99	-22.54		Cuts inclusion
SA21C_0205_1	0.2247	0.0061	2.82	0.21	0.0936	0.0072	1.275	0.021	13600	5100	52.68	0.95	41.46	0.9	62.6	3.2	1303	32	1329	55	1170	170	-11.37		Cuts resin
SA21C_0206_1	0.5248	0.0066	13.06	0.18	0.1788	0.0019	3.456	0.028	360000	130000	608.7	9.8	176.5	2.8	535	11	2716	28	2681	13	2638	18	-2.96	C	
SA21C_0207_1	0.2669	0.0038	3.613	0.075	0.0977	0.0016	1.503	0.013	158000	92000	876	16	588	14	853	15	1524	19	1546	16	1564	32	2.56	C	
SA21C_0208_1	0.1776	0.0026	1.702	0.055	0.0692	0.0022	1.358	0.01	84000	32000	433.8	6.2	322.5	4.4	367.2	7.6	1053	14	1004	20	862	65	-22.16	R	
SA21C_0209_1	0.1896	0.0043	1.92	0.13	0.0738	0.0052	1.091	0.013	25300	7200	85.6	1.4	79.7	1.3	92.2	3.4	1119	23	1058	44	780	150	-43.46	R	
SA21C_0300_1	0.522	0.0075	13.01	0.31	0.1803	0.0044	0.6308	0.0055	67000	23000	112.6	1.6	180.9	2.6	548	11	2704	32	2671	23	2627	40	-2.93	R	
SA21C_0301_1	0.1914	0.0034	2.119	0.081	0.08	0.0031	1.309	0.014	48000	18000	249.1	4.5	193.2	4	199.3	5.8	1128	19	1141	26	1114	81	-1.26	R	
SA21C_0302_1	0.2155	0.0031	2.498	0.06	0.0835	0.0018	1.611	0.013	154000	57000	726	16	452.3	9.7	510	11	1257	16	1268	17	1259	42	0.16		Cuts inclusion,

																									radiation damage
SA21C_0303_1	0.3211	0.0043	4.68	0.099	0.1051	0.0022	1.2532	0.0094	173000	62000	451.9	6.9	361.5	5.6	689	12	1794	21	1758	17	1690	39	-6.15	C	
SA21C_0304_1	0.1888	0.0026	1.967	0.051	0.0751	0.002	0.9419	0.0065	184000	51000	555.8	8.2	589.9	8.9	700	12	1114	14	1100	17	1039	51	-7.22	R	
SA21C_0305_1	0.2221	0.0051	2.43	0.15	0.079	0.0048	1.812	0.025	15900	6400	83.4	1.2	46.64	0.78	66	3.2	1290	27	1212	46	980	130	-31.63	C	
SA21C_0306_1	0.2261	0.004	2.64	0.1	0.0849	0.0032	1.528	0.019	28000	13000	153.4	2.6	102.9	1.9	143.6	4.6	1313	21	1300	30	1233	78	-6.49	R	
SA21C_0307_1	0.3174	0.0039	4.704	0.084	0.1066	0.0016	1.0472	0.0079	155000	68000	528.4	7.4	521.1	7.1	1037	18	1776	19	1762	15	1727	29	-2.84	C	
SA21C_0308_1	0.2263	0.0056	2.49	0.16	0.0815	0.0054	0.964	0.013	20200	7000	65.3	1	70.9	1.1	103.3	4.2	1312	29	1235	48	1020	140	-28.63	R	
SA21C_0309_1	0.0933	0.0044	1.061	0.092	0.0839	0.0067	1.079	0.033	15300	5100	98	4.2	97.9	4.8	49.4	3	573	26	698	47	970	180	40.93		Fracture, cuts inclusion
SA21C_0400_1	0.2931	0.0052	4.04	0.16	0.0996	0.0039	0.8283	0.0073	55000	32000	131.7	2.3	163.3	2.9	326	7.6	1654	26	1620	32	1540	76	-7.40		Cuts zones
SA21C_0401_1	0.1893	0.0058	2.26	0.22	0.0877	0.0092	1.863	0.037	-12800	6900	30.48	0.58	16.58	0.38	24.2	1.9	1114	31	1067	83	870	220	-28.05	R	
SA21C_0402_1	0.1219	0.0015	2.564	0.039	0.1509	0.002	3.373	0.026	-1130000	290000	1694	25	495.6	7.2	1348	20	741.2	8.4	1287	11	2349	23	68.45		Radiation damage
SA21C_0403_1	0.3072	0.0041	4.499	0.097	0.1052	0.0021	3.491	0.03	4400000	1100000	359.1	6.3	99.5	2	184.8	5.8	1725	20	1723	18	1699	36	-1.53	C	
SA21C_0404_1	0.2106	0.0049	2.98	0.13	0.1015	0.004	1.084	0.013	380000	100000	139.9	3.6	123.6	4	177	5.4	1232	26	1379	34	1581	75	22.07		Fractures, radiation damage
SA21C_0405_1	0.2707	0.0033	3.806	0.068	0.1014	0.0019	1.156	0.065	450000	120000	495.7	6.4	452	21	300.8	8.4	1543	17	1591	14	1639	33	5.86		Cuts resin
SA21C_0406_1	0.227	0.0033	2.6	0.085	0.0822	0.0027	1.882	0.018	86000	35000	243.2	4.1	122.6	2.2	211.1	6.4	1318	17	1286	24	1200	67	-9.83	R	
SA21C_0407_1	0.2131	0.0058	2.38	0.23	0.0825	0.0084	1.597	0.029	2600	4600	38.21	0.74	23.44	0.52	38.8	2.4	1242	31	1115	76	750	210	-65.60	C	
SA21C_0408_1	0.1921	0.0058	1.93	0.21	0.0735	0.0078	2.572	0.052	2100	4000	36.54	0.55	14.3	0.32	18.6	1.6	1129	31	959	79	550	220	-105.27	R	
SA21C_0409_1	0.1618	0.0038	2.595	0.063	0.1158	0.0017	0.966	0.025	205000	99000	1307	23	1410	22	2004	30	965	21	1291	18	1883	27	48.75		Hit existing spot
SA21C_0500_1	0.1891	0.0042	2.79	0.15	0.1075	0.0072	1.174	0.023	22000	20000	124.4	4.7	113.6	6.2	186	13	1115	23	1325	41	1620	120	31.17		Radiation damage
SA21C_0503_1	0.2391	0.0042	3.276	0.098	0.0988	0.0029	1.423	0.019	35000	73000	235.7	5.1	182.4	4.9	176.3	6.3	1380	22	1462	24	1567	56	11.93		Radiation damage
SA21C_0504_1	0.2245	0.0037	2.512	0.086	0.081	0.0027	1.567	0.013	14000	87000	203.6	3.1	141.7	2.3	273.6	7.2	1304	19	1269	25	1162	68	-12.22	R	
SA21C_0505_1	0.1912	0.0034	2.233	0.095	0.0847	0.0034	1.103	0.011	175000	78000	119.8	1.8	117.3	1.9	191.6	6	1127	18	1172	31	1212	82	7.01		Fracture, radiation damage

SA21C_0506_1	0.2235	0.0038	2.71	0.12	0.0878	0.0039	0.6173	0.0055	220000	150000	78.8	1.3	135.5	2	311.5	7.7	1299	20	1312	32	1265	96	-2.69	R	
SA21C_0507_1	0.1967	0.006	2.03	0.2	0.0772	0.0079	1.149	0.021	15000	11000	18.66	0.41	16.14	0.45	40.7	2.6	1153	32	1026	76	710	210	-62.39	C	
SA21C_0508_1	0.2816	0.0092	3.9	0.41	0.103	0.011	0.614	0.013	7000	6300	9.5	0.18	15.08	0.29	58.5	3.1	1591	46	1380	110	1060	240	-50.09		Cuts resin
SA21C_0509_1	0.2079	0.003	2.315	0.068	0.0803	0.0023	1.679	0.013	144000	85000	184	2.7	103.9	1.5	305.7	7.2	1218	16	1208	21	1169	58	-4.19	C	

Plesovice Standards

Standards A	206/238 Ratio	206/238 2SE	207/235 Ratio	207/235 2SE	207/206 Ratio	207/206 2SE	U/Th Ratio	U/Th Ratio 2SE			Approx U PPM	Approx U PPM 2SE	Approx Th PPM	Approx Th PPM 2SE	Approx Pb PPM	Approx Pb PPM 2SE	206/238 Age	206/238 2SE	207/235 Age	207/235 2SE	207/206 Age	207/206 2SE	% Discordance
Z_Plesovice_1	0.05367	0.00039	0.3915	0.0097	0.0538	0.0014	9.679	0.051			755.8	8	78.09	0.96	39	1.5	337	2.4	333.7	7	308	53	-9.42
Z_Plesovice_2	0.0537	0.00037	0.394	0.01	0.0536	0.0015	9.682	0.051			753.8	8.3	77.91	0.93	39	1.4	337.2	2.2	334.6	7.5	291	57	-15.88
Z_Plesovice_3	0.05363	0.00035	0.402	0.01	0.0546	0.0015	9.677	0.049			758.8	9.1	78.4	1.1	39	1.3	336.8	2.2	340.9	7.6	336	57	-0.24
Z_Plesovice_4	0.05375	0.00035	0.3897	0.0092	0.0525	0.0012	9.686	0.05			752.8	7.5	77.79	0.87	38.9	1.3	337.5	2.1	332	6.7	263	50	-28.33
Z_Plesovice_5	0.05369	0.00036	0.3938	0.0096	0.053	0.0013	9.667	0.048			760.3	8.7	78.6	1	39.2	1.4	337.1	2.2	335.4	7	287	51	-17.46
Z_Plesovice_6	0.05363	0.00035	0.3966	0.0088	0.0539	0.0013	9.693	0.048			751.2	8.1	77.55	0.92	38.8	1.4	336.8	2.1	337.3	6.4	321	50	-4.92
Z_Plesovice_7	0.05364	0.00036	0.3947	0.0092	0.0537	0.0013	9.679	0.047			754.4	9.4	78	1.1	39.1	1.3	336.8	2.2	335.6	6.7	308	50	-9.35
Z_Plesovice_8	0.05371	0.00033	0.3848	0.0089	0.0523	0.0013	9.672	0.044			757	8.2	78.33	0.97	38.8	1.2	337.2	2	329	6.6	254	51	-32.76
Z_Plesovice_9	0.05372	0.00035	0.4055	0.0095	0.0549	0.0013	9.678	0.05			757.3	6.6	78.14	0.75	39.4	1.2	337.3	2.2	343.4	6.8	357	50	5.52
Z_Plesovice_10	0.05365	0.00037	0.3898	0.0095	0.0532	0.0013	9.682	0.05			751.7	5.7	77.67	0.64	38.7	1.4	336.8	2.3	333	7.1	289	54	-16.54

Standards B	Final206_238	Final206_238_Int2SE	Final207_235	Final207_235_Int2SE	Final207_206	Final207_206_Int2SE	Final_U_Th_Ratio	Final_U_Th_Ratio_Int2SE	Final206_204	Final206_204_Int2SE	Approx_U_PPM	Approx_U_PPM_Int2SE	Approx_Th_PPM	Approx_Th_PPM_Int2SE	Approx_Pb_PPM	Approx_Pb_PPM_Int2SE	FinalAge206_238	FinalAge206_238_Int2SE	FinalAge207_235	FinalAge207_235_Int2SE	FinalAge207_206	FinalAge207_206_Int2SE	
Output_1_1	0.05345	0.00086	0.384	0.021	0.0522	0.0029	9.608	0.089	130000	430000	751	11	77.6	1.3	37.9	2.9	335.6	5.3	324	16	190	110	-76.63
Output_1_2	0.05471	0.00085	0.469	0.027	0.0619	0.0035	9.793	0.093	3000	110000	697	10	71.1	1.2	69.8	6.6	343.3	5.2	385	18	560	120	38.70
Output_1_3	0.05482	0.00085	0.415	0.019	0.0552	0.0025	9.662	0.096	252000	91000	709	11	73.7	1.3	43.4	3.2	344	5.2	350	14	328	94	-4.88

Output_1_4	0.05405	0.00079	0.405	0.018	0.0541	0.0024	9.728	0.085	-5.00E+06	1.80E+06	772	13	79.9	1.4	41.5	3	339.3	4.8	343	13	299	92	-13.48
Output_1_5	0.05339	0.00081	0.403	0.018	0.0546	0.0024	9.157	0.083	-174000	59000	736	11	81.1	1.3	41.6	3	335.2	5	340	13	321	92	-4.42
Output_1_6	0.05322	0.0008	0.389	0.019	0.0536	0.0026	9.491	0.084	-230000	480000	765.9	9.9	81.5	1.1	43.5	3.2	334.2	4.9	331	14	270	100	-23.78
Output_1_7	0.05348	0.00083	0.393	0.019	0.0538	0.0026	9.8	0.097	55000	25000	743	11	76.6	1.3	38	2.9	335.7	5.1	332	13	266	96	-26.20
Output_1_8	0.05361	0.00082	0.386	0.02	0.0521	0.0026	10.07	0.11	26000	16000	698.7	9.6	69.7	1.1	33.4	2.6	336.6	5	326	15	210	100	-60.29
Output_1_9	0.05356	0.00083	0.385	0.018	0.0529	0.0025	9.96	0.089	14000	14000	734	11	73.3	1.1	37.5	2.5	336.2	5.1	328	13	238	97	-41.26
Output_1_10	0.05367	0.00082	0.391	0.017	0.0527	0.0024	9.613	0.08	-140000	210000	758	11	78.4	1.2	38.9	2.8	336.9	5	332	13	260	95	-29.58
SA2	Final206_238	Final206_238_Int2SE	Final207_235	Final207_235_Int2SE	Final207_206	Final207_206_Int2SE	Final_U_Th_Ratio	Final_U_Th_Ratio_Int2SE	Final206_204	Final206_204_Int2SE	Approx_U_PPM	Approx_U_PPM_Int2SE	Approx_Th_PPM	Approx_Th_PPM_Int2SE	Approx_Pb_PPM	Approx_Pb_PPM_Int2SE	FinalAge206_238	FinalAge206_238_Int2SE	FinalAge207_235	FinalAge207_235_Int2SE	FinalAge207_206	FinalAge207_206_Int2SE	
Z_Plesovice_1	0.0536	0.001	0.377	0.027	0.0489	0.0034	9.72	0.13	116000	25000	760.1	7.6	78.6	1.1	31.6	3	336.4	6.1	316	20	70	130	-380.57
Z_Plesovice_2	0.05378	0.00097	0.398	0.025	0.0533	0.0036	9.51	0.12	50000	2.80E+06	731.4	8.3	75.5	1.1	37.5	3.4	337.6	5.9	335	18	190	130	-77.68
Z_Plesovice_3	0.05419	0.00071	0.379	0.025	0.0495	0.0034	10.06	0.11	-800000	150000	833.1	9	86.3	1.2	51.5	5.9	340.2	4.3	319	19	70	130	-386.00
Z_Plesovice_4	0.0526	0.001	0.389	0.029	0.0524	0.004	9.59	0.12	270000	170000	704.7	7.6	71.2	1.1	33.8	4.7	330.3	6.2	324	21	150	140	-120.20
Z_Plesovice_5	0.05306	0.00078	0.428	0.024	0.057	0.0034	9.59	0.1	-13000	54000	875	10	92.8	1.3	68.8	6	333.2	4.8	355	17	360	120	7.44
Z_Plesovice_6	0.0552	0.0012	0.453	0.06	0.0579	0.0074	10.64	0.14	55000	52000	716.9	7.6	71.9	1.1	40.3	6.6	346.5	7.4	339	31	170	190	-103.82
Z_Plesovice_7	0.05337	0.0009	0.398	0.03	0.0526	0.004	8.81	0.11	340000	200000	796.1	9.4	86.7	1.3	49.6	6.3	335.1	5.5	330	22	160	150	-109.44
Z_Plesovice_8	0.0547	0.00092	0.411	0.033	0.0537	0.0044	10.29	0.12	-54000	45000	737.1	8.4	74.6	1.1	39.1	5.3	343.2	5.6	337	24	170	160	-101.88
Z_Plesovice_9	0.05264	0.00088	0.347	0.034	0.0471	0.0046	8.982	0.095	44000	43000	766	8.5	81.3	1.1	40.8	5.8	330.6	5.4	291	26	-70	180	572.29
Z_Plesovice_10	0.0541	0.0011	0.404	0.027	0.0527	0.0036	10.24	0.13	520000	140000	751.2	8.3	76.6	1	38.1	3.7	339.7	6.5	338	20	220	140	-54.41
Z_Plesovice_11	0.05349	0.0009	0.384	0.025	0.0516	0.0034	9.64	0.12	92000	28000	747.8	9.1	77.8	1.2	40.5	3.6	335.8	5.5	327	19	160	130	-109.88
Z_Plesovice_12	0.05432	0.00094	0.389	0.025	0.0518	0.0034	9.98	0.11	98000	23000	780.7	8.7	81.1	1.1	43.3	3.6	341.6	5.6	329	19	170	130	-100.94
Z_Plesovice_13	0.05348	0.00099	0.419	0.031	0.056	0.0043	10.57	0.15	46000	12000	729.7	7.4	73.4	1.1	29.4	3.1	335.8	6.1	344	22	260	150	-29.15
Z_Plesovice_14	0.05349	0.00095	0.383	0.024	0.0506	0.0031	9.23	0.11	300000	120000	783.5	9.1	83.1	1.3	43	3.9	335.8	5.8	322	18	150	120	-123.87

SA3_1	Final206_238	Final206_238_Int2SE	Final207_235	Final207_235_Int2SE	Final207_206	Final207_206_Int2SE	Final_U_Th_Ratio	Final_U_Th_Ratio_Int2SE	Final206_204	Final206_204_Int2SE	Approx_U_PPM	Approx_U_PPM_Int2SE	Approx_Th_PPM	Approx_Th_PPM_Int2SE	Approx_Pb_PPM	Approx_Pb_PPM_Int2SE	FinalAge206_238	FinalAge206_238_Int2SE	FinalAge207_235	FinalAge207_235_Int2SE	FinalAge207_206	FinalAge207_206_Int2SE	
Z_Plesovice_1	0.0554	0.0012	0.397	0.026	0.052	0.0036	9.88	0.13	52000	23000	745.3	9.3	76.8	1.2	33.2	3	347.3	7.2	331	19	170	130	-104.29
Z_Plesovice_2	0.0524	0.00096	0.416	0.023	0.0582	0.0032	9.4	0.1	54000	14000	787	9.7	82.2	1.2	61.8	3.9	329.1	5.9	351	17	410	120	19.73
Z_Plesovice_3	0.0528	0.00095	0.384	0.022	0.0531	0.0031	9.92	0.12	51000	18000	745.7	8.8	76.4	1.2	39.5	3.2	331.5	5.8	326	16	230	120	-44.13
Z_Plesovice_4	0.0555	0.0011	0.395	0.026	0.0522	0.0034	9.79	0.13	51000	17000	732	10	76	1.2	39.2	2.9	348.2	6.7	331	19	190	130	-83.26
Z_Plesovice_5	0.05305	0.00089	0.394	0.02	0.0542	0.0028	9.58	0.11	54000	12000	773	10	80.5	1.4	48.1	3.8	333.1	5.4	332	14	290	110	-14.86
Z_Plesovice_6	0.05308	0.00083	0.397	0.021	0.0551	0.0029	9.64	0.1	50000	19000	770.8	8.8	79.5	1.1	48.5	3.5	333.3	5.1	336	15	310	110	-7.52
Z_Plesovice_7	0.05293	0.00095	0.388	0.024	0.0533	0.0033	9.66	0.12	52000	20000	728	10	75.4	1.3	41.5	3.8	333.1	6	326	17	230	120	-44.83
Z_Plesovice_8	0.05388	0.00097	0.406	0.025	0.0554	0.0035	9.72	0.11	53000	18000	772.4	8.1	80	1.1	35.2	2.9	338.9	6	341	18	300	130	-12.97
Z_Plesovice_9	0.0549	0.001	0.409	0.027	0.0546	0.0036	10.07	0.14	51000	17000	722.4	9.6	74.1	1.3	28.3	2.7	344.7	6.3	342	20	260	130	-32.58
Z_Plesovice_10	0.05392	0.00091	0.386	0.021	0.0526	0.0027	9.61	0.11	52000	15000	766	10	78.4	1.3	40	3.1	338.4	5.6	327	15	230	110	-47.13
Z_Plesovice_11	0.0538	0.0009	0.382	0.021	0.052	0.003	8.92	0.11	54000	15000	826	11	90.4	1.4	49	3.5	338.3	5.6	325	15	200	120	-69.15
Z_Plesovice_12	0.0529	0.001	0.368	0.025	0.0516	0.0035	11.47	0.15	51000	16000	722.8	9.1	72.2	1.2	24.8	2.6	332.1	6.2	311	18	150	130	-121.40
Z_Plesovice_13	0.056	0.0011	0.427	0.03	0.0566	0.0041	9.61	0.13	52000	21000	771	10	82.2	1.4	33.4	3	351.1	6.9	351	21	290	140	-21.07
Z_Plesovice_14	0.05302	0.0009	0.378	0.025	0.0518	0.0034	9.64	0.12	52000	17000	729.5	9.7	75	1.2	34	2.9	332.9	5.5	318	18	180	130	-84.94
Z_Plesovice_15	0.05323	0.00089	0.383	0.02	0.053	0.0027	9.649	0.098	53000	16000	769.9	9.7	79	1.3	45.3	3.3	334.2	5.4	324	15	250	110	-33.68
Z_Plesovice_16	0.05578	0.00097	0.391	0.02	0.0527	0.0028	9.22	0.1	50000	17000	791.7	8.9	84.3	1.2	53.8	3.5	349.8	5.9	334	15	240	110	-45.75
Z_Plesovice_17	0.05242	0.00097	0.407	0.025	0.0581	0.0038	10.06	0.11	53000	12000	733.7	8.9	74.9	1.1	34.5	3	329.2	5.9	341	19	380	130	13.37
Z_Plesovice_18	0.0536	0.0011	0.387	0.026	0.0536	0.0036	10.12	0.13	51000	19000	759	9.5	78.4	1.3	26.5	2.7	336.6	6.7	324	19	210	130	-60.29
Z_Plesovice_19	0.05466	0.00099	0.41	0.027	0.0555	0.0038	9.53	0.12	52000	20000	730.7	9.9	76.4	1.2	28.1	2.4	342.9	6.1	340	19	280	130	-22.46
Z_Plesovice_20	0.05397	0.00084	0.381	0.021	0.0528	0.003	9.75	0.1	51000	17000	733	11	75	1.3	52	3.3	338.7	5.2	323	15	220	110	-53.95
Z_Plesovice_21	0.05354	0.00087	0.413	0.019	0.0571	0.0027	9.358	0.092	58000	19000	890.1	8.3	95.9	1.1	84.2	4.8	336.1	5.3	348	14	412	98	18.42
Z_Plesovice_22	0.0532	0.00092	0.372	0.022	0.0525	0.0032	10.06	0.11	49000	16000	642.5	8.6	64.8	1.1	37.7	2.9	334	5.6	317	16	190	120	-75.79

Z_Plesovice_23	0.05288	0.00094	0.415	0.021	0.059	0.003	9.64	0.1	53000	18000	789.2	9.6	81.4	1.1	49.3	3.3	332.1	5.8	351	16	460	110	27.80
SA4	Final206_238	Final206_238_Int2SE	Final207_235	Final207_235_Int2SE	Final207_206	Final207_206_Int2SE	Final_U_Th_Ratio	Final_U_Th_Ratio_Int2SE	Final206_204	Final206_204_Int2SE	Approx_U_PPM	Approx_U_PPM_Int2SE	Approx_Th_PPM	Approx_Th_PPM_Int2SE	Approx_Pb_PPM	Approx_Pb_PPM_Int2SE	FinalAge206_238	FinalAge206_238_Int2SE	FinalAge207_235	FinalAge207_235_Int2SE	FinalAge207_206	FinalAge207_206_Int2SE	
Z_Plesovice_1	0.0536	0.001	0.355	0.022	0.0513	0.0032	10.14	0.12	50000	11000	745.7	9.7	74	1.1	32	2.6	336.2	6.4	304	17	160	120	-110.13
Z_Plesovice_2	0.0534	0.00099	0.442	0.024	0.0633	0.0036	8.88	0.11	58000	13000	763.8	9.3	86.6	1.2	55.5	3.4	335.2	6	367	17	560	120	40.14
Z_Plesovice_3	0.0537	0.0011	0.378	0.024	0.0528	0.0032	10.33	0.16	51000	13000	776	15	77.1	1.1	36.6	2.9	337	6.9	319	18	220	120	-53.18
Z_Plesovice_4	0.0542	0.0011	0.374	0.022	0.0531	0.0033	10.47	0.14	50000	12000	761	11	74.1	1.1	35.5	2.7	339.9	6.5	320	17	230	120	-47.78
Z_Plesovice_5	0.0537	0.001	0.428	0.025	0.0604	0.0036	8.94	0.11	47000	11000	745.9	9.3	83.3	1.1	52.6	3.5	336.8	6.3	355	18	470	120	28.34
Z_Plesovice_6	0.05368	0.00099	0.383	0.023	0.054	0.0033	10.46	0.12	55000	11000	738.5	8.3	71.65	0.98	30.4	2.7	337	6	323	17	250	120	-34.80
Z_Plesovice_7	0.05322	0.00097	0.404	0.023	0.0576	0.0034	9.31	0.12	49000	12000	783	10	87.4	1.4	42.6	3.2	334.1	5.9	341	17	380	120	12.08
Z_Plesovice_8	0.05374	0.00098	0.388	0.023	0.0541	0.0032	10.15	0.14	55000	12000	762	11	78	1.3	38	2.9	337.3	6	327	17	270	120	-24.93
Z_Plesovice_9	0.054	0.001	0.374	0.023	0.0525	0.0034	10.27	0.13	48000	11000	750	10	73.2	1.2	35.2	3	338.6	6.2	318	17	180	120	-88.11
Z_Plesovice_10	0.054	0.001	0.492	0.027	0.0694	0.0041	8.53	0.11	52000	11000	765.7	9.2	87.5	1.2	73.8	4.8	338.8	6.2	403	19	740	130	54.22
Z_Plesovice_11	0.05343	0.00094	0.387	0.024	0.0543	0.0033	10.42	0.14	48500	9800	714.2	9	68.2	1.1	30.9	2.9	335.5	5.7	325	18	260	130	-29.04
Z_Plesovice_12	0.0545	0.001	0.384	0.024	0.0523	0.0032	9.73	0.11	70000	12000	808.8	9.9	85.4	1.3	39.2	3.3	342.2	6.1	325	18	200	120	-71.10
Z_Plesovice_13	0.05359	0.00096	0.407	0.024	0.0561	0.0032	9.79	0.12	50000	11000	742.1	8.4	76.7	1.1	39	2.7	336.4	5.9	342	18	350	120	3.89
Z_Plesovice_14	0.0534	0.0011	0.384	0.021	0.0538	0.0031	9.63	0.11	53000	11000	753.6	8.6	78	1.1	36.6	3.3	335.4	6.5	327	15	280	110	-19.79
Z_Plesovice_15	0.05336	0.00092	0.373	0.023	0.0524	0.0033	9.65	0.11	46000	11000	756.3	8.8	78	1.1	40.7	3.1	335	5.6	317	17	180	120	-86.11
SA5	Final206_238	Final206_238_Int2SE	Final207_235	Final207_235_Int2SE	Final207_206	Final207_206_Int2SE	Final_U_Th_Ratio	Final_U_Th_Ratio_Int2SE	Final206_204	Final206_204_Int2SE	Approx_U_PPM	Approx_U_PPM_Int2SE	Approx_Th_PPM	Approx_Th_PPM_Int2SE	Approx_Pb_PPM	Approx_Pb_PPM_Int2SE	FinalAge206_238	FinalAge206_238_Int2SE	FinalAge207_235	FinalAge207_235_Int2SE	FinalAge207_206	FinalAge207_206_Int2SE	
Z_Plesovice_1	0.0547	0.0027	-0.07	0.3	-0.021	0.031	10.56	0.53	80000	49000	755	13	78.2	3.3	-78	73	342	17	120	240	-4030	970	108.49
Z_Plesovice_2	0.053	0.0024	0.409	0.077	0.054	0.01	9.94	0.43	118500	6800	758	15	78.9	3.2	53	14	332	15	300	54	-240	310	238.33
Z_Plesovice_3	0.0549	0.0027	0.452	0.084	0.073	0.015	9.29	0.4	47400	2700	753	10	76.8	2.9	34	9.2	345	17	313	54	30	340	-1050.00

Z_Plesovice_4	0.0526	0.0026	0.419	0.069	0.071	0.013	10.01	0.41	48000	2500	756	16	76.1	2.6	35	8.2	329	16	316	48	120	320	-174.17
Z_Plesovice_5	0.0532	0.003	0.381	0.071	0.055	0.011	9.46	0.45	68900	4100	763	25	82.7	2.7	51.1	9	333	18	281	48	-130	310	356.15
Z_Plesovice_6	0.0543	0.0027	0.392	0.069	0.059	0.01	9.65	0.44	49800	2800	753	24	77.4	2.6	39.3	8.9	340	17	293	47	-100	290	440.00
Z_Plesovice_7	0.0536	0.0028	0.372	0.067	0.0498	0.0098	9.39	0.4	38300	2400	757	17	77.3	2.6	35.4	7.8	336	17	273	46	-340	290	198.82
Z_Plesovice_8	0.0538	0.0026	0.382	0.07	0.051	0.01	9.23	0.43	77600	3300	743	21	75.2	2.8	39.5	8.3	337	16	286	50	-280	300	220.36
Z_Plesovice_9	0.054	0.0026	0.398	0.068	0.0534	0.0094	9.7	0.47	65300	3000	772	21	81.6	2.9	34.3	8.5	338	16	302	48	-190	280	277.89
Z_Plesovice_10	0.0534	0.0025	0.411	0.073	0.055	0.01	9.4	0.39	45500	2400	746	21	78.1	2.6	40	9.7	335	15	307	50	-120	290	379.17
Z_Plesovice_11	0.0525	0.0026	0.382	0.062	0.0559	0.0095	9.97	0.53	52400	3000	758	23	75	2.6	40.3	8.2	329	16	296	44	-80	280	511.25
Z_Plesovice_12	0.0545	0.0036	0.387	0.064	0.058	0.01	9.18	0.43	58300	3800	754	22	79.7	2.8	36.9	8.2	340	22	289	44	-90	280	477.78
Z_Plesovice_13	0.0553	0.0043	0.525	0.091	0.071	0.012	9.7	0.64	41200	2900	669	36	76.9	2.9	46.7	8.7	345	25	366	55	180	300	-91.67
Z_Plesovice_14	0.0481	0.0021	0.33	0.056	0.056	0.01	9.38	0.33	87900	3500	1080	22	132.5	4	57	12	303	13	268	43	-170	280	278.24
Z_Plesovice_15	0.0586	0.0042	0.62	0.16	0.129	0.043	11.49	0.8	31800	2900	474	22	44	3	44	15	365	25	323	82	-330	420	210.61
Z_Plesovice_16	0.0571	0.0031	0.356	0.089	0.049	0.013	10.62	0.5	45000	2900	745	19	73.8	3.6	29	10	357	19	236	59	-690	340	151.74
Z_Plesovice_17	0.0584	0.0029	0.434	0.085	0.052	0.011	9.83	0.4	66800	3700	878	22	104	4.5	33	11	365	18	293	57	-370	320	198.65
SA7	Final206_238	Final206_238_Int2SE	Final207_235	Final207_235_Int2SE	Final207_206	Final207_206_Int2SE	Final_U_Th_Ratio	Final_U_Th_Ratio_Int2SE	Final206_204	Final206_204_Int2SE	Approx_U_PPM	Approx_U_PPM_Int2SE	Approx_Th_PPM	Approx_Th_PPM_Int2SE	Approx_Pb_PPM	Approx_Pb_PPM_Int2SE	FinalAge206_238	FinalAge206_238_Int2SE	FinalAge207_235	FinalAge207_235_Int2SE	FinalAge207_206	FinalAge207_206_Int2SE	
Z_Plesovice_1	0.05394	0.00096	0.393	0.027	0.0537	0.0037	9.65	0.13	49000	27000	820	11	87.4	1.5	45.2	5.8	338.6	5.9	328	20	210	140	-61.24
Z_Plesovice_2	0.05314	0.00096	0.396	0.022	0.0549	0.0032	9.75	0.13	56000	19000	715	9.2	72.8	1.4	35.1	3.7	333.6	5.8	335	17	320	120	-4.25
Z_Plesovice_3	0.0537	0.001	0.392	0.025	0.0518	0.0033	9.66	0.12	48000	22000	783	10	80.4	1.4	40.1	3.4	337	6.2	329	18	180	130	-87.22
Z_Plesovice_4	0.05402	0.00089	0.392	0.024	0.0525	0.0033	9.64	0.12	54000	23000	737.2	9.2	75.8	1.2	40	3.5	339.1	5.5	329	18	190	130	-78.47
Z_Plesovice_5	0.0541	0.001	0.398	0.025	0.0562	0.0036	9.73	0.12	52000	27000	717.3	9.2	72.3	1.2	37.2	3.5	339.5	6.2	335	18	330	130	-2.88
Z_Plesovice_6	0.05296	0.00094	0.394	0.022	0.0565	0.0033	9.64	0.12	52000	30000	744.8	9.2	76	1.2	39.6	3.6	332.6	5.7	334	16	340	120	2.18
Z_Plesovice_7	0.0541	0.0011	0.391	0.024	0.0508	0.0032	9.64	0.12	47000	28000	760.9	9.9	77.7	1.3	39.9	3.4	339.2	6.5	330	18	160	120	-112.00
Z_Plesovice_8	0.0536	0.00093	0.398	0.024	0.0529	0.0031	9.99	0.12	51000	20000	703.1	9.5	71.1	1.1	33.6	3.8	336.4	5.7	334	17	240	120	-40.17

Z_Plesovice_9	0.05311	0.00089	0.394	0.024	0.0534	0.0033	9.39	0.12	65000	22000	827	12	91.2	1.7	42.2	3.1	333.5	5.5	331	17	220	120	-51.59
Z_Plesovice_10	0.05435	0.00094	0.391	0.025	0.0513	0.0033	9.7	0.11	43000	22000	811	12	87.4	1.4	39.1	2.9	341.1	5.7	330	18	160	130	-113.19
SA8	Final206_238	Final206_238_Int2SE	Final207_235	Final207_235_Int2SE	Final207_206	Final207_206_Int2SE	Final_U_Th_Ratio	Final_U_Th_Ratio_Int2SE	Final206_204	Final206_204_Int2SE	Approx_U_PPM	Approx_U_PPM_Int2SE	Approx_Th_PPM	Approx_Th_PPM_Int2SE	Approx_Pb_PPM	Approx_Pb_PPM_Int2SE	FinalAge206_238	FinalAge206_238_Int2SE	FinalAge207_235	FinalAge207_235_Int2SE	FinalAge207_206	FinalAge207_206_Int2SE	
Z_Plesovice_1	0.054	0.0011	0.402	0.027	0.0553	0.0039	9.68	0.12	97000	67000	753	13	78	1.6	39.1	3.4	338.9	6.7	335	19	250	130	-35.56
Z_Plesovice_2	0.0535	0.001	0.403	0.028	0.056	0.0039	9.69	0.13	69000	91000	761.5	8.9	78.8	1.3	39.8	3.8	335.8	6.4	337	20	290	140	-15.79
Z_Plesovice_3	0.0534	0.001	0.41	0.03	0.0568	0.0042	9.63	0.14	-400000	130000	749.2	9.3	77.6	1.3	37.9	4	335.1	6.4	339	21	300	150	-11.70
Z_Plesovice_4	0.0538	0.0012	0.37	0.029	0.0503	0.004	9.74	0.15	-5000	230000	751	10	76.8	1.5	38.9	4.2	337.7	7.2	312	21	90	150	-275.22
Z_Plesovice_5	0.054	0.0012	0.387	0.027	0.0528	0.0038	9.65	0.14	300000	270000	759.3	9.6	78.8	1.3	38.7	4.2	339	7.2	328	20	190	140	-78.42
Z_Plesovice_6	0.0535	0.0011	0.402	0.03	0.0544	0.0042	9.71	0.14	180000	210000	757.3	9.4	78.2	1.3	41.2	4.6	335.9	6.6	333	22	220	150	-52.68
Z_Plesovice_7	0.054	0.0012	0.389	0.029	0.053	0.004	9.67	0.14	-2000	150000	756	10	78.4	1.4	37.9	3.9	339.1	7.3	324	21	180	150	-88.39
Z_Plesovice_8	0.0536	0.001	0.392	0.028	0.053	0.0037	9.66	0.13	500000	110000	749.6	9.7	76.9	1.4	38.2	4	336.5	6.2	329	20	190	140	-77.11
Z_Plesovice_9	0.0532	0.001	0.376	0.026	0.051	0.0036	9.66	0.14	56000	84000	737	11	75.1	1.4	38.2	3.6	334.3	6.1	323	20	170	140	-96.65
Z_Plesovice_10	0.0535	0.001	0.391	0.028	0.0528	0.0037	9.87	0.13	14000	77000	756.7	8	77.6	1.1	38	3.1	336	6.2	326	20	190	140	-76.84
Z_Plesovice_11	0.05412	0.00093	0.389	0.023	0.0519	0.0031	9.4	0.11	122000	73000	820.1	9.4	92.5	1.3	48.7	3.6	339.7	5.7	327	17	180	120	-88.72
Z_Plesovice_12	0.0535	0.0011	0.413	0.029	0.0562	0.0041	10	0.14	52000	45000	704.5	9.5	70.1	1.1	35.2	3.4	335.9	6.7	344	21	280	140	-19.96
Z_Plesovice_13	0.05347	0.00096	0.399	0.028	0.0544	0.0039	9.62	0.12	48000	38000	760	10	78.7	1.3	37.2	3.9	335.7	5.9	332	20	240	140	-39.88
Z_Plesovice_14	0.0535	0.0012	0.398	0.027	0.0543	0.0037	9.66	0.14	53000	36000	765	10	79.7	1.5	40.5	3.9	336.1	7.1	332	20	250	140	-34.44
Z_Plesovice_15	0.0539	0.0011	0.388	0.027	0.0514	0.0036	9.74	0.13	56000	35000	753	10	77	1.4	37.4	3.9	338.5	6.9	324	20	140	140	-141.79
Z_Plesovice_16	0.0537	0.001	0.374	0.028	0.0508	0.004	9.67	0.13	54000	36000	728	10	75	1.3	38.8	3.7	336.9	6.4	313	20	80	140	-321.13
Z_Plesovice_17	0.0545	0.001	0.413	0.023	0.0544	0.003	9.64	0.13	51000	44000	796	11	84.4	1.5	40	3.5	341.9	6.2	347	17	300	120	-13.97
Z_Plesovice_18	0.05304	0.00099	0.406	0.025	0.0551	0.0034	9.66	0.12	57000	42000	763.7	9.9	79.5	1.2	42.5	3.7	333	6.1	339	18	290	130	-14.83
Z_Plesovice_19	0.0536	0.0011	0.386	0.027	0.0526	0.0036	9.77	0.14	52000	36000	730	10	73.9	1.4	35.2	3.6	336.1	6.7	326	20	180	140	-86.72
Z_Plesovice_20	0.0537	0.0011	0.423	0.028	0.0582	0.0042	9.62	0.13	44000	36000	766	10	79.2	1.3	40.2	3.9	337	6.6	353	21	340	140	0.88

Z_Plesovice_21	0.0541	0.001	0.378	0.028	0.0501	0.0038	9.75	0.13	52000	33000	740.4	9.3	75.8	1.3	37.3	4	339.2	6.4	319	21	90	140	-276.89
Z_Plesovice_22	0.05384	0.00098	0.394	0.026	0.0533	0.0036	9.55	0.12	34000	35000	792	10	83	1.2	45.2	4.4	338.6	6.1	332	19	210	140	-61.24
Z_Plesovice_23	0.053	0.0011	0.366	0.025	0.0495	0.0034	9.84	0.14	61000	29000	728	9.2	73.2	1.3	34.8	3.8	332.8	6.6	311	19	110	130	-202.55
Z_Plesovice_24	0.0539	0.001	0.413	0.029	0.0555	0.004	9.65	0.11	57000	31000	767	10	79.9	1.3	40.5	3.9	338.2	6.3	344	21	270	140	-25.26

SA10	Final206_238	Final206_238_Int2SE	Final207_235	Final207_235_Int2SE	Final207_206	Final207_206_Int2SE	Final_U_Th_Ratio	Final_U_Th_Ratio_Int2SE	Approx_U_PPM	Approx_U_PPM_Int2SE	Approx_Th_PPM	Approx_Th_PPM_Int2SE	Approx_Pb_PPM	Approx_Pb_PPM_Int2SE	FinalAge206_238	FinalAge206_238_Int2SE	FinalAge207_235	FinalAge207_235_Int2SE	FinalAge207_206	FinalAge207_206_Int2SE	
Z_Plesovice_1	0.05377	0.00039	0.386	0.01	0.0537	0.0015	9.915	0.053	737.9	6.6	75.6	0.76	31.1	1.2	337.7	2.3	328.8	7.7	293	59	-15.26
Z_Plesovice_2	0.05358	0.00038	0.408	0.01	0.0571	0.0015	9.603	0.045	757.4	7	79.93	0.87	44.2	1.5	336.6	2.4	346	7.4	430	56	21.72
Z_Plesovice_3	0.05369	0.00038	0.378	0.0097	0.0523	0.0014	9.699	0.047	795.4	8.3	82.27	0.96	35.9	1.4	337.3	2.3	323.2	7.1	247	55	-36.56
Z_Plesovice_4	0.05368	0.00037	0.406	0.011	0.0567	0.0015	9.787	0.048	724.6	6.8	73.76	0.81	46.7	1.8	337.2	2.3	344	7.9	420	58	19.71
Z_Plesovice_5	0.05368	0.00035	0.3923	0.0097	0.0552	0.0014	9.595	0.049	777.2	8.2	79.69	0.96	42.6	1.4	337	2.2	333.7	7.1	358	54	5.87
Z_Plesovice_6	0.05369	0.00036	0.4081	0.0092	0.0574	0.0014	9.264	0.043	796	7.6	84.63	0.86	57	1.7	337.1	2.2	346.5	6.8	447	51	24.59
Z_Plesovice_7	0.05366	0.00037	0.3907	0.0095	0.0541	0.0013	9.861	0.048	704.6	6.7	71.98	0.77	34.6	1.2	336.9	2.2	333.6	7.1	326	54	-3.34
Z_Plesovice_8	0.05369	0.00036	0.3916	0.0096	0.0524	0.0013	9.774	0.05	772	8.4	79.64	0.97	37.9	1.3	337.1	2.2	333.2	7	260	52	-29.65
Z_Plesovice_9	0.05369	0.00037	0.3857	0.0098	0.0535	0.0014	9.817	0.048	760.3	7.1	76.86	0.76	35.1	1.2	337.1	2.2	328.8	7.2	288	55	-17.05
Z_Plesovice_10	0.05365	0.00038	0.3726	0.0098	0.0528	0.0014	9.597	0.052	850.4	9.3	87.2	1	36	1.4	336.9	2.3	319.1	7.2	261	55	-29.08
Z_Plesovice_11	0.0537	0.00039	0.423	0.011	0.0563	0.0015	9.716	0.057	725.7	5.9	75.4	0.76	42.6	1.5	337.1	2.4	356.8	7.9	398	58	15.30

SA21C	Final206_238	Final206_238_Int2SE	Final207_235	Final207_235_Int2SE	Final207_206	Final207_206_Int2SE	Final_U_Th_Ratio	Final_U_Th_Ratio_Int2SE	Final206_204	Final206_204_Int2SE	Approx_U_PPM	Approx_U_PPM_Int2SE	Approx_Th_PPM	Approx_Th_PPM_Int2SE	Approx_Pb_PPM	Approx_Pb_PPM_Int2SE	FinalAge206_238	FinalAge206_238_Int2SE	FinalAge207_235	FinalAge207_235_Int2SE	FinalAge207_206	FinalAge207_206_Int2SE	
Z_Plesovice_1	0.05362	0.0009	0.445	0.02	0.0609	0.0029	10.17	0.1	370000	170000	837	13	88.2	1.5	51.8	2.8	336.6	5.5	369	14	532	97	36.73
Z_Plesovice_2	0.05361	0.00087	0.385	0.02	0.0527	0.0028	10.58	0.11	135000	74000	675.9	9.9	68.3	1.2	27.5	3	336.5	5.3	327	15	220	110	-52.95
Z_Plesovice_3	0.05365	0.00081	0.373	0.014	0.0506	0.0018	9.045	0.079	102000	39000	832	14	89	1.7	49.7	2.6	336.8	5	319	11	178	75	-89.21
Z_Plesovice_4	0.05367	0.00082	0.386	0.015	0.0523	0.002	9.128	0.078	54000	19000	755	11	77.8	1.2	51.1	2.9	336.9	5	329	11	243	80	-38.64

Z_Plesovice_5	0.05385	0.00096	0.394	0.018	0.0534	0.0025	9.97	0.1	53000	16000	752	11	77.8	1.2	37	2.3	338	5.9	333	13	260	96	-30.00
Z_Plesovice_6	0.05414	0.00091	0.376	0.019	0.0505	0.0025	9.92	0.1	44000	17000	756	14	78.1	1.6	29.9	2.2	339.8	5.5	320	14	141	99	-140.99
Z_Plesovice_7	0.05343	0.00086	0.449	0.022	0.0601	0.0027	9.65	0.1	57000	20000	755	11	78	1.3	47.1	2.7	335.4	5.3	371	15	521	99	35.62
Z_Plesovice_8	0.05317	0.00089	0.379	0.02	0.0517	0.0027	9.89	0.11	46000	17000	755	12	78	1.4	28.4	2.2	333.9	5.4	321	15	200	110	-66.95
Z_Plesovice_9	0.05393	0.00084	0.379	0.019	0.0508	0.0026	9.73	0.11	54000	15000	754	13	78.1	1.6	28.8	2.2	338.5	5.2	323	15	170	100	-99.12
Z_Plesovice_10	0.05374	0.00083	0.386	0.018	0.0518	0.0024	10.13	0.11	93000	32000	755	11	77.9	1.3	29.2	2.1	337.3	5.1	327	13	197	95	-71.22
Z_Plesovice_11	0.05358	0.00088	0.432	0.019	0.0583	0.0026	9.06	0.1	151000	48000	758	13	78.4	1.5	61.8	3	336.3	5.4	360	14	436	95	22.87
Z_Plesovice_12	0.05399	0.00092	0.415	0.019	0.0554	0.0024	10.4	0.11	43000	31000	751	11	77.7	1.3	34.1	2.3	338.8	5.6	348	14	349	90	2.92
Z_Plesovice_13	0.05369	0.00078	0.397	0.015	0.0537	0.002	9.847	0.086	-200000	200000	748	11	77	1.2	53.6	2.8	337.1	4.8	337	11	295	80	-14.27
Z_Plesovice_14	0.0539	0.00076	0.386	0.017	0.0523	0.0023	9.197	0.079	138000	62000	827	10	86.2	1.2	67.7	3.3	338.3	4.7	327	12	222	91	-52.39
Z_Plesovice_15	0.05367	0.00089	0.383	0.021	0.0518	0.0029	10.37	0.11	56000	31000	653.2	9.7	66.8	1.2	26.8	2.1	336.9	5.4	323	15	190	110	-77.32
Z_Plesovice_16	0.05325	0.00086	0.381	0.016	0.0519	0.0022	9.416	0.09	26000	38000	917	15	95.1	1.8	46.2	2.9	334.4	5.3	324	12	226	87	-47.96

NIST 610

Standards A	Final206_238	Final206_238_Int2SE	Final207_235	Final207_235_Int2SE	Final207_206	Final207_206_Int2SE	Final_U_Th_Ratio	Final_U_Th_Ratio_Int2SE			Approx_U_PPM	Approx_U_PPM_Int2SE	Approx_Th_PPM	Approx_Th_PPM_Int2SE	Approx_Pb_PPM	Approx_Pb_PPM_Int2SE
G_NIST610_1	0.2469	0.0016	30.25	0.2	0.9097	0.0049	0.8281	0.003			585.1	7.9	723	12	10600	110
G_NIST610_2	0.2453	0.0017	30.18	0.2	0.9095	0.0049	0.849	0.0031			524.9	6.3	618.5	8.4	9980	120
G_NIST610_3	0.2456	0.0015	30.4	0.19	0.9097	0.005	0.8482	0.0029			677.8	6.2	830.2	7.9	17650	110
G_NIST610_4	0.245	0.0017	30.36	0.21	0.9096	0.0049	0.8354	0.0031			709.3	9.7	913	14	11920	280

Standards B	Final206_238	Final206_238_Int2SE	Final207_235	Final207_235_Int2SE	Final207_206	Final207_206_Int2SE	Final_U_Th_Ratio	Final_U_Th_Ratio_Int2SE	Final206_204	Final206_204_Int2SE	Approx_U_PPM	Approx_U_PPM_Int2SE	Approx_Th_PPM	Approx_Th_PPM_Int2SE	Approx_Pb_PPM	Approx_Pb_PPM_Int2SE
G_NIST610_1	0.2506	0.0033	32.19	0.38	0.926	0.0077	0.771	0.0055	11840	310	582	11	745	14	11430	190
G_NIST610_2	0.2527	0.0032	32.04	0.34	0.9136	0.0084	0.7746	0.0053	17640	540	564	10	718	13	11130	180

G_NIST610_3	0.2521	0.0034	31.93	0.41	0.9141	0.0085	0.7851	0.0054	31930	930	551.7	9.6	695	13	11020	180
G_NIST610_4	0.249	0.0033	30.81	0.35	0.9019	0.008	0.8668	0.0069	-3910	99	445.7	7.6	508.5	9.1	7960	140
G_NIST610_5	0.2481	0.003	30.88	0.35	0.9063	0.0076	0.8687	0.006	-3588	82	441.9	7.5	501.7	9	7770	120
G_NIST610_6	0.2471	0.0033	30.62	0.35	0.9047	0.008	0.8808	0.006	-3260	81	440.3	6.8	491.3	7.9	7570	120
SA21C	Final206_238	Final206_238_Int2SE	Final207_235	Final207_235_Int2SE	Final207_206	Final207_206_Int2SE	Final_U_Th_Ratio	Final_U_Th_Ratio_Int2SE	Final206_204	Final206_204_Int2SE	Approx_U_PPM	Approx_U_PPM_Int2SE	Approx_Th_PPM	Approx_Th_PPM_Int2SE	Approx_Pb_PPM	Approx_Pb_PPM_Int2SE
G_NIST610_1	0.2417	0.0032	31.39	0.46	0.914	0.014	0.9293	0.0085	7590	340	437	5.9	476.1	6.9	5823	74
G_NIST610_2	0.2501	0.0036	32.08	0.48	0.905	0.015	0.9296	0.0075	9180	320	401.3	5.5	426.7	6.3	7189	92
G_NIST610_3	0.2403	0.0033	30.92	0.4	0.909	0.012	0.9301	0.0081	14950	720	304.8	4.3	338.9	5.1	7409	97
G_NIST610_4	0.2462	0.0032	31.64	0.39	0.905	0.012	0.9241	0.0072	19640	900	399.1	5.8	417	6.6	7960	100
G_NIST610_5	0.2418	0.0034	31.36	0.39	0.913	0.012	0.9171	0.0078	29000	1200	312.5	3.7	349.2	4.4	7827	93
G_NIST610_6	0.2476	0.0032	32.02	0.42	0.913	0.012	0.917	0.0079	44900	1900	511.6	7.1	581.7	9	8260	110
G_NIST610_7	0.2437	0.0034	31.18	0.41	0.904	0.013	0.9054	0.007	51700	2500	402.6	5	427.7	5.7	8065	92
G_NIST610_8	0.2494	0.0031	32.08	0.39	0.911	0.011	0.9065	0.0075	40000	1700	458.7	6.4	525.1	8.2	8490	110
G_NIST610_9	0.2445	0.0035	31.1	0.4	0.903	0.012	0.9045	0.0072	24800	1100	428.8	6.2	451.8	7.1	8350	120
G_NIST610_10	0.2481	0.0031	32.08	0.39	0.918	0.012	0.8985	0.0079	14990	530	468.1	6.8	546.3	8.7	8680	130
G_NIST610_11	0.2438	0.0033	31.49	0.41	0.916	0.012	0.8963	0.0078	11100	430	457.7	6.1	508.2	7.4	8680	110
G_NIST610_12	0.2491	0.0032	31.64	0.41	0.902	0.012	0.8946	0.0071	8740	300	476.5	7	555.8	8.7	8820	120
G_NIST610_13	0.2488	0.0035	31.87	0.4	0.913	0.013	0.889	0.0069	7470	320	548.9	7.3	635.6	9.1	8890	110
G_NIST610_14	0.2493	0.0032	31.66	0.4	0.906	0.013	0.8889	0.0078	6780	270	424.9	6.5	456.4	7.7	9040	130
SA3.1	Final206_238	Final206_238_Int2SE	Final207_235	Final207_235_Int2SE	Final207_206	Final207_206_Int2SE	Final_U_Th_Ratio	Final_U_Th_Ratio_Int2SE	Final206_204	Final206_204_Int2SE	Approx_U_PPM	Approx_U_PPM_Int2SE	Approx_Th_PPM	Approx_Th_PPM_Int2SE	Approx_Pb_PPM	Approx_Pb_PPM_Int2SE
G_NIST610_1	0.2487	0.0038	31.11	0.43	0.91	0.012	0.8245	0.0071	15750	540	650	11	811	14	9860	140

G_NIST610_2	0.2458	0.0036	30.64	0.44	0.905	0.01	0.8532	0.0061	4950	180	502.6	8	576.2	9.6	9990	140
G_NIST610_3	0.2447	0.0035	30.67	0.42	0.912	0.011	0.8598	0.0067	6580	220	508.5	8	594	9.6	9700	150
G_NIST610_4	0.2438	0.0035	30.54	0.41	0.912	0.01	0.8692	0.007	7250	260	525.8	7.8	614	10	9630	140
G_NIST610_5	0.2447	0.0036	30.64	0.43	0.913	0.011	0.8835	0.0078	4150	140	456.5	6.9	513.5	8.5	9540	130
G_NIST610_6	0.2498	0.0038	31.06	0.45	0.908	0.011	0.8874	0.0066	5830	190	434	6.2	485.9	7.7	9380	130
G_NIST610_7	0.2434	0.0031	30.38	0.4	0.913	0.011	0.867	0.0067	8170	290	509.5	7.8	584.9	9.7	9440	140
G_NIST610_8	0.2446	0.0035	30.25	0.42	0.901	0.01	0.8481	0.0069	7610	270	580.7	8.5	687	11	9200	130
G_NIST610_9	0.2436	0.0034	30.07	0.42	0.899	0.01	0.8383	0.0063	8280	290	641	10	787	13	9090	130
G_NIST610_10	0.2445	0.0034	30.53	0.39	0.916	0.012	0.8483	0.0062	5460	190	498.9	7.5	581	10	8940	120
G_NIST610_11	0.243	0.0033	30.28	0.43	0.913	0.011	0.8344	0.0068	3950	140	429.2	6.5	497.5	8.2	9050	130
G_NIST610_12	0.2432	0.0034	30.28	0.4	0.911	0.011	0.777	0.0059	5830	180	530.7	8.1	765	13	8830	120
G_NIST610_13	0.2431	0.0035	30.24	0.43	0.914	0.01	0.7675	0.0055	9070	320	630.3	9.4	856	14	8870	120
G_NIST610_14	0.2423	0.0037	30.24	0.39	0.918	0.011	0.8194	0.0066	7580	270	598.7	9.1	722	12	8800	120
G_NIST610_15	0.2435	0.0034	29.97	0.4	0.909	0.011	0.8801	0.0065	4890	170	451.4	6.9	506.6	8.5	8790	140
G_NIST610_16	0.2451	0.0033	30.02	0.44	0.906	0.011	0.8935	0.0069	4340	140	405.1	6.2	444.4	7.3	8710	130
G_NIST610_17	0.2431	0.0034	30.14	0.43	0.914	0.01	0.8399	0.0069	4340	130	513.1	7.8	620	10	8570	130
G_NIST610_18	0.2451	0.0037	29.84	0.39	0.903	0.011	0.8115	0.0069	7360	250	650.5	9.2	840	14	8570	120
G_NIST610_19	0.2446	0.0034	30.25	0.38	0.917	0.011	0.8305	0.0069	8610	280	589.9	9	709	11	8470	120
G_NIST610_20	0.247	0.0034	29.99	0.41	0.901	0.011	0.8808	0.0072	4610	140	395.9	6.5	447.1	7.9	8440	130
G_NIST610_21	0.2435	0.0034	29.85	0.41	0.914	0.011	0.9089	0.0068	3300	100	317.5	4.9	351.1	5.8	8350	120
G_NIST610_22	0.2439	0.0035	29.65	0.4	0.9035	0.0092	0.9046	0.0066	4420	140	408.3	5.8	458.5	7.2	8310	120
G_NIST610_23	0.246	0.0036	30.12	0.4	0.913	0.011	0.8742	0.0071	5150	180	475.4	6.9	542.8	9.2	8200	120
SA4	Final206_238	Final206_238_Int2SE	Final207_235	Final207_235_Int2SE	Final207_206	Final207_206_Int2SE	Final_U_Th_Ratio	Final_U_Th_Ratio_Int2SE	Final206_204	Final206_204_Int2SE	Approx_U_PPM	Approx_U_PPM_Int2SE	Approx_Th_PPM	Approx_Th_PPM_Int2SE	Approx_Pb_PPM	Approx_Pb_PPM_Int2SE

G_NIST610_1	0.2396	0.0036	28.66	0.37	0.913	0.012	0.9693	0.0094	2275	95	444.2	6.6	460.7	7.4	5511	76
G_NIST610_2	0.2418	0.0036	29.05	0.36	0.913	0.012	0.9684	0.0078	2133	84	405.9	6	419.7	6.8	5780	85
G_NIST610_3	0.2433	0.0035	29.14	0.39	0.908	0.012	0.9675	0.0091	2143	83	391	5.6	413.7	6.9	5890	80
G_NIST610_4	0.2419	0.0034	29.13	0.38	0.912	0.013	0.9553	0.0083	2094	81	403.6	5.2	433.9	6.1	6052	72
G_NIST610_5	0.2449	0.0036	29.25	0.39	0.901	0.011	0.9481	0.0079	2033	79	422	5.5	443.9	6.6	6103	81
G_NIST610_6	0.2444	0.0038	29.61	0.39	0.916	0.013	0.9416	0.0076	2020	84	427.1	6.3	459.3	7.1	6207	84
G_NIST610_7	0.2436	0.0032	29.36	0.39	0.907	0.013	0.9353	0.0077	1898	70	402.3	5.8	444.2	7.1	6221	80
G_NIST610_8	0.2449	0.0034	29.8	0.41	0.911	0.013	0.9275	0.0078	1909	75	400.2	5.8	445.1	7.3	6396	81
G_NIST610_9	0.2461	0.0035	29.45	0.39	0.899	0.012	0.927	0.0081	1943	76	426.2	6	462.2	6.9	6585	83
G_NIST610_10	0.2455	0.0035	29.89	0.42	0.911	0.011	0.9299	0.0083	1870	76	444.4	6.3	464.2	7	6559	88
G_NIST610_11	0.2466	0.0032	30.22	0.38	0.913	0.011	0.9162	0.0074	1812	65	464.9	5.8	499.2	6.7	6806	81
G_NIST610_12	0.2434	0.0036	29.84	0.4	0.912	0.012	0.9011	0.0071	1752	74	427.5	6.4	485.3	7.7	6781	94
G_NIST610_13	0.2456	0.003	30.2	0.39	0.912	0.011	0.8842	0.0069	1712	63	429.4	5.9	491.4	7.7	7090	95
G_NIST610_14	0.2468	0.0035	30.24	0.43	0.908	0.012	0.8752	0.0076	1687	59	430.8	5.7	491.1	7.3	7310	110
G_NIST610_15	0.2462	0.0032	30.21	0.39	0.91	0.012	0.8646	0.0064	1639	64	421.5	6.5	483.7	7.8	7400	110

SA5	Final206_238	Final206_238_Int2SE	Final207_235	Final207_235_Int2SE	Final207_206	Final207_206_Int2SE	Final_U_Th_Ratio	Final_U_Th_Ratio_Int2SE	Final206_204	Final206_204_Int2SE	Approx_U_PPM	Approx_U_PPM_Int2SE	Approx_Th_PPM	Approx_Th_PPM_Int2SE	Approx_Pb_PPM	Approx_Pb_PPM_Int2SE
G_NIST610_1	0.2335	0.0075	41.8	1.2	0.944	0.038	0.814	0.016	-57000	35000	486.2	6.9	613	9.9	14520	280
G_NIST610_2	0.2405	0.0063	31.04	0.87	0.911	0.033	0.798	0.014	11200	8900	556.5	7.8	673.6	9.6	9830	200
G_NIST610_3	0.2358	0.007	25.88	0.71	0.898	0.03	0.814	0.014	25000	11000	614.8	8.8	681.2	9.4	8010	140
G_NIST610_4	0.2355	0.0068	25.1	0.79	0.898	0.035	0.817	0.015	1100	3600	502.6	7.7	601.3	9.3	6770	120
G_NIST610_5	0.2378	0.0071	26.07	0.82	0.891	0.034	0.806	0.016	8800	5500	440.8	7	541	8.2	6170	120
G_NIST610_6	0.2339	0.0065	29.06	0.86	0.92	0.034	0.807	0.016	8200	7800	455.9	6.1	544.8	9	6280	110
G_NIST610_7	0.2373	0.006	30.7	0.86	0.894	0.03	0.802	0.015	3100	3700	512.9	7.3	581	8.8	6840	140
G_NIST610_8	0.236	0.0066	31.43	0.98	0.919	0.031	0.807	0.016	10800	5500	476.1	7.2	533.6	8.7	6880	140

G_NIST610_9	0.2326	0.0073	29.89	0.96	0.916	0.036	0.81	0.015	18100	9500	374.3	5.4	456	6.7	6170	110
G_NIST610_10	0.2377	0.0072	28.71	0.85	0.902	0.034	0.807	0.017	5000	3400	365.3	5.8	428.4	6	5504	97
G_NIST610_11	0.2318	0.0073	28.58	0.93	0.943	0.036	0.815	0.017	8000	4200	341	5.2	396.2	5.1	4704	84
G_NIST610_12	0.2265	0.0063	26.67	0.79	0.912	0.033	0.806	0.015	7100	4400	411.9	6.5	488.5	8.4	5630	110
G_NIST610_13	0.2306	0.0064	27.26	0.8	0.893	0.031	0.81	0.013	-500	3000	418.4	6.8	563.8	8.5	6370	110
G_NIST610_14	0.2255	0.0076	28.8	1.2	0.918	0.04	0.827	0.019	11200	8800	767	13	960	16	9510	240

SA7	Final206_238	Final206_238_Int2SE	Final207_235	Final207_235_Int2SE	Final207_206	Final207_206_Int2SE	Final_U_Th_Ratio	Final_U_Th_Ratio_Int2SE	Final206_204	Final206_204_Int2SE	Approx_U_PPM	Approx_U_PPM_Int2SE	Approx_Th_PPM	Approx_Th_PPM_Int2SE	Approx_Pb_PPM	Approx_Pb_PPM_Int2SE
G_NIST610_1																
G_NIST610_2	0.2456	0.0034	30.62	0.42	0.916	0.01	0.8328	0.0066	11700	430	611.1	8.4	729	11	11150	150
G_NIST610_3	0.2481	0.0035	31.88	0.48	0.909	0.011	0.836	0.0066	11450	450	597.8	8.6	706	11	11320	160
G_NIST610_4	0.2494	0.0037	31.45	0.41	0.899	0.011	0.8457	0.0065	12140	420	590.9	8.1	693	11	11450	160
G_NIST610_5	0.2454	0.0036	29.64	0.37	0.916	0.011	0.8388	0.0072	13480	450	583.2	8.6	680	11	11240	170
G_NIST610_6	0.2477	0.0038	29.93	0.39	0.907	0.012	0.8451	0.0067	14960	550	579.3	8.9	670	11	10740	160
G_NIST610_7	0.2484	0.0035	31.51	0.41	0.901	0.011	0.8431	0.0058	13910	480	563.2	8.6	655	10	10080	150
G_NIST610_8	0.2481	0.0036	31.68	0.41	0.918	0.011	0.8644	0.0066	10080	340	544.8	7.8	632.8	9.6	9220	130

SA8	Final206_238	Final206_238_Int2SE	Final207_235	Final207_235_Int2SE	Final207_206	Final207_206_Int2SE	Final_U_Th_Ratio	Final_U_Th_Ratio_Int2SE	Final206_204	Final206_204_Int2SE	Approx_U_PPM	Approx_U_PPM_Int2SE	Approx_Th_PPM	Approx_Th_PPM_Int2SE	Approx_Pb_PPM	Approx_Pb_PPM_Int2SE
G_NIST610_1	0.2408	0.0036	29.74	0.45	0.915	0.012	0.8003	0.0067	33900	1300	465.7	7.1	581	9.6	8520	120
G_NIST610_2	0.2415	0.0035	29.7	0.36	0.904	0.012	0.7838	0.0065	50000	1700	547.4	8.1	697	11	10330	140
G_NIST610_3	0.2438	0.0036	30.14	0.43	0.903	0.011	0.7755	0.0065	86600	3100	639	10	818	14	12460	180
G_NIST610_4	0.246	0.0034	30.81	0.44	0.912	0.011	0.7497	0.0064	156900	5600	720	12	949	16	14590	220
G_NIST610_5	0.2439	0.0035	30.42	0.43	0.907	0.013	0.742	0.0062	208700	7800	731	11	982	16	15130	210

G_NIST610_6	0.2451	0.0034	30.79	0.39	0.911	0.012	0.7379	0.0055	172700	5900	735	11	994	16	15040	210
G_NIST610_7	0.243	0.0034	30.59	0.44	0.906	0.011	0.7448	0.0059	121300	4900	733	11	983	17	14900	230
G_NIST610_8	0.2451	0.0034	30.97	0.4	0.91	0.011	0.7646	0.006	77000	2700	703	11	909	15	13470	200
G_NIST610_9	0.2444	0.0035	30.94	0.41	0.912	0.012	0.7849	0.0062	54300	1800	610.7	9.5	763	13	11140	170
G_NIST610_10	0.2426	0.0033	31.26	0.41	0.927	0.011	0.8202	0.0063	40900	1600	510	8.2	622	10	9330	140
G_NIST610_11	0.2436	0.0033	30.81	0.4	0.908	0.012	0.881	0.0076	31900	1200	480.3	7.6	579	10	8760	130
G_NIST610_12	0.241	0.0033	30.31	0.41	0.903	0.01	0.8218	0.0063	26470	940	570.5	8.9	698	11	10220	150
G_NIST610_13	0.2402	0.0033	30.82	0.4	0.923	0.011	0.7716	0.0064	23030	820	656	10	842	14	12680	180
G_NIST610_14	0.2411	0.0033	30.5	0.37	0.908	0.011	0.7548	0.0059	23020	900	686	10	906	14	13940	210
G_NIST610_15	0.2425	0.0034	30.68	0.37	0.908	0.011	0.7508	0.0068	21700	750	703	10	929	15	14080	200
G_NIST610_16	0.2446	0.0035	30.82	0.4	0.906	0.012	0.7705	0.006	21370	760	662	11	849	14	12860	190
G_NIST610_17	0.2444	0.0032	30.5	0.38	0.895	0.011	0.7931	0.0054	21710	720	583.3	8.6	745	11	11700	160
G_NIST610_18	0.242	0.0034	30.87	0.44	0.916	0.011	0.7933	0.0061	22420	850	575.8	8.6	733	11	11860	170
G_NIST610_19	0.247	0.0034	31.33	0.4	0.911	0.01	0.7705	0.0063	21850	750	649.8	9.5	833	13	13930	200
G_NIST610_20	0.2475	0.0033	31.01	0.42	0.9	0.011	0.7628	0.0063	22340	760	687	10	892	15	14770	220
G_NIST610_21	0.2433	0.0035	31.24	0.4	0.926	0.012	0.7593	0.0059	21610	810	689	10	901	15	14320	210
G_NIST610_22	0.2482	0.0034	31.57	0.42	0.91	0.011	0.7604	0.0061	19920	710	671	12	885	16	13520	210
G_NIST610_23	0.2486	0.0031	31.29	0.39	0.902	0.011	0.7477	0.0059	18470	650	692	11	910	14	13770	200
G_NIST610_24	0.2455	0.0034	31.31	0.37	0.915	0.011	0.7798	0.006	16050	510	633.7	9.8	808	13	12380	180

SA10	Final206_238	Final206_238_Int2SE	Final207_235	Final207_235_Int2SE	Final207_206	Final207_206_Int2SE	Final_U_Th_Ratio	Final_U_Th_Ratio_Int2SE			Approx_U_PPM	Approx_U_PPM_Int2SE	Approx_Th_PPM	Approx_Th_PPM_Int2SE	Approx_Pb_PPM	Approx_Pb_PPM_Int2SE
G_NIST610_1	0.2437	0.0014	29.65	0.16	0.9098	0.005	0.8749	0.0034			451.4	4.9	525	6.6	6781	64
G_NIST610_2	0.2414	0.0014	29.43	0.17	0.9087	0.0055	0.8767	0.0031			458.5	5.4	525	7	7225	77
G_NIST610_3	0.24	0.0014	29.27	0.17	0.9111	0.0052	0.8769	0.0032			454.2	5.4	516.5	6.9	7445	79

G_NIST610_4	0.242	0.0014	29.18	0.17	0.9085	0.005	0.8731	0.0032			449.6	5.5	507.2	6.9	7658	82
G_NIST610_5	0.2425	0.0014	29.41	0.17	0.9095	0.0048	0.8727	0.0031			456.2	5.3	514.4	6.7	7856	81
G_NIST610_6	0.2448	0.0014	29.95	0.17	0.9101	0.0049	0.8719	0.003			465.8	5.4	537.1	7	7986	82
G_NIST610_7	0.2425	0.0014	30.57	0.17	0.9097	0.005	0.869	0.003			477.2	5.4	553.8	7.1	8063	82
G_NIST610_8	0.2445	0.0013	30.19	0.17	0.9095	0.0049	0.865	0.0029			494.6	6.1	568.2	7.9	8084	91
G_NIST610_9	0.2426	0.0014	28.94	0.16	0.9093	0.0048	0.862	0.003			529.5	6.2	603.5	7.9	8061	87
G_NIST610_10	0.211	0.0012	26.83	0.16	0.9098	0.0046	0.8627	0.0031			607.2	7.8	708	10	8143	95
G_NIST610_11	0.1848	0.001	24.94	0.15	0.91	0.005	0.8599	0.0029			686.5	7.4	832	10	8008	78
G_NIST610_12	0.1844	0.0011	24.94	0.14	0.9093	0.0046	0.8595	0.003			713	7.7	866	11	8263	83

SA21C	Final206_238	Final206_238_Int2SE	Final207_235	Final207_235_Int2SE	Final207_206	Final207_206_Int2SE	Final_U_Th_Ratio	Final_U_Th_Ratio_Int2SE	Final206_204	Final206_204_Int2SE	Approx_U_PPM	Approx_U_PPM_Int2SE	Approx_Th_PPM	Approx_Th_PPM_Int2SE	Approx_Pb_PPM	Approx_Pb_PPM_Int2SE
G_NIST610_1	0.2489	0.0034	29.65	0.37	0.8717	0.0081	0.9162	0.0066	10970	290	610	12	772	17	8170	130
G_NIST610_2	0.2511	0.0034	29.83	0.35	0.8683	0.0076	0.9085	0.0067	18680	470	563.7	9.3	659	11	8760	130
G_NIST610_3	0.2526	0.0033	29.91	0.36	0.8641	0.0085	0.9017	0.0069	-14120	340	496.4	7.5	560.4	8.6	8650	120
G_NIST610_4	0.2505	0.0031	29.92	0.31	0.8668	0.0076	0.8769	0.0061	-4104	88	387.6	6.8	410.6	7.4	8870	140
G_NIST610_5	0.2494	0.0031	30.01	0.34	0.8711	0.0075	0.8585	0.0058	-4262	99	517.1	8.7	613	10	8960	140
G_NIST610_6	0.2502	0.0029	30.42	0.33	0.8771	0.0076	0.8396	0.0059	-5900	160	620	11	763	14	9020	150
G_NIST610_7	0.2511	0.0029	30.25	0.34	0.8676	0.0074	0.8271	0.0059	-6460	160	677	11	814	13	9330	140
G_NIST610_8	0.249	0.003	30.15	0.33	0.8714	0.0079	0.8083	0.0053	-6130	140	700	11	879	14	9570	150
G_NIST610_9	0.2501	0.0033	30.43	0.35	0.8757	0.0081	0.8026	0.0059	-5300	120	684	11	852	14	9540	140
G_NIST610_10	0.2477	0.0032	30.19	0.36	0.876	0.0076	0.8031	0.0057	-8020	200	619	10	808	13	9590	140
G_NIST610_11	0.2483	0.0032	30.28	0.36	0.8772	0.0078	0.8066	0.0061	16190	400	592.2	9.8	688	12	9640	150
G_NIST610_12	0.2485	0.0032	30.2	0.36	0.8761	0.0079	0.8162	0.0054	11530	260	592	10	764	14	9370	150
G_NIST610_13	0.2491	0.0032	30.26	0.32	0.8783	0.0082	0.8253	0.0053	-224000	11000	387.3	6.9	486.8	8.7	9810	150

G_NIST610_14	0.2495	0.003	30.34	0.33	0.882	0.0076	0.8416	0.0055	-15110	370	350.7	5.8	394.5	7.1	9890	160
G_NIST610_15	0.2496	0.0034	30.18	0.37	0.8797	0.0087	0.8467	0.006	-13500	340	436.6	6.4	514.3	7.5	9720	150
G_NIST610_16	0.2492	0.003	30.34	0.33	0.8871	0.0076	0.8508	0.0054	-12670	290	535.3	7.5	660.8	9.2	10170	150

6.3 Appendix 3

6.3.1 Palaeocurrents

Palaeocurrent data is measured from cross bedding at localities during sample collection and analysis. Measurements are taken to provide additional context to the study, however it is now understood that individual measurements likely form parts of larger structures such as accretionary bars and are not representative of the regional flow direction.

Palaeoflow	Locality	GPS
270°	SA20	N57.40596 W005.68389
180°	Log 4	In log section
140°	SA18	In log section
320°	Log 15	In log section
270°	Log 11	In log section
240°	SA15	In log section
270°	SA14	In log section
290°	SA13	N57.40806 W005.68418
240°	Log 3	N57.40762 W005.68536
180°	SA21	N57.46629 W005.78862
270°	SA23	N57.41926 W005.76290
135°	SA24	N57.41926 W005.60925